A Study of Extended-Range Forecasting Problems-Blocking

Final Report to NASA Grant No. NSG-5339

Tsing-Chang Chen, Project Director

MARCH 1981

DEPARTMENT OF EARTH SCIENCES
METEOROLOGY PROGRAM
IOWA STATE UNIVERSITY

FINAL REPORT

TO

The National Aeronautics and Space Administration

Washington, D.C.

Grant No. NSG-5339

A Study of the Extended-Range Forecasting Problem--Blocking

March 1981

from

Department of Earth Sciences

Iowa State University

Ames, IA 50011

PROJECT DIRECTOR: Tsing-Chang Chen

CONTENTS

Spectral Analysis and Maintenance of Large-Scale Moving Waves by Nonlinear Interactions at 200 mb in the GLAS General Circulation Model

by

Tsing-Chang Chen and Hal G. Marshall
Department of Earth Sciences
Iowa State University
Ames, IA 50011

and

J. Shukla
NASA/Goddard Space Flight Center
Laboratory for Atmospheric Sciences
Greenbelt, MD 20771

Department of Meteorology
Massachusetts Institute of Technology
Cambridge, MA 02139

Abstract

Wavenumber-frequency spectral analysis of a 90-day winter (Jan. 15 - April 14) wind field simulated by a climate experiment of the GLAS atmospheric circulation model is made using the space-time Fourier analysis which is modified with Tukey's numerical spectral analysis. Computations are also made to examine how the model wave disturbances in the wavenumber-frequency domain are maintained by nonlinear interactions. Results are compared with observation, especially Kao and Lee's study.

It is found that equatorial easterlies do not show up in this climate experiment at 200 mb. The zonal kinetic energy and momentum transport of stationary waves are too small in the model's Northern Hemisphere. The wavenumber and frequency spectra of the model are generally in good agreement with observation. However, some distinct features of the model's spectra are revealed. The wavenumber spectra of kinetic energy show that the eastward moving waves of low wavenumbers have stronger zonal motion while the eastward moving waves of intermediate wavenumbers have larger meridional motion compared with observation. Furthermore, the eastward moving waves show a band of large spectral value in the medium frequency regime. The frequency spectra in high frequency regime decrease faster than observation as frequency increases. The scheme proposed by Kao and Lee for the maintenance of kinetic energy spectra by nonlinear interactions in middle latitudes is not applicable over the whole model globe because of the disappearance of equatorial easterlies. The maintenance of momentum flux spectra by nonlinear interactions in NH middle latitudes is similar to that of kinetic energy spectra. The primary nonlinear interactions of kinetic energy and momentum flux are contributed by those

between mean zonal flow and long and medium waves with low and medium frequencies. The stationary waves do not play a significant role in the nonlinear interactions as found in observation.

1. Introduction

The development of the general circulation model (GCM) in the past two decades has reached the step where the GCM is not only used to simulate the atmospheric circulation, but also employed to make medium range forecasts and long-term climate study. The simulation of the GCM is conventionally verified against the long-term averaged spatial distribution of observed atmospheric circulation. In fact, numerous observational studies demonstrate that the life cycle of the atmospheric disturbances vary from about a week for cyclone waves to several weeks for planetary waves. Besides the evaluation of the GCM simulation in the space domain, it seems logical to assess the GCM simulation in the time domain, too.

In order to accomplish the second goal, Hayashi and Golder (1977) and Hayashi (1974) applied the lag-correlation method to make the space-time spectral analysis of the wave disturbances in midlatitudes and tropics of the GCM of the Geophysical Fluid Dynamics Laboratory (GFDL). The spectral analysis with a lag-correlation method is also employed by Pratt (1979) to analyze the midlatitude disturbances of the GCM of the National Center for Atmospheric Research (NCAR). Tsay (1974b), then, uses the space-time Fourier analysis proposed by Kao (1968) to examine the tropical disturbances of the NCAR GCM.

The technique of the aforementioned spectral analysis in space and time can be classified into two methods: space-time spectral analysis (Hayashi, 1971) and space-time Fourier analysis (Kao, 1968). The former uses a lag-correlation method, while the latter uses a direct Fourier transform method. Tsay (1974a) and Pratt (1976) show these two methods are equivalent at

a discrete frequency, if a frequency smoothing is applied. Recently, Kao and Lee (1977) revised Kao's original scheme by introducing Tukey's (1967) spectral analysis technique to make extensive spectral analysis of atmospheric disturbances.

The GCM developed at the Goddard Institute for Space Studies (GISS) (Sommerville et al., 1974) has been diagnostically analyzed in various physical aspects, e.g. spectral energetics (Tenenbaum, 1976). However, no attempt has been made to investigate the wave disturbances of the current GCM at GLAS in the time domain. In order to promote our understanding of the wave disturbances in the GLAS atmospheric circulation model, it is of interest to analyze the wave motions of this model using modified Kao's scheme and to verify the model simulation against Kao and Lee's (hereafter referred to as KL) results.

The detailed structure of the GLAS atmospheric circulation model is described in detail by Somerville et al. (1974). It is a 9-level primitive equation model in σ-coordinate system. The grid system is 4° latitude x 5° longitude. The model contains a hydrological cycle, parameterization of subgrid-scale cumulus convection and orography. The radiation computation includes the calculated cloud and water vapor distribution. Arakawa's (1966) scheme is applied to treat the horizontal advections. Recently, the 4th order finite difference scheme is introduced to the GCM at Goddard Laboratory for Atmospheric Sciences (Kalnay-Rivas, 1977). However, the climate run analyzed in the present study uses the second order model.

Data analyzed in this study are condensed from a 4-month climate experiment (D122) using the NMC analysis of 1 January 1975 as initial field. The

history output data for every 12 hr over a period of 90 days starting from 00GMT, 15 January 1975, are used. The data of the first 15 days in this climate experiment are not used to avoid the transition period.

The current study consists of two parts: space-time spectral analysis and the maintenance of large scale moving waves by non-linear interactions. The discussion of these two parts is presented respectively in Sections 2 and 3.

2. Spectral Analysis

a. Method

The analysis of wavenumber-frequency spectra in this study follows KL's procedure in which they apply the numerical spectral analysis of Tukey (1967) to Kao's original space-time Fourier analysis (Kao, 1968). The detailed procedure of computations can be found in KL. However, a brief summary of the modified Kao's scheme should sufficiently serve the purpose of illustration. Suppose an atmospheric variable, $q(\lambda,t)$, be a real single-valued function which is piecewise continuous in an interval $(0,2\pi)$ for both longitudinal λ and time t. The complex Fourier coefficients of this atmospheric variable, $Q(k,\pm n)$, can be evaluated by,

$$Q(k, \pm n) = \frac{1}{4\pi^2} \int_0^{2\pi} \int_0^{2\pi} q(\lambda,t) e^{i(k\lambda \pm nt)} ds dt, \qquad (1)$$

where k and n are wavenumber and frequency respectively. -n represents the eastward moving waves, while +n is westward.

The double Fourier transform is carried out in two steps. It is evaluated first in the space domain,

$$Q_q(k,t) = \frac{1}{2\pi} \int_0^{2\pi} q(\lambda,t) e^{ik\lambda} d\lambda \ . \qquad (2)$$

The wavenumber-frequency Fourier coefficients are calculated by performing the Fourier transform of wavenumber Fourier coefficients, $Q_q(k,t)$,

$$Q(k,\pm n) = \frac{1}{2\pi}\int_0^{2\pi} Q_q(k,t)e^{\mp int}dt \qquad (3)$$

Tukey's numerical spectral analysis is applied after $Q_q(k,t)$ is obtained from (2). Let us express

$$Q(k,\pm n) = Q_r(k,\pm n) + i\, Q_i(k,\pm n) \quad ,$$

where Q_r and Q_i are the real and imaginary parts of Q respectively. The wavenumber-frequency spectrum can be calculated by

$$E_{pq}(k,\pm n) = 2[P_r(k,\pm n)Q_r(k,\pm n) + P_i(k,\pm n)Q_i(k,\pm n)] \quad , \qquad (4)$$

where $P(k,\pm n) = P_r(k,\pm n) + i\, P_i(k,\pm n)$ is the Fourier coefficient of a variable $p(\lambda,t)$. $E_{pq}(k,\pm n)$ is a power spectrum if $p(\lambda,t) = q(\lambda,t)$, while $E_{pq}(k,\pm n)$ is the cospectrum of p and q if $p(\lambda,t) \neq q(\lambda,t)$.

b. Latitudinal distributions of mean zonal velocity, kinetic energy of stationary and transient waves, and meridional transport of westerly momentum

The linear theory of wave motions shows that the behavior of waves critically depends upon the zonal mean state. In order to obtain some background of the zonal mean flow and wave motions of the GLAS model at 200 mb, the latitudinal distributions of zonal mean velocity, kinetic energy and meridional transport of westerly momentum of stationary (n=o) and transient waves ($n\neq 0$) waves at this level are shown in Fig. 1a. The observations extracted from various studies for the period from December to February are shown in Fig. 1b to verify the simulation of the GLAS model.

The zonal mean wind of this climate run is close to the January simulation of Somerville et al. (1974) and the observation, except the equatorial easterlies surprisingly disappear. In fact, the examination of 500 mb zonal mean wind in this climatological experiment does not show the disappearance of easterlies in the model tropics.

The model kinetic energies of the transient waves of zonal and meridional velocities, K_{tu} and K_{tv}, are very much larger than their counterparts of stationary waves, K_{su} and K_{sv}. The observational K_{su} peaks at the equator and at 35°N and has a larger value than the model's. It is obvious that the stationary waves are not well simulated in the model. The comparison of the kinetic energies of stationary and transient waves between the GLAS model and the observation at the 200 mb level shows that the smaller eddy kinetic energy of the model is mainly due to the zonal motion of stationary waves.

Both K_{tu} and K_{tv} have maximum values occurring at the same locations of the maximum zonal mean flow in the Southern and Northern Hemisphere (hereafter referred as SH and NH). The same situation occurs in the observation. The model maximum values of K_{tv} in the SH is much smaller than observational values. The observational kinetic energy of the transient waves is almost equally distributed in K_{tu} and K_{tv} in the NH (KL, 1977). This equal partition of K_{tu} and K_{tv} does show in the model to some extent. It should be also noted that the model K_{tu} and K_{tv} are larger than observational values in the tropics.

The latitudinal distribution of meridional transport of westerly momentum displayed in Fig. 1 shows clearly that the model transport is equatorward in the regions north of 40°N and south of 40°S, and is poleward in the global belt between 40°N and 40°S. The meridional transport of westerly momentum in the model is mainly contributed by the transient waves. The contribution from the

stationary waves is concerted constructively with the transient waves. The meridional transports of westerly momentum by stationary and transient waves in the observational study are about the same in the NH, while the later is dominant in the SH. The comparison of the westerly momentum transport between the GLAS model and the observational study shows that the transport is too strong by model transient waves and too weak by model stationary waves in the NH. In addition, the momentum transport by the model transient waves in the SH is slightly weaker than observational values.

The January (Somerville et al., 1974) and July (Stone et al., 1977) simulations of the GISS model have shown that the model total eddy transport of momentum is too weak. Although the maximum value of meridional transport of westerly momentum in this climatological experiment is comparative to KL's observational value, it may be inferred that the weak eddy transport of momentum in the January and July simulation of the GISS model is due to the small contribution of stationary waves shown in Fig. 1a.

It has long been well known that eddy kinetic energy is too small and eddy transport of momentum is too weak in the numerical general circulation models. Manabe et al. (1970) and Wellck et al. (1971) demonstrate that the increasing of the horizontal resolution of numerical general circulation can enhance the magnitude of eddy energies and energy conversions. This suggests that the increasing of horizontal resolution may well be one of the very likely ways to improve the simulation of stationary waves in the GLAS atmospheric circulation model. In fact, it has also long been realized that stationary waves are generally determined by the forcing of topography and stationary heat sources (e.g., Derome and Wiin-Nielsen, 1971). The sophisticated general circulation models usually have realistic orography, even though it is smoothed.

The increase of horizontal resolution, of course, can make the topography more realistic. The stationary heat sources must depend upon the treatment of diabatic heating. In other words, the refinement of model diabatic heating scheme could be another important factor to improve the simulation of stationary waves.

c. Wavenumber and frequency spectra of zonal and meridional kinetic energy

In order to shed light on the wave characteristic of the GLAS model in space, the wavenumber spectral analysis is made. The wavenumber kinetic energy spectra of zonal and meridional motions are displayed in Fig. 2.

The zonal kinetic energy spectra show that the eastward moving waves have larger energy than the westward moving waves. However, the energies of these two classes of waves become closer, especially in the high wavenumber regime, as the equator is approached. The contrast of zonal kinetic energies between the eastward and westward waves is consistent with KL's study. The close comparison between the GLAS model and KL's observational result shows that the eastward moving waves of the model's low wavenumber regime, which possesses most of the wave energy, have larger energy content than KL values. In contrast, the model's westward moving waves have less energy than the KL values. It is interesting to note that the zonal kinetic energy of both eastward and westward waves at the equator is larger than that of KL.

Both the observational and model kinetic energy of zonal motion in the SH shown in Section 2a are mainly due to the transient waves. Desbois (1975) also shows that the zonal kinetic energy spectrum at 45°S decreases monotonically as wavenumber increases. The eastward moving waves may have higher energy content. Since Desbois' finding does not appear in this energy spectra at 38°S shown in Fig. 2a, we could infer that the zonal kinetic energy of model eastward moving wave of low wavenumber regime may be smaller in the SH middle latitudes.

The zonal kinetic energy of the model stationary wave one becomes dominant at 18°N and 2°N. Krishnamurti (1971) and Krishnamurti et al. (1973) show that wave one, associated with the east-west circulation at 200 mb over the tropics, possesses the most significant part of wave energy and is quasi-stationary. This particular feature of wave one in the tropics is also confirmed recently by Chen (1980) and shown very clearly in KL's result. Compared with KL's result, the zonal kinetic energy of this wave in the equatorial area of the GLAS model is still too weak.

In the high wavenumber regime, Tenenbaum (1976) has shown that the overall NH kinetic energy spectrum of the GISS model has a slope of -2.6 between waves 8 and 15. Fig. 2a shows that the -3 power law is applicable in high and middle latitudes. However, the slope of the zonal kinetic energy spectrum in the high wavenumber regime becomes -2 as it approaches the equator.

Model meridional kinetic energy spectra at various latitudes are shown in Fig. 2b. The most striking difference of the spectral distribution of meridional kinetic energy from that of zonal kinetic energy is the former always shows a band of maximum values over the scales in which exist the maximum baroclinic instability (KL, 1977; Pratt, 1977, Desbois, 1975). The GLAS model, in general, reproduces fairly well the meridional kinetic energy spectra. However, careful inspection shows that the meridional kinetic energy in the low wavenumber regime is too small and too large over the band of maximum values. In other words, the long waves have less north-south motion, while the most baroclinically unstable waves have too strong north-south motion. The model westward moving waves have more meridional kinetic energy than the model eastward moving waves at the equator. The slope of meridional energy spectra in the high wavenumber regime is close to -3, but the slope becomes -2 near the equator. Furthermore, the comparison between the zonal and meridional kinetic

energy spectra shows that the energy content of eastward moving waves in the high wavenumber regime of meridional kinetic energy spectra is larger than those of zonal kinetic energy spectra, except at 2°N and 58°S.

In order to compare the time characteristics of model disturbances with the observational study of KL, the frequency spectra of zonal and meridional motion of the eastward and westward motion at 200 mb of the GLAS model are shown in Fig. 3. There is no pronounced difference between the frequency spectra of zonal and meridional motion as the wavenumber spectra of these two motions. The spectra of the eastward moving waves have larger energy content than the westward moving waves, except some low frequency components of zonal motion at 58°N and intermediate frequency disturbances of meridional motion at 2°N. The difference of frequency spectra between eastward and westward motions decreases as it approaches the equator. Furthermore, the spectra decrease as the frequency increases. These general features of frequency spectra ar. similar to KL's analysis. Notice that some differences exist between KL's and the model results. The model frequency spectra of eastward moving waves have a band of large values between 5-20 cycles (90 days)$^{-1}$ in the middle and high latitudes of the NH and 38°S. The most distinct feature is that the eastward moving waves peak at 7 cycles (90 days)$^{-1}$ which has a period of 12.9 days in the frequency spectra of zonal motion at 58°N, 38°N, 18°N, and meridional motion at 58°N, 38°N and 38°S. In fact, Hayashi and Golder (1977) also find a 12-day wave in the zonal and meridional motion at 190 mb of the GFDL model. They interpretate the 12-day disturbance as strong cyclones. Miller (1974) also shows a 14-15 day vacillation of atmospheric energy. In any event, this type of wave disturbance does not show in the KL observational analysis. Through careful comparison between the frequency spectra of KL and GLAS model, one finds that the low frequency (< 5 cycles/ 90 days) regime of the GLAS model has less

energy than KL's observational spectra. Pratt (1979) also finds that both the GFDL and NCAR models in middle and high latitudes have less wave activity than the atmosphere in the planetary-scale wave domain of 1-3 week period. The frequency spectra of the GLAS model in the high frequency regime obviously follow a power law as KL's analysis. The slope of the model frequency spectra varies from -2 to -3, with one -4 at 58°S for zonal motion. In other words, the frequency spectra of the GLAS model decrease faster with increasing frequency than the observation.

d. Wavenumber and frequency spectra of momentum transport

The general feature of the momentum transport in the wavenumber domain of the NH in the study of KL, and Hayasti and Golder (1975) is: (a) the equatorial transport at high latitudes by stationary and transient waves of low wavenumber regime; (b) the poleward transport in middle latitudes by the planetary-scale stationary waves and baroclinically unstable transient waves and (c) the southward transport at the equator by planetary-scale stationary waves. The SH in Desbois' (1975) study shows a somewhat different picture: (a) the poleward transport in the middle latitudes is attributed to the baroclinically unstable waves and (b) the equatorward transport at high latitudes is due to low-wavenumber waves.

The wavenumber cospectra of momentum transport of the GLAS model at 200 mb for various latitudes are shown in Fig. 4a. The momentum is transported equatorward at 58°N by wavenumber 4 and 5 of the stationary and eastward moving waves, while wavenumber 3 of the stationary wave transports momentum northward. The equatorward transport by wavenumber 2 of the stationary and eastward moving waves found by KL is not shown in the model. The poleward transport at 38°N is mainly accomplished by baroclinically unstable eastward moving waves and stationary wavenumber 3 and 5. Notice that the transport by baroclinic

unstable eastward moving waves is much larger than the atmosphere in KL's analysis. The pronounced transports of stationary wavenumbers 1 and 5 of the westward moving waves are missing in the model. The poleward transport at 18°N is weak and is attributed to stationary wave one and cyclone-scale eastward moving waves. The pronounced southward transport at the equator by stationary wavenumbers 2 and 4 of the KL analysis does not exist in the model, while the model stationary wavenumber 1 provides northward transport. Comparing the momentum transport in the SH of the GLAS model at 200 mb with Desbois' result, we can see that the maximum transport is attributed to the eastward moving wave 7 rather than wavenumber 5 as the observational study shows. In addition, the equatorward transport of momentum by the low wavenumber regime in Desbois' analysis disappears in the model. This transport is mainly contributed by the cyclone-scale eastward moving waves.

The frequency cospectra of momentum transport at high latitudes is mainly performed by eastward moving waves of low frequency. In middle latitudes, the momentum is mainly transported poleward by the eastward moving waves, especially those with a period of 5, 8, and 16 days, and by the westward moving waves of low frequency. The transport is not significant at the equator by the moving waves.

Except at the equator, the contribution to the model momentum transport by the westward moving waves is not significant over most frequencies. At 58°N, the equatorward transport is mainly executed by the eastward moving waves, especially with frequency 7 and 13 cycles (90 days)$^{-1}$, the eastward moving waves of low frequency transport the momentum poleward. In the middle latitudes and subtropics of the NH, the poleward transport of momentum is mainly carried out by the eastward moving waves with peak values at 7 and 11 cycles (90 days)$^{-1}$ at 38°N and 7 cycles (90 days)$^{-1}$ at 18°N. The southward transport at the equator

is more sigaificant than observed and performed by the westward moving waves of low frequency especially 1, 4 and 8 cycles (90 days)$^{-1}$. In the middle latitudes and subtropics of the SH, the poleward transport of momentum is mainly provided by the eastward moving waves with frequency less than 20 cycles (90 days)$^{-1}$. The momentum transport is not significant at 50°S.

In summary, the momentum transport by the stationary waves of low wavenumber and the westward moving waves of low frequency are not simulated well by the GLAS model.

e. Wavenumber-frequency spectra of zonal and meridional kinetic energy, and momentum transport

It was mentioned in the introduction that two methods were employed to make spectral analysis of atmospheric motions: the lag-correlation method and the direct Fourier transform method. Hayashi and Golder (1977) and Pratt (1977) use the former method, while Kao and his colleagues (Kao and Wendell, 1970; Wendell, 1969; Kao et al., 1970; Kao and Kuczek, 1973) use the latter method. The general finding of their wavenumber-frequency spectra of kinetic energy and momentum is the following. In the middle latitudes, the preferred spectral band is oriented from low wavenumber, low frequency of westward moving waves to high wavenumber and high frequency of eastward moving waves. The wave motion of the atmosphere in the dominant region of the spectral density is essentially of the Rossby type. In the tropics, the spectral band is oriented from low wavenumber and frequency to high wavenumber and low frequency.

Figs. 5-7 display the frequency-wavenumber spectra of zonal motion, meridional motion, and momentum transport at 200 mb and various latitudes of the GLAS model. The common features of these spectra is a preferred band of spectra that extends from a region of low wavenumber and low frequency of the westward moving waves to a region of high wavenumber and high frequency of

the eastward moving waves in the middle and high latitudes in both hemispheres. The preferred band of spectra in the tropics extends from the region of low wavenumber and frequency to a region of high wavenumber and low frequency. These common features of the GLAS model spectra are similar to Kao's.

The contrast of zonal spectra in both hemispheres shows that the Northern Hemisphere has higher wave activities. This is expected because the climate run of present analysis is the later winter and earlier spring. The maximum values of spectra at 38°N and 58°N occur at wavenumbers 3 and 4 with frequency of 7 cycles (90 days)$^{-1}$. Notice that wavenumbers 7 and 8 with frequency of 15 cycles (90 days)$^{-1}$ at 38°S has a significant power signal which does not appear in the Northern Hemisphere.

The meridional spectra show that the maximum spectral values are wavenumber 6 with frequency of 10 cycles (90 days)$^{-1}$ at 38°N and wavenumber 8 with frequency of 15 cycles (90 days)$^{-1}$ at 38°S. In addition, the westward moving waves at the equator have higher power than the eastward moving waves. This is also consistent with the analysis of Kao and Kuczek (loc cit).

The comparison between zonal and meridional spectra shows that the maximum spectral values of the former spectra appear in the lower wavenumber than that of the latter spectra. In addition the contrast between the spectra in both hemispheres shows that the maximum spectral values in the NH appear in the lower wavenumber, while they appear in the higher wavenumber in the SH. The same situation also applies to the spectra of momentum transport.

The spectra of momentum transport show significant northward transport at 38°N and significant southward transport at 38°S. The maximum values of spectra exists at wavenumber 4 with a frequency of 7 cycles (90 days)$^{-1}$ at 38°N and wavenumber 7 with a frequency of 15 cycles (90 days)$^{-1}$. The interhemispheric contrast of zonal and meridional spectra also applies to the spectra of momentum transport.

3. Maintenance of large-scale moving waves by nonlinear interactions

a. Formation and computations

The maintenance of the moving waves by the nonlinear interactions in the GLAS model will be analyzed in terms of the kinetic energy equations of zonal and meridional motions and the momentum flux equation. The derivation of these equations in the wavenumber-frequency domain can be found in Kao (1968). The classification of wavenumber-frequency domain in the practical computations follow KL. Therefore, a brief description of the formulation and computations here should be sufficient.

The kinetic energy equations of zonal and meridional motions and the momentum flux equation in the physical domain can be expressed as:

$$\underset{}{\frac{1}{2}\frac{\partial u^2}{\partial t}} = \underset{(u1)}{-\frac{u^2}{a\cos\phi}\frac{\partial u}{\partial \lambda}} \underset{(u2)}{-\frac{uv}{a}\frac{\partial u}{\partial \phi}} \underset{(u3)}{+\frac{\tan\phi}{a}u^2 v} \underset{(u4)}{+ fu(v-v_g)} \underset{(u5)}{+ uF_1}, \tag{5}$$

$$\underset{}{\frac{1}{2}\frac{\partial v^2}{\partial t}} = \underset{(v1)}{-\frac{uv}{a\cos\phi}\frac{\partial v}{\partial \lambda}} \underset{(v2)}{-\frac{v^2}{a}\frac{\partial v}{\partial \phi}} \underset{(v3)}{-\frac{\tan\phi}{a}u^2 v} \underset{(v4)}{- fv(u-u_g)} \underset{(v5)}{+ uF_2}, \tag{6}$$

$$\frac{\partial}{\partial t}(vu) = \underset{(vu1)}{-\frac{u}{a\cos\phi}\frac{\partial}{\partial t}(vu)} \underset{(vu2)}{-\frac{v}{a}\frac{\partial}{\partial \phi}(vu)} \underset{(vu3)}{-\frac{\tan\phi}{a}u(u^2-v^2)}$$

$$\underset{(vu4)}{- f[u(u-u_g) - v(v-v_g)]} \underset{(vu5)}{+ vF_1 + uF_2}. \tag{7}$$

The notations used are conventional. Let us use capital letters to designate the Fourier coefficients of atmospheric variables, equations (5)-(7) in the wavenumber-frequency domain can be written in the form (Kao, 1968):

$$|U(k,n)|^2_{(EUU)} = \frac{T}{2\pi}\Bigg\{U(-k,-n)\,\frac{i}{n}\sum_j\sum_m\underbrace{\left[\frac{i}{a\cos\phi}\,jU(j,m)U(k-j,n-m)\right]}_{(U1)}$$

$$-\,U(-k,-n)\,\frac{i}{na}\sum_j\sum_m\underbrace{[U_\phi(j,m)V(k-j,n-m)]}_{(U2)}$$

$$-U(-k,-n)\,i\,\frac{\tan\phi}{na}\sum_j\sum_m\underbrace{[U(j,m)V(k-j,n-m)]}_{(U3)}$$

$$-\underbrace{U(-k,-n)\,\frac{i}{n}\,f[V(k,n)-V_g(k,n)]}_{(U4)}-\underbrace{\frac{i}{n}\,U(-k,-n)G_1(k,n)}_{(U5)}\Bigg\}, \quad (8)$$

$$|V(k,n)|^2_{(EVV)} = \frac{T}{2\pi}\Bigg\{V(-k,-n)\,\frac{i}{n}\sum_j\sum_m\underbrace{\frac{i}{a\cos\phi}\,[jV(j,m)U(k-j,n-m)]}_{(V1)}$$

$$+V(-k,-n)\,\frac{i}{na}\sum_j\sum_m\underbrace{[V_\phi(j,m)V(k-j,n-m)]}_{(V2)}$$

$$+V(-k,-n)\,\frac{i\,\tan\phi}{na}\sum_j\sum_m\underbrace{[U(j,m)U(k-j,n-m)]}_{(V3)}$$

$$+\underbrace{V(-k,-n)\,\frac{i}{n}\,f[U(k,n)-U_g(k,n)]}_{(V4)}-\underbrace{\frac{i}{n}\,V(-k,-n)G_2(k,n)}_{(V5)}\Bigg\}, \quad (9)$$

$$E_{uv}(k,n) = \frac{T}{2\pi a}\left\{\frac{-1}{\cos\phi}\frac{1}{n}\sum_j\sum_m jU(k-j,n-m)[U(j,m)V(-k,-n) + V(j,m)U(-k,-n)]\right.$$

(VU1)

$$+\frac{i}{n}\sum_j\sum_m V(k-j,n-m)[U_\phi(j,m)V(-k,-n) + V_\phi(j,m)U(-k,-n)]$$

(VU2)

$$\left.+\frac{i}{n}\tan\phi\sum_j\sum_m U(j,m)[U(-k,-n)U(k-j,n-m) - V(-k,-n)V(k-j,n-m)]\right\}$$

(VU3)

$$+\frac{ifT}{2\pi n}\{U(-k,-n)[U(k,n) - U_g(k,n)] - V(-k,-n[V(k,n) - V_g(k,n)]\}$$

(VU4)

$$+\frac{T}{2\pi n}\ U(-k,-n)G_2(k,n) - V(-k,-n)G_1(k,n) \qquad (10)$$

(VU5)

The left-handed side of (8) to (10) is respectively kinetic energy of zonal and meridional velocity, and momentum flux of moving waves with wavenumber k and frequency n. For convenience of future discussion, particular notations are designated to every term on the right-hand side of these equations. ( )1 and ( )2 represent the longitudinal and latitudinal convergence of either energy or momentum flux respectively by nonlinear interactions. ( )3 is sphericity effect and ( )4 + ( )5 is a combination of the ageostrophic effect, friction and computational errors. This combining effect can be determined by the residual method.

Every nonlinear interaction term on the right-hand side of (8) to (10) has a double summation which involves wavenumber and frequency. Following Kao's analysis, the range of wavenumber and frequency in the computation of this study covers $-20 \leq j \leq 20$ and $-90 \leq m \leq 90$. Since a great number of possible interactions is involved in these computations, Kao's classification of the wavenumber-frequency space into some particular domains is also adopted for the purpose of analysis. Tables 1 and 2 show the classifications of wavenumber and frequency, respectively.

Notice that the classification shown in Tables 1 and 2 can provide 28 domains and 406 possible interactions. A combination of a wavenumber and frequency classification represent a domain, for example, (k_s, n_ℓ) designates the domain of long waves moving eastward with low frequency. The interactions are specified by placing the wavenumber-frequency domains side by side, e.g. $(k_s, n_m)(k_m, -n_\ell)$.

b. Maintenance of spectral energy of moving waves by nonlinear interactions

Wendell (1969) and sequential studies of Kao and collaborators have shown that the sum of the spectral energy of six wavenumber-frequency categories shown in Table 3 can explain most of the kinetic energy associated with moving waves. In order to examine how the spectral kinetic energy of model moving waves is maintained through the nonlinear interactions, only these six categories of moving waves will be analyzed using equations (8) and (9). The contributions of various interactions for various latitudes at 200 mb of the GLAS model are shown in Table 3.

It is of interest to point out that EUU and EVV of long waves shown in Table 3 possess more spectral energy in the Northern Hemisphere, while medium waves have more spectral energy in the Southern Hemisphere. The

longitudinal convergences of kinetic energy flux, U1 and V1, over the model globe supply kinetic energy to eastward moving waves, but extract kinetic energy from the westward moving waves. The function of U1 and V1 at the equator at 200 mb of the GLAS model is opposite to that of KL's observational analysis at 500 mb where U1 and V1 extract kinetic energy from eastward moving waves and supply to westward moving waves. The disappearance of the easterly flow in the model equatorial area shown in Section 2b may cause the reversal of longitudinal convergence of kinetic energy flux at 200 mb of the GLAS model. It is also of interest to point out that UI and VI of long waves are very significant in the NH, but those of medium waves are generally significant in the SH. This feature is consistent with the latitudinal distribution of EUU and EVV.

The latitudinal convergence of kinetic energy flux, U2 and V2, is generally smaller than U1 and V1, especially the contrast between V1 and V2. Furthermore, U2 and V2 are not exactly of opposite sign to U1 and V1 as KL found at the 500 mb analysis. In fact, the signs of U2 and V2 are randomly distributed to some extent. The sphericity effect, U3 and V3, is generally very small and is essentially zero near the equator.

The residual term, (U4 + U5) and (V4 + V5), which is a combination of the ageostrophic effect, friction, and computational error, is the same order of magnitude as U1 and V1. However, (U4 + U5) and (V4 + V5) have the opposite function to maintain the spectral energy of moving waves as compared with U1 and V1. In other words, (U4 + U5) and (V4 + V5) supply kinetic energy to westward moving waves and extract kinetic energy from eastward moving waves

over the whole model globe, except for the eastward moving waves with medium frequency at some latitudes. Notice that the function of (U4 + U5) and (V4 + V5) is also opposite to KL's finding at the equator where KL found that (U4 + U5) and (V4 + V5) supply kinetic energy to both eastward and westward moving waves.

Based upon their analysis for the linear and nonlinear interactions in spectral kinetic energy equations, KL proposed a scheme for the maintenance of spectral energy of moving waves in the westerly regime of the middle latitudes, shown in Fig. 8, and in the easterly regime of the tropics. Although U2 and V2 of the GLAS model at 200 mb do not show such a regularity as KL found in their analysis, KL's scheme for the maintenance of spectral energy of moving waves in the westerly regime is in general applicable to the moving waves of the GLAS model at 200 mb.

It is also of interest to point out that our further examination on the contributions of various interactions to the spectral energy of moving waves reveals that the primary nonlinear interactions (not shown) is due to those involving the mean zonal flow with the long and medium waves of low and intermediate frequency. Our analysis in Section 2b shows that the model stationary waves are weak. KL found that the stationary waves play an important role in the nonlinear interactions. However, the present study shows that the role played by the model stationary waves is not vital.

c. Maintenance of spectral momentum transport flux of moving waves by nonlinear interactions

Equation (9) is used to examine how the spectral momentum transport flux of moving waves is maintained through nonlinear interactions for various wavenumber-frequency domains and various latitudes. The resultant values of

various interactions for the six wavenumber-frequency categories described in Section 3b are displayed in Table 8.

The spectral flux of momentum in various wavenumber-frequency domains shown in Table 8 directs toward north at 38°N, 18°N and 58°S, but toward south at 58°N, 2°N, 18°S and 38°S. The exception occurs to the low-frequency westward moving waves of long wavelength at 38°N where these waves present the southward transport of momentum flux.

The longitudinal convergence of momentum transport, VU1, is still generally the dominant process, and its function on the momentum transport is more complicated than its counterpart of the zonal and meridional kinetic energy discussed in Section 3b. At 38°N (midlatitude) and 18°N (subtropics) VU1 provides the northward transport of momentum to the eastward moving waves, but extract it from the westward moving waves. However, the reversed process occurs at 38°S and 18°S, except (k_s, $+n_\varphi$) at 38°S and (k_s, $+n_\varphi$) at 18°S. At the equator, VU1 is generally small, but provides northward transport of momentum to both the westward and eastward moving waves. At high latitudes of the SH (58°S), VU1 behaves in a similar way as its counterpart at the equator. However, VU1 at 58°N acts randomly as far as the direction of momentum transport is concerned.

The contribution of latitudinal convergence of momentum transport, VU2, is generally smaller than VU1, and is random. In some wavenumber-frequency categories at high latitudes (58°N) and low latitudes (2°N and 18°N), VU2 becomes more significant than VU1. The effect of sphericity, VU3, is generally small and almost zero at 2°N. The residual term which involves the combination of the ageostrophic effect, frictional and computational errors, has the comparative magnitude with respect to VU1 and has an opposite sign except the wave categories belong to intermediate frequency domain.

Following their scheme for maintaining the spectral energy of the moving waves by nonlinear interactions, ageostrophic effect, and friction, KL propose a similar scheme to show how the spectral momentum flux of the moving wave is maintained by various processes. In KL's scheme at 40°N, VU1 + VU3 supply northward spectral momentum flux to the eastward moving waves, while VU2 + (VU4 + VU5) extract northward spectral momentum flux from eastward moving waves. As for the westward moving waves, the functions of VU1 + VU3 and VU2 + (VU4 + VU5) are reversed. At the equator, VU1 + VU2 extract northward spectral momentum flux from both the eastward and westward moving waves, while (VU4 + VU5) supply northward spectral momentum transport to both the eastward and westward moving waves. The comparison between Table 8 and KL's result shows that KL's scheme may not be applied to the GLAS model completely, especially at the equator where the easterlies do not show in the GLAS model. At 38°N and 18°N of the GLAS model, we move VU3 to the group VU2 + (VU4 + VU5) and obtain the top diagram in Fig. 8. That is, VU1 supplies northward spectral momentum flux to the eastward moving waves, while VU2 + VU3 + (VU4 + VU5) extract northward spectral momentum flux from the eastward moving waves. The effect of VU1 and VU2 + VU3 + (VU4 + VU5) on the westward moving waves are opposite to that on the eastward moving waves. This scheme is reversed at 38°S and 18°S. It is because the eddy transport of westerly momentum is south-poleward. At the equator of the GLAS model, VU2 generally is larger than VU1 and is not so regular in sign. This does not show in KL's observational analysis. In order to compare with KL's study, we also modify KL's scheme at the equator by moving VU2 to (VU4 + VU5). The maintenance of spectral momentum flux at the equator of the GLAS model is opposite to KL's scheme in sign. In other words, VU1 supplies northward spectral momentum

transport to both eastward and westward moving waves, while VU2 + (VU4 + VU5) extract northward spectral momentum transport from both eastward and westward moving waves.

It should be also pointed out that the detailed analysis of the contributions from various interactions to the spectral momentum transport (not shown) are those between the mean zonal flow and the long and medium waves with low and intermediate frequency. Again, the stationary waves do not play any significant role in nonlinear interactions.

4. Summary

The space-time Fourier spectral analysis and the equations of kinetic energy and momentum transport in the wavenumber-frequency domain proposed by Kao (1968) and modified by Kao and Lee (1977) using Tukey's numerical spectral analysis are employed to analyze the 200-mb wind fields of a 4-month climate experiment of the GLAS atmospheric circulation model. This climate run covers the period from January 1 to April 30, 1975. This study analyzes a 90-day (January 15-April 14, 1975) wind field of this climate run. Comparison between the present study and observation, mainly Kao and Lee's study, leads to the following conclusions.

1. The 200-mb latitudinal distributions of model mean zonal wind, zonal and meridional kinetic energy and momentum transport of eddies agree fairly well with observations. However, some difficiencies of this climate run are revealed: equatorial easterlies disappear, and zonal kinetic energy and momentum transport of stationary waves are too small in the model Northern Hemisphere (NH).
2. The general features of wavenumber spectra of the model zonal and meridional kinetic energy for moving waves are consistent with observation. The model zonal kinetic energy in wavenumber one of stationary

wave is too small in the NH subtropics and equator. Furthermore, the zonal kinetic energy of the model eastward moving waves in low wavenumber regime is larger in NH and smaller in SH than observation. The meridional kinetic energy spectra of both hemispheres have smaller values in low wavenumber regime and larger values in intermediate wavenumber regime than observation.

3. The frequency spectra of zonal and meridional kinetic energy of eastward moving waves show a band [5 $\sim$ 20 cycles (90 days)$^{-1}$] of large values in middle and high latitudes and peaks at 7 cycles (90 days)$^{-1}$ $\sim$ 12.9 days. In addition, the frequency spectra have a slope of -2 $\sim$ -3 in a high frequency regime, rather than -1 as Kao finds.

4. The model momentum transport in the wavenumber domain is mainly performed by the eastward moving and stationary waves of intermediate wavenumber in middle and high latitudes of the NH and only by the eastward moving waves of intermediate wavenumbers in middle and high latitudes of the SH. The southward momentum transport at the equator is due to the eastward moving waves of intermediate wavenumber. The momentum transport by the stationary waves of low wavenumber is too weak in the model. In the frequency domain, the momentum transport is principaly carried by the eastward moving waves of 5 $\sim$ 20 cycles (90 days)$^{-1}$ in both hemispheres, and 1 $\sim$ 20 cycles (90 days) at 2°N. The momentum transport by the low-frequency waves is not significant in the model as found in observation.

5. The model wavenumber-frequency spectra of zonal and meridional motion and momentum transport have a preferred band which is oriented from low wavenumber and low frequency of the westward moving waves to high wavenumber and high frequency of eastward moving waves in middle and high latitudes.

The preferred band of spectra in the tropics extends from low wavenumber and low frequency to high wavenumber and low frequency. Furthermore, maximum spectral value of zonal motion appears in lower wavenumber than that of meridional motion. These features of model wavenumber-frequency spectra are consistent with the spectral studies of Kao, Hayashi and Pratt. Another interesting feature of model spectra is that the maximum spectral value in NH occurs in lower wavenumber than in SH.

6. The mean westerlies exist over the whole model globe at 200 mb in this climate experiment. The nonlinear interactions by the longitudinal convergence of kinetic energy flux (U1 and V1) and a combination of ageostrophic effect and dissipation (U4 + U5) and (V4 + V5) are dominant and comparable. U1 and V1 provides kinetic energy to the eastward moving waves, but extract kinetic energy from the westward moving waves. (U4 + U5) and (V4 + V5) function oppositely as U1 and V1 do. The primary interactions of kinetic energy in wavenumber-frequency domain are largely through the interactions between mean zonal flow and the long and medium waves of low and medium frequencies. The significant role played by the stationary waves shown in Kao and Lee's does not appear in the model.

7. The maintenance of momentum transport spectra by linear and non-linear processes in the NH is similar to that of kinetic energy spectra. However, the functions of longitudinal convergence of momentum transport flux (VU1) and a combination of ageostrophic effect and dissipation (VU4 + VU5) in SH is opposite to those in NH. At the equator, VU1 supplies meridional flux of westerly momentum to both the eastward and westward

moving waves, but VU4 + VU5 extracts from both moving waves. This scheme is opposite to Kao and Lee's in direction. The primary interactions of meridional flux of westerly momentum is similar to those of kinetic energy.

Acknowledgments

Suggestions and discussions provided by Drs. S.-K. Kao, J.J. Tribbia and David M. Straus were most helpful for the present study. We thank Dr. Milgon Halem for his interest in this study. The constructive comments given by one of the anonymous reviewers are very helpful to clarify the presentation of this paper. The history tape of the GLAS atmospheric circulation model was prepared by Mr. William Byerly. This study is supported by the NASA grant NSG-5339.

References

Arakawa, A., 1966: Computational design of long term numerical integration of the equations of fluid motion: Two dimensional incompressible flow. Part I. J. Comput. Phys. 1:119-143.

Chen, T.-C., 1980: On the energy exchange between the divergent and rotational components of atmospheric flow over the tropics and subtropics at 200 mb during two northern summers. Mon. Wea. Rev. 108:896-912.

Derome, J. and A. Wiin-Nielsen, 1971: The response of a middle-latitude model atmosphere to forcing by topography and stationary heat source. Mon. Wea. Rev. 99:654-676.

Desbois, M., 1975: Large-scale kinetic energy spectra from Eulerian analysis of EØLE wind data. J. Atmos. Sci. 32:1838-1847.

Hayashi, Y., 1971: A generalized method of resolving disturbances into progressive and retrogressive waves by space Fourier and time cross-spectral analysis. J. Met. Soc. Japan 49:125-128.

_____, 1974: Spectral analysis of tropical disturbances appearing in a GFDL general circulation model. J. Atmos. Sci. 31:180-218.

_____ and D.G. Golder, 1977: Space-time spectral analysis of mid-latitude disturbances appearing in a GFDL general circulation model. J. Atmos. Sci. 34:237-262.

Kalnay-Rivas, E., A. Bayliss, and J. Storeh, 1977: The 4th order GISS model of the global atmosphere. Cont. Atmos. Phys. 50:299-311.

Kao, S.-K., 1968: Large-scale atmospheric motion and transports in frequency wavenumber space. J. Atmos. Sci. 25:32-38.

_____ and L.L. Wendell, 1970: The kinetic energy of the large-scale atmospheric motion in wavenumber-frequency space: I. Northern Hemisphere. J. Atmos. Sci. 27:359-375.

_____, C.Y. Tsay, and L.L. Wendell, 1970: The meridional transport of angular momentum in wavenumber-frequency space: J. Atmos. Sci. 27:614-626.

_____ and R.J. Kuczek, 1973: The kinetic energy of large-scale atmospheric motion in wavenumber-frequency space: III. The tropics. J. Atmos. Sci. 30:308-312.

_____ and H.N. Lee, 1977: The nonlinear interactions and maintenance of the large-scale moving waves in the atmosphere. J. Atmos. Sci. 34:471-485.

Krishnamurti, T.N., 1971: Tropical east-west circulations during the northern summer. J. Atmos. Sci. 28:1342-1347.

_____, M. Kanamitsn, W. J. Koss, and J.D. Lee, 1973: Tropical east-west circulations during the northern winter. J. Atmos. Sci. 30:780-787.

Manabe, S., J. Smagorinsky, J.L. Holloway, Jr. and H.M. Stone, 1970: Simulated climatology of a general circulation model with a hydrologic cycle. III. Effects of increased horizontal computational resolution. Mon. Wea. Rev. 98:175-212

Miller, A.J., 1974: Periodic variation of atmospheric circulation at 14-16 days. J. Atmos. Sci. 31:720-726.

Morel, P., and M. Desbois, 1974: Mean 200-mb circulation in the Southern Hemisphere deduced from EØLE balloon flights. J. Atmos. Sci. 31:394-407.

Pratt, R.W., 1976: The interpretation of space-time spectral quantities. J. Atmos. Sci. 33:1060-1066.

_____, 1977: Space-time kinetic energy spectral in mid-latitude. J. Atmos. Sci. 34:1054-1057.

_____, 1979: A space-time spectral comparison of the NCAR and GFDL general circulation models to the atmosphere. J. Atmos. Sci. 36:1681-1691.

Somerville, R.C.J., P.H. Stone, M. Halem, J.E. Hansen, J.S. Hogan, L.M. Druyan, G. Russell, A.A. Lacis, W.J. Quirk and J. Tenenbaum, 1974: The GISS model of the global atmosphere. J. Atmos. Sci. 31:84-117.

Stone, P.H., S. Chow, and W.J. Quirr, 1977: The July climate and a comparison of the July and January climates simulated by the GISS general circulation model. Mon. Wea. Rev. 105:170-194.

Tenenbaum, J., 1976: Spectral and spatial energetics of the GISS model atmosphere. Mon. Wea. Rev. 104:15-30.

Tsay, C.Y., 1974a: A note on the methods of analyzing travelling waves. Tellus 26:412-415.

_____, 1974b: Analysis of large-scale wave disturbances in the tropics simulated by an NCAR global circulation model. J. Atmos. Sci. 31:330-339.

Tukey, J.W., 1967: Spectrum calculations in the new world of the fast Fourier transform. Advanced Seminar on Spectral Analysis of Time Series, B.

Webster, P.J., and D.G. Curtin, 1974: Interpretations of the EØLE experiment. 1. Temporal variation of Eulerian quantities. J. Atmos. Sci. 31:1860-1875.

Wellck, R., A. Kasahara, W. Washington and G. de Santo, 1971: Effect of horizontal resolution in a finite-difference model of the general circulation. Mon. Wea. Rev. 99:673-683.

Wendell, L.L., 1969: A study of the large-scale atmospheric trubulent kinetic energy in wavenumber-frequency space. Tellus 21:760-788.

Figure Captions

Fig. 1. Latitudinal distribution of zonal mean velocity, kinetic energy of zonal and meridional velocities of stationary and transient waves, meridional transport of westerly momentum at 200 mb. (a) GLAS model and (b) observation from various sources. The observations north of 20°S come from KL, while south of 15°S are from EØLE study in which zonal mean velocity and kinetic energy are drawn from Morel and Desbois (1974), and momentum transport from Webster and Curtain (1974). The solid line denotes transient waves, while the dashed line represents stationary waves.

Fig. 2. Wavenumber spectra of (a) zonal and (b) meridional kinetic energy of the GLAS model at 200 mb and various latitudes.

Fig. 3. Same as Fig. 2, except for frequency spectra.

Fig. 4. (a) Wavenumber co-spectra of momentum transport associated with stationary and moving waves of the GLAS model at 200 mb and various latitudes. (b) Same as (a) except for frequency co-spectra.

Fig. 5. Wavenumber-frequency spectra of zonal motion at 200 mb of the GLAS model.

Fig. 6. Wavenumber-frequency spectra of meridional motion at 200 mb of the GLAS model.

Fig. 7. Wavenumber-frequency co-spectra of momentum transport at 200 mb of the GLAS model.

Fig. 8. Schematic diagram for maintenance of spectral energy of moving waves at 200 mb of the GLAS model.

Fig. 9. Schematic diagram for maintenance of spectral momentum transport flux of moving waves at 200 mb of the GLAS model.

Table 1. Wavenumber Classification

Wavenumber k	Classification	Symbol
0	zonally averaged flow	0
1-5	long waves (small wavenumber)	k_s
6-9	medium waves	k_m
10-20	short waves (large wavenumber)	k_ℓ

Table 2. Frequency Classification

Frequency n (cycles per 90 days)	Period (days)	Classification (frequency)	Direction of wave motion	Symbol
-90 to -31	1-3	high	west to east	$+n_h$
-30 to -11	3-9	medium	west to east	$+n_m$
-10 to -1	9-90	low	west to east	$+n_\ell$
0		zero	stationary	0
1 to 10	9-90	low	east to west	$-n_\ell$
11 to 30	3-9	medium	east to west	$-n_m$
31 to 90	1-3	high	east to west	$-n_h$

Table 3. Linear and nonlinear contributions to energy spectra in various wavenumber-frequency domains at various latitudes at 200 mb.

		FUU =	U1 +	U2 +	U3 +	(U4+U5)	EVV =	V1 +	V2 +	V3 +	(V4+V5)
	58°N	15.25 =	104.67	+ 15.50	- 3.11	- 101.81	28.55 =	143.96	- 4.28	- 16.50	- 94.03
	38°N	45.85 =	345.70	- 61.87	- 9.09	- 228.98	8.60 =	201.85	+ 4.18	- 8.60	- 188.83
	18°N	18.25 =	40.99	+ 10.64	+ 0.20	- 33.58	4.29 =	15.86	- 0.20	+ 3.13	+ 14.00
$(k_g, +n_\ell)$	2°N	11.67 =	5.79	+ 14.35	+ 0.01	- 8.47	0.90 =	1.07	+ 0.43	+ 0.01	+ 0.61
	18°S	20.36 =	46.14	+ 90.72	+ 0.19	- 116.69	2.91 =	12.22	- 1.38	+ 0.71	- 8.64
	38°S	37.97 =	243.63	+ 40.24	+ 1.72	- 247.05	5.36 =	132.73	+ 6.66	+ 3.09	- 133.12
	58°S	18.59 =	90.82	+ 20.54	- 3.58	- 89.18	5.28 =	32.19	- 3.95	- 7.88	- 15.08
	58°N	16.53 =	-68.76	+ 1.26	+ 2.26	+ 81.77	5.32 =	-49.06	+ 9.66	+ 3.04	+ 41.68
	38°N	11.20 =	-113.16	- 2.86	+ 8.29	+ 118.43	9.19 =	-257.42	+ 6.48	+ 14.80	+ 245.33
	18°N	9.14 =	-20.82	+ 12.15	- 0.35	+ 18.17	1.67 =	-13.00	+ 0.51	- 1.40	+ 15.56
$(k_g, -n_\ell)$	2°N	7.62 =	-25.47	+ 0.88	+ 0.01	+ 32.20	1.75 =	-1.42	- 0.02	+ 0.03	+ 3.16
	18°S	8.44 =	-12.00	- 15.79	- 0.27	+ 36.30	3.08 =	-1.98	+ 0.13	+ 0.03	+ 5.02
	38°S	7.75 =	-60.11	- 37.90	+ 2.57	+ 103.19	2.64 =	-52.73	+ 2.83	+ 3.67	+ 48.87
	58°S	8.57 =	-20.85	- 3.14	- 1.68	+ 34.24	7.95 =	-8.80	+ 0.59	- 5.55	+ 21.71
	58°N	13.66 =	25.94	+ 2.00	- 2.79	- 11.49	12.66 =	32.51	+ 1.10	- 4.93	- 16.02
	38°N	21.18 =	48.64	+ 6.48	- 1.26	- 32.68	6.72 =	18.02	+ 0.11	- 2.02	- 9.39
	18°N	11.00 =	6.97	- 4.04	- 0.03	+ 8.04	1.40 =	0.95	+ 0.05	+ 0.13	+ 0.27
$(k_g, +n_m)$	2°N	4.48 =	1.02	- 1.87	- 0.00	+ 5.33	1.05 =	0.02	- 0.02	+ 0.00	+ 1.50
	18°S	8.31 =	3.57	+ 1.65	- 0.03	+ 3.11	0.75 =	0.30	+ 0.06	+ 0.08	+ 0.31
	38°S	12.28 =	24.71	- 1.48	+ 0.08	- 11.03	2.74 =	5.66	- 0.29	+ 0.14	- 2.77
	58°S	9.02 =	6.04	+ 1.41	+ 0.01	+ 1.56	1.43 =	2.67	+ 0.26	- 0.53	- 0.97
	58°N	2.50 =	29.10	- 2.10	- 0.45	- 24.05	5.52 =	38.30	- 1.11	- 2.56	- 29.11
	38°N	4.24 =	61.98	- 12.76	- 5.83	- 39.16	11.20 =	132.92	- 1.14	- 12.13	- 106.45
	18°N	4.81 =	19.08	+ 9.83	+ 0.14	- 24.24	4.23 =	31.00	+ 0.58	+ 0.30	- 27.65
$(k_m, +n_\ell)$	2°N	4.49 =	5.53	+ 1.84	- 0.00	- 2.88	1.06 =	2.36	- 0.43	- 0.01	- 0.88
	18°S	6.36 =	31.79	- 9.91	- 0.41	- 15.11	6.53 =	83.40	+ 3.67	- 0.57	- 49.97
	38°S	4.97 =	67.95	+ 14.27	- 7.91	- 69.34	25.52 =	182.32	+ 7.73	- 15.89	- 148.64
	58°S	3.13 =	20.00	- 1.06	- 1.05	- 14.76	4.67 =	19.71	- 0.16	- 2.46	- 12.42
	58°N	0.64 =	-8.71	- 4.91	- 0.43	+ 14.69	1.38 =	-13.45	+ 0.35	- 0.41	+ 14.89
	38°N	1.02 =	-39.01	- 5.03	+ 2.61	+ 39.20	0.87 =	-45.67	+ 3.28	+ 4.85	+ 38.41
	18°N	2.83 =	-9.25	+ 10.47	- 0.14	+ 1.75	0.97 =	-28.69	- 2.71	- 0.42	+ 32.78
$(k_m, -n_\ell)$	2°N	3.00 =	-3.55	+ 2.59	+ 0.00	+ 3.96	1.92 =	-2.12	- 0.69	- 0.02	+ 4.75
	18°S	3.48 =	-12.96	+ 8.80	+ 0.63	+ 7.01	3.92 =	-21.17	- 2.24	+ 1.12	+ 26.21
	38°S	13.89 =	-27.90	+ 9.65	+ 2.33	+ 29.81	0.74 =	-33.65	+ 3.22	+ 4.43	+ 26.94
	58°S	1.57 =	-5.82	+ 2.12	+ 0.07	+ 5.20	0.88 =	8.30	+ 0.53	+ 0.79	+ 7.86
	58°N	5.33 =	17.79	- 1.04	- 1.33	- 12.75	15.42 =	39.20	+ 0.88	- 2.90	- 21.76
	38°N	8.56 =	41.13	- 0.48	- 2.84	- 29.25	18.02 =	121.53	- 0.12	- 6.43	- 96.96
	18°N	6.25 =	7.90	- 3.10	+ 0.10	+ 1.35	5.14 =	5.86	- 0.00	+ 0.09	- 0.81
$(k_m, +n_m)$	2°N	2.39 =	1.22	- 0.11	- 0.00	+ 1.28	1.15 =	0.87	- 0.02	- 0.00	+ 0.30
	18°S	9.28 =	6.98	+ 0.13	+ 0.09	+ 2.08	7.10 =	6.76	+ 0.30	+ 0.15	- 0.11
	38°S	12.91 =	61.08	+ 3.25	- 5.85	- 45.57	64.70 =	192.48	- 0.35	- 11.04	- 116.39
	58°S	7.63 =	16.01	- 0.49	- 0.91	- 6.98	3.43 =	8.92	- 0.11	- 1.63	+ 1.74

Table 4. Linear and nonlinear contributions to northward momentum transport spectra in various wavenumber-frequency domains at various latitudes at 200 mb.

		EVU	=	VU1	+	VU2	+	VU3	+	(VU4 + VU5)
	58°N	-1.99	=	30.55	+	65.08	-	2.53	-	94.76
	38°N	19.25	=	184.04	-	2.35	-	1.67	-	110.77
	18°N	8.19	=	30.25	-	2.67	-	0.82	-	18.57
$(k_s, +n_\ell)$	2°N	-1.54	=	3.81	+	6.42	+	0.04	-	11.81
	18°S	-3.24	=	-9.09	+	12.22	+	2.11	-	8.98
	38°S	-10.75	=	-100.28	-	16.21	+	0.47	+	105.27
	58°S	6.55	=	51.90	-	0.05	+	3.61	-	48.91
	58°N	-1.32	=	-24.89	-	16.84	+	1.62	+	38.79
	38°N	-0.71	=	80.48	-	7.15	+	12.12	-	86.16
	18°N	1.60	=	-9.50	-	8.95	-	0.92	+	20.97
$(k_s, -n_\ell)$	2°N	-1.67	=	2.32	+	8.73	-	0.00	-	12.72
	18°S	-0.76	=	2.24	-	27.55	-	0.23	+	24.78
	38°S	-0.01	=	-13.08	-	8.11	+	2.31	+	18.87
	58°S	1.19	=	2.05	+	11.61	-	0.34	-	12.13
	58°N	-6.99	=	-15.07	+	4.11	-	2.58	+	6.55
	38°N	27.51	=	27.16	+	0.26	-	1.44	+	1.53
	18°N	7.37	=	0.34	+	1.03	+	0.02	+	5.92
$(k_s, +n_m)$	2°N	-1.64	=	0.14	-	0.58	+	0.00	-	1.20
	18°S	-4.13	=	-0.86	+	0.19	+	0.01	-	3.47
	38°S	-15.20	=	-13.52	-	0.02	+	0.31	-	1.97
	58°S	7.65	=	0.96	+	1.09	-	0.18	+	5.78
	58°N	-7.34	=	1.85	+	9.44	-	0.08	-	18.55
	38°N	29.10	=	30.81	+	16.11	-	6.27	-	11.55
	18°N	10.27	=	17.35	+	1.77	+	0.36	-	9.21
$(k_m, +n_\ell)$	2°N	-2.03	=	-1.49	-	1.25	-	0.01	+	0.72
	18°S	-6.10	=	-7.92	+	6.36	-	0.09	+	4.45
	38°S	-18.40	=	-29.20	+	3.58	-	7.69	+	15.41
	58°S	10.89	=	16.44	-	4.02	-	0.48	-	1.05
	58°N	-7.47	=	7.95	+	6.15	-	0.75	-	20.82
	38°N	29.48	=	-33.61	+	29.48	+	1.84	+	31.77
	18°N	11.42	=	-7.70	+	16.27	+	0.09	+	2.76
$(k_m, -n_\ell)$	2°N	-2.79	=	1.44	-	2.14	+	0.00	-	2.09
	18°S	-6.04	=	-9.22	-	9.88	+	0.11	+	12.95
	38°S	-18.56	=	5.79	+	15.58	+	2.61	-	42.54
	58°S	12.22	=	-4.61	+	0.45	-	0.12	+	16.50
	58°N	-11.33	=	-9.06	+	1.26	-	1.22	-	2.31
	38°N	37.89	=	37.86	-	2.53	-	2.78	+	5.34
	18°N	12.10	=	0.26	+	0.99	+	0.27	+	10.58
$(k_m, +n_m)$	2°N	-2.77	=	0.15	+	0.57	-	0.00	-	3.03
	18°S	-8.12	=	-2.26	-	2.97	+	0.15	-	3.04
	38°S	-27.52	=	-32.02	+	9.39	-	5.25	+	0.36
	58°S	14.30	=	5.65	+	0.28	-	0.90	+	9.27

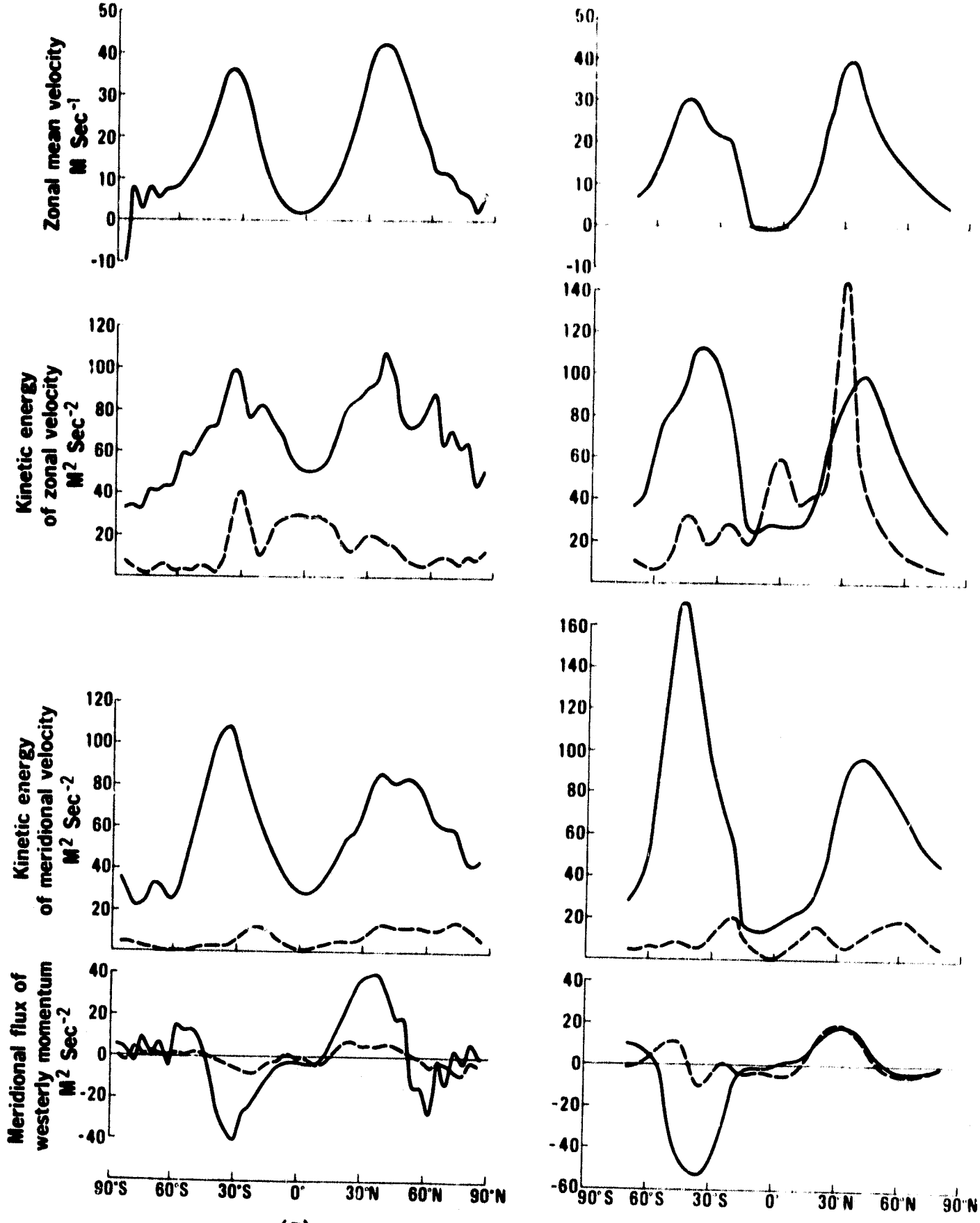
Zonal mean velocity
M Sec-1
50
40
30
20
10
0
-10
Kinetic energy
of zonal velocity
M2 Sec-2
120
100
80
60
40
20
Kinetic energy
of meridional velocity
M2 Sec-2
120
100
80
60
40
20
Meridional flux of
westerly momentum
M2 Sec-2
40
20
0
-20
-40
90°S
60°S
30°S
0°
30°N
60°N
90°N
(a)
50
40
30
20
10
0
-10
140
120
100
80
60
40
20
160
140
120
100
80
60
40
20
40
20
0
-20
-40
-60
90°S
60°S
30°S
0°
30°N
60°N
90°N
(b)

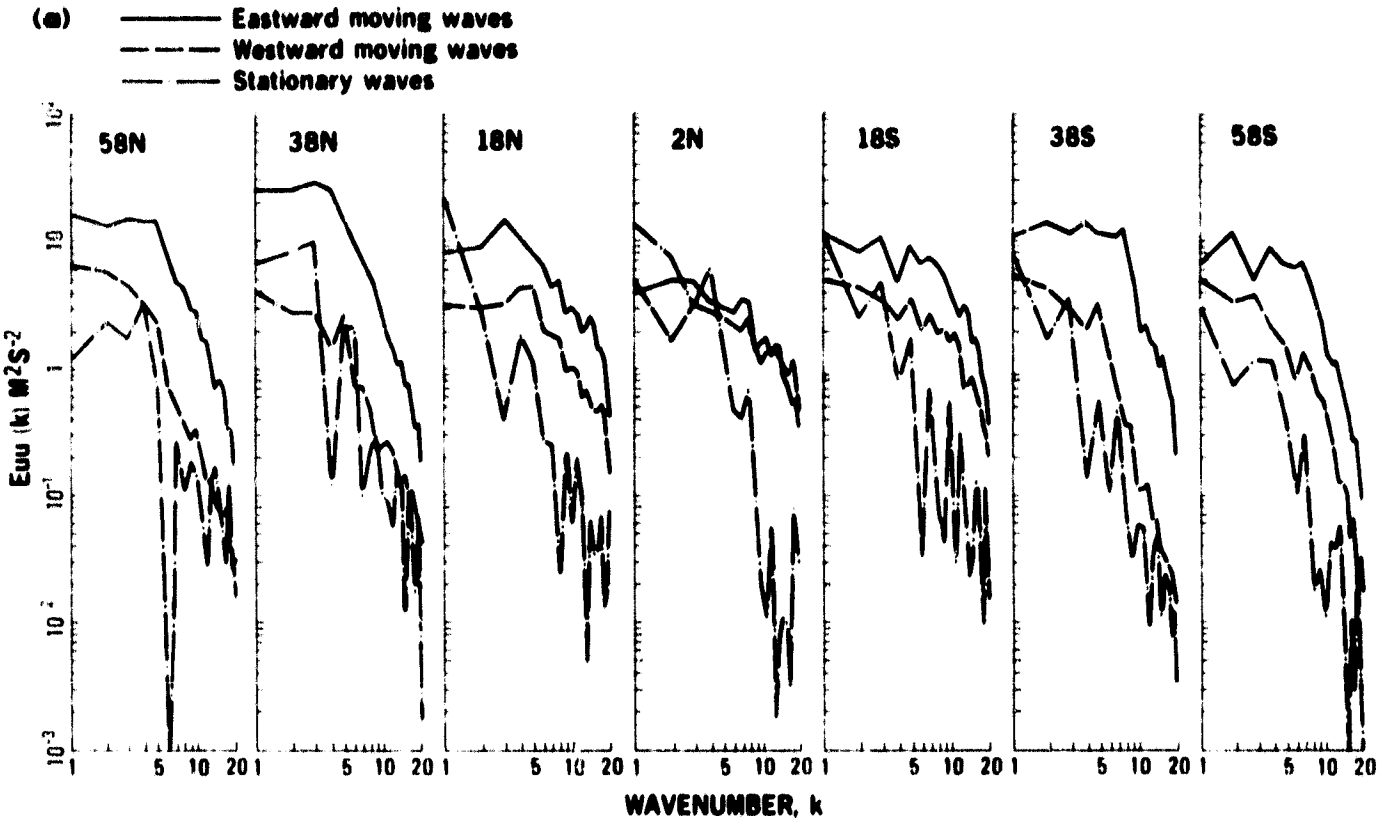
(a)
Eastward moving waves
Westward moving waves
Stationary waves
58N
38N
18N
2N
18S
38S
58S
Euu (k) M²S⁻²
WAVENUMBER, k

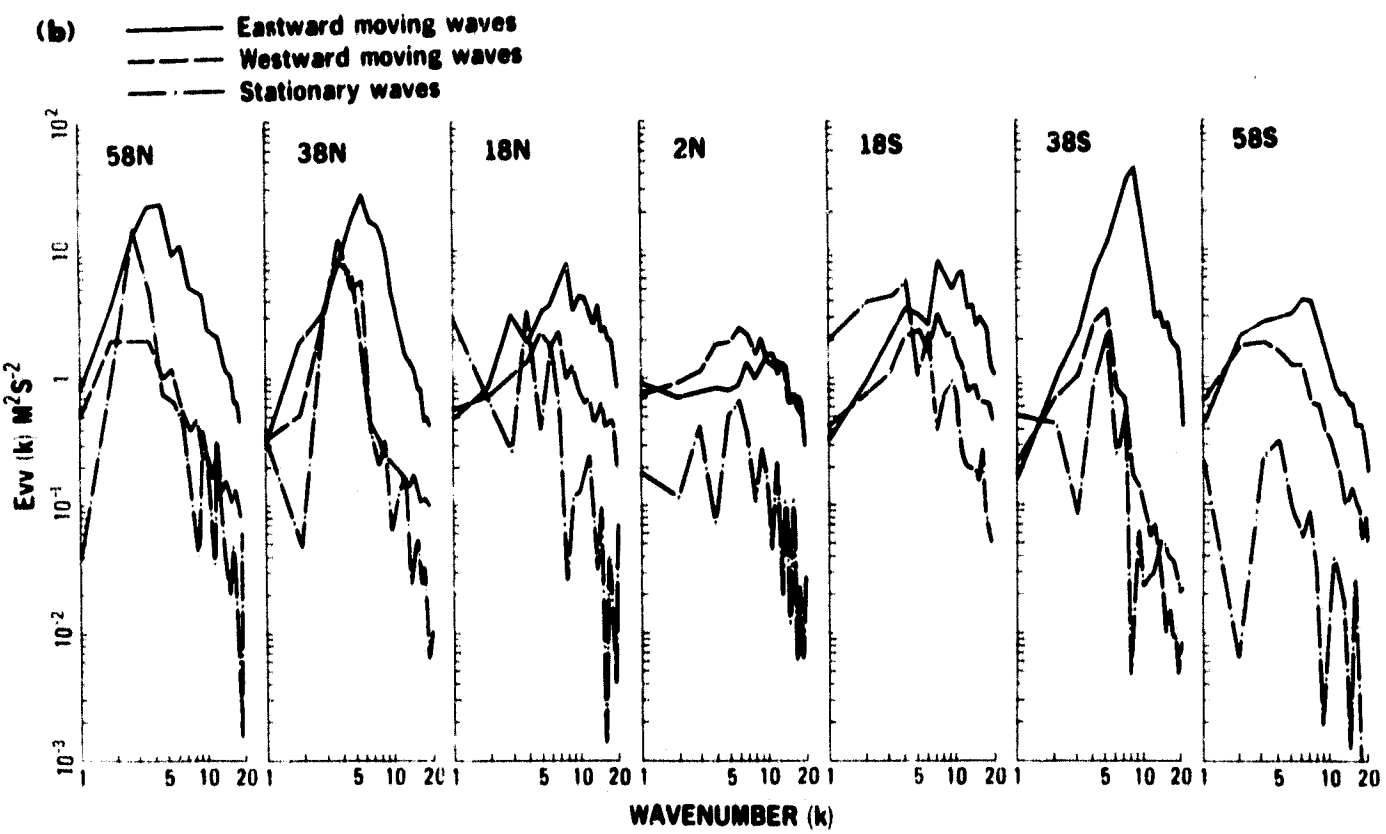
(b)
Eastward moving waves
Westward moving waves
Stationary waves
58N
38N
18N
2N
18S
38S
58S
Evv (k) M²S⁻²
WAVENUMBER (k)

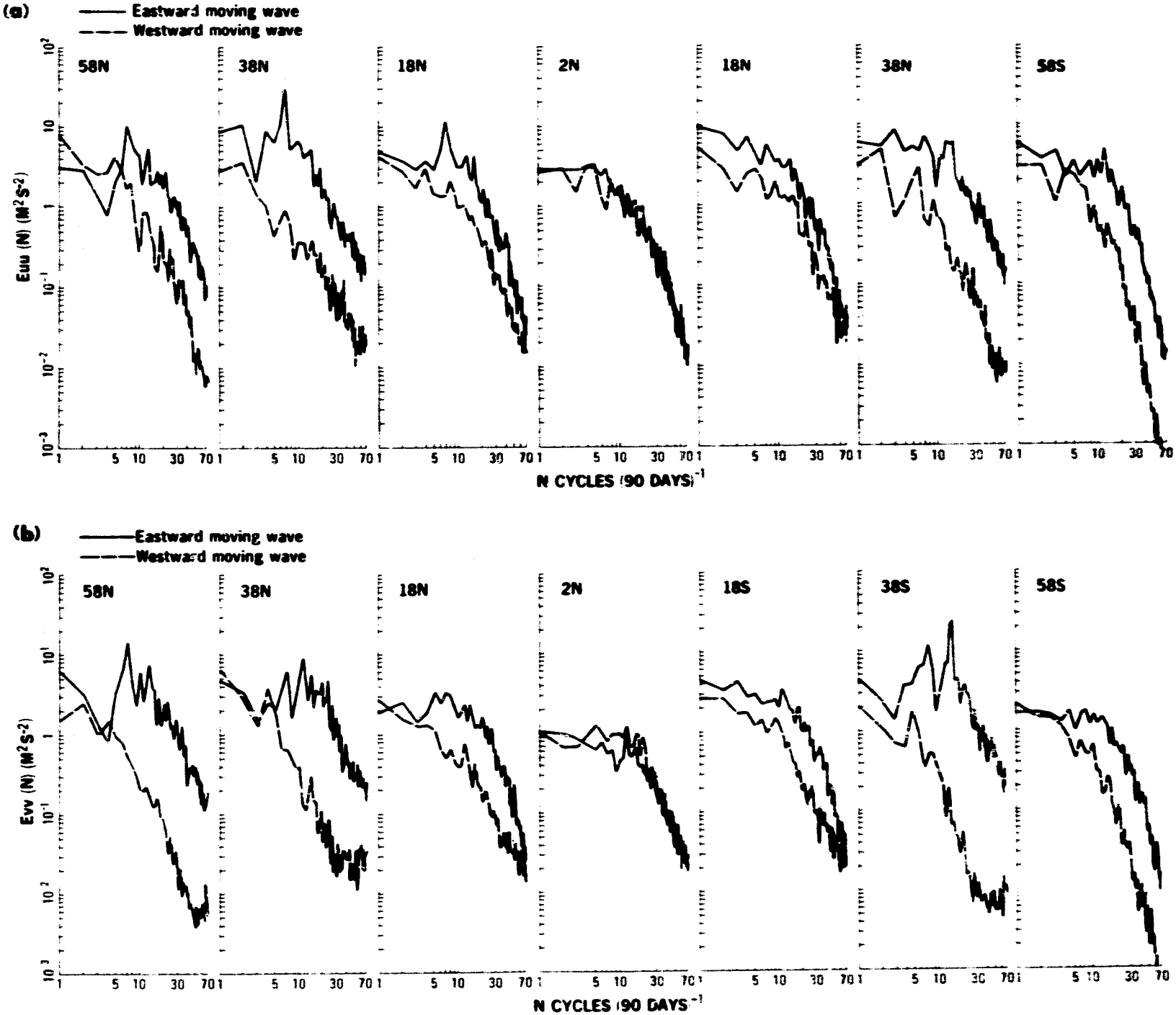
(a)
Eastward moving wave
Westward moving wave
58N
38N
18N
2N
18N
38N
58S
Euu (N) (M²S⁻²)
N CYCLES (90 DAYS)⁻¹
(b)
Eastward moving wave
Westward moving wave
58N
38N
18N
2N
18S
38S
58S
Evv (N) (M²S⁻²)
N CYCLES (90 DAYS)⁻¹

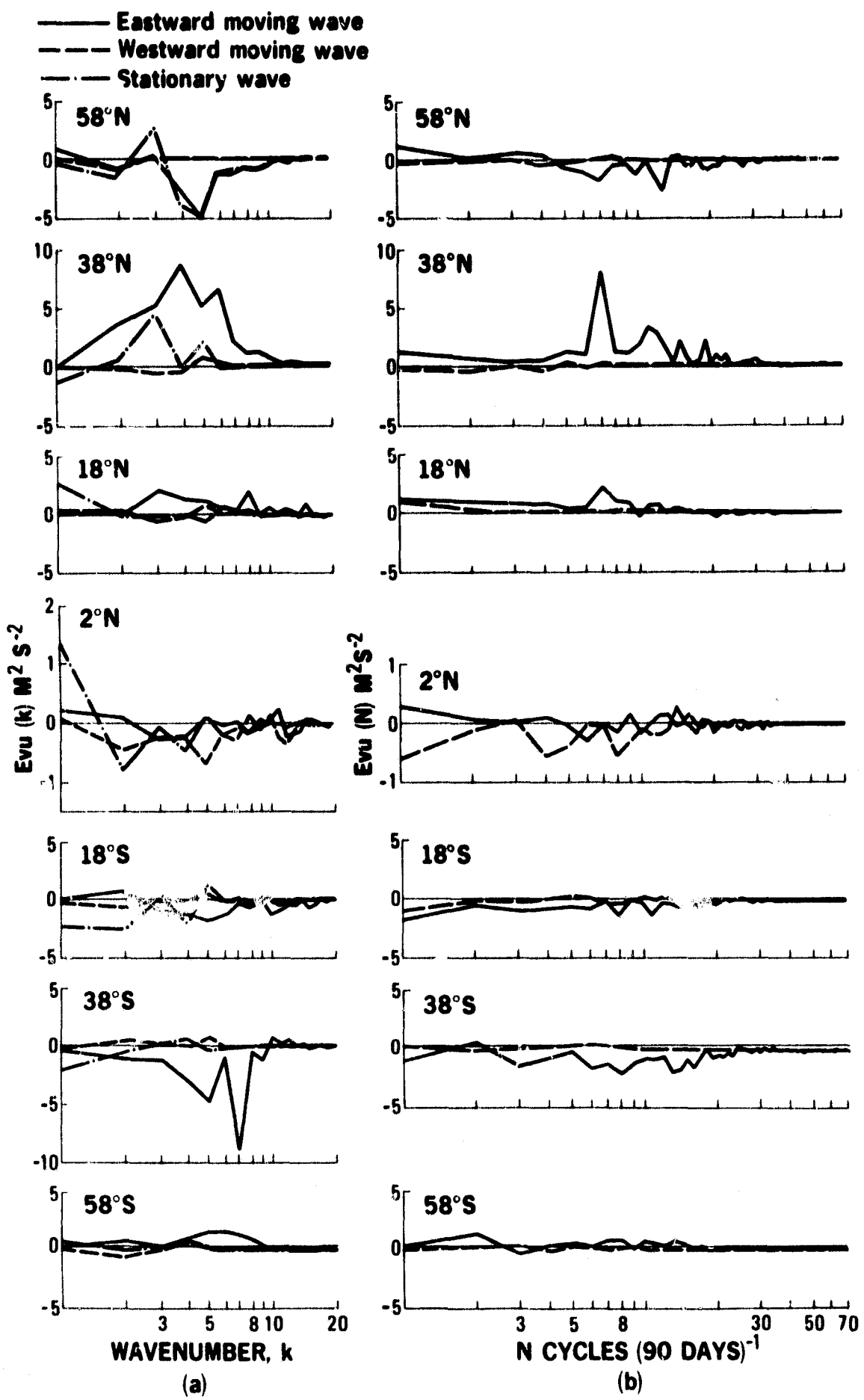
Eastward moving wave
Westward moving wave
Stationary wave
58°N
38°N
18°N
2°N
18°S
38°S
58°S
Evu (k) M² S⁻²
Evu (N) M²S⁻²
WAVENUMBER, k
N CYCLES (90 DAYS)⁻¹
(a)
(b)

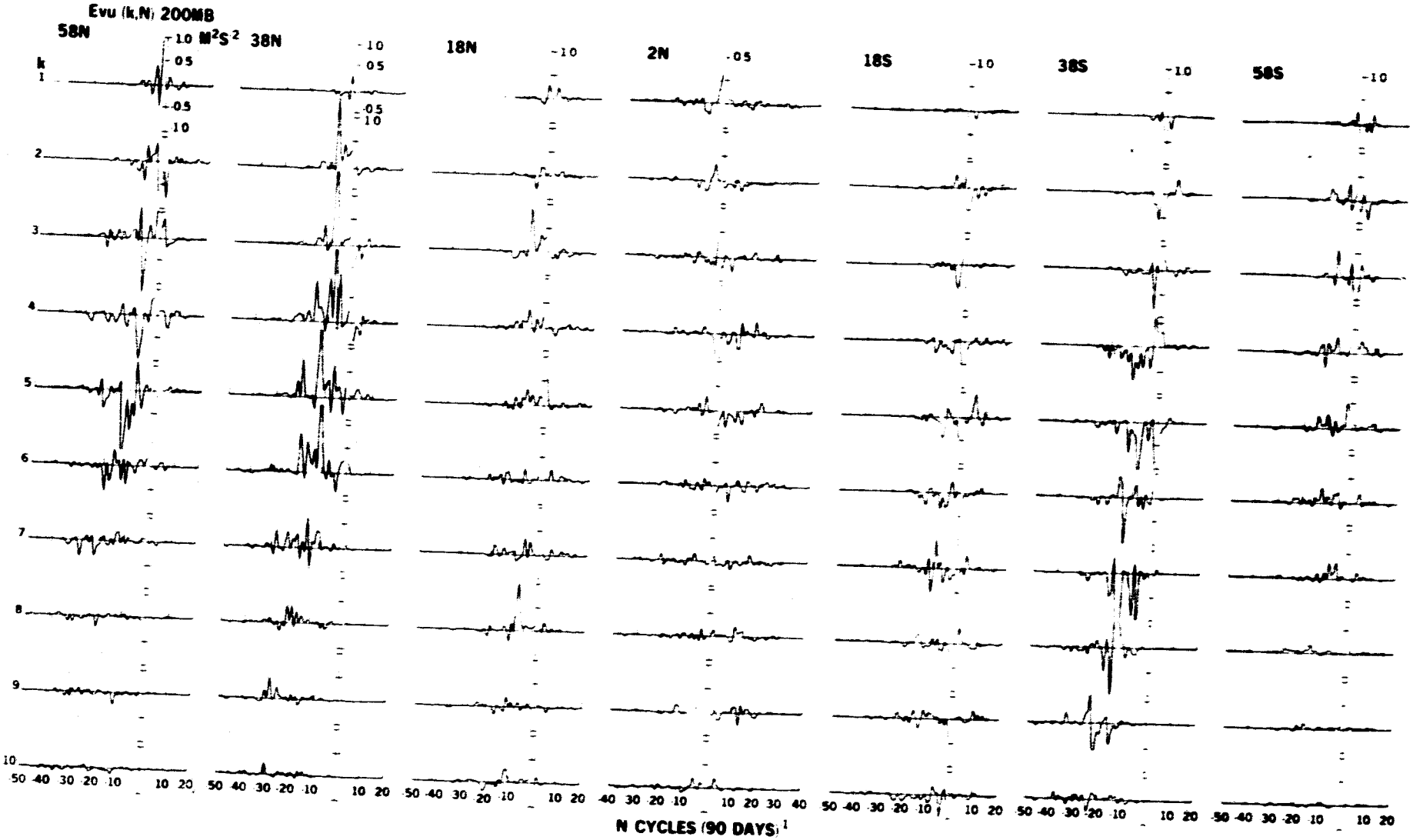
Evu (k,N) 200MB
58N
38N
18N
2N
18S
38S
58S
M²S⁻²
k
N CYCLES (90 DAYS)⁻¹

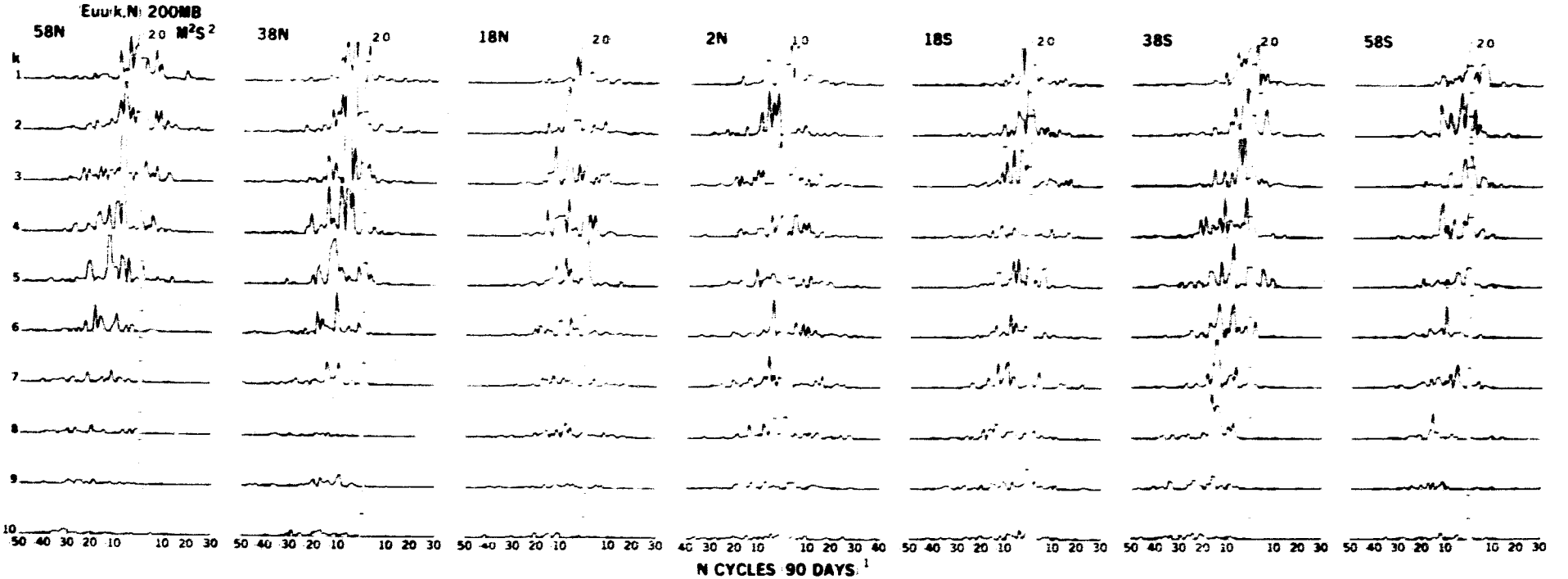
Eddy N 200MB
58N
20
M²S²
38N
20
18N
20
2N
20
18S
20
38S
20
58S
20
k
1
2
3
4
5
6
7
8
9
10
50 40 30 20 10 10 20 30
50 40 30 20 10 10 20 30
50 40 30 20 10 10 20 30
40 30 20 10 10 20 30 40
50 40 30 20 10 10 20 30
50 40 30 20 10 10 20 30
50 40 30 20 10 10 20 30
N CYCLES 90 DAYS⁻¹

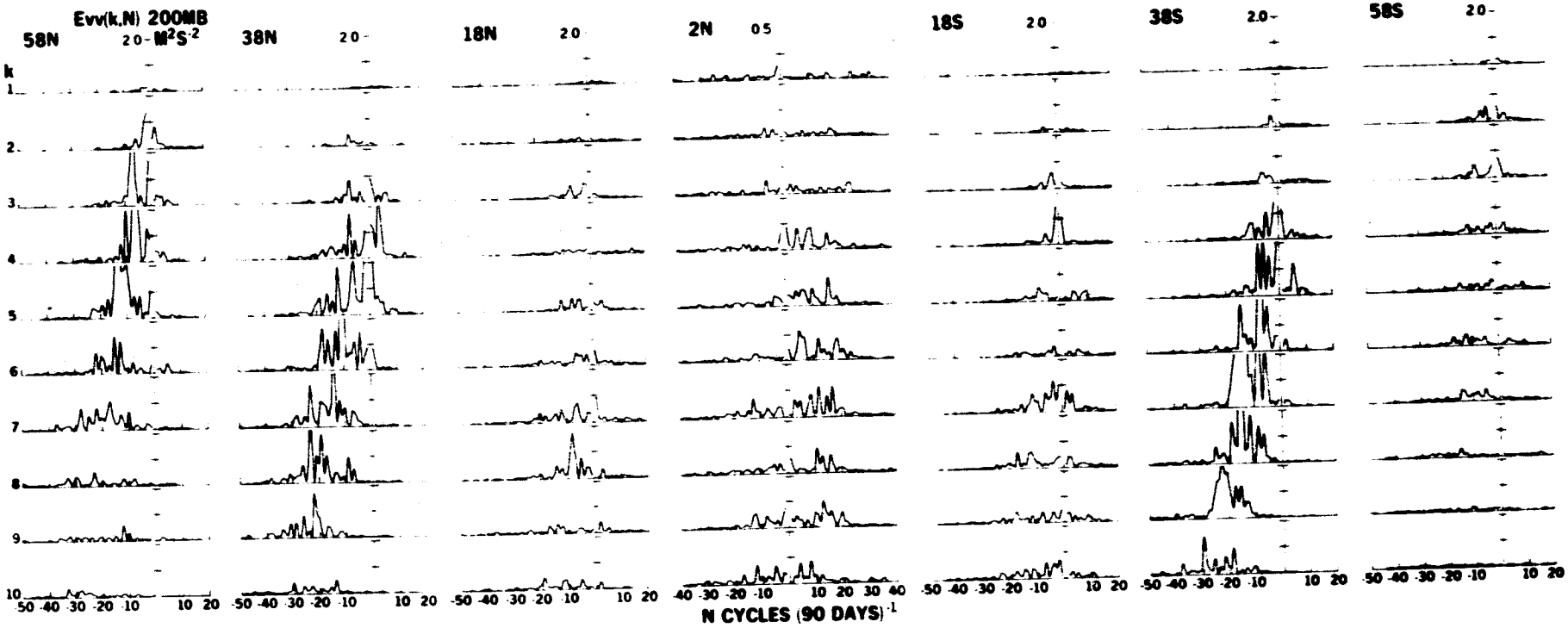
Evv(k,N) 200MB
M²S⁻²
58N
38N
18N
2N
18S
38S
58S
20
05
k
1
2
3
4
5
6
7
8
9
10
-50 -40 -30 -20 -10 10 20
-40 -30 -20 -10 10 20 30 40
N CYCLES (90 DAYS)⁻¹

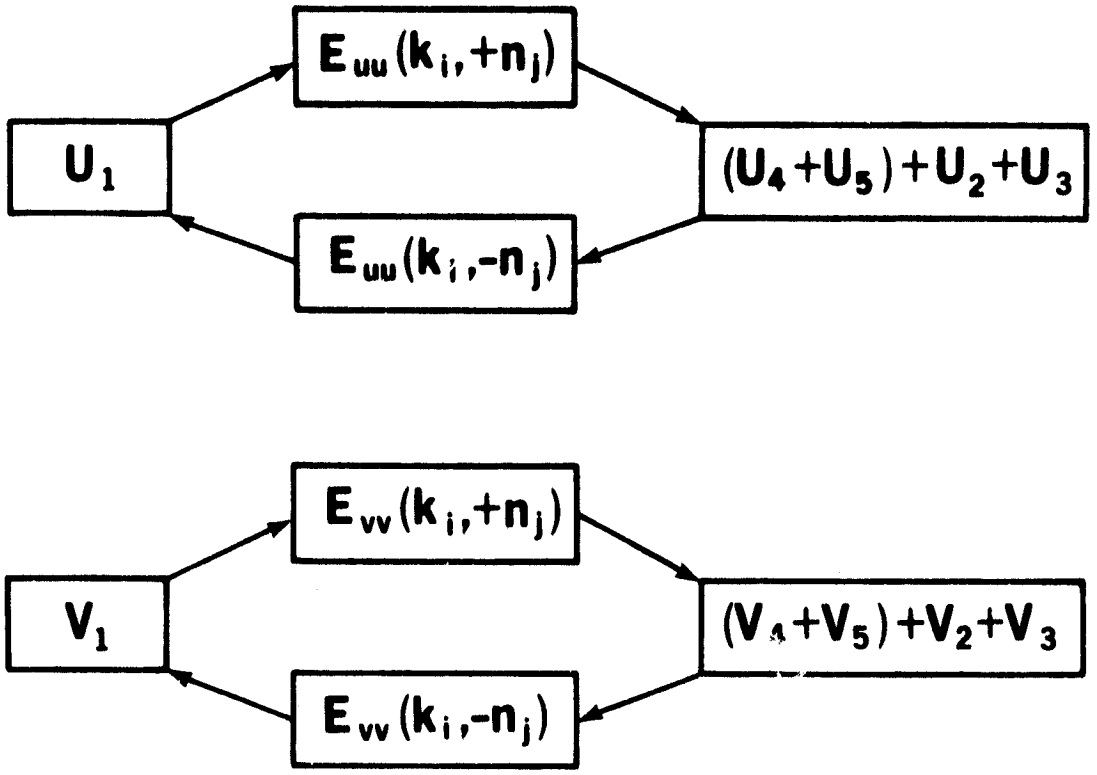
$E_{uu}(k_i,+n_j)$
U_1
$(U_4+U_5)+U_2+U_3$
$E_{uu}(k_i,-n_j)$
$E_{vv}(k_i,+n_j)$
V_1
$(V_4+V_5)+V_2+V_3$
$E_{vv}(k_i,-n_j)$

At 18° N and 38°N

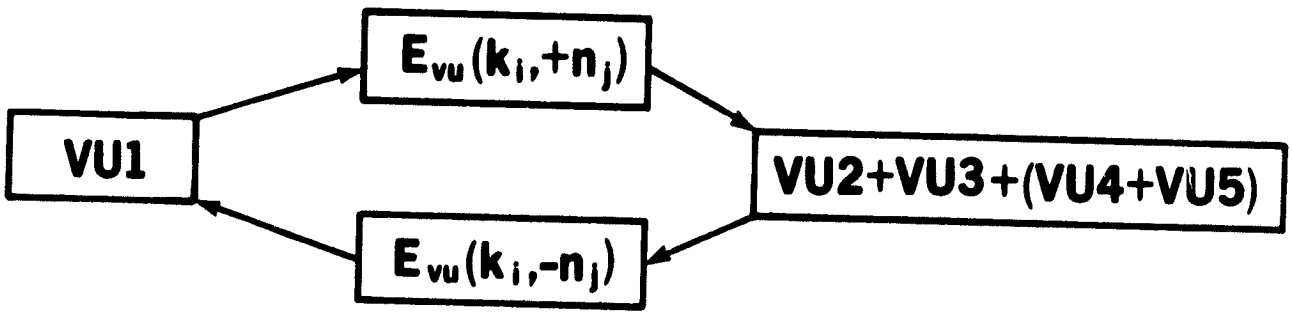

At 2° N

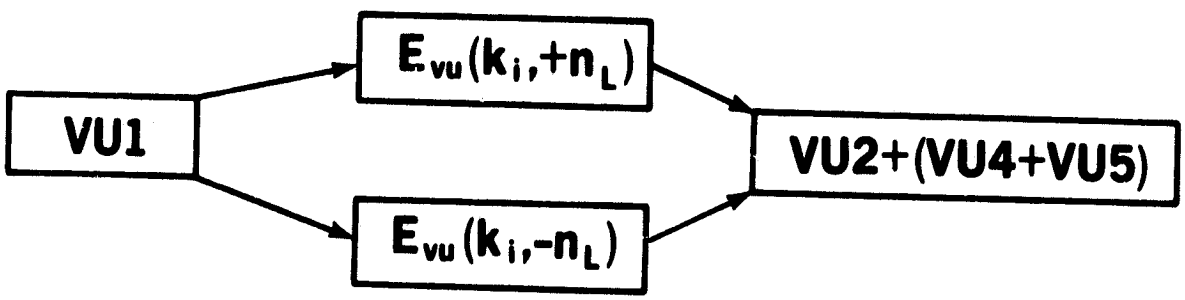

At 18°S and 38°S

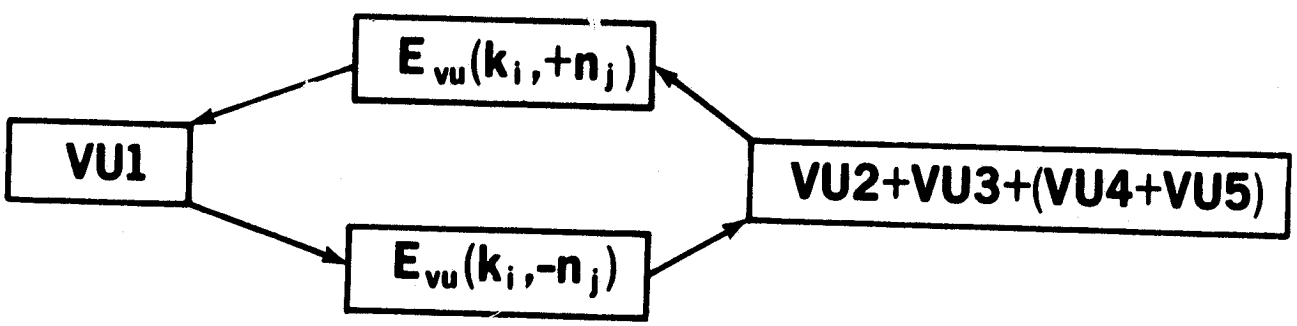

Spectral energetics analysis of ultralong waves and blocking ridges generated in the GLAS atmospheric model due to the North Pacific SST anomaly

by

Tsing-Chang Chen
Department of Earth Sciences
Iowa State University
Ames, Iowa 50011

and

J. Shukla
Laboratory for Atmospheric Sciences
NASA-Goddard Space Flight Center
Greenbelt, MD 20771

Abstract

Two experiments were performed previously by Shukla and Bangaru (1979) to test the response of the general circulation model of the Goddard Laboratory for Atmospheric Sciences to a North Pacific sea surface temperature anomaly: (1) control run in which the climatological mean SST was used and (2) anomaly run in which an invarient Pacific SST anomaly of 1976-1977 winter was imposed on the control run. It is found that the ridges and troughs appearing in control run are amplified and become stationary in anomaly run. The purpose of this study is to examine the effect of SST anomaly on the long waves in terms of spectral analysis.

The spectrally filtered Hovmöller diagrams show that wavenumber 2 and 3 in the anomaly run become stationary around the climatological locations of observational study when the persistent blocking ridges were generated in this experiment. The constructive interference of wavenumber 2 and 3 in the anomaly run forms two persistent blocking ridges: one in the west coast of North America and the other in western Europe.

Spectral energetics analysis of the anomaly run during the appearance of persistent blocking ridges shows that A_2 and A_3, available potential energy of wavenumber 2 and 3, are supplied by the conversion from zonal available potential energy. K_2 and K_3, kinetic energy of these two waves are maintained in different processes. K_2 is provided by $C(A_2, K_2)$, conversion from A_2 to K_2, while K_3 is mainly furnished by $-C(K_3, K_Z)$, conversion from K_3 to K_Z, zonal kinetic energy. In other words, K_2 is supported by baroclinic energy conversion and K_3 is essentially supplied by barotropic energy conversion.

The atmospheric circulation conditions in January 1963 and 1976-1977 winter were similar to that in the anomaly run during the existence of persistent blocking ridge. The spectral energetics of these two periods of time are used to compare that of the anomaly run. It is concluded that the necessary condition to have blocking ridges formed is the constructive interference of stationary long waves. The other condition for the formation of blocking ridges is how these long waves are amplified and maintained. The spectral energetics of blocking ridges shows that the amplification and maintenance of stationary long waves can be due to various physical processes.

1. Introduction

The ocean has long been known as an important energy reservoir to the overlying atmospheric circulation which would be modified through the release of thermal energy (sensible and latent heat) from the ocean. Therefore, it is inferred that the appearance of the sea surface temperature (SST) anomaly may alter the atmospheric circulation pattern and generate anomalous weather. The observational studies in the past decades provided evidences of the large-scale feedback interaction between the atmosphere and ocean.

Bjerknes (1966, 1969) showed that the SST anomaly over the tropical Pacific Ocean could cause the change of intensity of trade wind and Hadley circulation, and, in turn, might cause the anomalous atmospheric circulation in middle latitudes. Recently, Namias (1978) indicated that the anomalous west-east SST gradients over the Pacific Ocean enhanced atmospheric baroclinicity and also increased the upper level southerly flow. This anomalous southerly flow was not only to affect the local circulation pattern, but also the downstream circulation which might in turn affect the weather of North America. Ratcliffe and Murray (1970) also found a feedback relationship between the Atlantic and western Europe. The appearance of negative SST anomaly over a wide area south of Newfoundland is associated with blocked atmospheric patterns the following month over northern and western Europe, while a positive SST anomaly in the same general area favor more progressive synoptic types.

The observational studies described above indicates that SST anomalies may influence vitally the climate dynamics and long-term forecast. To examine how the large-scale air-sea interaction affects the atmospheric circulation, one has to study the ocean-atmosphere system as an entity. Since the

whole atmosphere-ocean system is too complicated, the general circulation model (GCM) has been used in the past decade as a quantitative tool to investigate the large-scale air-sea interaction. Moreover, Namias (1970) has noted that the SST anomalies, once formed, may persist for a long period of time, despite iterations with the overlying atmosphere. Therefore, the effects of the persistent SST anomalies on the atmospheric circulation are examined by inserting SST anomalies over the sea surface of a noninteractive model.

Rowntree (1972) used the Geophysical Fluid Dynamics Laboratory 9-layer hemispheric model to test the effect of the warm anomaly in the tropical east Pacific Ocean. The hypothesis proposed by Bjerknes (1966) was confirmed by Rowntree's numerical experiment. The Goddard Institute for Space Study version of the 2-layer Mintz-Arakawa model and multilevel version (Somerville et al., 1974) were employed by Spar (1973a, b) and Spar and Atlas (1975) to test the effect of SST and SST anomalies on the long-term forecast. No significant impact has been found in their numerical experiments.

The 5°-mesh version of the national Center for Atmospheric Research atmospheric model has been used for a series of tests of the model response to SST anomalies. Houghton et al. (1974) tested the SST anomalies over the north Atlantic Ocean on the simulated climate. They found that the warm anomaly case showed good agreement with Ratcliff and Murray's result. Chervin et al. (1976) imposed the dipolar SST anomalies on the Pacific. Their statistic analysis of 1.5 km temperature did not show downstream teleconnections between North Pacific SST anomalies and atmospheric temperature over the North American continent with high statistic significance. Kutzbach et al. (1977) made more extensive analysis for the experiments performed by Chervin et al. (1976) and also tested the effect of longitudinal location of SST anomalies.

In addition to the response of local circulation, wavelike perturbations also extended downstream from the region of SST anomalies. Chervin et al. (1980) made more experiments with various SST anomalies. Their experiments showed that the midlatitude anomaly response involved near downstream wavelike changes and the subtropic anomaly response was more confined to the vicinity of the SST anomaly.

The observational study by Namias (1978) to examine the effect of the Pacific on the anomalous circulation pattern in 1976-77 winter indicated that the anomalous west-east SST gradients over the north Pacific was one of the major factors to cause a persistent open blocking ridge located in the west coast of North America. Following Namias' findings, two numerical experiments were performed to test the response of the Goddard Laboratory for Atmospheric Sciences (GLAS) atmospheric model to the SST anomalies over the north Pacific in the 1976-77 winter (Shukla and Bangaru, 1979). These two experiments are one using the climatological mean SST and the other imposed invariant SST anomaly of 1976-77 winter, in addition to the climatological mean SST. The pronounced model response to the SST anomaly is shown in the amplification of large-scale waves. The most remarkable aspect is the appearance of two persistent open blocking ridges located in the west coast of North America and western Europe. In order to understand how these two persistent blocking ridges are formed and maintained, our major effort in the present study is aimed at examining the alternation of the long-wave behavior due to SST anomalies and the spectral energetics of these long waves.

A brief description of the GLAS model and numerical experiments is provided in Section 2. Section 3 discusses the synoptic and spectral analysis of the experiments and the formation of persistent blocking ridges. Section 4

presents the spectral energetics how the long waves which form the blocking ridges are maintained. A comparison of the model simulation to the observational analysis of the long waves and their spectral energetics is made in Section 5. Section 6 offers the summary and discussion.

2. Description of the GLAS general circulation model and experimental design

Model

The general circulation model used in this study is the second-order version of the Goddard Laboratory for Atmospheric Sciences (GLAS). This GCM was originally developed at Goddard Institute for Space Study (GISS) by Somerville et al. (1974) for a winter season simulation. A summer simulation with essentially the same GCM was carried out by Stone et al. (1977). The model was recently modified by Halem et al. (1978) at the GLAS in the model's longwave radiation parameterization, the surface boundary processes, and some numerical treatment of the time differential approximation.

The model is a global primitive-equation model which is developed in the sigma vertical coordinate system (Phillips, 1957) with nine levels between the surface and the top at 10 mb. Horizontal grid spacing is 4° latitude and 5° longitude. A variable horizontal grid with coarser spacing near the pole is introduced. In addition, the time-altering space-uncentered difference scheme of Arakawa (1972) was removed and a high order two-grid point filter developed by Shapiro (1970) was applied there. The time step is 10 minutes in the model integration.

The model also includes a detailed parameterization of no explicit subgrid scale processes. The condensation and cloud are generated by two different mechanisms: large-scale supersaturation and parameterized subscale moist convection. Short-wave radiation is calculated by a parameterization based

on detailed radiative calculations, including multiple scattering. Long wave radiation fluxes are calculated using a new scheme developed by Wu (1980). These long- and short-wave radiation transfers were calculated at 5-hour intervals. The ground temperature are evaluated from the net heating and cooling at the surface by radiation, sensible heat and latent heat fluxes. The geographic distribution of the continent, topography, albedo, and ice and snow cover are specified. The soil moisture is predicted as treated in the UCLA model (Gates, 1972). Sea surface temperatures adopt the monthly mean observed values provided by the NCAR (Washington and Thiel, 1970). These temperatures were updated daily by a linear interpolation between the midpoints of two consecutive months.

The verification of the GLAS atmospheric model simulation of winter and summer seasons can be found in Halem et al. (1978).

Numerical Experiments

In the winter of 1976-77, the severe weather occurred over North America, extreme cold dominated the eastern part of the United States and record drought affected the far west. In addition, abnormal warmth occurred over Alaska and much of the Canadian Arctic. Namias (1978) examined the possible factors to cause this severe winter weather. He found that the SST in the north Pacific was characterized by abnormally cold temperatures in its central and western parts with a warm pool off the west coast of the United States shown in Figure 1. In addition, the anomalous changes in SST are in phase with the normal month-to-month changes. In other words, the normal SST gradient between 160°W-140°W was greatly strengthened in this winter. The enhanced west-east SST gradient over the Pacific increased baroclinicity in the overlying atmosphere and also increased the upper level southly east

of 140°W. This flow helped steer storms northward to Alaska and produced a meridionally extensive ridge over the west coast of North America, and a trough in the east. Therefore, Namias suggested that the North Pacific SST anomalies might have been one of the multiple causes of the abnormally cold temperatures in eastern North America during the winter of 1976-77.

A numerical experiment with the GLAS general circulation model was carried out to test Namias' hypothesis (Shukla and Bangaru, 1979). The experiments were performed by firstly integrating the GLAS model for 45 days with the climatological mean SST (Washington and Thiel, 1970) and the observed initial conditions for January 1, 1975. This integration is referred to as the control run. The climatological SST field was then changed by adding a time invariant anomaly field and therefore, although the climatological SST varied with season, the imposed anomaly field remained constant with time. The distribution of the imposed SST anomalies is shown in Figure 1. Notice that the numerical values used in the experiments were exaggerated by considering them in °C rather than °F shown in Namias' study (1978). The model was integrated again for 45 days and will be referred to as the anomaly run. Since this is not a coupled ocean-atmosphere model, SST anomalies were assumed to persist for the whole period of integration. This assumption is justified by the observed fact that SST anomalies do persist for a period of several months (Namias, 1970). The purpose of this numerical experiment is not to simulate the actual events of the 1976-77 winter but to examine the effects of similar SST anomalies on the model atmosphere. It should be noted that the atmospheric conditions in the control run correspond to the winter of 1975.

3. Synoptic and spectral analysis

Synoptics

The comparison of the synoptics between the control and anomaly runs will provide the first glance of the response of the model atmosphere to the SST anomalies shown in Figure 1. The examination of model daily charts (not shown) of both runs reveals that a two ridge-trough system always exist. Furthermore, the anomaly run generates two persistent blocking ridges in the west coast of North America and West Europe in the first two weeks of model February, i.e. the last two weeks of the anomaly run. In order to have an overview of the synoptic difference between these two runs, the mean height fields for the first two weeks of model February at 500 and 850 mb are shown in Figure 2.

The two-week mean height fields display the circulation pattern of two ridge-trough system at 500 mb of both runs. The open troughs become close lows at 850 mb. Two ridges exist along the west coast of North America and western Europe at both 500 and 850 mb. The ridges of the anomaly run are amplified very remarkably compared to the control run, especially at 500 mb. The 500 mb trough over the Atlantic is deepened very much in the anomaly run. The 500 mb trough over the Pacific is very broad. However, the 850 mb close low, which is 500 mb open trough, over the Pacific also demonstrates its deepening in the anomaly run. It is also interesting to note that both the trough and ridge lines tilt from southeast to northwest. In addition, the ridge of the anomaly run over western Europe is shifted westward at 500 mb and eastward at 500 mb with respect to that of the control run. This contrast between both runs is especially pronounced north of 60°N.

The deepening of the low (or trough) over the Pacific and the intensification of the ridge over the west coast of North America can be understood due to the enhancement of the model baroclinicity by the imposed west-east SST anomaly gradient and also possibly by the interaction between the positive SST anomalies over the east North Pacific and the Rockys. In other words, the persistent blocking ridge appearing on the west coast of North America can be intuitively understood as the near downstream teleconnection. Furthermore, the amplification of the ridge over western Europe and the deepening of the trough (or low) over the Atlantic naturally demonstrates that the GLAS model atmosphere also respond to the Pacific SST anomaly with a far downstream teleconnection.

Spectral Analysis

Hovmöller's diagram, i.e. longitude-time trough-ridge system, (Hovmöller, 1949) has long been used to examine the amplification and propagation of atmospheric long waves. Recently, Somerville (1980) suggested that the spectrally filtered (SF) Hovmöller diagram is a more effective mean to isolate the interesting features of long waves and to examine the four-dimensional development of long waves.

The comparison of the height fields between both runs reveals clearly that the most distinguishable difference is in the large-scale features. In other words, the major response of the GLAS model atmosphere to the SST anomalies over the North Pacific shows in the long waves. For this reason, it would be instructive to use the SF Hovmöller diagram to illustrate the spectral response of the model atmosphere to the SST anomalies. Furthermore, 50°N, which is located in the middle of the north-south extent of the ridges,

is chosen to depict the SF Hovmöller diagrams. Figure 3 shows these diagrams of three different wave groups: wavenumber 1-15, wavenumber 1-4, and wavenumber 5-15, at 500 mb. The first wave group is regarded as the total wave disturbances, the second wave group as the long waves, and the third wave group as short waves.

The SF Hovmöller diagrams of wavenumber 1-15 for both the anomaly and control runs, Figures 3a and d, show that two ridge-trough systems exist over most of the simulation period. The trough-ridge system in the anomaly run is stationary, while that is eastward propagating in the control run. Comparison between Figures 3a and d also reveals that the trough-ridge systems in both runs in the third week of January are still similar to some extent. This similarity of the SF Hovmöller diagrams for total wave disturbances may indicate that the GLAS model has memory of the initial height field and the model response to the Pacific SST anomalies does not become significant in the first three weeks of the model simulation.

In order to examine the role played by the long and short wave regimes, the SF Hovmöller diagrams of wavenumber 1-4 and 5-15 are also displayed in Figures 3b, c, e and f, respectively. The comparison between the long-wave SF Hovmöller diagrams and the total-wave SF Hovmöller diagrams shows very clearly that the large-scale pattern of the ridge-trough system in both runs are mostly explained by the long-wave regime. The contribution from the short-wave regime is the fine structure of the ridge-trough system. The long-wave SF Hovmöller diagrams show that the persistent blocking ridges in the anomaly run are mainly constructed by the stationary long waves.

The short-wave SF Hovmöller diagrams characterize the eastward propagation of the short waves over most of the longitudes and time. However, both the

control and anomaly runs have stationary ridges located at 30°E in the first two weeks of February. In addition, the troughs and ridges of the short-wave regime in the anomaly run between 150°E and 120°W are quasi-stationary. Recall that the SST anomalies are imposed in the North Pacific with the boundary of positive and negative anomalies around 140°W. It is understood that the strong west-east SST gradient would enhance the baroclinicity of the overlying atmosphere. This may, in turn, increase the cyclogenesis in the enhanced baroclinic zone. In any event, the quasi-stationarity of the short-wave ridges and troughs may indicate the stationarity of forcing from the Pacific SST anomalies. This argument is consistent with previous experiments using the NCAR atmospheric model by Chervin et al. (1976), Kutzbach et al. (1977) and Chervin et al. (1980). The intensification of the ridge located at 30°E is a very surprising downstream teleconnection in the GLAS atmospheric model.

To further our understanding of the long-wave response to the Pacific SST anomalies, the SF Hovmöller diagrams for each individual long wave from wave-number 1 to 4 are depicted in Figure 3. The most pronounced difference between two runs are wavenumbers 2 and 3. These two waves "lock in" the anomaly run. In other words, the west-east Pacific SST anomalies force these two waves to be stationary. It is also interesting to note that the super-imposition of wavenumbers 2 and 3, Figure 3e, provides a reasonable explanation of the double persistent blocking ridges, shown in Figures 2a or b.

Based upon the occurrence of blocking observed by Rex (1958) and the latitudinal distribution of planetary-wave phase at 500 mb analyzed by Eliasen (1958), Austin (1980) claims that the formation of blocking can be classified in the following ways due to the constructive interference and amplication of planetary waves:

	Wavenumber 1	Wavenumber 2	Wavenumber 3
Atlantic Blocking	large	large	small
Pacific Blocking	small	large	large
Double Blocking	large	large	large

Although the anomaly run does not generate the Rex-type blocking, the amplification of two persistent blocking ridges in the first two weeks of February seems to be similar to double blocking; one ridge is located between the eastern North Pacific off the west coast of the North American continent, and the other is situated between the eastern North Atlantic and western Europe.

It would be interesting to compare the spectral analysis of the anomaly run with Austin's compilation of observational studies. Wavenumber 1 in the anomaly run is shifted about 50° westward with respect to Eliasen's result. Wavenumber 2 of the anomaly run has about the same location as observation, while, wavenumber 3 of the anomaly run is shifted eastward about 10°. The SF Hovmöller diagram of wavenumber (2+3), Figure 4e, shows clearly that the eastward shift of wavenumber 3 makes the formation of double blocking ridges only by wavenumbers 2 and 3 possible. The amplification and westward shift of wavenumber 1 helps the filling of the trough between two persistent blocking ridges formed by wavenumbers 2 and 3, and the intensification of the Atlantic blocking ridge.

Tung and Lindzen (1979) proposed resonance theory to explain the development of atmospheric blocking. "To be resonant, the wind condition in the atmosphere has to be such that the phase speed of the free traveling wave is reduced to zero, so that the wave becomes stationary with respect to the surface of the Earth and hence, also to the topographic forcing and land-sea differential heating." This is Tung and Lindzen's "stationary condition". The discussion

above clearly shows that the insertion of the Pacific SST anomalies make wavenumbers 2 and 3 "lock in". This lock-in effect enable wavenumbers 2 and 3 in the anomaly run satisfy the necessary condition for the occurrance of the persistent blocking ridges. Furthermore, one has to face another problem, that is the amplification of the stationary waves. Austin (1980) speculated that the imposed SST anomalies enhance the thermal forcing which, in turn, amplifies stationary waves to form blocking. In order to understand this problem, we shall apply the spectral energetics to examine how long waves are amplified after becoming stationary in Section 4.

It has been shown that wavenumbers 2 and 3 in the anomaly run are so vital to determine the formation of persistent blocking ridges. It would be of interest and informative to examine the synoptic structure of these two waves. The persistent blocking ridges obtain their maximum intensity on February 4. It would be illustrative to show the spectrally filtered synoptic charts of wavenumbers 2, 3 and combination of them at 12 GMT 4 Feb for height and temperature at 500 mb, Figure 5.

The highs of wavenumber 2 located at Alaska Bay and north Central Europe, while those of wavenumber 3 are anchored at the west coast of Canada, the North Sea and Siberia. The combination of these two waves forms two highs at the west coast of Canada and the North Sea with a deep low located at Labrador and another broad low extending from north Africa to the northwestern Pacific. The combination of temperature wavenumbers 2 and 3 is very similar to the height except the warmth centered at the Alaska Bay is shifted westward with respect to the high of height field. The comparison of individual waves of height and temperature shows that wavenumber 2 has a significant phase lag between height and temperature and wavenumber 3 does not. In fact, the

observations of daily spectral analysis reveal that wavenumber 2 height leads wavenumber 2 temperature from 10° to 30° longitude. On the contrary, height and temperature of wavenumber 3 does not show very significant phase lag on the basis of daily variation. This indicates that wavenumber 2 is baroclinic and wavenumber 3 is relatively barotropic. The remarkable difference of synoptic structure between these two waves must be related to the difference of physical processes to develop and maintain them.

4. Energetics

Energetics Scheme

In order to examine the development and maintenance of the blocking ridges in terms of spectral analysis, Saltzman's (1957) spectral energetics scheme is employed to a latitudinal zonal between 26°N and 86°N. Following Saltzman's formulation and Steinberg et al.'s (1971) expression, spectral energy equations in symbolic form can be written as:

$$\frac{dK_Z}{dt} = \sum_{n=1}^{N} C(K_n, K_Z) + C(A_Z, K_Z) + F(K_Z) - D(K_Z), \tag{1}$$

$$\frac{dK_n}{dt} = - C(K_n, K_Z) + CK(n|m,\ell) + C(A_n, K_n) + F(K_n) - D(K_n), \tag{2}$$

$$\frac{dA_Z}{dt} = - \sum_{n=1}^{N} C(A_Z, A_n) - C(A_Z, K_Z) + F(A_Z) + G(A_Z), \tag{3}$$

$$\frac{dA_n}{dt} = C(A_Z, A_n) - C(A_n, K_n) + C(n|m,\ell) + F(A_n) + G(A_n), \tag{4}$$

where K and A represent kinetic and available potential energy. The subscripts Z and n denote zonal and wave components. The rate of change of various energy components on the left-hand side is contributed by the various energetic processes on the right-hand side. C(P,Q) represents the energy conversion from P to Q. Note that $\sum_{n=1}^{N} C(K_n, K_Z) = C(K_E, K_Z)$ and $\sum_{n=1}^{N} C(A_Z, A_n) = C(A_Z, A_E)$. CX(n/m,ℓ) is the gain rate to wavenumber n of quantity x due to triplet interactions between all possible combinations of m and ℓ with n. F(x) gives the contribution due to the flux across the lateral boundary of the open region. G(A) and D(K) are generation of available potential energy and dissipation of kinetic energy, respectively.

Equations for eddy energies, $K_E = \sum_{n=1}^{N} K_n$ and $A_E = \sum_{n=1}^{N} A_n$, can be obtained by summing equations (2) and (4) from n = 1 to N,

$$\frac{dK_E}{dt} = - C(K_E, K_Z) + C(A_E, K_E) + F(K_E) - D(K_E), \tag{5}$$

$$\frac{dA_E}{dt} = C(A_Z, A_E) - C(A_E, K_E) + F(A_E) + G(A_E). \tag{6}$$

The traditional Lorenz energy cycle consists of equations (1), (3), (5) and (6). A schematic energy diagram is shown in the appendix to illustrate the maintenance of wavenumber n energetics.

Overview of model energetics during blocking situations

Time variations of various energies, A_Z, A_E, K_Z and K_E, and various energy conversions, $C(A_Z, A_E)$, $C(A_E, K_E)$ and $C(K_E, K_Z)$ from January 16 to February 14 in the anomaly run are depicted in Figure 5. Let us recall the amplification of blocking ridges located in the west coast of North America and western Europe in the anomaly r[illegible]overs the first two weeks of February. Observation of Figure 6 reveals that A_Z and K_Z start to decline on January 30, while A_E and K_E increase. Then, A_E [illegible]d K_E, especially the latter, decrease around February 7, and both increase about February 10 again. Notice that both A_Z and K_Z increase, in general, when A_E and K_E decrease, or vice versa.

The energy conversions, $C(A_Z, A_E)$ and $C(A_E, K_E)$ are always positive. In addition, their time variations go hand-in-hand and are also consistent with the time variations of A_E and K_E. It is surprising to note that $C(K_E, K_Z)$ is negative over most of the time period in the anomaly run. This indicates that the eddy disturbances are barotropically maintained by the energy conversion from the zonal flow.

Lejenäs (1977) compiled the time variations of A_Z, A_E, K_Z and K_E from the energetics study of atmospheric blocking by Winston and Kreuger (1961) and Miyakoda (1963) and energy conversions by Paulin (1968). Lejenäs sketched a characteristic picture of the energy changes and energy conversions during a blocking situation in Figure 7. We may not be able to expect that the energetics for the development of the persistent blocking ridges in the anomaly run is the same as the atmospheric cases analyzed by either Winston and Kreuger or Miyakoda. However, the energetics during the development of model blocking ridges depicted in Figure 4 shows a very striking similarity to Lejenäs' schematic picture.

Dynamical transports of wavenumbers 2 and 3 during blocking

It was observed in Section 3 that the life period of the blocking ridges generated in the anomaly run was about two weeks. In addition to examine how the blocking ridges are formed, we have to face how the blocking ridges are maintained for such a long period of time. The spectral analysis in Section 3 shows that the formation of the blocking ridges are essentially due to the constructive interference of wavenumbers 2 and 3. On the other hand, the spectral energetics of these two waves would shed light on the maintenance of blocking ridges.

Before we investigate the spectral energetics of wavenumbers 2 and 3 in detail, the examination of the dynamic transport activities would provide some informative property of these two waves. Figure 8 depicts the time variation of zonal flow and temperature at 500 mb for the anomaly run. The zonal flow between 26°N-62°N starts to decrease when the blocking ridges develop at the end of January. The zonal flow increases again after about 4 days. An interesting feature about the zonal flow is the appearance of easterlies in high latitudes (60° - 70°N) from February 3-9. This is obviously caused by the warming at high latitudes shown in Figure 8b. The warming at high latitudes indicates that the blocking ridges channel the warm air to high latitudes.

The time variations of momentum and sensible heat transports* for waves 2 and 3, $\bar{u}\bar{v}(2)$, $\bar{u}\bar{v}(3)$, $\bar{v}\bar{T}(2)$ and $\bar{v}\bar{T}(3)$, are displayed in Figures 9 and 10, respectively. It can be seen clearly that the transport activities by wavenumbers 2 and 3 mainly occur in high latitudes. This is consistent with the

*$\bar{v}\bar{T}(n)$ and $\bar{u}\bar{v}(n)$ will be used hereafter to denote the sensible heat and momentum transport by wavenumber n. The combining contribution from two waves, e.g. 2 and 3, will be denoted by $\bar{v}\bar{T}(2+3)$ and $\bar{u}\bar{v}(2+3)$. $\bar{(\ )}$ = zonal average.

observational spececctral analysis of these two transports by W'in-Neilsen et al. (1964). It is interesting to note that $\overline{uv}(2)$ and $\overline{uv}(3)$ ($\overline{vT}(2)$ and $\overline{vT}(3)$) are, in general, southward (northward) in high latitudes. Surprisingly, uv(3) becomes northward from midlatitudes to high latitudes during the mature stage of blocking ridges. $\overline{vT}(2)$ is very significant northward transport during the existence of blocking ridges, but $\overline{vT}(3)$ is significantly southward over some period during the developing stage of blocking ridges. This may manifest that $\overline{vT}(2)$ is important factor to cause the warming in high latitude shown in Figure 8.

The blocking ridges shown in Figure 2 reach their maximum intensity on February 4. The geographic distribution of $\overline{uv}$, $\overline{vT}$ and $\overline{\omega T}$ of wavenumbers 2 and 3, and sum of these two waves at 500 mb on February 4 are also shown in Figure 11. Observation of these figures reveals that $\overline{uv}(3)$ is more significant than $\overline{uv}(2)$, while $\overline{vT}(2)$ and $\overline{\omega T}(2)$ are larger than $\overline{vT}(3)$ and $\overline{\omega T}(3)$. This contrast of transport properties between wavenumbers 2 and 3 is consistent with the synoptic analysis that wavenumber 2 is baroclinic and wavenumber 3 is relatively barotropic. $\overline{uv}(2+3)$, $\overline{vT}(2+3)$ and $\overline{\omega T}(2+3)$ are significant in the western hemisphere. It is interesting to note that $\overline{vT}(2+3)$ and $\overline{\omega T}(2+3)$ show three areas of large value: eastern Pacific, North America, and eastern Atlantic. The superimposition of height and temperature geographic distributions for the sum of wavenumbers 2 and 3, shown in Figure 5, explain well the distribution of $\overline{vT}(2+3)$. Positive $\overline{vT}(2+3)$ at eastern Pacific and eastern Atlantic is due to northward warm air advection, while positive $\overline{vT}(2+3)$ at North America is because the southward cold air advection. $-\overline{\omega T}$ represents the vertical transport of sensible heat which usually is in phase with $\overline{vT}$. In addition, $-\overline{\omega T}$ also denotes the conversion between A_E and K_E, namely, the release of available potential energy. The "lock-in" effect by imposing Pacific SST anomalies in the anomaly run seems

to increase the release of A_E to enhance stationary wavenumbers 2 and 3 and, in turn, to amplify the intensity of blocking ridges.

Kutzbach et al. (1977) imposed a dipole SST anomaly on the Pacific of the NCAR model with warm part to the east and cold part to the west. The spacing between the centers of warm and cold SST anomaly is about 45° of longitude which is about wavelength of wavenumber 4. The model temperature changes have the greatest magnitude and vertical extent over the warm ocean anomaly, rather than a wavenumber 4 response. Kutzbach et al., therefore, speculated that the warm anomaly and its longitudinal position with respect to the continents may be of primary importance to describe the pattern of mid-troposphere response. The geographic distribution of $\overline{vT}(2+3)$ and $\overline{\omega T}(2+3)$ in the present study may support their conjecture.

Spectral energetics of wavenumber 2 and 3

A_n and K_n of various long waves in the anomaly run as a function of time are shown in Fig. 9. The inclusion of wavenumber 1 and 4 is to provide a comparison of energy contents in different long waves. Although A_1 is dominant over some period in February, the SF Hovmöller diagrams show that the formation of the persistent blocking ridges is mainly due to the constructive interference of wavenumber 2 and 3. Note that both A_n and K_n of wavenumber 2 and 3 increase from the end of January when the persistent blocking ridges shown in Fig. 2 start to develop. Furthermore, our spectral energetics analysis indicates that the major contributions to various energy conversions of Lorenz energy cycle in the long wave regimes are from wavenumber 2 and 3 in the anomaly run.

Let us first deal with the energetics of wavenumber 2 with the aid of spectral energy diagram displayed in the appendix. A_2 is maintained by

$C(A_Z, A_2)$, $C(A_2, K_2)$ and $CA(2|m,\ell)$. Both $C(A_Z, A_2)$ and $C(A_2, K_2)$ are positive over the time period concerned in our analysis. Furthermore, the time variation of $C(A_Z, A_2)$ and $C(A_2, K_2)$ are in concert with that of A_2. This in-phase variation indicates that A_2 is provided by $C(A_Z, A_2)$, but is consumed by $C(A_2, K_2)$. The nonlinear interaction $CA(2|m,\ell)$ actually also extracts energy out of A_2 over most of the blocking period.

K_2 is virtually maintained by $C(A_2, K_2)$, $C(K_2, K_Z)$ and $CK(2|m,\ell)$. $C(A_2, K_2)$ was found to be always positive. $C(K_2, K_Z)$ is positive over most of the time except in the second week of February. $CK(2|m,\ell)$ is generally negative except when $C(A_2, K_2)$ drops significantly during February 8-9. It is obvious that $C(A_2, K_2)$ maintains K_2, and $C(K_2, K_Z)$ and $CK(2|m,\ell)$ diminish K_2.

$C(A_Z, A_2)$ and $C(A_2, K_2)$ involve the baroclinic processes of horizontal and vertical sensible heat transport, respectively, while $C(K_2, K_Z)$ is due to the barotropic process of momentum transport. The maintenance of A_2 and K_2 are provided by $C(A_Z, A_2)$ and $C(A_2, K_2)$, respectively. Recall that the synoptic analysis in Section 3 showed that wavenumber 2 temperature always has a phase lag behind wavenumber 2 height. These observational evidences indicate that the development and maintenance of wavenumber 2 is due to the baroclinic process.

The time variations of various energy conversions to maintain A_3 and K_3 are depicted in Figure 11. It was shown in Figure 9 that A_3 does not increase very much compared with A_1 and A_2 during the development of blocking ridges, but K_3 increases very significantly. Let us follow the argument for the maintenance of A_2 and K_2 to examine the energetics of wavenumber 3. $C(A_Z, A_3)$

and $CA(3|m,\ell)$ are major channels to support A_3. However, the small value of $C(A_Z, A_3)$ compared with $C(A_Z, A_2)$ may explain the reason why A_3 is not increased very much during the development of the blocking ridges. Furthermore, the magnitude of $C(A_3, K_3)$ is not large either. It may be because $C(A_Z, A_3)$ is small. K_3 is essentially supplied by $-C(K_3, K_Z)$, the barotropic conversion releasing the available zonal kinetic energy, rather than $C(A_3, K_3)$, the baroclinic conversion to release the eddy available potential energy. It is very clear that the physical processes to maintain the energetics of K_3 is different from those to K_2. As we discussed previously in Section 3 that wavenumber-3 height and temperature do not possess any significant phase lag between them. In addition, the momentum transport of wavenumber 3 becomes very significant during the development of blocking ridges. In any event, these arguments provide evidences that wavenumber 3 is mainly developed and maintained barotropically during the existence of blocking ridges in the anomaly run.

The contrast of physical processes to develop and maintain wavenumber 2 and 3 during the existence of persistent blocking ridges in the anomaly run is very apparent. In fact, the energetics of the blocking ridges occurred in January 1963 are similar to that generated in the anomaly run to a great extent. The spectral energetics study for this peculiar month, which will be discussed in further detail in the next section, by Wiin-Nielsen et al. (1964), Wiin-Nielsen (1964) and Murakami and Tomatsu (L965) showed that wavenumber 2 and 3 were dominant in this month. Wavenumber 2 were maintained mainly by baroclinic processes, while wavenumber 3 were supported by barotropic processes.

5. Comparison with observational studies

The model atmosphere is not a real one and the model response to the SST anomalies may not be the same as the response of the real atmosphere.

Nevertheless, the comparison of the present analysis of the anomaly run with some observational studies may shed some light on the physical mechanism which causes the persistent blocking ridges generated in the anomaly run. Under this guidance, we select January 1963 and January-February 1977. The reasons to select these two winters are as follows.

It was pointed out by Tung and Lindzen (1979) that the United States experienced very similar abnormal circulation patterns and severe winter conditions in January 1963 and January 1977; a persistent and enormously amplified ridge existed in the eastern Pacific. Furthermore, the spectral energetics of the anomaly run during the existence of the persistent blocking ridges is similar to that of January 1963 analyzed by Wiin-Nielsen et al. (1964) and Murakami and Tomatsu (1967) to a great extent. Examining the large-scale interaction between atmosphere and North Pacific, Namias (1978) suggested that the North Pacific SST anomalies in 1976-1977 winter could be the major factor to maintain the quasi-stationary amplified long waves over the North Pacific and North America. The anomaly run in the current study adopts the North Pacific SST anomalies compiled by Namias (1978). Of course, we do not expect these SST anomalies can force the model to generate the same circulation condition as the real atmosphere in 1976-1977 winter. However, it would be interesting to see whether the model response to the Pacific SST anomalies in the same direction as Namias' suggestion of the SST anomalies on the atmospheric circulation.

(a) January, 1963

Synoptics

It was observed that the existence of an unusual type of January 1963 atmospheric circulation which had an extreme amplification (O'Connor, 1963).

The average circulation of 700 mb is shown in Figure 14. The pronounced features of the atmospheric circulation in this month are enormously amplified ridge in the eastern Pacific, a blocking highs of Rex type prevailed through the mouth between Iceland and Britain, and mother strong ridge over the central Asia. These three ridges were accompanied with the abnormally amplified eastern North American trough, deep Azores low, European trough and the pacific low extending from the west Pacific to Hawaii. The cold artic air was brought to the northeast North America, Europe and Far East, and caused very severe cold weather over these three areas. The unusual warmth was occurred over Alaska and Greenland. In addition, most of the trough and ridge lines tilted from south-east to northwest. This circulation condition is similar to the existence of the persistent blocking ridges in the anomaly run.

Energetics

The energetics analysis of January 1963 discussed in the following based upon studies of Wiin-Nielsen (1964), Wiin-Nielsen et al. (1964) and Murakami and Tomatsu (1967). The Lorenz energy cycle of this month is shown in Figure 15c. The directions of energy conversions, $C(A_Z, A_E) = 6.43$ Watt m^{-2} and $C(A_E, K_E) = 2.96$ Watt m^{-2}, are the same as conventional studies (Lorenz, 1967). Surprisingly, $C(K_E, K_Z)$ of this month has a large negative value of -1.29 Watt m^{-2} which indicates that the eddies were barotropically unstable in this month. The time variations of various energy components in January 1963 are depicted in Figure 15a and b. Note that A_E and K_E increase (decrease) when A_Z and K_Z decrease. The overall picture of time variation of January 1963 atmospheric energetics shown in Figure 15 is similar to Lejenäs' during a blocking situation described in Figure 7.

The spectral energetics of January 1963 is displayed in Figure 16. The spectra of A_n, Figure 16a, and K_n, Figure 16b, show that wavenumber 2 and 3 have the largest values, although A_1 is comparable to A_2 or A_3. This may indicate that the atmospheric circulation of this month is mainly described by wavenumber 2 and 3. It may also manifest that the persistent blocking ridges in January were due to the constructive interference of these waves. $C(A_n, K_n)$ is extracted from the result of Murakami and Tomatsu (1965) which was integrated over 30°N-70°N and 1000-500 mb. In any rate, it still gives some indication of $C(A_n, K_n)$ over the whole layer of atmosphere. $C(A_Z, A_n)$, Figure 16c, and $C(A_n, K_n)$, Figure 16e, of wavenumber 2 and 3 are positive and dominant, while $C(K_3, K_Z)$, shown in Figure 16d, has very large negative value of -1.14 Watt m^{-2}. Comparing Figure 16d and Figure 15c, we can see that $-C(K_3, K_2)$ explains most part of $-C(K_E, K_Z)$. This shows that wavenumber 3 is barotropically unstable. These discussions above indicate that A_2 and A_3 are supported by $C(A_Z, A_2)$ and $C(A_Z, A_3)$, respectively. Note that $C(A_Z, A_2) > C(A_Z, A_3)$ may explain why $A_2 > A_3$. Furthermore, K_2 is maintained by $C(A_2, K_2)$, baroclinic energy conversion, while K_3 is sponsored by both $C(A_3, K_3)$ and $-C(K_3, K_2)$. In other words, K_3 is supplied by a very significant barotropic conversion in addition to baroclinic conversion. The energetics of wavenumber 2 and 3 in January 1963 is very similar to that in the anomaly run.

Let us recall that wavenumber 2 and 3 "lock in" by imposing the Pacific SST anomalies of 1976-1977 winter in the anomaly run. The spectral energetics of wavenumber 2 and 3 in January 1963 and the anomaly run is similar. We may speculate that the mechanisms to cause the "lock-in" of these two waves in these two cases may be the same. However, the pattern of Pacific SST anomaly in the 1962-1963 winter was an extensive and persistent warmth over central

and eastern North Pacific (Namias, 1963) which is not the same as that of 1976-1977 winter.

(B) January - February 1977

Synoptics and spectral analysis

The main features of atmospheric circulation in 1976-77 winter were very persistent through the whole season (Taubensee, 1977; Wagner, 1977; Dickson, 1977). The mean 700 mb circulation of this winter is shown in Figure 7 (Namias, 1978). Deep troughs persisted over the central Pacific ocean and eastern North American while a strong persistent open blocking ridge located near the west coast of North America. Therefore, the warm air was channeled to Alaska by the southerly to the west of the ridge and the cold artic air accompanying with heavy snows was brought to the northeast and droughts also occurred in the west. In addition, some blockings occurred over the North Atlantic and the pole in January and February.

The spectral analysis of wave motions are illustrated by the 500 mb SF Hovmöller diagrams at 50°N, Figure 18. The total-wave SF Hovmöller diagram presents two very persistent blocking ridges: a very strong narrow blocking ridge between 90°W-150°W and a broad weak blocking ridge between 30°W-90°E. The long-wave SF Hovmöller diagram explain the major feature of the blocking ridges as we have seen in the anomaly run. The strong narrow blocking ridge between 90°W-150°W existed since the first week of January 1977 and decayed at the end of the third week of February. The short-wave SF Hovmöller diagram show that the small waves have strong eastward propagation. However, exception occurs between 120°W and 120°E, i.e. over the Pacific, where the ridges and troughs composed of short waves becomes relatively stationary. Namias (1978) claimed that the significant west-east Pacific SST gradient enhanced the

cyclogensis and the upper level southerly which steered the storm northward. The quasi-stationarity of short-wave ridges and troughs may manifest that the cyclogensis occurs in the same areas very often. This feature is also found in the anomaly run.

The SF Hovmöller diagrams of individual waves are also displayed in Figure 15d-h. All long waves (n=1-4), during January-February 1977 at 50°N were quasi-stationary. The two-month mean locations of these long-wave ridges are very close to Eliasen's (1958) values which are displayed in Figure 1 of Austin (1980). It is interesting to note that the very strong narrow blocking ridge decayed when wavenumber 3 and 4 became moving and weak.

Let us compare the SF Hovmöller diagrams of individual long waves in the anomaly run, Figure 3, and those during January-February 1977. The ridge of model wavenumber 1 is located around 60°W, when this wave becomes stationary in the anomaly run. The ridge of observational wavenumber 1 is located around 0° of longitude. This discrepancy may be due to the difference of seasonal forcing between the model simulation and observation. When wave-number 2 and 3 become stationary in the anomaly run the ridge positions of these two waves are very close to Eliasen's observation. Wavenumber 4 is essentially eastward moving wave in the anomaly run. The effect of the Pacific SST anomalies make wavenumber 2 and 3 stationary in the positions as these two waves found either in January-February 1977 or in Eliasen's (1958) study.

Energetics*

Our energetics computations for January-February 1977 reveal that time variations of A_E and K_E were not very significant, and A_Z and K_Z increased somewhat in February (not shown). The slight enhancement of A_Z and K_Z is due to the intensity decrease of the persistent trough and ridge in this winter (Dickson, 1977). Figure 18 shows that an Atlantic blocking existed in the first ten days of January. Time variations of various energies during this period of time are the same as Lejenäs' schematic diagram, Figure 5.

Lorenz energy cycle of these two months is depicted in Figure 19. The directions of various energy conversions are the same as conventional studies. A remarkable difference between the energy cycle of January-February 1977 and that of the anomaly run is $C(K_E, K_Z)$. $C(K_E, K_Z)$ is negative in the anomaly run, while it is positive in January-February 1977. In other words, the eddies of this winter is barotropically stable. Namias (1978) suggests that the seasonal forcing is another factor to decide the atmospheric circulation pattern. The contrast of $C(K_E, K_Z)$ between January-February 1977 and the anomaly run seems to indicate again that the seasonal forcing of the GLAS model is different from 1976-1977 winter. In addition, Rosen and Salstein (1980) pointed out that 1976-1977 winter has strong $C(K_E, K_Z)$ which is due to the highly amplified nature of atmospheric waves.

The spectral energetics of January-February 1977 is displayed in Figure 20. A_3 is somewhat smaller than A_1 and A_2, but K_3 is comparable to K_1 and

---

*The computations use the observational data analyzed by the National Meteorological Center (NMC) and archived at the National Center for Atmospheric Research (NCAR). The region of integration covers 30°-80°N. The ω fields, which were used to calculate $C(A_E, K_E)$, were evaluated by the scheme proposed by Chen et al. (1981).

blocking ridge in the west coast of North America is mainly due to the constructive interference of wavenumber 2 and 3. In order to compare with the energetics of anomaly run, we shall focus on these two waves. $C(A_Z, A_2)$ and $C(A_Z, A_3)$ dominate $C(A_Z, A_E)$ and are the sources to supply A_2 and A_3, respectively. K_2 and K_3 are maintained by $C(A_2, K_2)$ and $C(A_3, K_3)$, respectively. The most pronounced difference of spectral energetics between these two waves is that K_3 has a large energy sink, $C(K_3, K_Z)$ which explains 45% of $C(K_E, K_Z)$. Note that $C(K_2, K_Z)$ is small compared to $C(K_3, K_Z)$. The comparison of $C(K_3, K_Z)$ between this winter and the anomaly run shows that wavenumber 3 is barotropically stable in January-February 1977, and barotropically unstable in the anomaly run. In other words, wavenumber 3 has opposite physical functions in these two atmospheric circulations.

6. Concluding remarks and discussion

The general circulation model of the Goddard Laboratory for Atmospheric Sciences was used to test the model response to a Pacific sea surface temperature (SST) anomaly. Two experiments were performed: (1) control run in which the climatological mean SST compiled by Washington and Thiel (1971) was used, and (2) anomaly run in which an invarient Pacific SST anomaly of 1976-1977 winter compiled by Namias (1978) was imposed on the control run.

The ridges and troughs appearing in control run are amplified and become stationary in anomaly run. The most pronounced difference between these two runs is that the Pacific SST anomalies seem to change the behavior of long waves. The spectrally filtered Hovmöller diagram is employed to examine the propagation and amplification of long waves. It is found that wavenumber 2 and 3 in the anomaly run became stationary around the climatological locations

of observational study (Austin, 1980). The constructive interference of wavenumber 2 and 3 in the anomaly run forms two persistent open blocking ridges: one is in the west coast of North America and the other in the western Europe.

Since the persistent blocking ridges can be formed by the constructive interference of stationary long waves, the next problem we have to examine is how these persistent blocking ridges are amplified and maintained. The spectral energetics is carried out to answer this problem. Firstly, the total energy budget analysis displays that the time variation of the blocking ridge energetics over its life span is the same as that during the typical blocking situation as sketched by Lejenäs (1977). Spectral energetics of wavenumber 2 and 3 shows that A_2 and A_3 are supplied by $C(A_Z, A_2)$ and $C(A_Z, A_3)$, respectively. Note that $A_3 < A_2$ may be caused by $C(A_Z, A_3) < (C(A_Z, A_2)$. K_2 is provided by $C(A_Z, K_2)$, while K_3 is maintained by $-C(K_3, K_Z)$. In other words, K_2 is furnished by baroclinic energy conversion and K_3 is supplied by barotropic energy conversion.

Tung and Lindzen (1979) pointed out that the severe weather patterns of January 1963 and 1976-1977 winter were similar to some extent. Since the pattern of the pacific SST anomaly used in anomaly run is 1976-1977 winter, it would be of interest to compare the spectral analysis and energetics between the anomaly run and these two winters. The spectral energetics studies of Wiin-Nielsen (1964), Wiin-Nielsen et al. (1964), and Murakami and Tomatsu (1965) show that the energetics of wavenumber 2 and 3 is similar to the anomaly run, especially wavenumber 3 in January 1963 was vitally furnished by the barotropic energey conversion $-C(K_3, K_Z)$. The anomaly run began from January 1. We, therefore, start the spectral analysis and energetics of

1976-1977 winter from the same day. First of all, the spectrally filtered Hovmöller diagrams show that long waves (n=1-4) are stationary over most of this time period. The open blocking ridge located in the west coast of North America in this winter was mainly formed by the constructive interference of wavenumber 2, 3 and 4, especially 2 and 3. The blocking ridge decayed when these wavenumber 3 and 4 became moving. The development and maintenance of wavenumber 2 and 3 in this winter is different in some way from either in January 1963 or the anomaly run. A_n and K_n of wavenumber 2 and 3 are supported by $C(A_Z, A_n)$ and $C(A_n, K_n)$ respectively. On the other hand, K_3 is very significantly depleted by $C(K_3, K_Z)$. That is, wavenumber 3 is barotropically stable in this winter. It is opposite to the dynamical behavior of wavenumber 3 either in January 1963 or the anomaly run.

The summary provided above indicates that the necessary condition to have blocking ridges formed is the constructive interference of stationary long waves. The other condition for the formation of blocking ridges is how these long waves are amplified and maintained. The spectral energetics of blocking ridges shows that the amplification and maintenance of stationary long waves can be due to various physical processes: baroclinic and barotropic. In fact, it is also possible due to nonlinear interaction between cyclone-scale and planetary-scale waves as proposed by Gall et al. (1979) in a numerical experiment and observed by Hansen and Chen (1981) in diagnostic analysis of observational study.

Namias (1978) suggests that the Pacific SST anomaly of 1976-1977 winter is an important factor to cause the persistent blocking ridge in the west coast of North America. His hypothesis is confirmed by the numerical experiments analyzed in this study. In other words, the SST anomaly may

cause the stationarity of ultralong waves. It has been a well known problem in the sophisticated atmospheric model that the energy content of long waves are too small compared to observational study. This problem is also found recently in the GLAS model (Chen et al., 1981) and the operational model of European Center for Medium Range Weather Forecasts (Hollingsworth et al., 1980). Although Spar (1973a, b) and Spar and Atlas (1975) show that SST anomaly may not improve very much the long-term forecast using the GISS atmospheric model, our present analysis indicates that the careful treatment of the SST anomaly may be important to the simulation of long waves which may in turn improve the long-term forecast.

It has been observed that the stratospheric major warming always associated with the tropospheric blocking (e.g. Labitzke, 1967; Schoeberl, 1979). Our present analysis and observational study of Austin (1980) show that the persistent open blocking ridges or Rex-type blockings are established due to the constructive interference of stationary long waves. It is shown in the anomaly run that the SST anomalies may force long waves stationary. The introduction of SST anomalies to a general circulation with stratosphere may increase the possibility of success to simulate the stratospheric warming as Miyakoda et al. (1970).

Acknowledgment

The authors appreciate the help provided by Mrs. Hal Marshall and J. E. Nielsen. This study is supported by the NASA grant NSG-5339.

References

Arakawa A., 1972: Design of the UCLA atmospheric general circulation model. Tecn. Rep. No. 7, Department of Meteorology, University of California, Los Angeles.

Austin, J. F., 1980: The blocking of middle latitude westerly winds by planetary waves. Quart. J. R. Met. Soc., 106, 327-350.

Bjerknes, J., 1966: A possible response of the atmospheric Hadley circulation to equatorial anomalies of ocean temperature. Tellus, 18, 820-829.

_____, 1969: Atmospheric teleconnections from the equatorial pacific. Mon. Wea. Rev., 97, 163-172.

Chen, T.-C., H. G. Marshall and J. Shukla, 1981: Spectral analysis and maintenance of large-scale moving waves by nonlinear interactions at 200 mb in the GLAS general circulation model. Mon. Wea. Rev. (In press).

_____, A. R. Hansen and J. J. Tribbia, 1981: A note on the release of available potential energy. J. Meteor. Soc. Japan (submitted).

Chervin, R. M., W. M. Washington and S. H. Schneider, 1976: Testing the statistical significance of the response of the NCAR general circulation model to North Pacific Ocean surface temperature anomalies. J. Atmos. Sci., 33, 413-423.

_____, J. E. Kutzbach, D. D. Houghton and R. G. Gallimore, 1980: Response of the NCAR general circulation model to prescribed changes in ocean surface temperature. Part II: Midlatitude and subtropical changes. J. Atmos. Sci., 37, 308-332.

Dickson, R. R., 1977: Weather and circulation of February 1977 - Widespread drought. Mon. Wea. Rev., 105, 684-689.

Eliasen, E., 1958: A study of the long atmospheric waves on the basis of zonal harmonic analysis. Tellus, 10, 206-215.

Gall, R., R. Blakeslee and R. C. J. Somerville, 1979: Cyclone-scale forcing of ultralong waves. J. Atmos. Sci., 36, 1692-1698.

Gates, W. L., 1972: The January global climate simulated by the two-level Mintz-Arakawa model: a comparison with observation. Rept. R-1005-ARPA, Rand Corporation.

Halem, M., J. Shukla, Y. Mintz, M. L. Wu, R. Godbale, G. Herman, and Y. Sud, 1978: Comparisons of observed seasonal climate features with a winter and summer numerical simulation produced with the GLAS general circulation. Proceedings of the JOC Study Conference on Climate Models. April 3-7, 1978. Washington, D.C.

Hansen, A. R. and T.-C. Chen, 1981: Spectral energetics of atmospheric blocking. (Submitted to Mon. Wea. Rev.)

Harnack, R. P., 1980: An appraisal at the circulation and temperature pattern for winter 1978-79 and a comparison with the previous two winters. Mon. Wea. Rev., 108, 37-55.

Hollingsworth, A., K. Arpe, M. Tiedtke, M. Capaldo and H. Savjarvi, 1980: The performance of a medium-range forecast model in winter - impact of physical parameterizations. Mon. Wea. Rev., 108, 1736-1773.

Houghton, D. D., J. E. Kutzbach, M. McClintock and D. Suchman, 1974: Response of a general circulation model to a sea temperature perturbation. J. Atmos. Sci., 31, 857-868.

Hovmäller, E., 1949: The trough-and-ridge diagram. Tellus, 1, 62-66.

Kutzbach, J. E., R. M. Chervin and D. D. Houghton, 1977: Response of the NCAR general circulation model to prescribed changes in ocean surface temperature. Part I: Midlatitude changes J. Atmos. Sci., 34, 1200-1213.

Labitzke, K., 1965: On the mutual relation between stratosphere and troposphere during periods of stratospheric warmings in winter. J. Appl. Meteor., 4, 91-99.

Lejenäs, H., 1977: On the breakdown of the westerlies. Atmosphere, 15, 89-113.

Miyakoda, K., 1963: Some characteristic features of winter circulation in the troposphere and the lower stratosphere. Univ. of Chicago Tech. Rept. No. 14 (Dec.).

Murakami, T., R. F. Strickler and G. D. Hembree, 1970: Numerical simulation of the breakdown of a polar-night vortex in the stratosphere. J. Atmos. Sci., 27, 139-154.

_____, and K. Tomatsu, 1965: Energy cycle in the lower atmosphere. J. Meteor. Soc. Japan, 43, 73-89.

Namias, J., 1963: Large-scale air-sea interactions over the North Pacific from summer 1962 through the subsequent winter. J. Geophys. Res., 15, 6171-6186.

_____, 1970: Macroscale variations in sea-surface temperatures in the North Pacific. J. Geophys. Res., 75, 565-582.

_____, 1978: Multiple causes of the North American abnormal winter 1976-1977. Mon. Wea. Rev., 106, 279-295.

Phillips, N., 1957: A coordinate system having some special advantages for numerical forecasting. J. Meteor., 14, 184-185.

Taubensee, R. E., 1977: Weather and circulation of December 1976. Mon. Wea. Rev., 105, 368-373.

Tung, K. K. and R. S. Lindzen, 1979: A theory of stationary long waves. Part I: A simple theory of blocking. Mon. Wea. Rev., 107, 714-734.

Wagner, A. J., 1979: Weather and circulation of January 1977. Mon. Wea. Rev., 105, 553-560.

Wintson, J. S. and A. F. Krueger, 1961: Some aspects of a cycle of available potential energy. Mon. Wea. Rev., 81, 307-318.

Wiin-Nielsen, A., 1964: Some new observational studies of energy and energy transformations in the atmosphere. World Meterol. Organization, Tech. Note 66, Geneva, 177-207.

_____, J. A. Brown and M. Drake, 1964: Further studies of energy exchange between the zonal flow and eddies, Tellus, 16, 168-180.

Wu, M. L., 1980: The exchange of infrared radiative energy in the troposphere. J. Geophys. Res., 85, 4084-4090.

Appendix:

The spectral energy equations (1)-(4) can be illustrated by the following energy diagram, Figure A1. The notations used have been explained in Section 4.

Figure Captions

Figure 1. Observed Pacific sea surface temperature anomalies (°F) during the winter of 1976-1977 (after Namias, 1978).

Figure 2. Two-week (February 1-14) mean height fields: (a) 850 mb control run, (b) 850 mb anomaly run, (c) 500 mb control run, and (d) 500 mb anomaly run.

Figure 3. Spectrally filtered Hovmöller diagrams at 500 mb and 50°N for three wave groups: (a) wavenumber 1-15, (b) wavenumber 1-4, and (c) wavenumber 5-15.

Figure 4. Spectrally filtered Hovmöller diagrams at 500 mb and 50°N for four ultralong waves and combination of wavenumber 2 and 3.

Figure 5. Spectrally filtered synoptic charts of height and temperature of wavenumber 2, 3 and combination of them at 500 mb on February 4.

Figure 6. Time variations of energies: (a) A_Z and A_E, (b) K_Z and K_E, and (c) energy conversions: $C(A_Z, A_E)$, $C(A_E, K_E)$ and $C(K_E, K_Z)$.

Figure 7. Schematic picture of the energy changes and energy conversions during a blocking situation. Day $t = t_o$ is the onset of the blocking (after Lejenäs, 1977).

Figure 8. Time variation of (a) zonal flow and (b) zonal temperature at 500 mb for the anomaly run.

Figure 9. Time variation of momentum transport by wavenumber 2, $\overline{uv}(2)$, and by wavenumber 3, $\overline{uv}(3)$, at 500 mb for the anomaly run.

Figure 10. The same as Figure 9, except for sensible heat transport, i.e. $\overline{vT}(2)$ and $\overline{vT}(3)$.

Figure 11. Geographic distribution of $\overline{uv}$, $\overline{vT}$ and $\overline{\omega T}$ for wavenumber 2, 3 and combination of them at 500 mb on February 4.

Figure 12. Time variation of (a) available potential energy and (b) kinetic energy for wavenumber 1, 2, 3 and 4 in the anomaly run.

Figure 13. Spectral energetics of (a) wavenumber 2 and (b) wavenumber 3 in the anomaly run.

Figure 14. Average contours of 700 mb surface (tens of feet) for January 1963. Troughs are indicated by solid lines (after O'Connor 1963).

Figure 15. Energetics of January 1963: (a) time variation of A_Z and A_E, (b) time variation of K_Z and K_E, and (c) Lorenz energy cycle (after Wiin-Nielsen, 1964). Unit of energy conversions: Wm^{-2}.

Figure 16. Spectral energetics of January 1963: (a) A_E spectrum, (b) K_E spectrum, (c) $C(A_Z, A_n)$ spectrum, (d) $C(K_n, K_Z)$ spectrum and (e) time variation of $C(A_n, K_n)$. These figures are extracted from various studies: (a) and (b) from Wiin-Nielsen (1964), (c) and (d) from Wiin-Nielsen et al. (1964), and (e) from Murakami and Tomatsu (1965).

Figure 17. Mean 700 mb contours (tens of feet) of winter 1976-77 (December, January, and February) (after Namias, 1978).

Figure 18. Spectrally filtered Hovmöller diagrams at 500 mb and 50°N for January-February 1977.

Figure 19. Energy cycle of January-February 1977. Unit of energy conversions: Wm^{-2}.

Figure 20: Spectral energetics of January-February 1977: (a) A_E spectrum, (b) K_E spectrum, (c) $C(A_Z, A_n)$ spectrum, (d) $C(A_n, K_n)$ spectrum, (e) $C(K_n, K_Z)$ spectrum, (f) $CA(N|m,\ell)$ and (g) $CK(n|m,\ell)$.

Figure A1. Schematic energy diagram for wavenumber n.

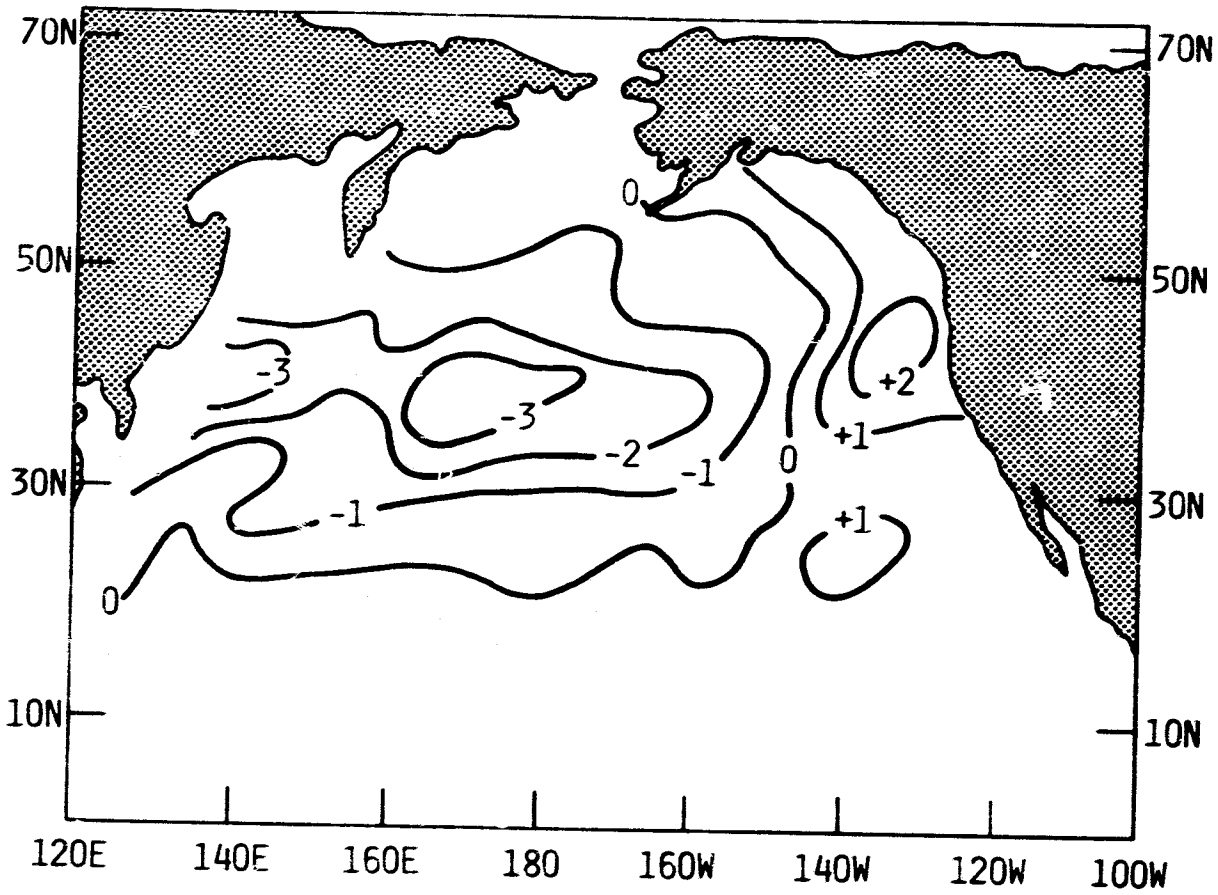
70N
50N
30N
10N
120E
140E
160E
180
160W
140W
120W
100W
0
-3
-3
-2
-1
0
+1
+2
+1
-1
0

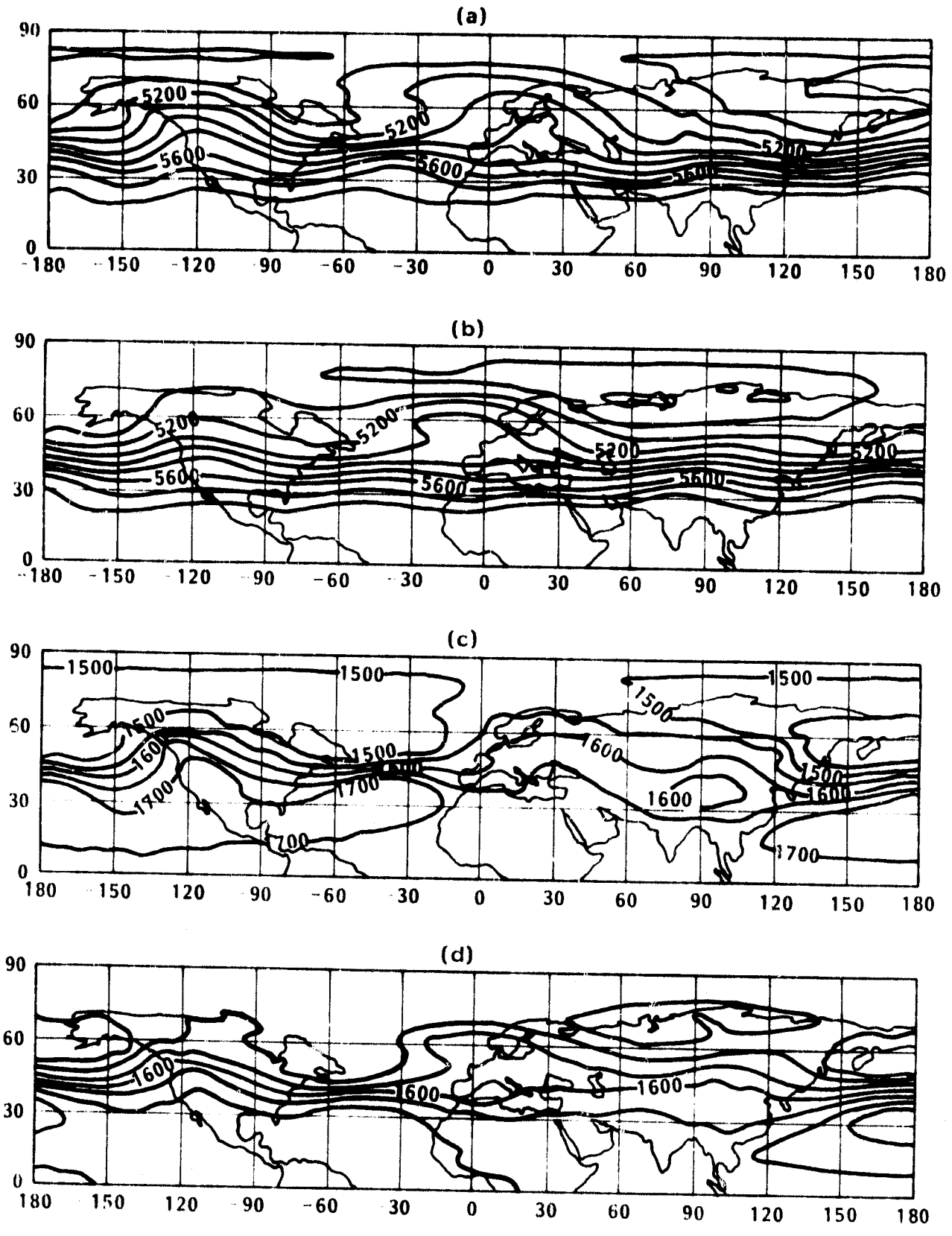
(a)
90
60
30
0
5200
5600
-180 -150 -120 -90 -60 -30 0 30 60 90 120 150 180
(b)
90
60
30
0
5200
5600
-180 -150 -120 -90 -60 -30 0 30 60 90 120 150 180
(c)
90
60
30
0
1500
1600
1700
180 150 120 90 -60 30 0 30 60 90 120 150 180
(d)
90
60
30
0
1600
180 150 120 90 -60 30 0 30 60 90 120 150 180

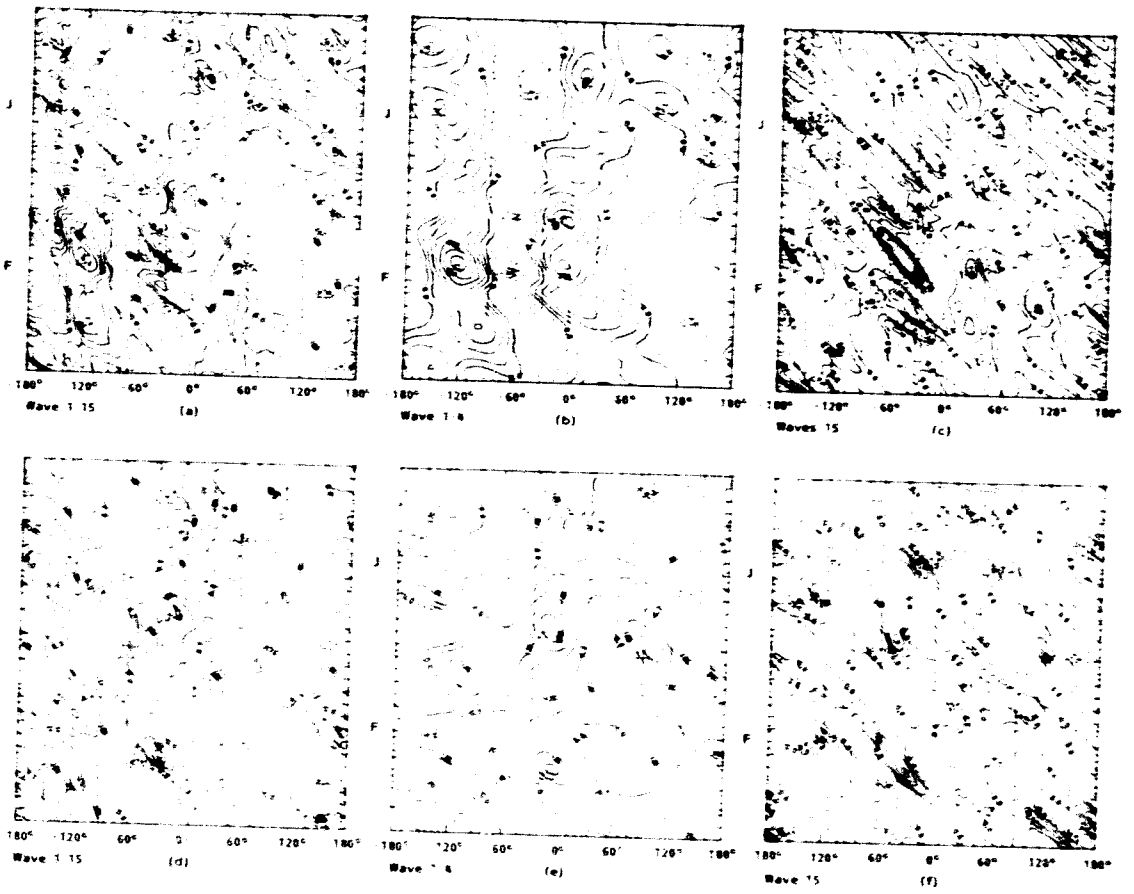
180° 120° 60° 0° 60° 120° 180°
(a)
(b)
(c)
(d)
(e)
(f)

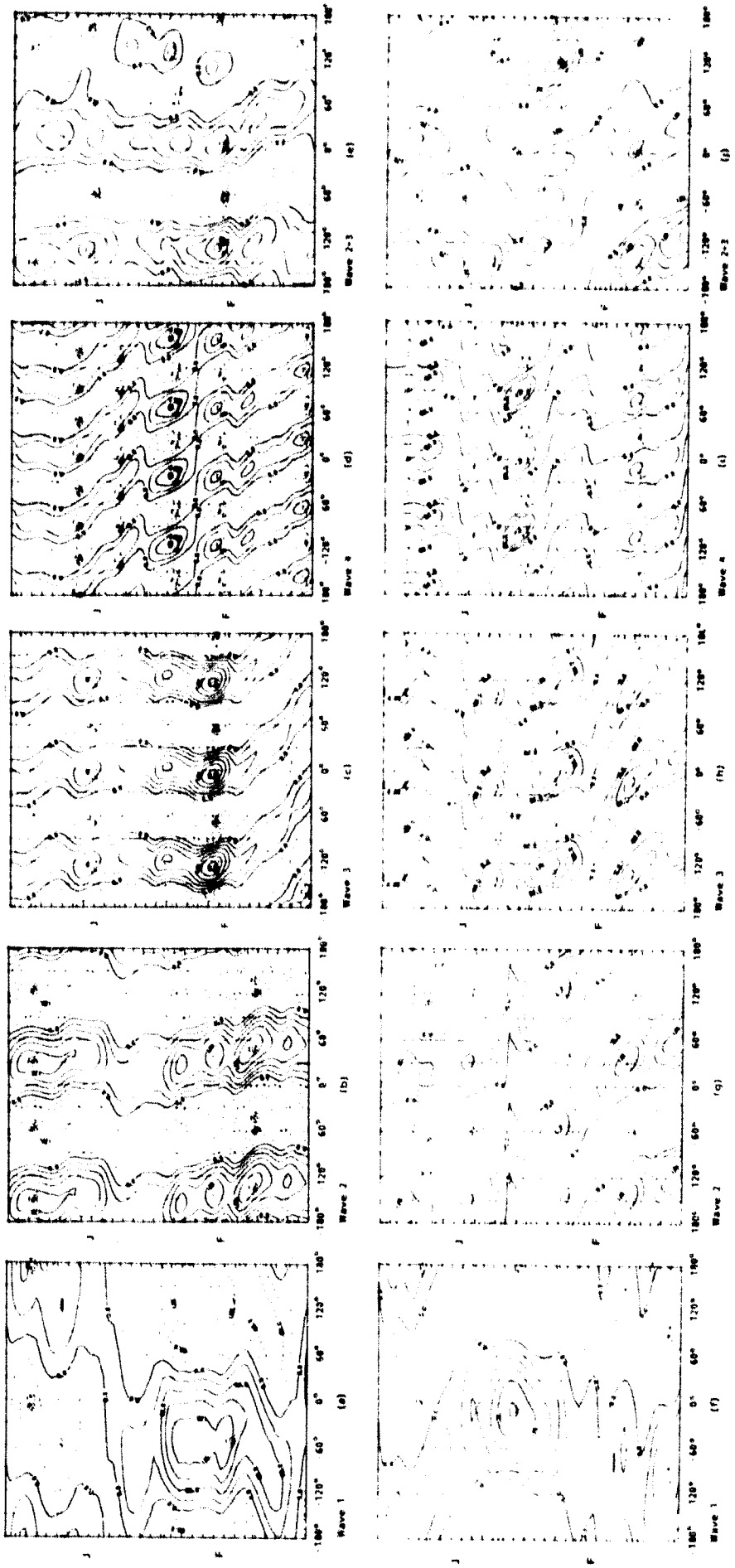

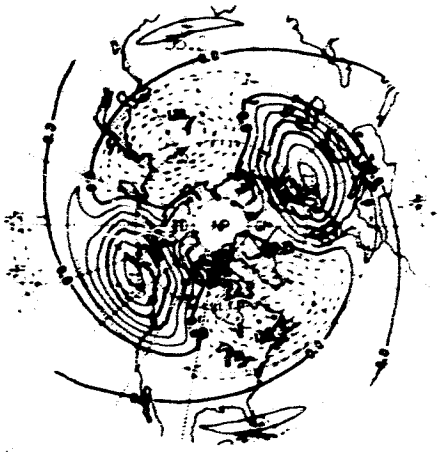

(a) Height Wave 2

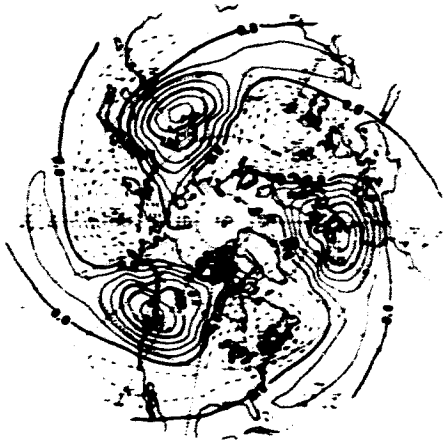

(b) Height Wave 3

(c) Height Wave 2+3

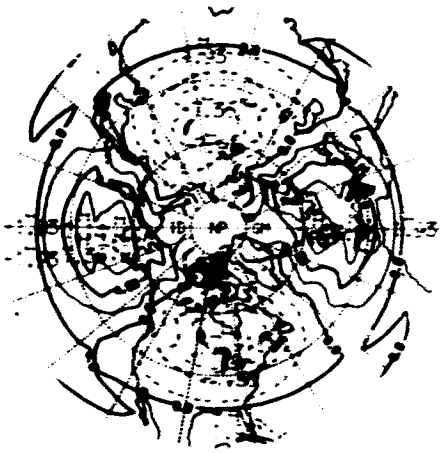

(d) Temperature Wave 2

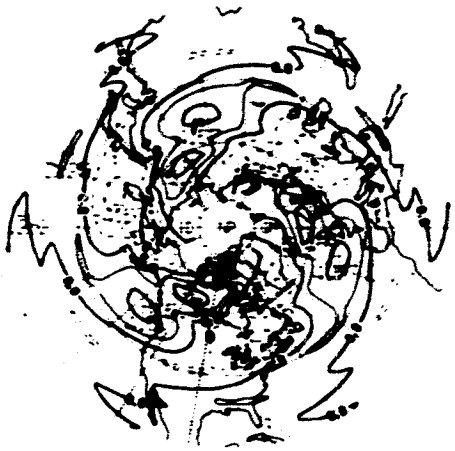

(e) Temperature Wave 3

(f) Temperature Wave 2+3

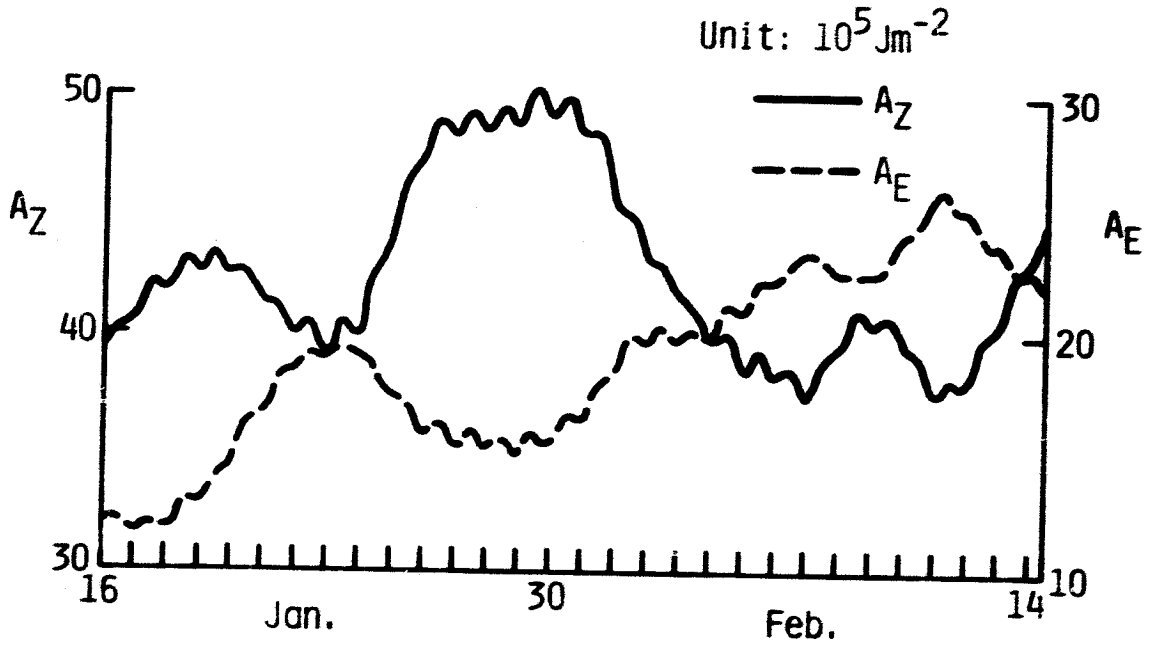

(a)

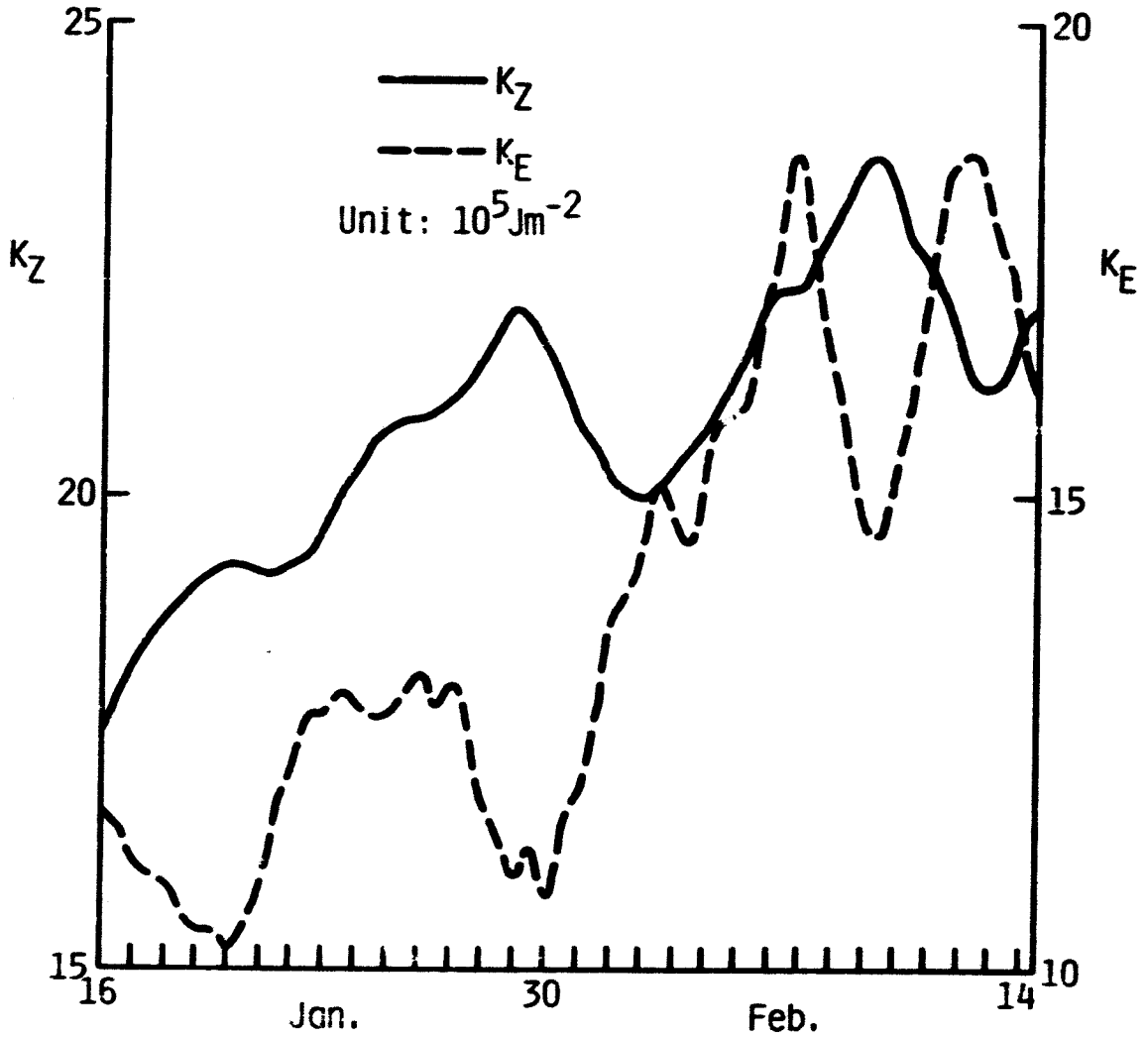

(b)

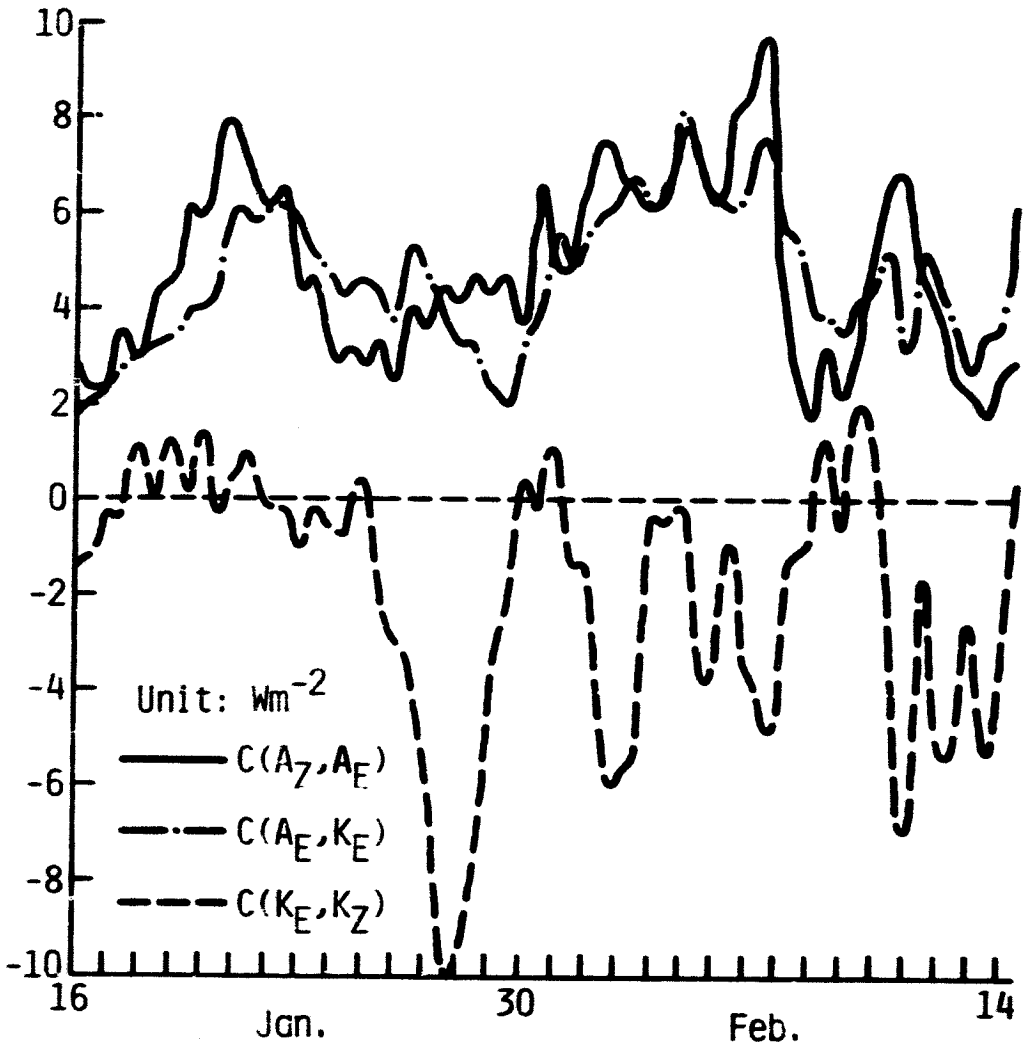

(c)

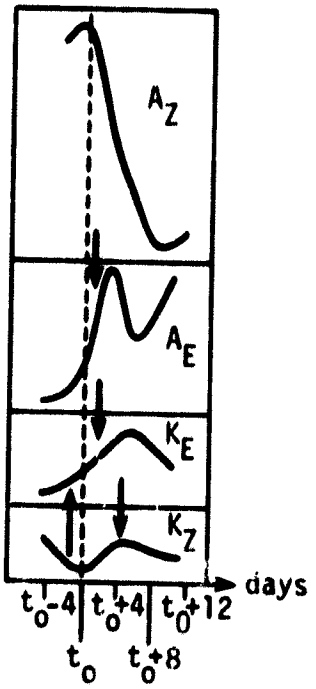
A_Z
A_E
K_E
K_Z
days
t_o-4
t_o+4
t_o+12
t_o
t_o+8

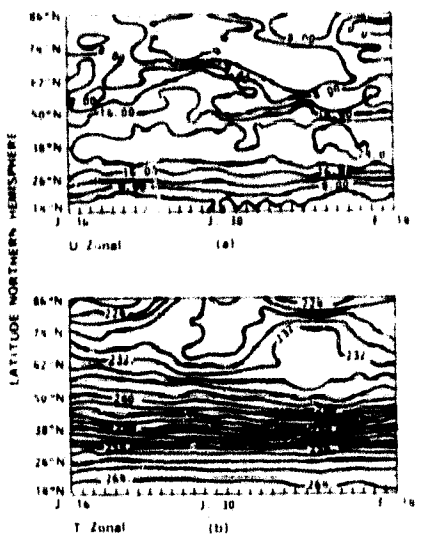
LATITUDE NORTHERN HEMISPHERE
U Zonal
(a)
T Zonal
(b)

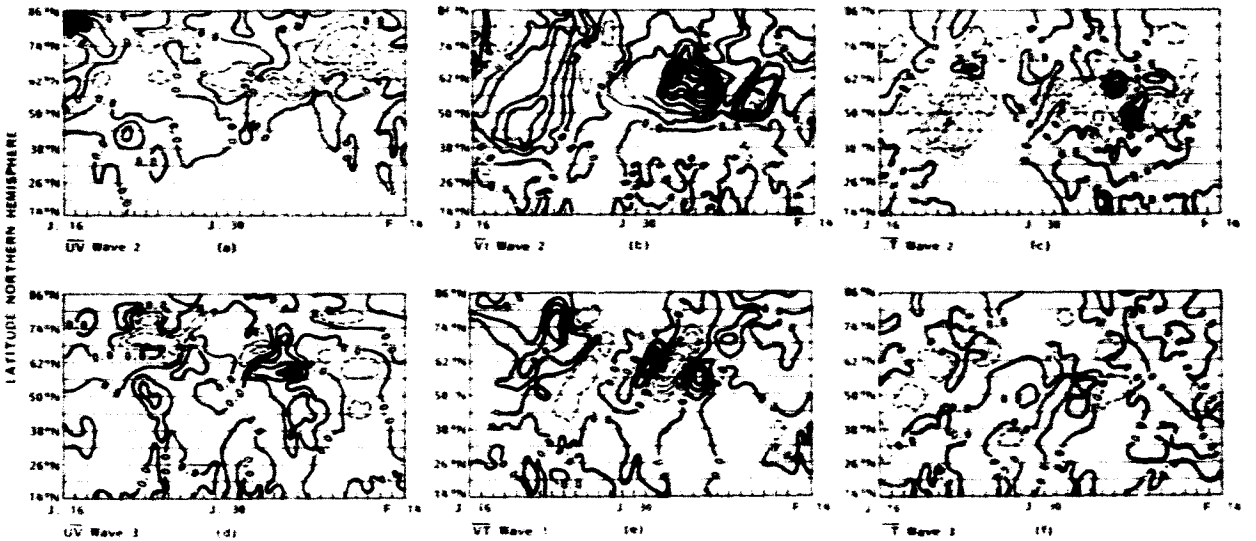
LATITUDE NORTHERN HEMISPHERE
J 16
J 30
F 13
(a)
(b)
(c)
(d)
(e)
(f)

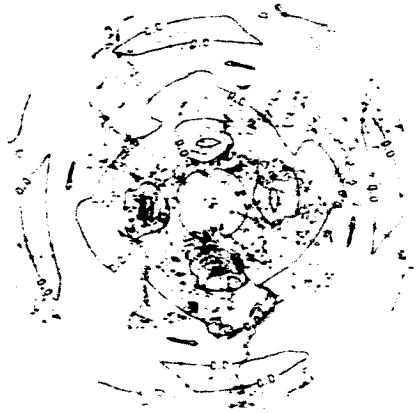

(a) UV Transport Wave 2

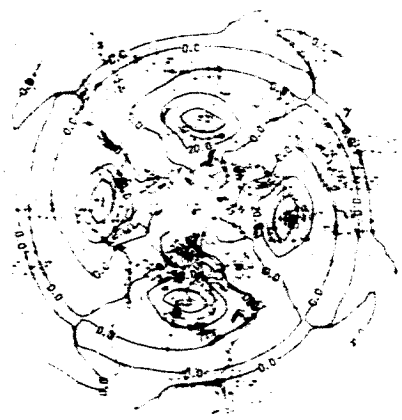

(b) VT Transport Wave 2

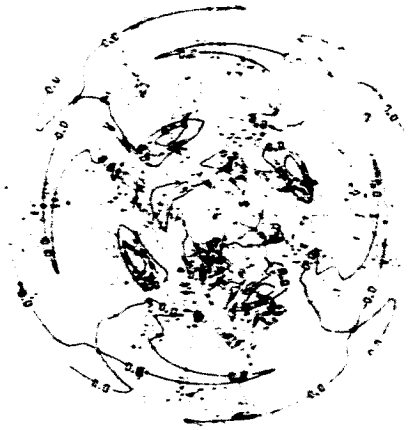

(c) ωT Transport Wave 2

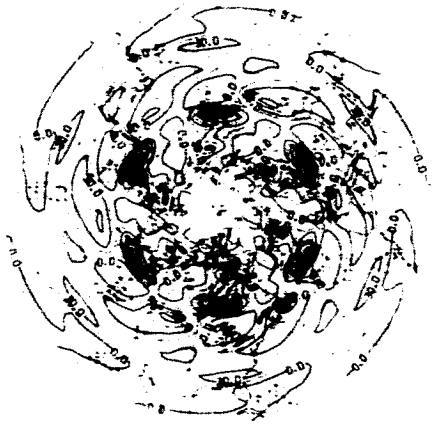

(d) UV Transport Wave 3

(e) VT Transport Wave 3

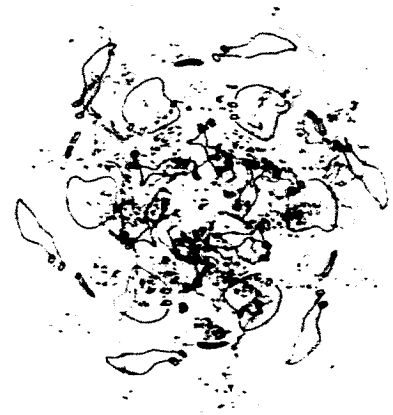

(f) ωT Transport Wave 3

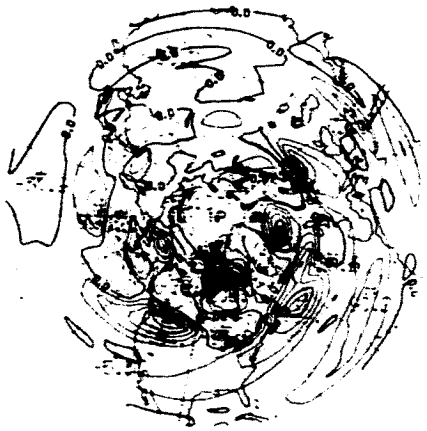

(g) UV Transport Wave 2+3

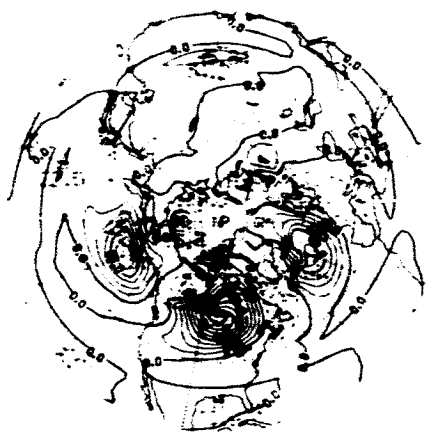

(h) VT Transport Wave 2+3

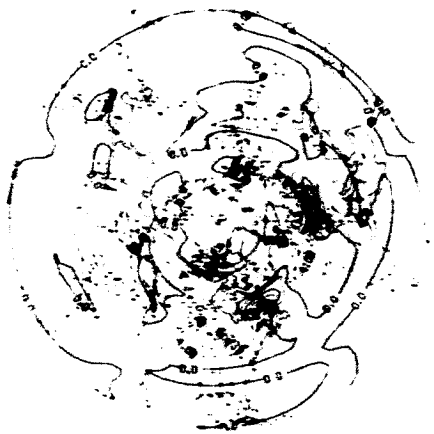

(i) ωT Transport Wave 2+3

C-2

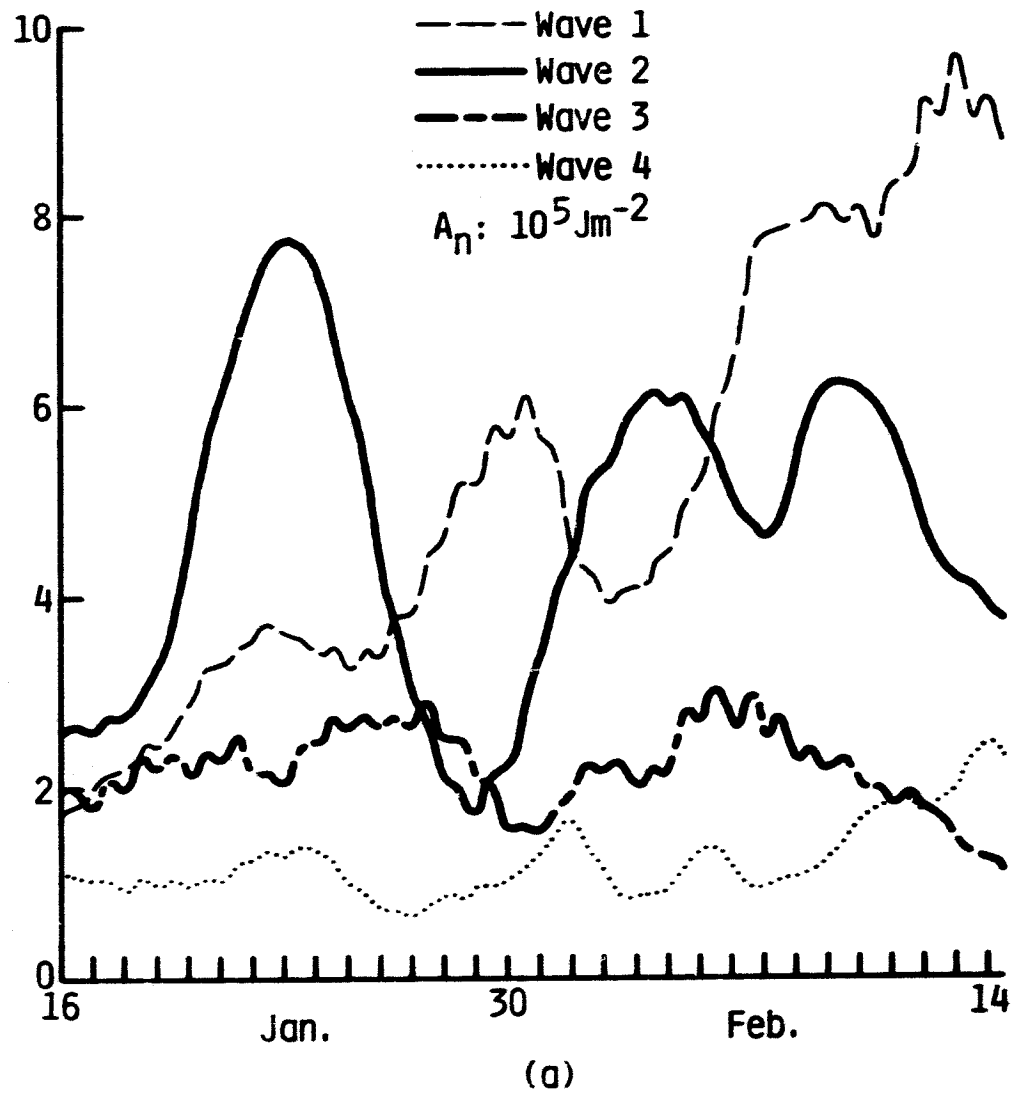

(a)

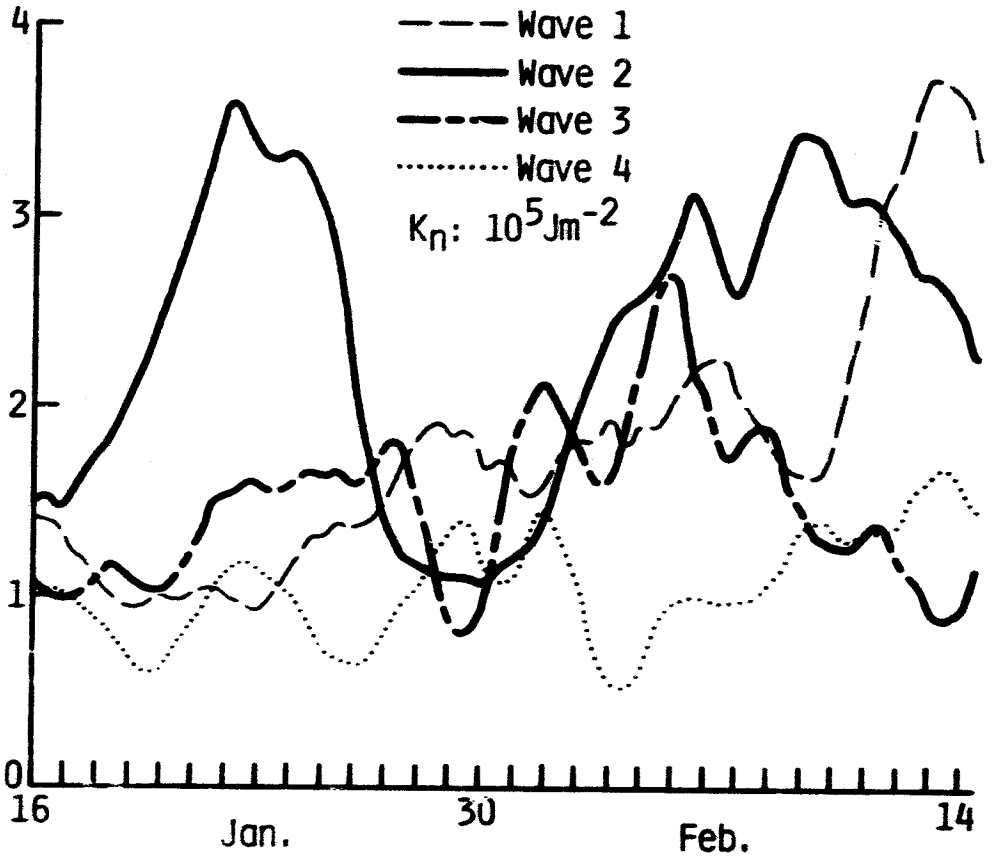

(b)

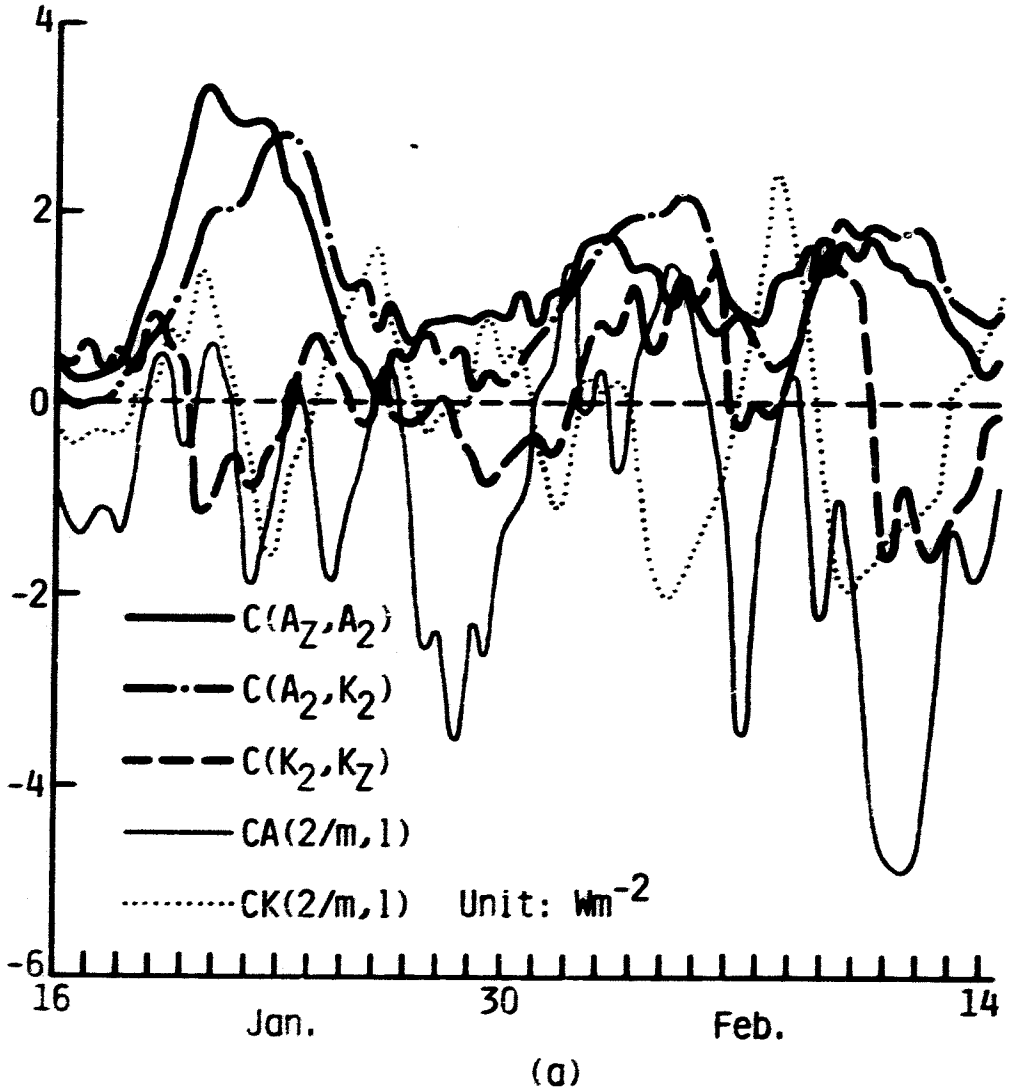
4
2
0
-2
-4
-6
16
Jan.
30
Feb.
14
C(A_Z,A_2)
C(A_2,K_2)
C(K_2,K_Z)
CA(2/m,1)
CK(2/m,1)
Unit: Wm^-2

(a)

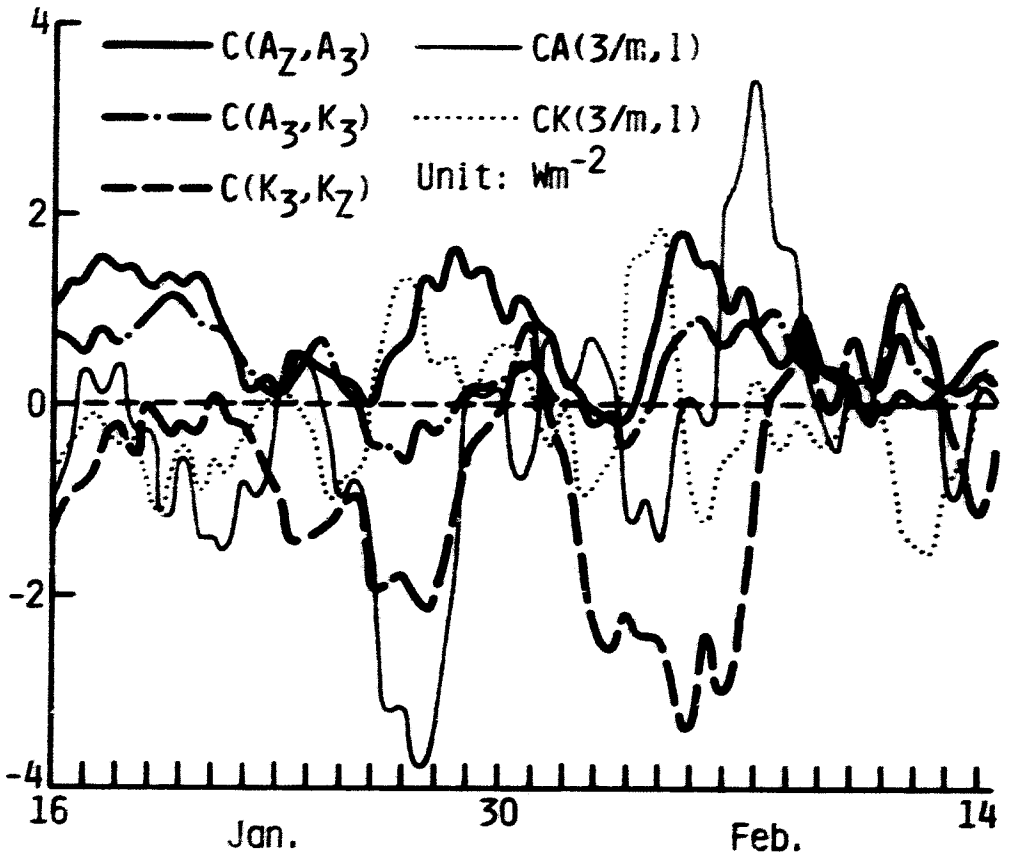

(b)

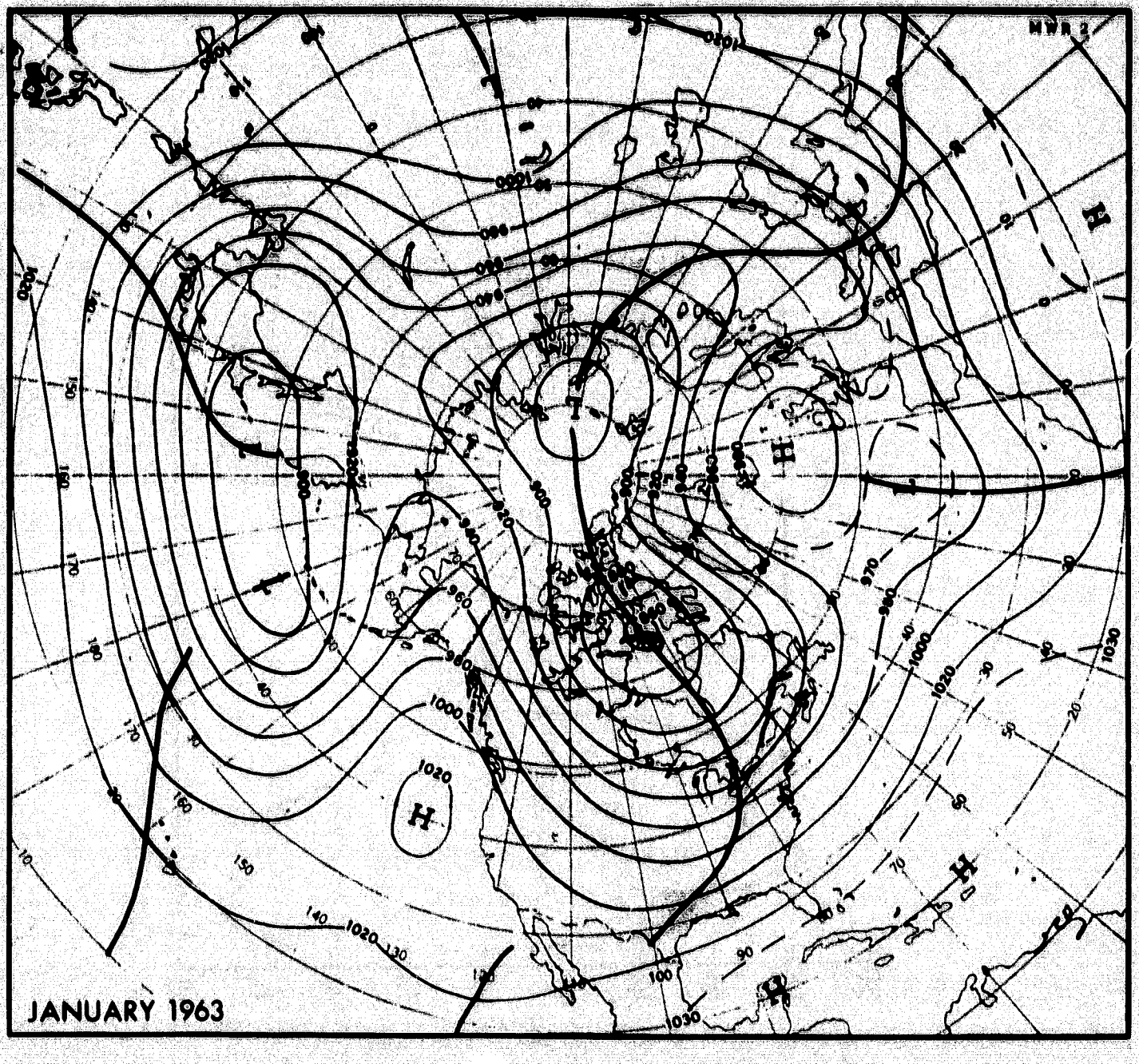
JANUARY 1963

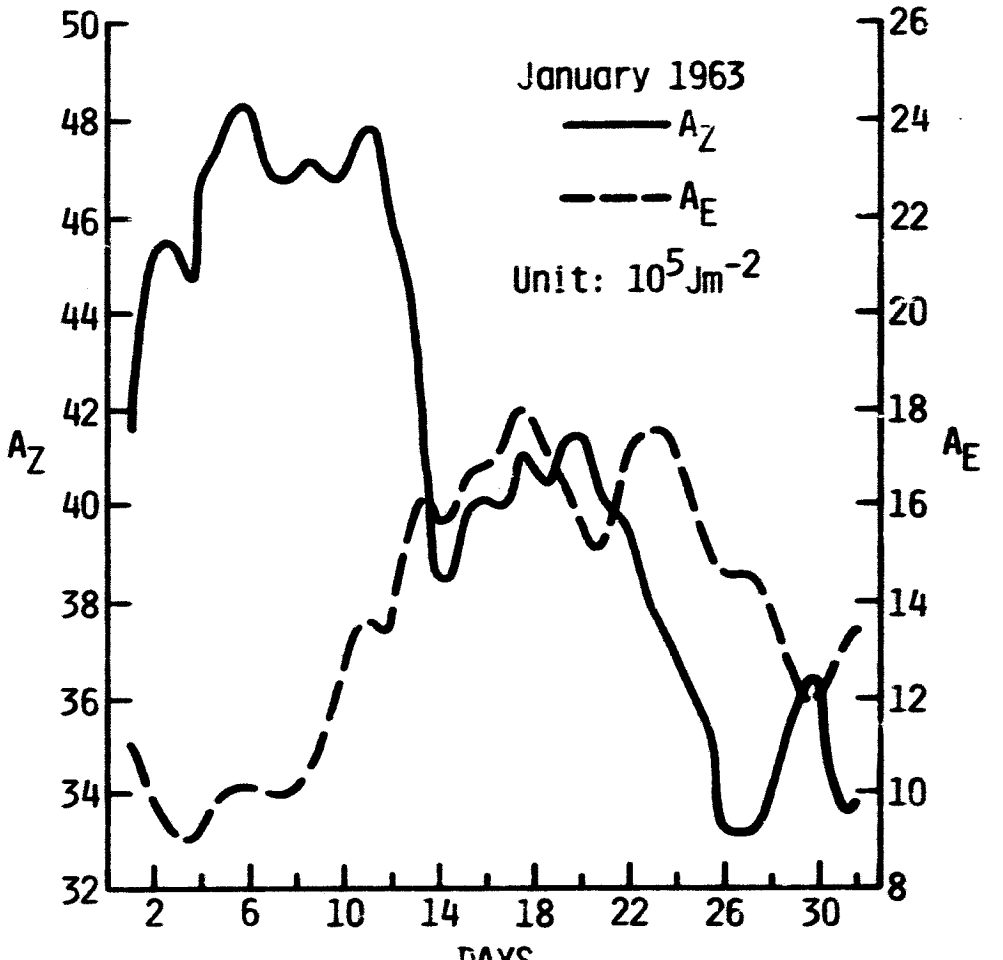
January 1963
A_Z
A_E
Unit: $10^5 Jm^{-2}$
A_Z
A_E
50
48
46
44
42
40
38
36
34
32
26
24
22
20
18
16
14
12
10
8
2
6
10
14
18
22
26
30
DAYS

(a)

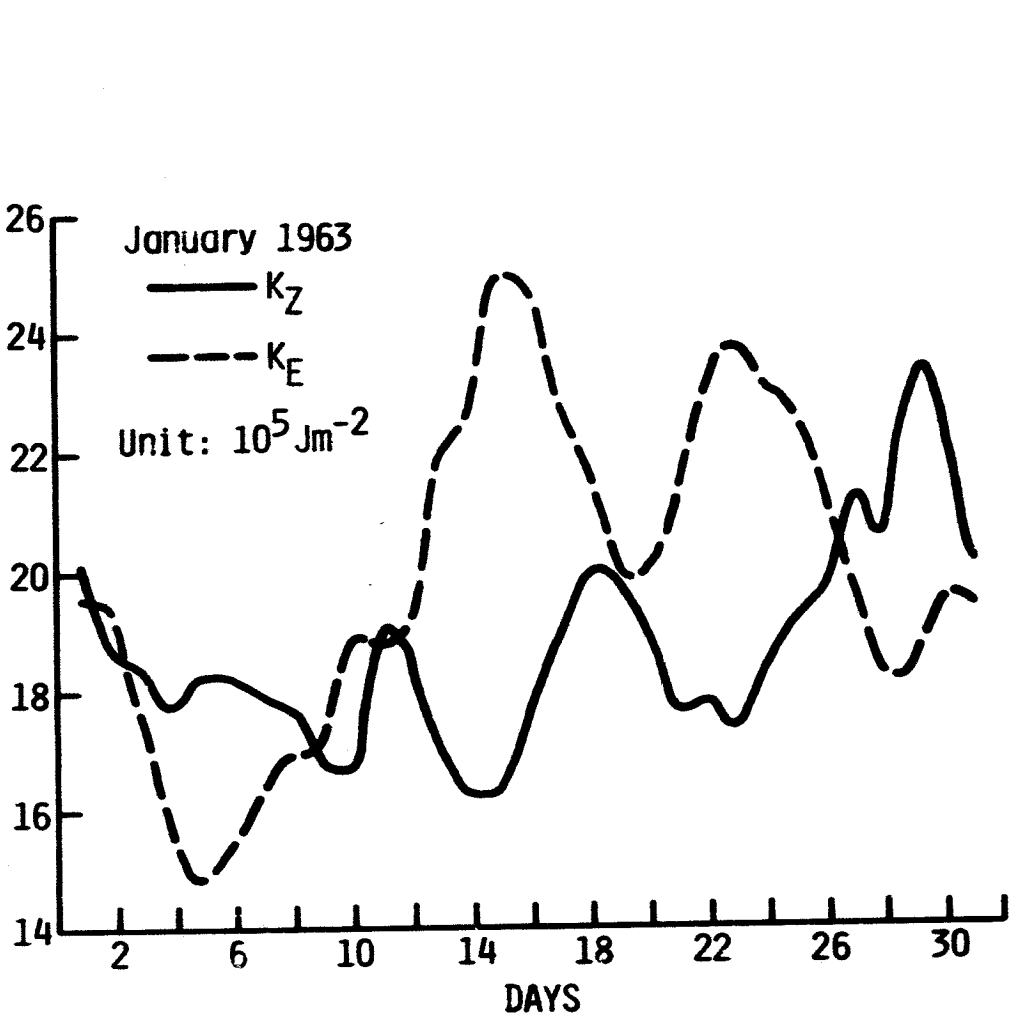
January 1963
K_Z
K_E
Unit: $10^5 Jm^{-2}$
26
24
22
20
18
16
14
2
6
10
14
18
22
26
30
DAYS

(b)

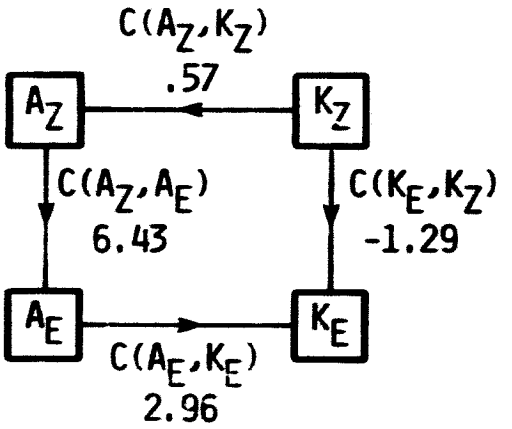

(c)

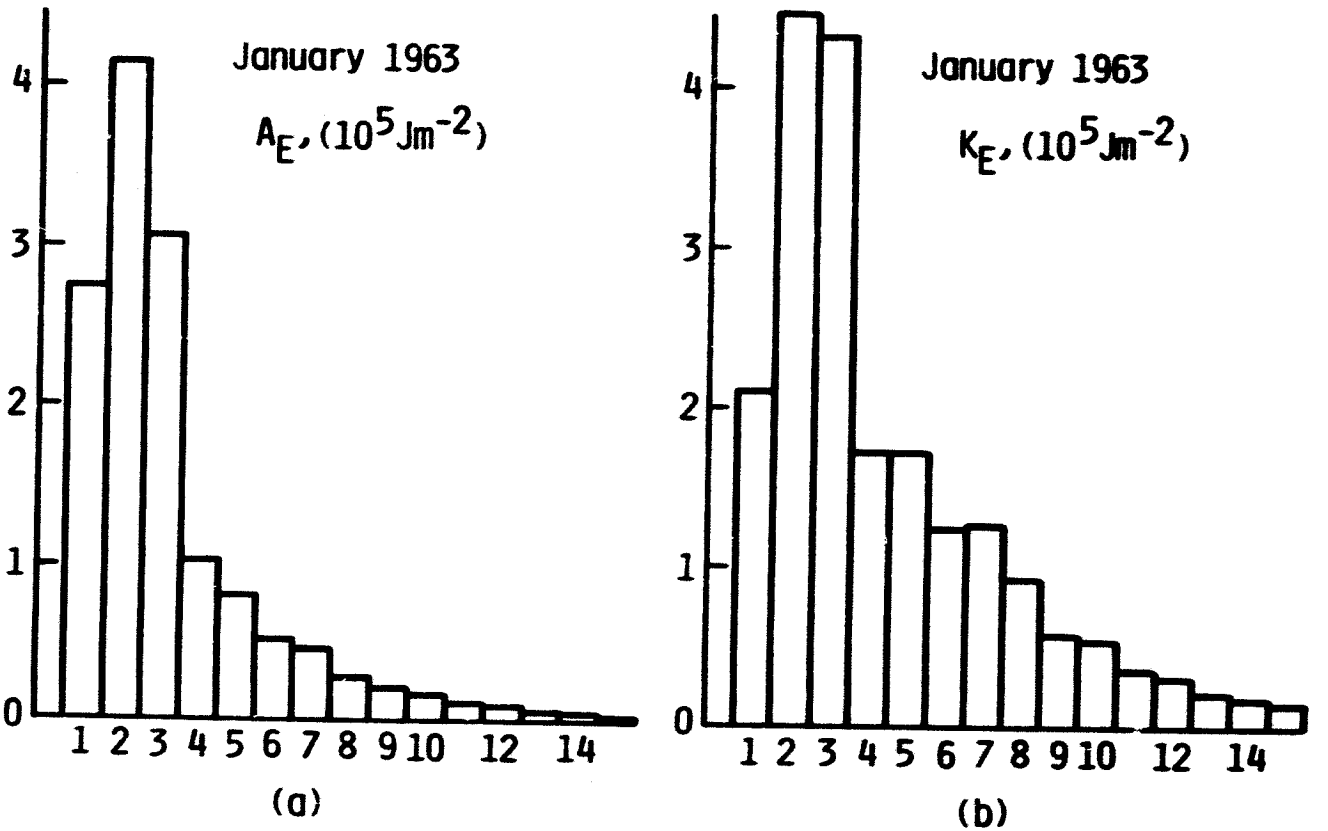
January 1963
A_E, (10^5 Jm^{-2})
0
1
2
3
4
1 2 3 4 5 6 7 8 9 10 12 14
(a)
January 1963
K_E, (10^5 Jm^{-2})
0
1
2
3
4
1 2 3 4 5 6 7 8 9 10 12 14
(b)

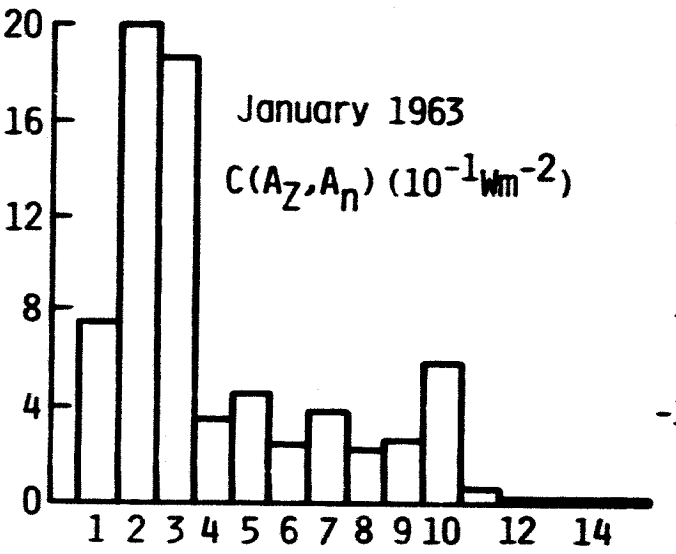
20
16
12
8
4
0
1 2 3 4 5 6 7 8 9 10 12 14
January 1963
C(A_Z, A_n) (10^-1 Wm^-2)

(c)

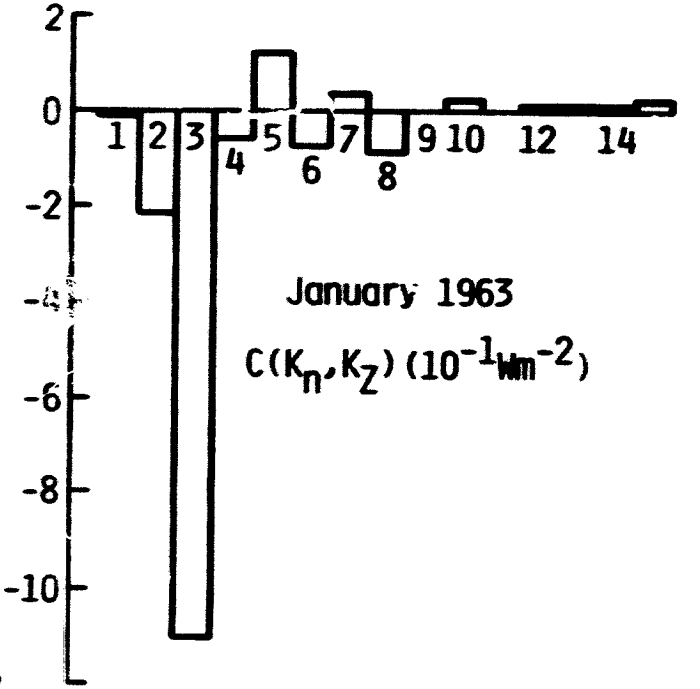
2
0
-2
-6
-8
-10
1 2 3 4 5 6 7 8 9 10 12 14
January 1963
C(K_n, K_Z) (10^-1 Wm^-2)

(d)

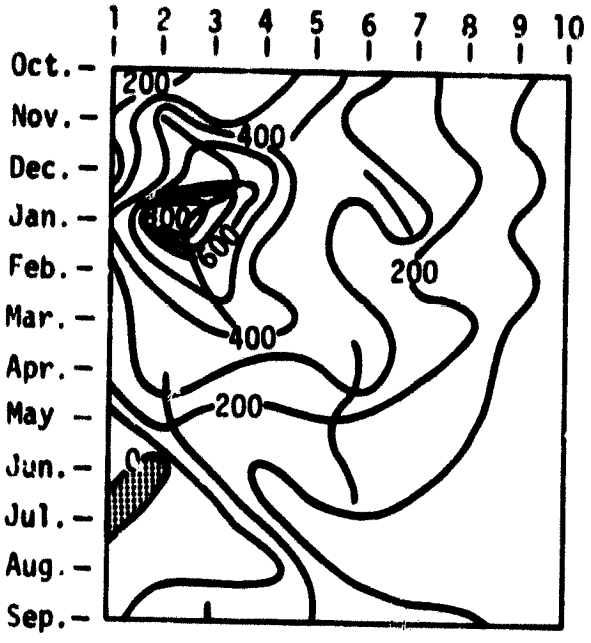
1 2 3 4 5 6 7 8 9 10
Oct.
Nov.
Dec.
Jan.
Feb.
Mar.
Apr.
May
Jun.
Jul.
Aug.
Sep.
200
400
600
200
400
200

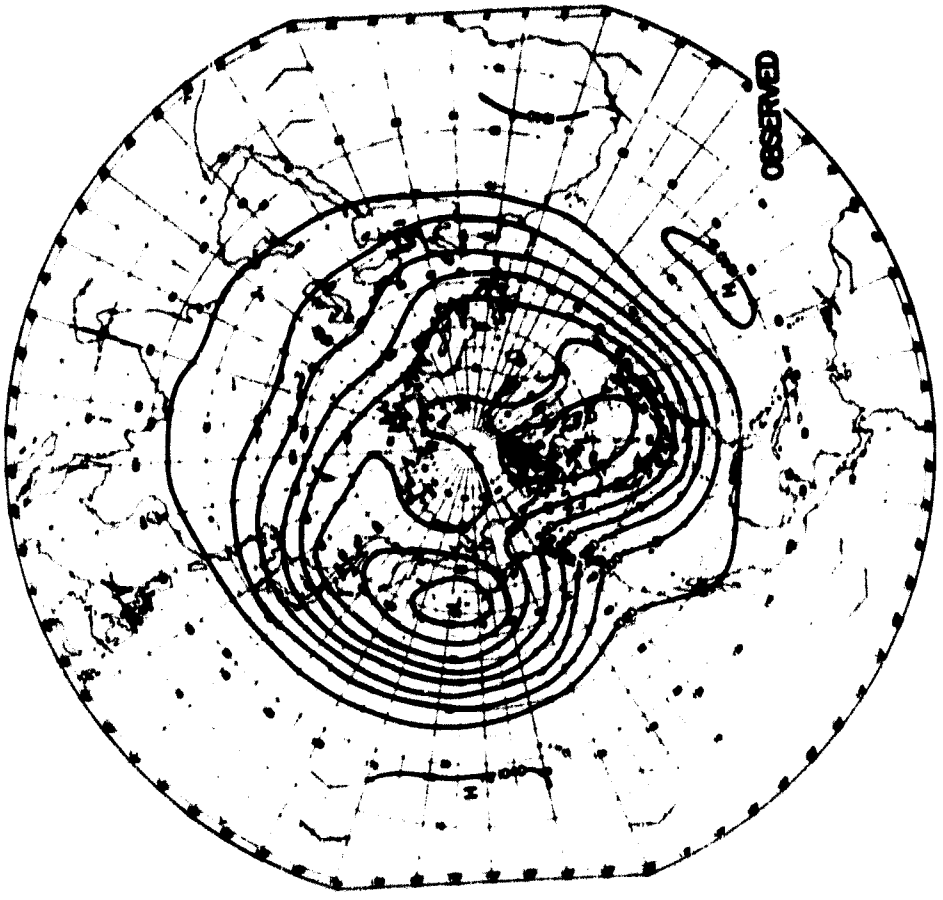

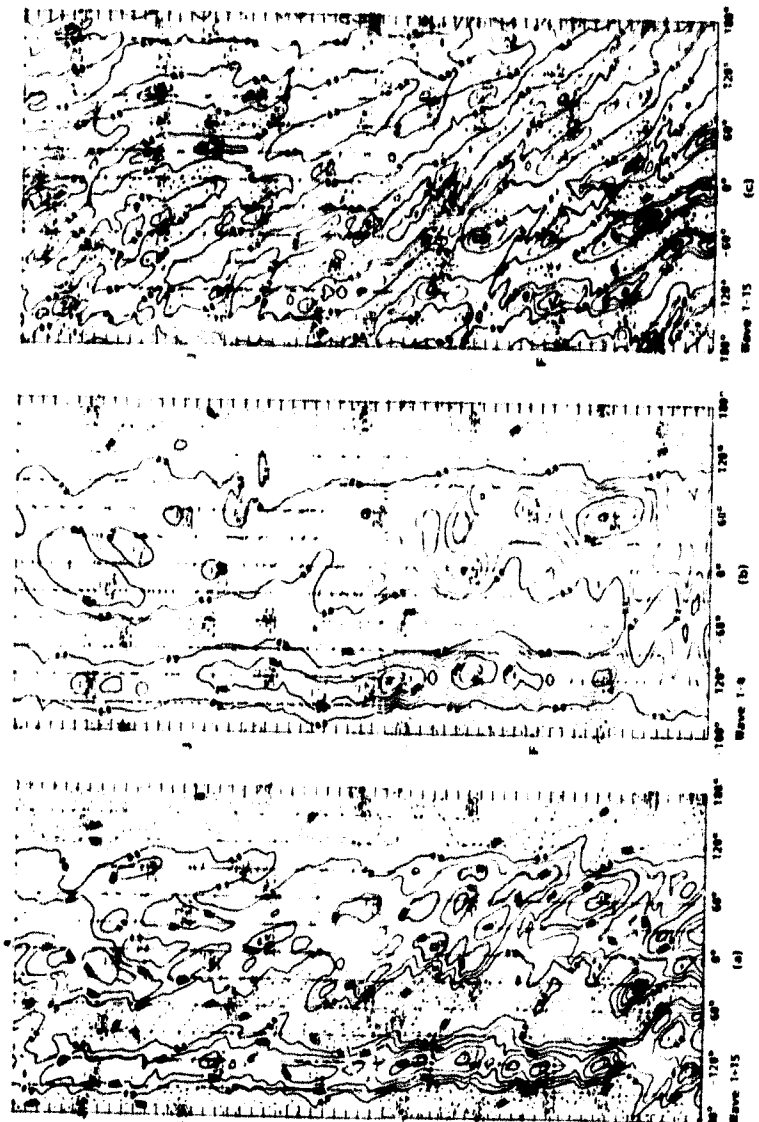

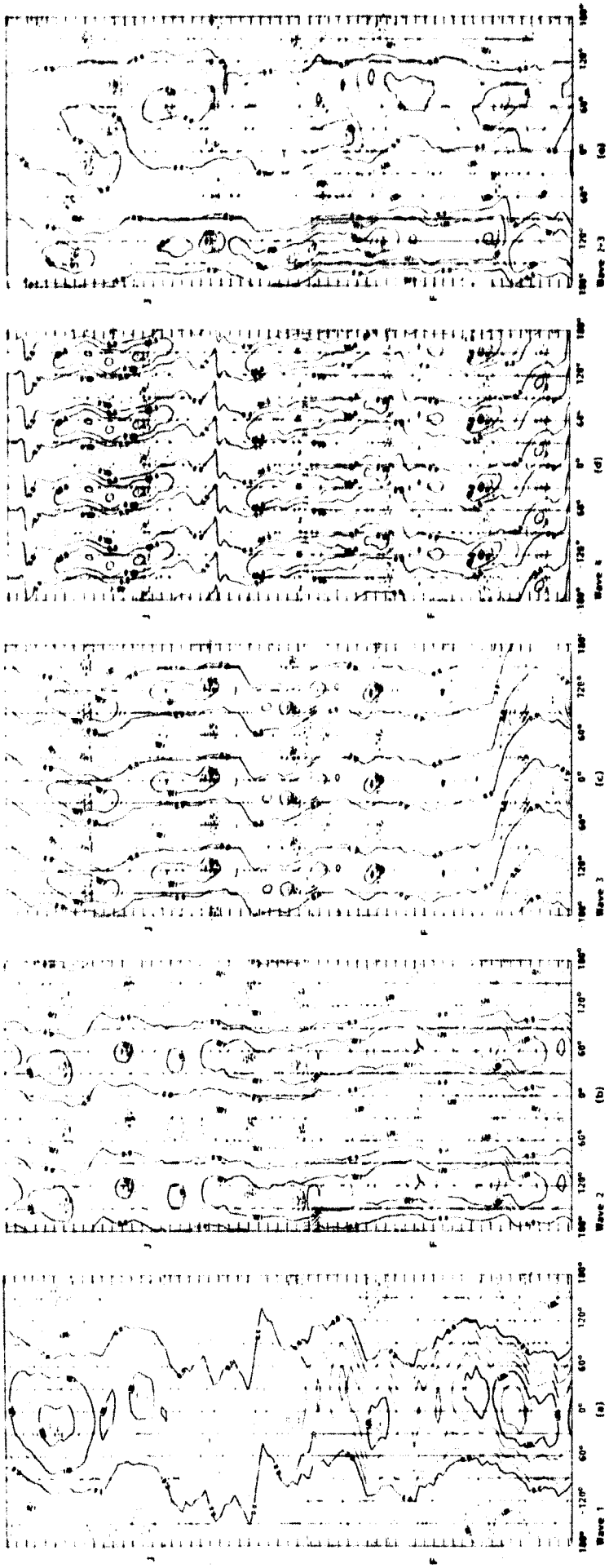

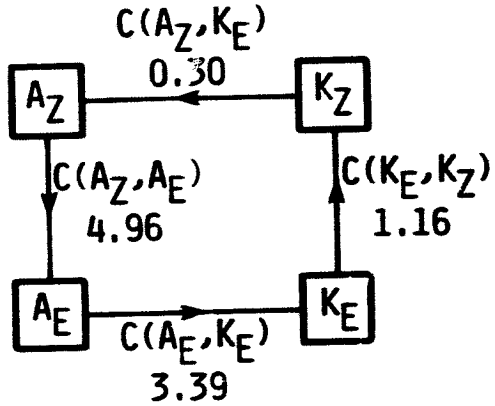
C(A_Z, K_E)
0.30
A_Z
K_Z
C(A_Z, A_E)
4.96
C(K_E, K_Z)
1.16
A_E
K_E
C(A_E, K_E)
3.39

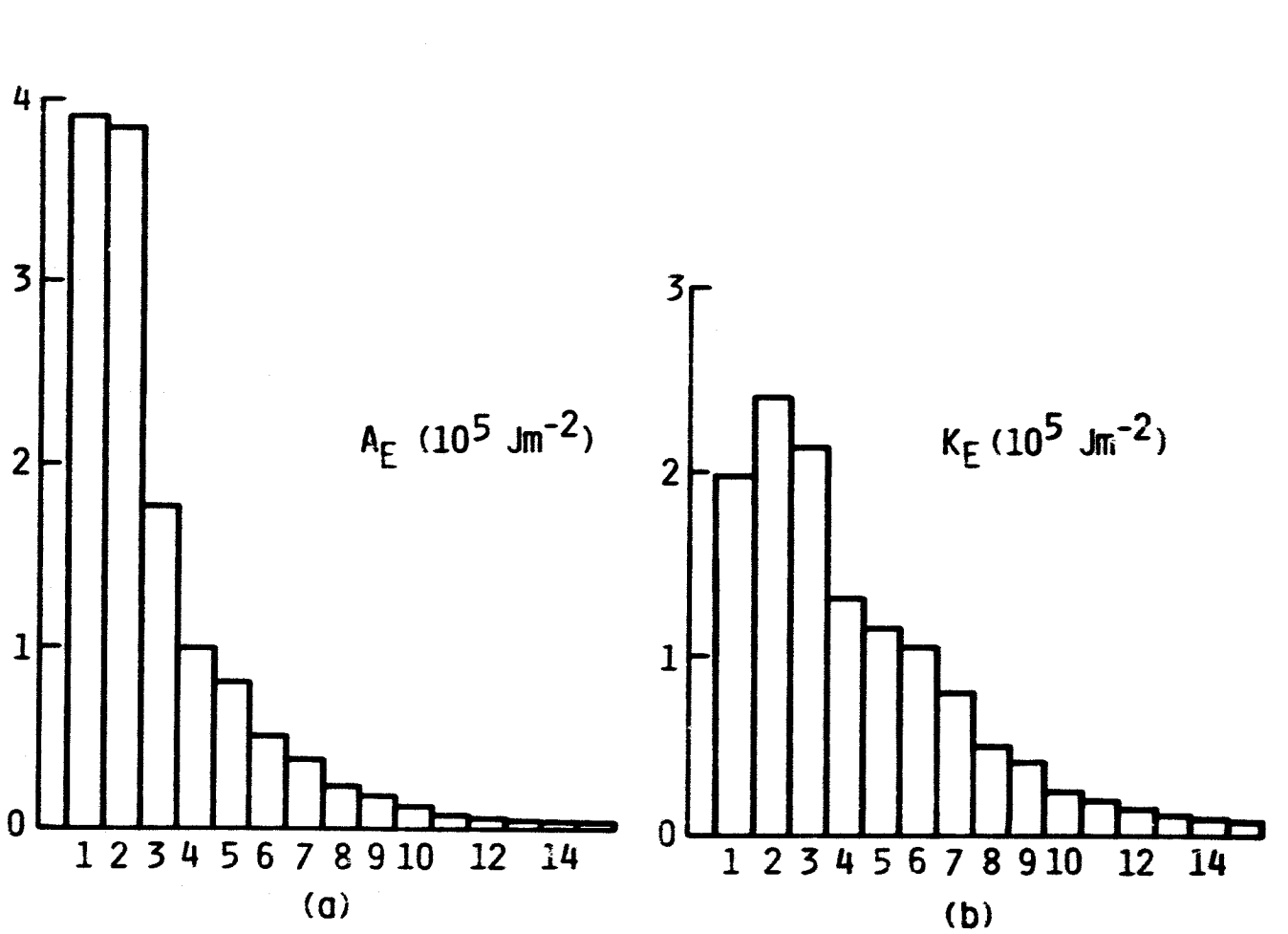
4
3
2
1
0
A_E (10^5 Jm^{-2})
1 2 3 4 5 6 7 8 9 10 12 14
(a)
3
2
1
0
K_E (10^5 Jm^{-2})
1 2 3 4 5 6 7 8 9 10 12 14
(b)

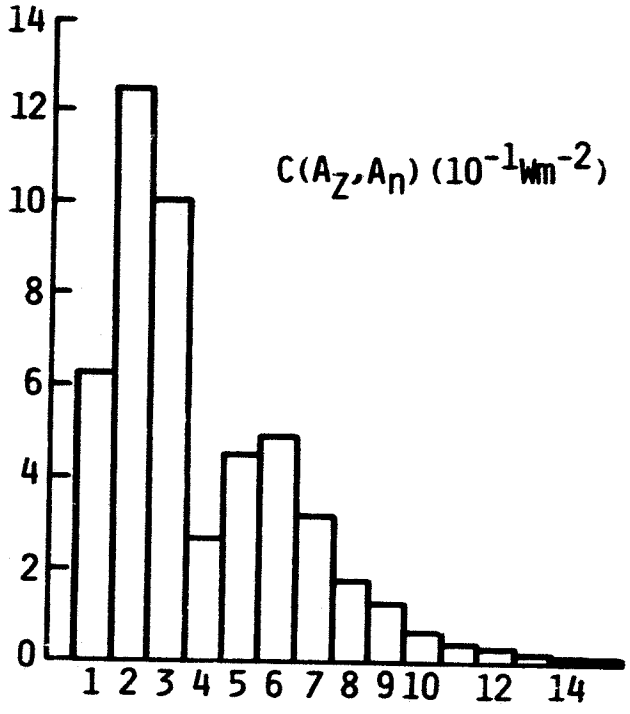
14
12
10
8
6
4
2
0
$C(A_Z, A_n)$ $(10^{-1}Wm^{-2})$
1 2 3 4 5 6 7 8 9 10 12 14

(c)

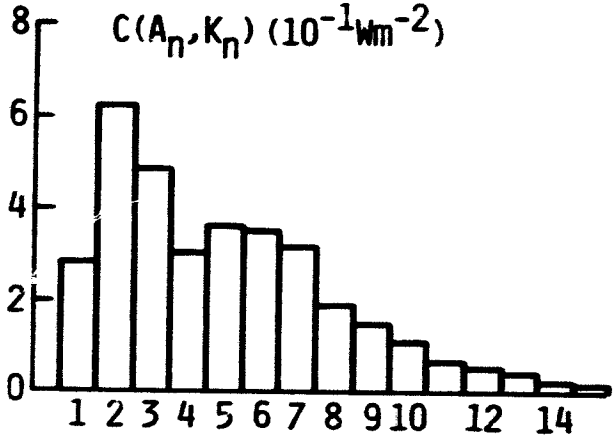
8
6
4
2
0
$C(A_n, K_n)$ $(10^{-1}Wm^{-2})$
1 2 3 4 5 6 7 8 9 10 12 14

(d)

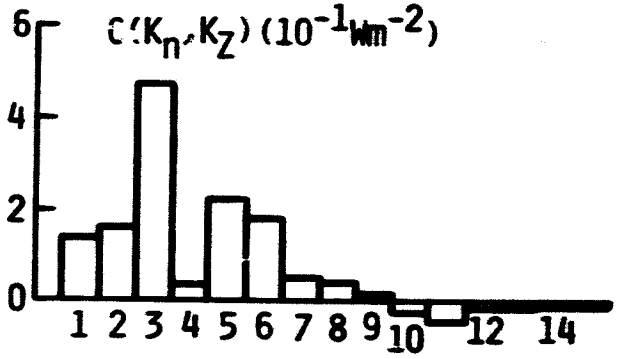
6
4
2
0
$C(K_n, K_Z)$ $(10^{-1}Wm^{-2})$
1 2 3 4 5 6 7 8 9 10 12 14

(e)

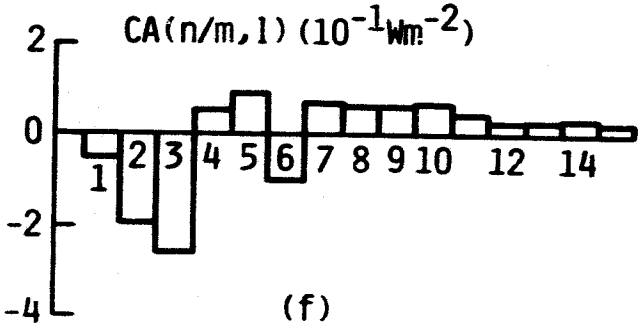
2
0
-2
-4
$CA(n/m, 1)$ $(10^{-1}Wm^{-2})$
1 2 3 4 5 6 7 8 9 10 12 14

(f)

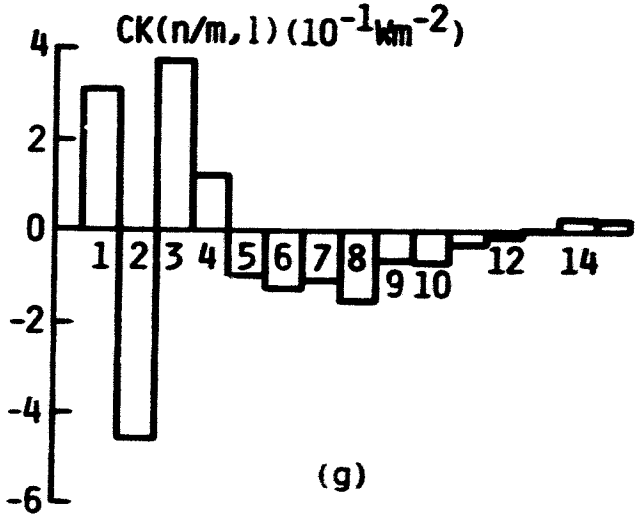
4
2
0
-2
-4
-6
$CK(n/m, 1)$ $(10^{-1}Wm^{-2})$
1 2 3 4 5 6 7 8 9 10 12 14

(g)

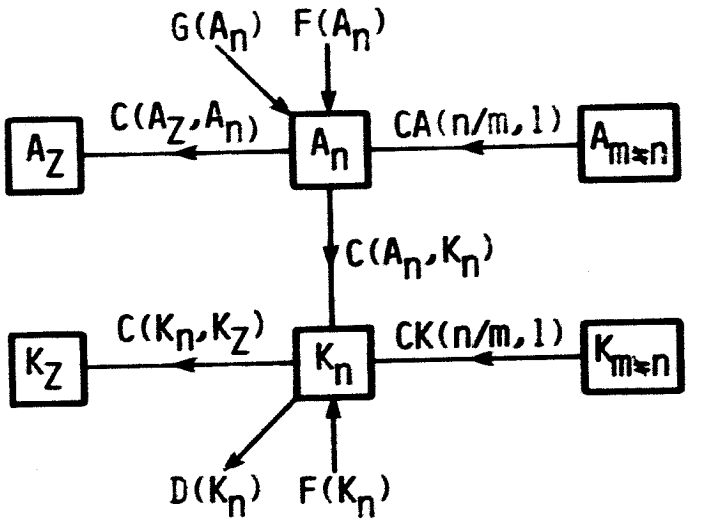
G(An)
F(An)
C(AZ,An)
AZ
An
CA(n/m,1)
Am≠n
C(An,Kn)
C(Kn,KZ)
KZ
Kn
CK(n/m,1)
Km≠n
D(Kn)
F(Kn)

A spectral energetics analysis of atmospheric blocking

Anthony R. Hansen and Tsing-Chang Chen

Department of Earth Sciences
Iowa State University
Ames, IA 50011

Abstract

The spectral energetics of two blocking case studies from the winter of 1978-79 are calculated. One case occurred over the North Atlantic and the other over the North Pacific. The temporal evolution and geographical distribution of the energetics of the planetary-scale (zonal harmonic wavenumbers 1-4) and the intermediate-scale (wavenumbers 5-10) wave ensembles are examined to identify the physical mechanisms important in the blocking process.

Two distinct forcing mechanisms were found. The Atlantic block was forced by the nonlinear interaction of intense baroclinic cyclone-scale waves with ultralong waves. The Pacific blocking resulted from the baroclinic amplification of planetary-scale waves. At least two necessary conditions are required for the development of blocking. First, one of the forcing mechanisms must be in operation, and second, the phase of the antecedent planetary-scale waves must be such that the forcing mechanism can amplify them into a blocking pattern.

In each of the cases studied, the block developed downstream of intense intermediate- or large-scale cyclogenesis. The possible relationship between this cyclogenesis, subsequent block development, and the pattern of sea surface temperature anomalies in the western portions of the oceans is discussed.

1. Introduction

Blocking action can result in significant local distortions of normal seasonal climatic trends (Rex, 1950b). Recent abnormal record setting winters in North America, particularly 1976-77 and 1978-79, have stimulated renewed interest in the blocking problem. Numerous articles discussing various aspects of this subject have appeared in recent literature. A problem frequently encountered when studying blocking action is establishing exactly what is meant by the term blocking. Any persistent, quasistationary ridge that impedes the normal eastward progression of cyclone-scale waves can be called a block. Our primary interest is in high latitude blocking ridges that have lifetimes of 10 to 15 days and that generally satisfy Rex's (1950a) definition of blocking.

The fact that blocking can cause large, seasonal climatic anomalies and that the physical mechanisms responsible for its formation are not well understood suggests that additional diagnostic studies of blocking are needed. The spectral energetics method provides a powerful diagnostic tool for the qualitative identification of mechanisms important in block development. Examination of the temporal evolution of the energetics can be particularly useful, especially if an effort is made to relate salient features of the energetics analysis to synoptically observable events.

We have calculated the evolution of the spectral energetics of two cases of blocking from the winter of 1978-79. The forcing mechanisms of these two ridges were quite different. The first case occurred over the North Atlantic in December 1978. This block was forced by the nonlinear interaction of baroclinic cyclone-scale waves with planetary waves. The second case occurred over the North Pacific in late December 1978 and early January 1979. This block developed as a result of the baroclinic amplifi-

cation of planetary-scale waves. The forcing mechanisms of these blocking episodes are representative of other cases of Atlantic and Pacific blocking (Hansen, 1981).

2. Background

Early investigators (Berggren, et al., 1949; Elliott and Smith, 1949; Rex, 1950a, b) established the synoptic behavior and climatology of blocking. According to Rex (1950a), blocking exists when the basic westerly current at upper levels splits into two branches that extend over at least 45° of longitude, with each branch trasnporting appreciable mass. A sharp transition from zonal flow upstream to meridional flow downstream of the current split must be observed and this pattern must persist for at least ten days. Rex (1950b) noted that blocking occurs most frequently over the northeastern portions of the Atlantic and Pacific Oceans, normally persists for 12 to 16 days, and is relatively stable in position. The climatological mean position of the blocks is, of course, just downstream from the normal position of the major midlatitude jet streams. The original single westerly jet is replaced by two westerly branches with a zone of easterly flow in between. A pronounced warming occurs in the northern part of the blocked zone with cooling in the southern part. The mean meridional temperature gradient across the blocked zone is greatly reduced or even reversed (Rex, 1950b).

Rex (1950a) observed that the formation of a blocking anticyclone is initiated by a "finite external-impulse" provided by a sufficiently intense cyclonic disturbance. Cyclone-scale waves apparently played an important role in developing the Atlantic block studied by Berggren et al. (1949). What, if any, cause and effect relationship exists between the cyclones and subsequent blocking cannot be determined from synoptic studies alone.

Ratcliffe and Murray (1970) found that cold sea surface temperature (SST) anomalies in a wide area south of Newfoundland are associated with blocked weather patterns over northern and western Europe. Warm SST anomalies in the same area favor more progressive flow patterns. Namias (1964) made a similar observation and suggested that cold SST anomalies near Newfoundland cause increased western Atlantic cyclogenesis which in turn leads to block development over northern Europe. It is difficult to confirm this speculation because the proposed processes occur in data sparse regions over the ocean.

Recently, several new theories for blocking have been proposed. Egger (1978, 1979) uses a barotropic channel model to show that blocking can result from the nonlinear interaction of forced stationary waves with slowly moving free waves. Charney and Devore (1979) use a low-order, barotropic channel model to suggest that for a given forcing, both high and low index equilibrium flows can exist. Blocking could be a meta-stable equilibrium of the low index type. Charney and Strauss (1980) have extended this idea to a baroclinic model, where they found that orography played an indirect, catalytic role in development of a low-index, blocked state. The transition to this blocked state may occur, in their opinion, through a combination of orographic and baroclinic instability. Tung and Lindzen (1979) show analytically that blocking may be caused by linear, resonant amplification of planetary-scale waves forced by topography and surface heating. If the atmospheric flow is such that it renders a wave stationary with respect to the earth's surface, the wave can interact resonantly with the stationary forcing.

None of the recent theories specifically incorporate the forcing of planetary-scale waves by cyclone-scale waves. However, Gall et al. (1979)

have suggested that the nonuniform spacing and intensity of cyclones around a latitude zone will lead to forcing of the ultralong waves by axially asymmetric cyclone-scale heat transports. The resulting pattern of high latitude warming and lower latitude cooling shown by Gall et al. resembles that associated with Rex blocking. The asymmetric cyclone-scale heat transports in turn force large-scale vertical motion and corresponding large-scale baroclinic energy conversions that provide the kinetic energy source for ultralong wave development.

Previous energetics analyses of blocking, using primarily time-averaged results, indicate that blocking is accompanied by strong baroclinic energy conversions. Julian and Labitzke (1965) noted increased vigor in the vertical motion field during the onset of blocking and concluded that the energy variations associated with it were largely baroclinic. Paulin (1970) and Murakami and Tomatsu (1965) found that large conversions of zonal to eddy available potential energy and, then to eddy kinetic energy accompanied block development. The maximum monthly mean baroclinic conversions occurred at zonal harmonic wavenumbers 2 and 3. Winston and Krueger (1961) discovered similar baroclinic energy conversions during the development phase of an Atlantic block.

All the aforementioned studies use data from the entire middle and high latitudes of the Northern Hemisphere. Zonally averaged results like these cannot distinguish whether diagnosed processes are associated with blocking or with some other aspect of the circulation. In addition, the calculation of monthly means can easily mask important energetics processes because the lifetime of blocking is usually only 10 to 15 days.

More recently, Hartman and Ghan (1980) used a statistical approach to examine the heat and vorticity budgets of composited Atlantic and Pacific blocks. They suggested that Pacific blocks may be caused by largely barotropic mechanisms, while Atlantic blocks may be largely baroclinic. Austin (1980) has shown that blocking can be represented by the constructive interference of planetary-scale zonal harmonic waves with normal phases but much greater than normal amplitudes.

However, so far no mechanism has been isolated to explain the initial development of blocking. Although it appears from most studies that baroclinic processes are important, the temporal evolution fo the spectral energetics of blocking has not yet been precented.

3. Data and Procedures

The equations governing atmospheric energetics in wavenumber domain were first formulated by Saltzman (1957). The complete spectral energetics formulation can be found in numerous other sources (e.g., Hansen, 1981; Saltzman, 1970) and will not be repeated here. Note that the nonlinear interaction represents a redistribution of energy between the various waves and is neither a source nor a sink of kinetic energy. When summed over all wavenumbers, the nonlinear interaction should yield no net change in total eddy kinetic energy (Steinberg et al., 1971). We have reformulated the spectral energetics equations in such a way that the wavenumber domain equations can be reconciled with the physical domain equations, and the nonlinear interaction terms sum to zero. Our reformulation of the nonlinear interaction terms is given in the Appendix.

The data used in this study are the output of the National Meteorological Center's (NMC) operational analysis. Twice daily Northern Hemisphere data for the horizontal wind (u, v), the geopotential height (z), and the temperature (T) on a 2.5° by 2.5° grid at the 10 mandatory levels in the troposphere (1000, 850, 700, 500, 400, 300, 250, 150 and 100 mb) were obtained from the National Center for Atmospheric Research. In order to measure the release of available potential energy (APE) through baroclinic energy conversion, it is necessary to compute the vertical motion in the atmosphere. The vertical velocity in pressure coordinates (ω) was calculated from a spectral form of the quasigeostrophic ω-equation assuming $\omega = 0$ at 1000 mb and 100 mb (Chen et al., 1981). Fourier coefficients of u, v, z, T and ω at each latitude circle and every level were calculated using a standard fast Fourier transform technique. The zonal harmonic expansion of the dynamical variables was truncated after wavenumber 18.

The spectral energetics results were integrated over the latitude zone from 30°N to 80°N. This zone was selected because it completely includes the features of the middle and high latitude circulation associated with blocking, while excluding the influences of the tropical Hadley cell circulation. The meridionally averaged results are also integrated in the vertical from 1000 to 100 mb.

In order to more easily relate the spectral energetics results to observable features of the circulation, ensembles of planetary-scale (wavenumbers 1-4) and intermediate-scale waves (wavenumbers 5-10) were formed. A similar approach has been used in previous energetics studies (Wiin-Nielsen et al., 1963, 1964; Chen et al. 1981). By examining the results for these

ensembles, we can isolate atmospheric energetics processes occurring on planetary or intermediate scales as well as nonlinear interactions between these scales. Smaller scale processes (wavenumbers $\geq$ 11) were found to play no significant role in blocking development.

It is not possible to determine from the time evolution of the spectral energetics alone whether the diagnosed energy or energy conversions have anything to do with the development of blocking. We should not expect that the development or existence of a blocking high will necessarily have a profound effect on the zonally averaged spectral energetics. Contributions from other regions can easily mask the energy processes related to blocking. We need to determine the spatial distribution of the energetics results in order to draw more definite conclusions.

Polar stereographic projections of planetary- and intermediate-scale ensemble kinetic energy, transports, height and temperature fields and baroclinic conversions were made for individual observation times when energy values or energy conversions were maximum or rapidly changing. These plots provide considerable insight into the distribution of energetics processes around the hemisphere and make it much easier to identify important processes related to blocking. To supplement the spectral energetics calculation, limited area energetics calculations were also performed. Specific information we wish to obtain from the limited area calculation is the location of wave-wave energy transfers.

4. A Case of High Latitude Atlantic Blocking

A. Synoptic Behavior

During the second half of December 1978, a major blocking ridge rapidly developed over the North Atlantic Ocean. Preceding the development, strong westerly flow between 40°N and 50°N dominated the Northern Hemisphere

circulation. A short wave 500 mb trough appeared over the western Great Lakes on 17 December in a region of strong zonal flow. This feature developed rapidly into a significant northwest-southeast tilted trough with strong warm advection apparent on its downstream side. By 0000 GMT 19 December, the trough had deepened considerably into a 494 dam closed low centered just north of Maine, with a trough extending southeastward over the Atlantic. A ridge was building south of Greenland ahead of this trough. The trough had acquired a very pronounced northwest-southeast tilt by 0000 GMT 21 December (Fig. 1) as the ridge continued to develop.

The block reached maturity at 0000 GMT 22 December as a 568 dam closed high centered at 68°N over the Greenland shore of the Denmark Strait. The original trough was still northwest-southeast tilted but it had greatly weakened. A stable, blocking high remained over Greenland centered near 70°N with 500 mb heights ranging from 560 to 569 dam until the 28th. Strong 500 mb easterlies along 60°N persisted throughout this period. At 1200 GMT of the 25th, easterlies extended from the Norwegian coast to Baffin Island and the 500 mb pattern had a classic Rex blocking structure (Fig. 2).

Beginning on roughly 28 December, high latitude retrogression of the blocking ridge was evident. At 1200 GMT 29 December (Fig. 3) the 500 mb pattern still resembled Rex blocking, but extension of the 500 mb ridge over Baffin Island and the Queen Elizabeth Islands was apparently the result of retrogression. Further height rises in this vicinity, particularly over the Beaufort Sea occurred between the 29th and the end of the month. By 0000 GMT 1 January 1979, the Atlantic block had completely decayed.

The development phase of the block was from roughly 19 to 22 December, the mature phase from 22 to 29 December, and decay occurred rapidly from 29 December to 1 January. The synoptic behavior of the case is very

similar to that described by Berggren et al. (1949). A spectrally filtered Hovmoller diagram of the planetary-scale 500 mb height field (z_{1-4}) at 70°N clearly shows the strong ultralong wave ridge amplifying during 19-22 December and persisting until the end of the month (Fig. 4) with retrogression apparent after roughly 27 December. The mean longitude of the high center is about 30°W. As we shall see, the largest energy conversions in the entire hemisphere at this time were associated with the development of this block.

B. Energetics

Before examining the various aspects of the ensemble results for this case, let us first consider the time evolution of the overall energy cycle. The vertical integration of the zonal kinetic energy (K_Z), eddy kinetic energy (K_E), zonal APE (A_Z) and eddy APE (A_E) averaged between 30°N and 80°N are shown in Fig. 5a. The conversions between these quantities are given in Fig. 5b.

K_Z had maintained a relatively large, steady value until 14 December corresponding to the aforementioned strong zonal flow in mid-December. K_Z dropped sharply from the 14th to the 16th, eventually reaching a minimum on the 20th. Minimum values of $C(A_Z, A_E)$ and $C(A_E, K_E)$ on 14 and 15 December correspond to a period of rapidly increasing A_Z. However, beginning on 15 December, both $C(A_Z, A_E)$ and $C(A_E, K_E)$ increased dramatically, reaching striking maxima on the 17th and 18th, respectively. They remained relatively large until the 22nd after which they declined sharply. As a result of these baroclinic processes, A_Z declined rapidly, and K_E and A_E rose from minima on 15 and 16 December to marked maxima on the 19th and 21st, respectively. Notice the negative correlation between A_Z and K_E (Fig. 5a)

that is consistent with these conversions. Lejenäs (1977) has noted a similar energy cycle during blocking in the work of previous investigators.

The decline in K_Z, rapid growth and decay of A_Z and minima in K_E and A_E precede the onset of blocking. Very large baroclinic processes [$C(A_Z, A_E)$ and $C(A_E, K_E)$] just prior to and during the development stage of the block account for the observed increases in A_E and K_E in the third week of December, with a much smaller contribution to K_E from $C(K_Z, K_E)$. The largest eddy kinetic energy values correspond to the developing phase of the block. K_E declines and remains relatively low during the mature stage. A_E reached its maximum as the block reached maturity.

The ensemble results give a clearer picture of the energetics of this case. The vertically integrated energetics of the planetary-scale ensemble (wavenumbers 1-4) and the intermediate ensemble (wavenumbers 5-10) are shown in Figs. 6a and 6b.

The large values of $C(A_Z, A_{1-4})$ and $C(A_{1-4}, K_{1-4})$ on 16 and 17 December and the $C(K_Z, K_{1-4})$ maximum on the 18th (Fig. 6a) are primarily associated with a deepening ultralong-wave trough over East Asia. However, the intermediate-scale kinetic energy and energy conversions from 15 to 22 December (Fig. 6b) were concentrated over eastern North America and the western Atlantic. The intermediate-scale kinetic energy (K_{5-10}) increased dramatically from a minimum on 14 December to a striking maximum on the 19th. K_{5-10} accounted for roughly half of the total eddy kinetic energy which was also maximum on that date. The intermediate-scale APE (A_{5-10}) underwent a similar but less dramatic increase. These energy increases are the result of large baroclinic energy conversions. The larger magnitude of $C(A_Z, A_{5-10})$ than $C(A_{5-10}, K_{5-10})$ accounts for the

increase in A_{5-10} from 16 to 18 December. Note that the intermediate-scale conversions represent most of the total A_Z to A_E and A_E to K_E conversions before and during the block's development. The decline in A_Z from 16 to 19 December has a marked negative correlation with the increases in A_{5-10} and K_{5-10} during the same period.

The major features of the intermediate-scale 500 mb height field at 1200 GMT 18 December (Fig. 7a) were a deep, northwest-southeast tilted trough extending from eastern North America into the western Atlantic with strong cyclone-scale ridges both upstream and downstream of the trough. The position of the trough over eastern North America in the synoptic chart for this date corresponds exactly to the intermediate-scale trough position in Fig. 7a. The cyclone-scale baroclinic energy conversion was maximum at this time and $C(A_{5-10}, K_{5-10})$ was concentrated around the eastern North American cyclone system (Fig. 7b). The largest conversion is over Laborador in southeasterly flow on the downstream side of the trough.

$C(A_Z, A_{5-10})$ was also very large at 1200 GMT 18 December. The cyclone-scale heat transports and therefore $C(A_Z, A_{5-10})$ were concentrated around the same trough-ridge system. Northward transport of warm air east of the trough axis and southward transport of cold air west of the trough axis can be inferred. By 1200 GMT 19 December, the heat transport associated with this trough had increased, especially the northward warm air transport on the trough's east side, and the convergence of the cyclone-scale heat transport had reached the south tip of Greenland. The zonal asymmetry of the cyclone-scale heat transport was particularly striking at 850 mb (Fig. 8).

The northwest-southeast tilting of the trough-ridge system caused considerable southward transport of westerly momentum (northward transport of

easterly momentum). The negative cyclone-scale momentum transport at 1200 GMT of the 19th was especially prominant over Newfoundland and south of Greenland (Fig. 9a). The ultralong wave 500 mb height field at this time (Fig. 9b) shows a diffuse ridge over the North Atlantic with the suggestion of easterly (geostrophic) flow from south of Greenland to over Hudson Bay (a similar pattern existed at 300 mb). Thus from 18 to 22 December there was convergence of cyclone-scale easterly momentum into a region of planetary-scale easterly flow (compare Figs. 9a and b). This coincides with the period of large nonlinear interaction between the intermediate and planetary-scale waves. A clear negative correlation between the planetary-scale and intermediate-scale kinetic energy existed from 19 to 23 December, consistent with the diagnosed nonlinear interaction (compare Figs. 6a and b). The period of declining K_{5-10} and large nonlinear transfer of energy to the rapidly rising K_{1-4} from 19 through 22 December corresponds exactly to the time of the rapid development of the North Atlantic blocking.

Comparison of the intermediate-scale and planetary-scale kinetic energy distributions over eastern North America and the North Atlantic on the 19th and 23rd supports the contention that intermediate-scale kinetic energy was transferred nonlinearly to the ultralong waves in this region. On the 19th, K_{5-10} had a very remarkable, zonally asymmetric distribution in this area (Fig. 10a) but K_{1-4} was nearly nonexistent. By 1200 GMT 23 December, this pattern had reversed. The K_{5-10} maxima over the Atlantic had completely disappeared. There are no contours over eastern North America or the Atlantic in the K_{5-10} plot at the time (not shown). However, very large K_{1-4} values, associated with the blocking high over Greenland, had replaced the intermediate-scale kinetic energy (Fig. 10b). Easterly flow south of Greenland

was particularly strong. Thus, the mechanism for the large diagnosed energy transfer from intermediate to planetary scale was apparently the northward transport of easterly momentum by cyclone waves into a region of planetary-scale easterly flow over the North Atlantic, resulting in the acceleration of the easterly flow.

At 1200 GMT 19 December, when the blocking ridge was rapidly developing, $C(A_{1-4}, K_{1-4})$ was divided, for the most part, between the North Pacific sector and a region just south of Greenland (Fig. 11). The large-scale ascent of warm air south of Greenland could have been forced by the strong cyclone-scale heat flux convergence in this area in a manner similar to that proposed by Gall et al. (1979). In any event, the source of K_{1-4} provided by the nonlinear interaction was as large or larger than the baroclinic source when the block was developing from 19 through 22 December (Fig. 6a), but the baroclinic conversion was distributed in various locations during this time. Therefore, we can conclude that the nonlinear interaction was the primary source for the kinetic energy of the block.

The equivalent barotropic structure of the ultralong waves over the Atlantic during the block's development is shown by comparing the planetary-scale height and temperature fields. At 1200 GMT 19 December , the weak ridges in the 500 mb height and temperature fields over the Atlantic were in phase. Even after the block had reached maturity at 1200 GMT 23 December, the amplified z_{1-4} and T_{1-4} ridge axes over Greenland were still almost exactly in phase at 500 mb (compare Figs. 12a and b), as well as at 850 mb and 300 mb. Notice the very large increase in the amplitude of the ridge over Greenland from the 19th to the 23rd (compare Figs. 9b and 12a). The thermal ridge experienced a correspondingly large amplification, consistent with the increase in A_{1-4}.

A maximum in the planetary-scale APE on 22 and 23 December corresponds to the time when the thermal ridge associated with the Atlantic block had its greatest amplitude. A major source of this APE was provided by the excess of $C(A_Z, A_{1-4})$ over $C(A_{1-4}, K_{1-4})$ between 1200 GMT 19 December and 0000 GMT 23 December (Fig. 6a). The $C(A_Z, A_{1-4})$ maximum on the 22nd was associated with significant net positive planetary-scale heat transports in the vicinity of the block (Fig. 13), although part of the marked northward warm air transport centered over Baffin Bay at 500 mb was counterbalanced by southward transport just east of Greenland. This viewpoint is supported by the build-up, noted earlier, of the planetary-scale thermal ridge over Greenland between 19 and 23 December.

An additional source of A_{1-4} during the development phase was the nonlinear transfer of intermediate-scale APE to the ultralong waves. Normally, the planetary waves export APE to smaller scales but a small positive contribution of A_{5-10} to A_{1-4} was maintained from 9 December to 21 December (not shown). The cyclone-scale heat transports over the western Atlantic with their attendant A_Z to A_{5-10} conversion were apparently followed by a transfer of some A_{5-10} to the planetary waves. (Note the decline in A_{5-10} during this time in Fig. 6b). The positive A_{5-10} to A_{1-4} transfer in this region was evidently large enough to more than counterbalance the normal negative transfers that were most likely occurring in the rest of the hemisphere, thus yielding the net positive transfer in the zonally averaged energetics.

The nonlinear interactions that forced the development of the Atlantic block dropped to zero on 23 December by which time the planetary-scale kinetic energy was very large (Fig. 10b) and an amplified ultralong wave

ridge was in place over Greenland (Fig. 12a). Notice the very obvious wavenumber 1 pattern north of 60°N in Fig. 12a.

All of the large-scale energy conversions fell to nearly zero on 23 and 24 December and K_{1-4} declined rapidly (Fig. 6a). No significant net energy sources are apparent in the vicinity of the block throughout its mature phase as the kinetic energy around the block declined markedly. However, the amplitudes of the planetary-scale height and thermal ridges over Greenland remained high from 22 to 28 December. The z_{1-4} and T_{1-4} ridges remained approximately in phase during this period.

By 1200 GMT 28 December, the block had begun to retrograde across northern Canada. The Greenland thermal ridge was still fairly strong on the 28th but by 30 December the effects of retrogression had greatly diminished the Greenland block. Southward transport of warm air by the large-scale flow at 850 mb and 500 mb just south of Greenland on 30 December may also have aided the decline of the block. This southward heat transport was the result of the retrograde height wave moving out of phase with the thermal wave.

In the last few days of December, the large planetary-scale energy conversions (Fig. 6a) were associated with developments in the Pacific sector that will be discussed in the next section. Intermediate-scale processes were unimportant during the block's mature and decay phases.

Corroboration of the nonlinear forcing of the block's development can be gained from the limited area energetics. We calculated the energetics within the sector bounded by 85°W, 20°W, 35°N and 75°N. This region contains the blocking high as well as the cyclone system that preceded it. The maxima in K_E and A_E on the 19th, and large values of $C(A_Z, A_E)$ and

$C(A_E, K_E)$ from 18 to 22 December within the limited area correspond very closely to the intermediate-scale ensemble results (compare Fig. 14 with Fig. 6b). The large east-west flux of K_E around the 19th was largely the result of cyclone-scale K_E entering the western boundary of the limited area. The very large transfer of eddy kinetic energy to the mean flow that followed the K_E maximum corresponds to the nonlinear transfer of intermediate-scale kinetic energy to the planetary waves in the spectral calculation (again, compare Fig. 14 to Fig. 6b). The area used in the limited area energetics calculation equals roughly 1/6 of the spectral domain, and the magnitude of $C(K_Z, K_E)$ within the limited area was about six times the magnitude of the nonlinear K_E transfer in the spectral calculation. Thus, the limited area energetics confirms that the location of the large nonlinear interaction from 18 to 23 December 1978 was over eastern North America and the western Atlantic. This result strengthens our argument that the resulting blocking ridge was forced primarily by this nonlinear interaction.

In summary, the development of this case of Atlantic blocking was preceded by a high index circulation with a large baroclinic instability as indicated by a large value of A_Z. The nonlinear transfer of kinetic energy from baroclinically active cyclone-scale waves to the planetary-scale waves provided the major source of kinetic energy for the block. The marked zonal asymmetry of the cyclone-scale heat transports coupled with large-scale zonal to eddy APE conversion caused the amplification of the thermal ridge associated with the block. During its mature stage, no active energy conversions were apparent in the vicinity of the block and K_{1-4} declined. The decay of the block was directly linked to the westward retrogression of the height wave. Slight baroclinic damping may have aided the block's demise.

The energy cycle during the development of this nonlinearly forced case can be summarized schematically as follows:

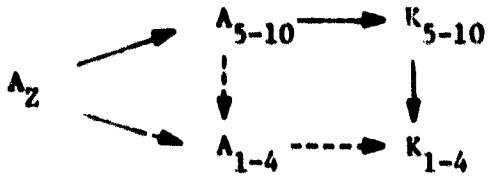

The dotted arrows represent relatively smaller magnitude energy conversions.

5. A Case of Pacific Blocking

A. Synoptic Behavior

Development of a major blocking ridge over Alaska and the eastern Pacific in late December 1978 and early January 1979 closely followed the development of the December 1978 Atlantic block. The Pacific block could be viewed as a westward redevelopment of the earlier feature, but we will treat it as a new development, keeping in mind the possible importance of the retrogression of the blocking high across northern Canada.

On 25 December 1978 westerly flow at 500 mb existed between 30°N and 60°N from central Asia to south of Kamchatka where the westerly current narrowed. The strongest westerlies in the eastern Pacific were between 50°N and 60°N across the Bering Sea and the Alaskan Gulf. A mean ridge was present over the eastern Pacific off the U.S. West coast. By 29 December a ridge had amplified along 140°W extending from ~ 45°N northward over the Alaskan peninsula, and an ultralong wave trough was developing over East Asia. A major closed low had formed in southwestern Canada in response to cold air plunging southward on the lee side of the Pacific ridge. At 1200 GMT 30 December (Fig. 15), there was further indication of regrogression of high 500 mb heights across northern Canada and the large-scale

trough over eastern Siberia had deepened noticeably. The pattern over the Pacific qualifies as blocking on this date.

A closed 557 dam high was positioned over Alaska at 0000 GMT 1 January 1979. In the previous three days, the East Asian trough had progressed eastward out of Siberia and was centered just east of Kamchatka on the first.

A closed 557 dam high was positioned over Alaska at 00Z 1 January 1979. In the previous three days, the East Asian trough had progressed eastward out of Siberia and was centered just east of Kamchatka on the first. Between 1 and 4 January further amplification of the Alaskan high took place. The pattern during this period can be called an omega block because of the deep ultralong wave lows over the Bering Sea and Hudson Bay flanking the high centered at 65°N, 140°W (Fig. 16).

The 500 mb height over Alaska remained at or above 560 dam from 4 to 8 January. The ridge developed a northwest-southeast tilt during this time and movement of the Bering Sea low to south of the Aleutian Islands gave the pattern the appearance of strong, Rex blocking.

Another ultralong wave trough began to progress slowly eastward from northeast Siberia on or before 8 January, reaching a maximum depth of 472 dam just off the Siberian coast on 11 January. Concurrently, the block began to decay and by 12 January it has weakened considerably (Fig. 17). Westerlies had reestablished themselves across the Pacific and the high center had moved north of Alaska and lost amplitude. Remnants of the ridge completely disappeared over the next 3 to 4 days.

During the first week of January when the Pacific block was in its mature stage, strong cyclogenesis occurred over eastern North America followed by the development of a major midlatitude ridge over the Atlantic.

The longitude versus time section of the planetary-scale height field (wavenumbers 1-4) at 60°N (Fig. 18) shows the stationary position of the blocking ridge along 140°W throughout its life cycle. Note the troughs both upstream and downstream of the blocking ridge during its mature stage (30 Dec. to 8 Jan.).

B. Energetics

The time history of the vertically integrated energy cycle for the zonal mean and eddy components of the flow during the December 1978-January 1979 Pacific blocking are given in Figs. 19a and b. Steadily increasing baroclinic processes consistent with rising K_E and declining A_Z, coupled with a relatively large $C(K_Z, K_E)$ mark the energy cycle during the block's developing phase in the last few days of December. $C(A_Z, A_E)$ and $C(A_E, K_E)$ increased steadily from 25 December to 1 January, while $C(K_Z, K_E)$ was strongly positive from the 28th to the 1st.

Most of the dramatic energy conversions that occurred in the zonally averaged energy cycle from 2 through 8 January were related to developments downstream from the Pacific ridge.

After 8 January as the Pacific block decayed, K_Z rose slowly while A_Z declined. The negative value of $C(K_Z, K_E)$ during this period may explain the K_Z increase. Only a slight increase in A_E and K_E accompany the $C(A_Z, A_E)$ and $C(A_E, K_E)$ maxima on the 9th. Notice that A_Z is negatively correlated with both A_E and K_E throughout the block's history. This relationship emphasizes the importance of baroclinic processes in the zonally averaged energetics during this period.

The planetary waves account for the large majority of the energy total conversions shown in late December. These energy conversions were primarily

associated with developments over the North Pacific and East Asia. The planetary-scale kinetic energy was steady from 26 through 28 December (Fig. 20a), but it rose sharply from the 29th to the 31st. Large-scale baroclinic processes [$C(A_Z, A_{1-4})$ and $C(A_{1-4}, K_{1-4})$] were very large in the last six days of December. On the 26th and 27th, negative $C(K_Z, K_{1-4})$ and wave-wave interactions counterbalance the baroclinic kinetic energy generation. However, from the 28th through the 31st, $C(K_Z, K_{1-4})$ became strongly positive and the nonlinear interaction remained near zero allowing the very large $C(A_{1-4}, K_{1-4})$ and the large $C(K_Z, K_{1-4})$ to cause the large-scale kinetic energy to increase sharply.

Substantial southward transport of cold air under the ultralong wave East Asian trough and northward transport of warm air over Alaska and the Bering Strait had developed by 28 December. The horizontal plots for 1200 GMT 30 December are representative of the 28 to 31 December period when large-scale baroclinic and barotropic processes were quite large. The East Asian planetary-scale low was centered just south of Kamchatka at 1200 GMT 30 December and the retrograde ridge over Alaska had begun to amplify (Fig. 21a). $C(A_Z, A_{1-4})$ was near a marked maximum on this date (Fig. 20a) and the most significant ultralong wave heat transports through the depth of the troposphere were over the Bering Sea and along the Asian coast. The northward transport of warm air is particularly strong at 850 mb and 500 mb over the Bering Sea (Fig. 21b). Comparison of the heat transport with the 500 mb planetary-scale ensemble temperature pattern over the Pacific (Fig. 21c) shows that the convergence of the planetary-scale eddy heat flux is acting to further amplify the thermal pattern by transporting warm (cold) air into the region of the thermal high (low). This is consistent with the large observed $C(A_Z, A_{1-4})$.

The large-scale baroclinic energy conversion at 500 mb (Fig. 21d) shows a very strong energy conversion in ascending warm air over the Bering Sea. A broad area of positive energy conversion is associated with sinking cold air beneath the East Asian trough. Comparing the 500 mb planetary-scale height and temperature fields at 1200 GMT 30 December (Figs. 21a and 21c), we see that the phase of the temperature field is shifted to the west of the height field. (The phase shift is more obvious in the lower troposphere (not shown).) This phase shift is consistent with the observed heat transports and $C(A_{1-4}, K_{1-4})$ noted above, and clearly demonstrates the baroclinic structure of the ultralong waves over the Pacific during the initial development of the block.

In addition, the planetary-scale ensemble's 300 mb momentum transport (Fig. 22) shows strong northward transport between 25°N and 40°N south and east of Japan on the south side of the East Asian trough. This suggests that the majority of the diagnosed transfer of K_Z to the ultralong waves occurred in conjunction with the intensification of the East Asian low.

The effect of these energy conversions on the planetary-scale kinetic energy budget is shown in the K_{1-4} distribution over the Pacific at 1200 GMT 31 December (Fig. 23) when K_{1-4} was at a maximum. The large values of K_{1-4} in the vicinity of the blocking high over the Aleutian Islands, the Bering Straits, and north of the Bering Straits are primarily from the baroclinic sources. The very large values in K_{1-4} east of Japan associated with intensification of the Japan jet are due to both barotropic and baroclinic processes. The corresponding K_{1-4} distribution on 28 December (not shown) had only very weak maxima over extreme northeastern Siberia and southwest of Japan. Intermediate-scale processes (Fig. 20b) were of no discernable importance in the Pacific sector.

Further amplification of the block occurred between 31 December 1978 and 4 January 1979. $C(A_Z, A_{1-4})$ remained relatively strong during this period, reaching another marked maximum on 3 January, but $C(A_{1-4}, K_{1-4})$ and $C(K_Z, K_{1-4})$ dropped sharply on 31 December and 1 January, respectively (Fig. 20a). Very strong planetary-scale heat transports existed over Alaska and the Bering Straits during this period on the upstream side of the blocking ridge (Fig. 24). Warm air was transported northward into the region of the thermal high associated with the block (Fig. 25a). The greater amplitude of the Alaska thermal ridge at 500 mb on 4 January (Fig. 25b) compared with 30 December (Fig. 21c) shows the cumulative effect of the large-scale heat transports and the resultant positive $C(A_Z, A_{1-4})$ in this region. Comparison of the planetary-scale height and temperature fields at 00Z 4 January (Figs. 25a and b) shows that there is still a slight phase shift of 10-15° longitude between the two. The phase shift is more noticeable at 850 mb (not shown). The continued existence of the phase lag is consistent with the planetary-scale heat transports, and is further evidence of the baroclinic nature of this blocking ridge.

Nothing particularly unusual had occurred in the intermediate-scale energy budget until the significant K_{5-10} maximum on 3 January (Fig. 20b). This peak was caused by baroclinic processes and was followed by a very large transfer of intermediate-scale kinetic energy to the planetary waves. The large buildup of cyclone-scale kinetic energy in early January took place over eastern North America and the Atlantic. A large increase in K_{1-4} over the Atlantic sector (not shown) is evidence of this interaction. Thus, the large, diagnosed nonlinear interaction during the block's mature phase had nothing to do with maintaining the Pacific block.

The sharp drop in A_Z and increases in A_E and K_E from 2 to 8 January (Fig. 21a) were associated with these Atlantic developments.

Meanwhile, all large-scale energy conversions and transfers fell to near zero on 6 January as K_{1-4} dropped sharply to a minimum on the 9th. Offsetting positive and negative heat transports (and $C(A_{1-4}, K_{1-4})$) on the upstream and downstream sides of the high were typical during the block's mature stage. However, by 7 January southward warm air transport over northwestern Canada exceeded the positive contribution over the Bering Straits. The axis of ridge in the height field over Alaska had moved slightly to the west of the thermal ridge axis resulting in the observed net southward heat transport. The amplitude of the large-scale height and temperature waves on the 7th was quite large, but by 9 January, the maximum height (z_{1-4}) near Alaska had moved north of the peninsula and had fallen by about 100 meters.

The large values of $C(A_Z, A_{1-4})$ and $C(A_{1-4}, K_{1-4})$ on 8 through 10 January were associated with the developing, progressive ultralong wave trough over eastern Siberia and the western Pacific. This trough development caused the transition of the large-scale Pacific pattern from strong blocking on the 8th to a pattern dominated by an extensive, northwest-southeast tilted East Asian trough on the 13th.

In summary, the initial development of the Pacific block in late December 1978 was the result of very significant, planetary-scale baroclinic processes [$C(A_Z, A_{1-4})$ and $C(A_{1-4}, K_{1-4})$]. It appears that the development was triggered by the retrograde surge of high heights across northern Canada from the North Atlantic in late December. Additional amplification of the block from 31 December to 4 or 5 January 1979 was due

to large-scale heat transports. During the block's mature phase (4 to 8 January), the zonally averaged energy converaions are quite small and no active energetics processes appeared to be occurring in the vicinity of the block. Decay of the block may have been partially due to baroclinic and barotropic damping. The baroclinic development of a prograde East Asian ultralong wave trough coincided with the block's decay phase. This active trough development and its eastward progression in particular appears to have destroyed the energetically inactive block.

The energy cycle during the development of this case of Pacific blocking can be summarized schematically as follows:

$$A_Z \longrightarrow A_{1-4} \longrightarrow K_{1-4} \dashleftarrow K_Z.$$

Here again, the dotted arrow represents a smaller magnitude conversion.

6. Discussion

There have been a number of suggestions in recent literature that intense cyclogenesis can act to force ultralong wave development. Earlier observational studies have also indicated an apparent relationship between intense cyclogenesis and blocking (Berggren et al., 1949; Rex, 1950a). Gall et al. (1979) have shown in model simulations that zonally asymmetric cyclone-scale heat transports can amplify planetary-scale waves through a type of nonlinear interaction. Namias (1980), Harnack (1980), and Sanders and Gyakum (1980) have all noted a correlation between intense cyclogenesis in the western and central North Atlantic and the recurrent strong blocking over the Greenland-Iceland area that occurred during the winter of 1978-79. We have found that the blocking high over Greenland in December 1978

was, in fact, forced by intense, baroclinic cyclone-scale waves. A block over Greenland in mid to late January 1979 was forced in a very similar manner (Hansen, 1981).

The very intense cyclogenesis over the western and central North Atlantic during the 1978-79 winter was enhanced by the presence of very strong sea surface temperature (SST) gradients off the east coast of North America (Sanders and Gyakum, 1980) that resulted from significant SST anomalies east of Newfoundland and Nova Scotia (Harnack, 1980). Increased baroclinicity in the ocean automatically induces atmospheric baroclinicity at the surface and through the depth of the lower atmosphere that is in convective exchange with the surface (Bjerknes, 1962). A larger than normal SST gradient can lead to very intense cyclogenesis in the vicinity of the largest gradient (Sanders and Gyakum, 1980). To maximize the SST gradient and therefore the low level baroclinic instability, the SST anomalies must be in phase with the normal SST distribution.

The probability that blocking can form over the North Atlantic is increased if cold SST anomalies exist east and south of Newfoundland (Ratcliffe and Murray, 1970). The position and strength of the cold SST anomalies in December and January given by Ratcliffe and Murray, based on several years with significant negative anomalies, are very similar to the cold SST anomaly in the same area for the 1978-79 winter given by Harnack (1980). In fact, the 1978-79 anomaly appears to be colder than Ratcliffe and Murray's mean. These SST anomalies create a larger than normal SST gradient off the east coast of North America which in turn leads to an enhanced baroclinic zone in the atmosphere in this area. Explosive cyclogenesis with very strong northward warm air flow on the east side of the trough is spawned by this baroclinicity. A blocking anticyclone

develops north of the cyclone wave due to the intense, zonally asymmetric cyclone-scale heat transports and nonlinear transfer of kinetic energy from intermediate to large-scale waves. Thus, the explosive cyclogenesis that results from the enhanced baroclinic zone in turn leads to stronger cyclone-scale forcing of the planetary-scale waves and subsequent block development. Namias (1964) has suggested that a similar sequence of events can lead to blocking.

However, strong cyclogenesis followed be substantial nonlinear transfer of kinetic energy from intermediate to large scales does not insure the development of blocking. For example, the development of the short duration (5 day) midlatitude ridge over the Atlantic Ocean in early January 1979 was energetically very similar to the development of the high latitude Rex blocks in the same region that preceded and followed it. The similarity appeared in both the spectral and limited area energecics calculations. In all three developments, marked baroclinic energy conversion by cyclone-scale waves over eastern North America and the western Atlantic preceded strong nonlinear interaction between these waves and the planetary-scale waves. However, in two cases Rex blocking resulted, but in the third it did not. The explanation of the different response of the regional flow field to apparently similar forcing lies in the antecedent structure of the regional flow (as represented by the zonal mean flow plus the planetary waves). In the 1978-79 examples, the Rex blocking was preceded by a weak large-scale ridge over the Greenland-Iceland area and the absence of a large-scale low over eastern Canada. The midlatitude ridge development was preceded by a well developed Hudson Bay low.

Simmons and Hoskins (1978, 1980) used a system with one zonal harmonic wave (wavenumber 6 or 9) and a variable mean flow to show that the structure

of the mean flow can affect the growth rate and maximum amplitude of baroclinic waves through barotropic effects. The initial growth of the waves in their model is baroclinic, but as the waves occlude their barotropic decay rate is profoundly affected by the nature of the mean flow in which they are embedded and with which they interact.

In the real atmosphere, the growth and decay of baroclinic waves are probably also profoundly affected by barotropic interactions with the mean flow within a given sector. The structure of the flow field given by the axially symmetric flow and existing planetary waves determines the growth rate, amplitude, and decay rate of baroclinically unstable waves through modulating barotropic interactions. These interactions can be with the zonal mean flow or with the planetary waves. The spectral results of Kao and Chi (1978) and Tsay and Kao (1978) show that nonlinear barotropic processes play an important role in determining the growth and decay rates of both large-scale and cyclone-scale waves.

Our study shows that strongly amplified cyclone waves can have a profound effect on the development of ultralong waves through nonlinear interaction. The nature of the regional flow field in which finite amplitude cyclone waves occur not only has an effect on how the cyclones develop, but also on how they ultimately alter the regional flow field through interactions with it. This interaction involves both barotropic energy transfer and significant sensible heat fluxes. The result can be the development of a short duration mid-ocean ridge with accelerated westerlies across the North Atlantic, or development of a blocking high over Greenland and Iceland that persists for nearly two weeks.

The growth of the blocking high over Alaska was accompanied by baroclinic development of an ultralong wave trough over East Asia and the western Pacific. The western Pacific large-scale trough development occurred over a region of large, mean SST gradients although the magnitude of the SST gradient in the North Pacific is typically about one half of that in the western North Atlantic (Sanders and Gyakum, 1980). Siberian snow cover can further enhance the atmospheric baroclinicity in this region. This would lead to more vigorous cyclogenesis in this region, just as it does over the Atlantic (Sanders and Gyakum, 1980). Although it should be checked more carefully, it appears from our analysis that the zonal scale of the major baroclinic disturbances in the middle and upper troposphere is larger over the Pacific than over the Atlantic. Thus, the major cyclonic developments over the Pacific are described primarily by the ultralong waves, whereas Atlantic cyclogenesis is described by intermediate-scale waves. Enhanced baroclinicity in either region due to SST anomalies and/or high surface albedo due to unusually heavy snow cover increases the activity of the dominant energetic scale in that region. Thus Pacific blocking can result from the baroclinic amplification of ultralong waves that is stimulated by an enhanced baroclinic zone in the western Pacific.

Of course, large-scale baroclinic development over eastern Siberia and the western Pacific does not necessarily lead to the development of Alaskan blocking. In fact, it can accompany the demise of Alaskan blocking as in the January 1979 case. Some additional factor is needed to allow the large-scale baroclinic energy conversion to create a blocking ridge. This may be related to the interaction of the finite amplitude baroclinic

wave with the mean flow in which it is embedded just as in the Atlantic case. The 1978-79 Pacific blocking was apparently triggered by retrogression of the blocking high across northern Canada. However, it is not clear that this particular behavior is a necessary condition for Pacific blocking. Other factors, such as the role of the stationary forcing over the Pacific, should also be considered.

We would expect that large-scale stationary forcing is a more dominant factor over the Pacific Basin than other the Atlantic. This is because the Pacific Ocean has a much larger zonal extent and a much larger surface area than the Atlantic. In addition, the Himalayan Massif provides a larger upstream orographic obstruction to the mean flow than does the North American Cordillera. As a result, blocking theories that invoke the stationary forcing of orography and land-sea differential heating as the mechanism for block development should be more applicable to the Pacific region.

Tung and Lindzen (1979) suggested that blocking could result from the resonant amplification of a free Rossby wave that becomes stationary at a position where it is in phase with the stationary forcing of orography and differential heating. This proposed behavior is at least superficially similar to the 1978-79 Pacific case, where the blocking ridge retrograded until it was over Alaska and in phase with the eastern Pacific standing wave ridge. It then amplified rapidly due to baroclinic processes in conjunction with the deepening western Pacific trough. However, the growth rate of this Alaskan ridge may have been too rapid to be explained by linear resonance. Many more case studies would have to be examined to determine if the 1978-79 behavior is typical of Pacific blocking. Tung

and Lindzen's theory may be more favorably applied to longer period circulation features such as the very persistent eastern Pacific ridge in the winter of 1976-77 (Chen and Shukla, 1981).

Interannual variations in the stationary forcing caused by alterations in sea surface temperatures can affect the intensity of baroclinic cyclogenesis and thus the strength of the mechanisms that force block development (by changing the SST gradients), as well as the structure of the standing waves. Mean conditions promoting explosive cyclogenesis should also favor more frequent and stronger blocking. The observed preponderance of blocked weather patterns during certain winter seasons as opposed to others may be explained as a result of these variations.

7. Conclusion

From our spectral energetics analysis of winter season blocking case studies, we have found two different mechanisms through which baroclinic processes can lead to the development of blocking: 1) the nonlinear forcing of ultralong waves by intense, baroclinic cyclone-scale waves, and 2) baroclinic amplification of planetary-scale waves. The second mechanism can be augmented by barotropic transfer of mean flow kinetic energy to the planetary-scale eddies. The energy source for the blocking comes from the local region or just upstream of the ridge. The intermediate-scale cyclogenesis that accompanied the development of the Greenland block in December 1978 may have been fostered by abnormally strong SST gradients near Newfoundland. An enhanced baroclinic zone over the western Pacific may also have stimulated the large-scale cyclogenesis that accompanied the Alaskan block's development, but this is less certain.

In addition, it appears that at least two necessary conditions must be met to allow a block to form. One of the above forcing mechanisms with a large source of potential energy (A_Z) must be in operation, and the orientation of existing planetary-scale waves must be such that the forcing mechanism can amplify them into a blocking pattern.

Finally, we see two major implications of our results to numerical weather prediction and extended range forecasting. We have found that the forcing of the ultralong waves by cyclone-scale waves can be very strong. Furthermore, the nonlinear interaction between intermediate and large-scale waves in the atmosphere is not continuous. It occurs in discrete episodes when the rate of energy transfer is very large. This is in contrast to the baroclinic energy source for the ultralong waves which maintains a steadier rate. Thus, errors in the prediction of cyclone-scale waves will lead to errors in the forecasting of ultralong wave development (Gall et al., 1979). Models must be able to predict explosive cyclogenesis if they are to be able to properly forecast the development of the ultralong waves and blocking. In addition, the models must accurately handle the position and phase of the antecedent planetary-scale waves so that they can correctly forecast the effects of intense nonlinear or baroclinic forcing on the evolution of the existing long wave pattern. These are areas where existing forecast models have exhibited a marked deficiency.

Acknowledgments

The major part of this project was supported by the National Aeronautics and Space Administration under Grant NSG-5339. The computations were performed under the sponsorship of National Science Foundation Grant ATM-7915800 at the National Center for Atmospheric Research (NCAR). Thanks go to the staff of the NCAR Computing Facility for their assistance, to Susan Snyder for drafting some of the figures and to Helen Fowler for typing the manuscript.

APPENDIX

The complete formulation of the spectral energetics equations used in this study are given by Hansen (1981). The only difference between our formulation and that given by Saltzman (1970) is in the nonlinear terms. Saltzman's flux term should be multiplied by 1/2, and the remaining half of the original term should be added to the nonlinear interaction term (Kanamitsu et al., 1972). The resulting formulation of the nonlinear interaction terms are given below.

In the spectral kinetic energy equation

$$C_K(n|m, n\pm m) = \sum_{\substack{m=-N \\ m\neq 0}}^{N} \left[\frac{1}{2} \left\{ \frac{-1}{a \cos\phi} \left[U_{-m}\left((n+m)U_{-n}U_{n-m} - (n-m)U_n U_{-n-m}\right) \right.\right.\right.$$

$$\left. + V_m\left((n+m)V_{-n}U_{n-m} - (n-m)U_n U_{-n-m}\right)\right] + \frac{1}{a}\left[V_{n-m}\left[\left(U_m \frac{\delta U_{-n}}{\delta\phi} - U_{-n}\frac{\delta U_m}{\delta\phi}\right)\right.\right.$$

$$\left. + \left(V_m \frac{\delta V_{-n}}{\delta\phi} - V_{-n}\frac{\delta V_m}{\delta\phi}\right)\right] + V_{-n-m}\left[\left(U_m \frac{\delta U_n}{\delta\phi} - U_n\frac{\delta U_m}{\delta\phi}\right) + \left(V_m \frac{\delta V_n}{\delta\phi}\right.\right.$$

$$\left.\left. - V_n \frac{\delta V_m}{\delta\phi}\right)\right]\right] + \left[\Omega_{n-m}\left[\left(U_m \frac{\delta U_{-n}}{\delta p} - U_{-n}\frac{\delta U_m}{\delta p}\right) + \left(V_m \frac{\delta V_{-n}}{\delta p} - V_{-n}\frac{\delta V_m}{\delta p}\right)\right]\right.$$

$$\left.\left. + \Omega_{-n-m}\left[\left(U_m \frac{\delta U_n}{\delta p} - U_n \frac{\delta U_m}{\delta p}\right) + \left(V_m \frac{\delta V_n}{\delta p} - V_n \frac{\delta V_m}{\delta p}\right)\right]\right]\right\} + \frac{\tan\phi}{a}$$

$$\left.\left[V_m\left(U_{-n}U_{n-m} + U_n U_{-n-m}\right) - U_m\left(V_{-n}U_{n-m} + V_n U_{-n-m}\right)\right]\right]$$

represents the rate of change of wavenumber n kinetic energy due to nonlinear transfer of kinetic energy to wavenumber n from all other waves. The zonal harmonic expansion was truncated at wavenumber N. U, V, and Ω refer to the Fourier coefficients of u, v, and ω, ϕ is the latitude, p is the pressure, and a is the radius of the earth. When summed over all wavenumbers, 1 to N, this formulation of $C_K(n|m, n\pm m)$ yields no net change in the total eddy kinetic energy.

$$C_A(n|m, n\pm m) = \frac{1}{\bar{\sigma}}\left(\frac{R}{p}\right)^2 \cdot \sum_{\substack{m=-N \\ m\neq 0}}^{N} \left[\frac{1}{2}\left\{\frac{-i\,T_m}{a\cos\phi}\left[(n\pm m)T_{-n}U_{n-m} - (n-m)T_nU_{-n-m}\right]\right.\right.$$

$$+ \frac{1}{a}\left[V_{n-m}\left(T_m\frac{\delta T_{-n}}{\delta\phi} - T_{-n}\frac{\delta T_m}{\delta\phi}\right) + V_{-n-m}\left(T_m\frac{\delta T_n}{\delta\phi} - T_n\frac{\delta T_m}{\delta\phi}\right)\right]$$

$$\left.\left. + \left[\Omega_{n-m}\left(T_m\frac{\delta T_{-n}}{\delta p} - T_{-n}\frac{\delta T_m}{\delta p}\right) + \Omega_{-n-m}\left(T_m\frac{\delta T_n}{\delta p} - T_n\frac{\delta T_m}{\delta p}\right)\right]\right\}\right.$$

$$\left. + \frac{R}{C_p p}T_m\left(T_{-n}\Omega_{n-m} + T_n\Omega_{-n-m}\right)\right]$$

is the nonlinear transfer of APE from all other waves to wavenumber n. $\bar{\sigma}$ is the static stability, R is the gas constant, C_p is the specific heat of air at constant pressure, and T is the Fourier coefficient of the temperature. Note that the contribution to $C_A(n|m, n\pm m)$ given by the fourth term

$$\left[\frac{R}{C_p p}T_m\left(T_{-n}\Omega_{n-m} + T_n\Omega_{-n-m}\right)\right]$$

does not sum to zero when summed over all wavenumbers whereas contributions from all the other terms do sum to zero.

REFERENCES

Austin, J.F., 1980: The blocking of middle latitude westerly winds by planetary waves. Quart. J. Roy. Meteor. Soc., 106, 327-350.

Berggren, R., B. Bolin, and C.-G. Rossby, 1949: An aerological study of zonal motion, its perturbation and breakdown. Tellus, 1, 14-37.

Bjerknes, J., 1962: Synoptic survey of the interaction of sea and atmosphere in the North Atlantic. Geof. Publ., 24, 115-145.

Charney, J.G., and J.G. Devore, 1979: Multiple flow equilibria in the atmosphere and blocking. J. Atmos. Sci., 36, 1205-1216.

Charney, J.G., and D.M. Strauss, 1980: Form-drag instability, multiple equilibria and propagating planetary waves in baroclinic, orographically forced planetary wave systems. J. Atmos. Sci., 37, 1157-1176.

Chen, T.C., A.R. Hansen, and J.J. Tribbia, 1981: A note on the release of available potential energy. Submitted to J. Meteor. Soc. Japan.

Chen, T.C., and J. Shukla, 1981: Response of the GLAS general circulation model to a Pacific SST anomaly. In preparation.

Egger, J., 1978: Dynamics of blocking highs. J. Atmos. Sci., 35, 1788-1801

Egger, J., 1979: Stability of blocking in barotropic channel flow. Beitr. Phys. Atmos. 52, 27-43.

Elliott, R.D., and T.B. Smith, 1949: A study of the effects of large blocking highs on the general circulation in the northern-hemisphere westerlies. J. Meteor., 2, 67-85.

Gall, R., R. Blakeslee, and R.C.J. Somerville, 1979: Cyclone-scale forcing of ultralong waves. J. Atmos. Sci., 36, 1692-1698.

Hansen, A.R., 1981: A diagnostic study of the spectral energetics of blocking. Ph.D. Dissertation, Iowa State University, 180 pp.

Harnack, R.P., 1980: An appraisal of the circulation and temperature pattern for winter 1978-79 and a comparison with the previous two winters. Mon. Wea. Rev., 108, 37-55.

Hartman, D.L., and S.J. Ghan, 1980: A statistical study of the dynamics of blocking. Mon. Wea. Rev., 108, 1144-1159.

Julian, P.R., and K.B. Labitzke, 965: A study of atmospheric energetics during the January-February 1963 stratospheric warming. J. Atmos. Sci. 22, 597-610.

Kanamitsu, M., T.N. Krishnamurti, and C. Depradine, 1972: On scale interactions in the tropics during the northern summer. J. Atmos. Sci., 29, 698-706.

Kao, S.K., and C.N. Chi, 1978. Mechanism for the growth and decay of long- and synoptic-scale waves in the mid-troposphere. J. Atmos. Sci., 35, 1375-1387.

Lejenäs, H., 1977: On the breakdown of the westerlies. Atmosphere, 15, 89-113.

Murakami, T., and K. Tomatsu, 1965: Energy cycle in the lower atmosphere. J. Meteor. Soc. Japan, 43, 78-88.

Namias, J., 1964: Seasonal persistance and recurrance of European blocking during 1958-1960. Tellus, 16, 394-407.

Namias, J., 1980: Causes of some extreme Northern Hemisphere climatic anomalies from summer 1978 through the subsequent winter. Mon. Wea. Rev., 108, 1333-1346.

Paulin, G., 1970: A study of the energetics of January 1959. Mon. Wea. Rev., 98, 795-809.

Ratcliffe, R.A.S., and R. Murray, 1970: New lag associations between North Atlantic sea surface temperatures and European pressure applied to long range forecasting. Quart. J. Roy. Meteor. Soc., 96, 226-246.

Rex, D.F., 1950a: Blocking action in the middle troposphere and its effect upon regional climate. I. An aerological study of blocking action. Tellus, 2, 196-211.

Rex, D.F., 1950b: Blocking action in the middle troposphere and its effect on regional climate. II. The climatology of blocking action. Tellus, 2, 275-301.

Saltzman, B., 1957: Equations governing the energetics of the larger scales of atmospheric turbulence in the domain of wavenumber. J. Meteor., 14, 513-523.

Saltzman, B., 1970: Large-scale atmospheric energetics in the wavenumber domain. Rev. Geophys. Space Phys., 8, 289-302.

Sanders, F. and J.R. Gyakum, 1980: Synoptic-dynamic climatology of the "bomb". Mon. Wea. Rev., 108, 1589-1606.

Simmons, A.J., and B.J. Hoskins, 1978: The life cycles of some nonlinear baroclinic waves. J. Atmos. Sci., 35, 414-432.

Simmons, A.J., and B.J. Hoskins, 1980: Barotropic influences on the growth and decay of nonlinear baroclinic waves. J. Atmos. Sci., 37, 1679-1684.

Steinberg, H.L., A. Wiin-Nielsen, and C.-H. Yang, 1971: On nonlinear cascades in large-scale atmospheric flow. J. Geophys. Res., 76, 8829-8840.

Tsay, C.-Y., and S.K. Kao, 1978: Linear and nonlinear contributions to the growth and decay of the large-scale atmospheric waves and jet stream. Tellus, 30, 1-14.

Tung, K.K., and R.S. Lindzen, 1979: A theory of stationary long waves. Part I: A simple theory of blocking. Mon. Wea. Rev., 107, 714-734.

Wiin-Nielsen, A., J.A. Brown, and M. Drake, 1963: On atmospheric energy conversions between the zonal flow and the eddies. Tellus, 15, 261-279.

Wiin-Nielsen, A., J.A. Brown, and M. Drake, 1964: Further studies of energy exchange between the zonal flow and the eddies. Tellus, 16, 168-180.

Figure Captions

Figure 1. 500 mb heights and temperatures at 0000 GMT 21 December 1978.

Figure 2. 500 mb heights and temperatures at 1200 GMT 25 December 1978.

Figure 3. 500 mb heights and temperatures at 1200 GMT 29 December 1978.

Figure 4. Spectrally filtered Hovmoller diagram of the planetary-scale height field (z_{1-4}) at 70°N for December 1978 (contour interval is 100 m, positive values are contoured with solid lines, negative values are contoured with dashed lines).

Figure 5a. Temporal evolution of the vertically integrated (1000-100 mb) energy cycle for 30°N to 80°N for 14 to 31 December 1978.

Figure 5b. Vertically integrated energy conversions in the same domain during late December 1978.

Figure 6a. Planetary-scale (wavenumbers 1-4) energetics for 14-31 December 1978. The upper part of the figure shows the evolution of K_{1-4} (solid line) and A_{1-4} (dashed line) and the lower part shows $C(A_Z, A_{1-4})$ (heavy solid line); $C(A_{1-4}, K_{1-4})$ (dashed line); $C(K_Z, K_{1-4})$ (dot-dashed line) and the contribution to K_{1-4} due to nonlinear interactions of waves 1-4 with all other waves (thin solid line).

Figure 6b. Intermediate-scale (wavenumbers 5-10) energetics for 14-31 December 1978. The upper part of the figure shows K_{5-10} (solid line) and A_{5-10} (dashed line), and the lower part shows $C(A_Z, A_{5-10})$ (thick solid line); $C(A_{5-10}, K_{5-10})$ (dashed line); $C(K_Z, K_{5-10})$ (dot-dashed line); and the rate of change of K_{5-10} due to nonlinear interactions with all other waves (thin solid line).

Figure 7a. The intermediate-scale height field (z_{5-10}) at 500 mb at 1200 GMT 18 December 1978 (contour interval is 100 m, solid contours indicate positive values and dashed contours indicate negative values in this and all other polar sterographic projections).

Figure 7b. $C(A_{5-10}, K_{5-10})$ at 500 mb on 1200 GMT 18 December 1978 (contour interval is 2.5×10^{-3} m^2/s^3.

Figure 8. The intermediate-scale heat transport (vT_{5-10}) at 850 mb on 1200 GMT 10 December 1978 (contour interval is 50°C m/s).

Figure 9a. The intermediate-scale momentum transport (uv_{5-10}) at 300 mb on 1200 GMT 19 December 1978 (contour interval is 100 m^2/s^2).

Figure 9b. z_{1-4} at 500 mb on 1200 GMT 19 December 1978.

Figure 10a. K_{5-10} at 500 mb on 1200 GMT 19 December 1978 (contour interval is 100 m^2/s^2).

Figure 10b. K_{1-4} at 500 mb on 1200 GMT 23 December 1978 (contour interval as in a).

Figure 11. $C(A_{1-4}, K_{1-4})$ at 500 mb on 1200 GMT 19 December 1978.

Figure 12a. z_{1-4} at 500 mb on 1200 GMT 23 December 1978 (contours every 100 m).

Figure 12b. T_{1-4} at 500 mb on 1200 GMT 23 December 1978 (contours every 5°C).

Figure 13. vT_{1-4} at 500 mb on 1200 GMT 21 December 1978 (contours every 50°C m/s).

Figure 14. Limited area energetics for the region bounded by 85°W, 20°W, 30°N and 75°N.

Figure 15. 500 mb heights and temperatures at 1200 GMT 30 December 1978.

Figure 16. 500 mb heights and temperatures at 0000 GMT 4 January 1979.

Figure 17. 500 mb heights and temperatures at 0000 GMT 12 January 1979.

Figure 18. Spectrally filtered Hovmoller diagram of z_{1-4} at 60°N for late December 1978 to mid January 1979.

Figure 19a. Energy cycle for late December 1978 to mid January 1979 (otherwise same as Figure 5a).

Figure 19b. $C(A_Z, A_E)$, $C(A_E, K_E)$ and $C(K_Z, K_E)$ for the same period.

Figure 20a. Planetary-scale energetics for 24 December 1978 to 12 January 1979 (otherwise same as Figure 6a).

Figure 20b. Intermediate-scale energetics for the same period (same as Figure 6b otherwise).

Figure 21a. z_{1-4} at 500 mb on 1200 GMT 30 December 1978.

Figure 21b. vT_{1-4} at 500 mb on 1200 GMT 30 December 1978.

Figure 21c. T_{1-4} at 500 mb on 1200 GMT 30 December 1978.

Figure 21d. $C(A_{1-4}, K_{1-4})$ at 500 mb on 1200 GMT 30 December 1978.

Figure 22. uv_{1-4} at 300 mb at 1200 GMT 30 December 1978.

Figure 23. K_{1-4} at 500 mb on 1200 GMT 31 December 1978.

Figure 24. vT_{1-4} at 500 mb on 0000 GMT 4 January 1979.

Figure 25a. T_{1-4} at 500 mb on 0000 GMT 4 January 1979.

Figure 25b. z_{1-4} at 500 mb on 0000 GMT 4 January 1979.

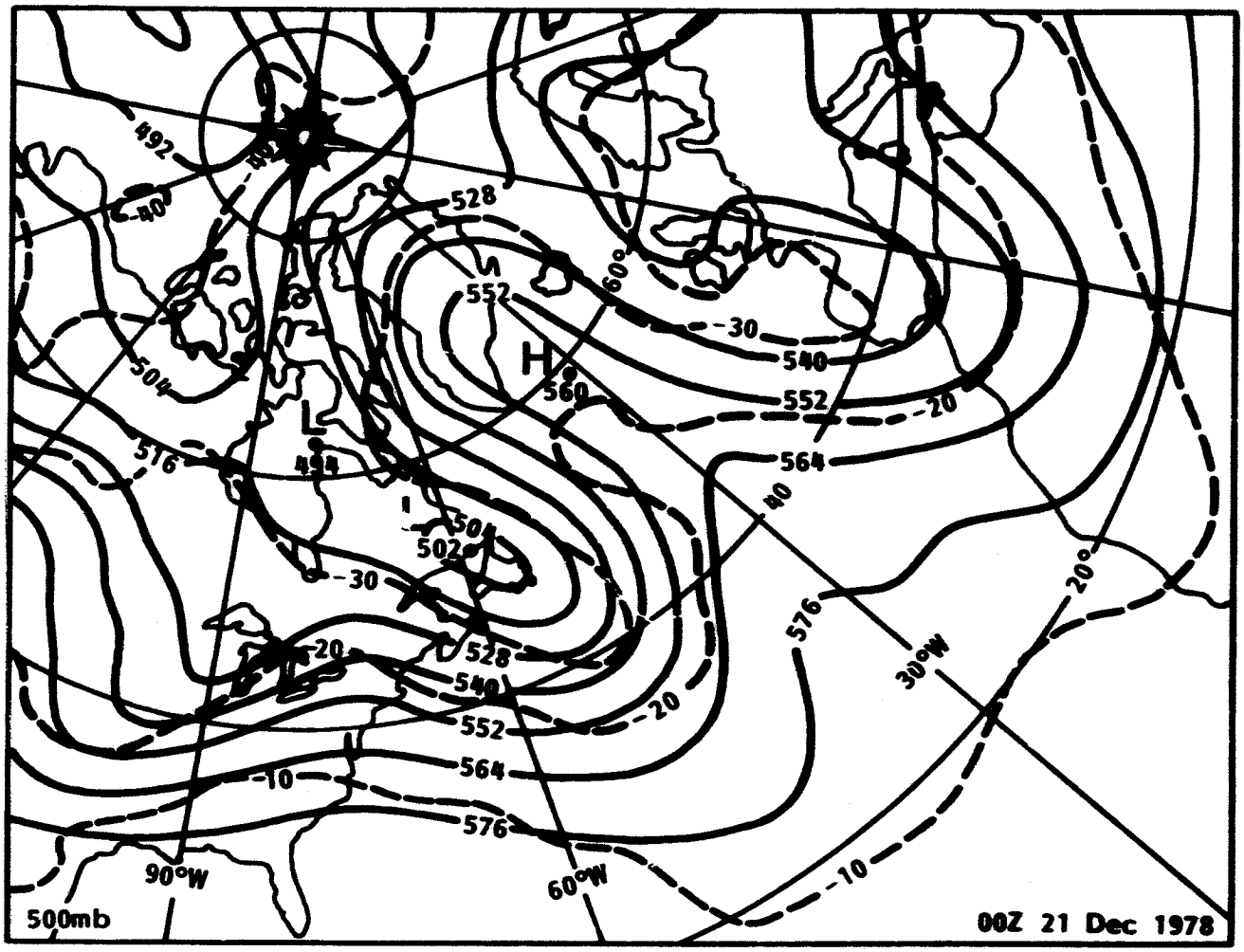
492
528
552
564
576
540
504
516
488
502
H
560
-30
-20
-10
-40
-60
20°
30°W
90°W
60°W
500mb
00Z 21 Dec 1978

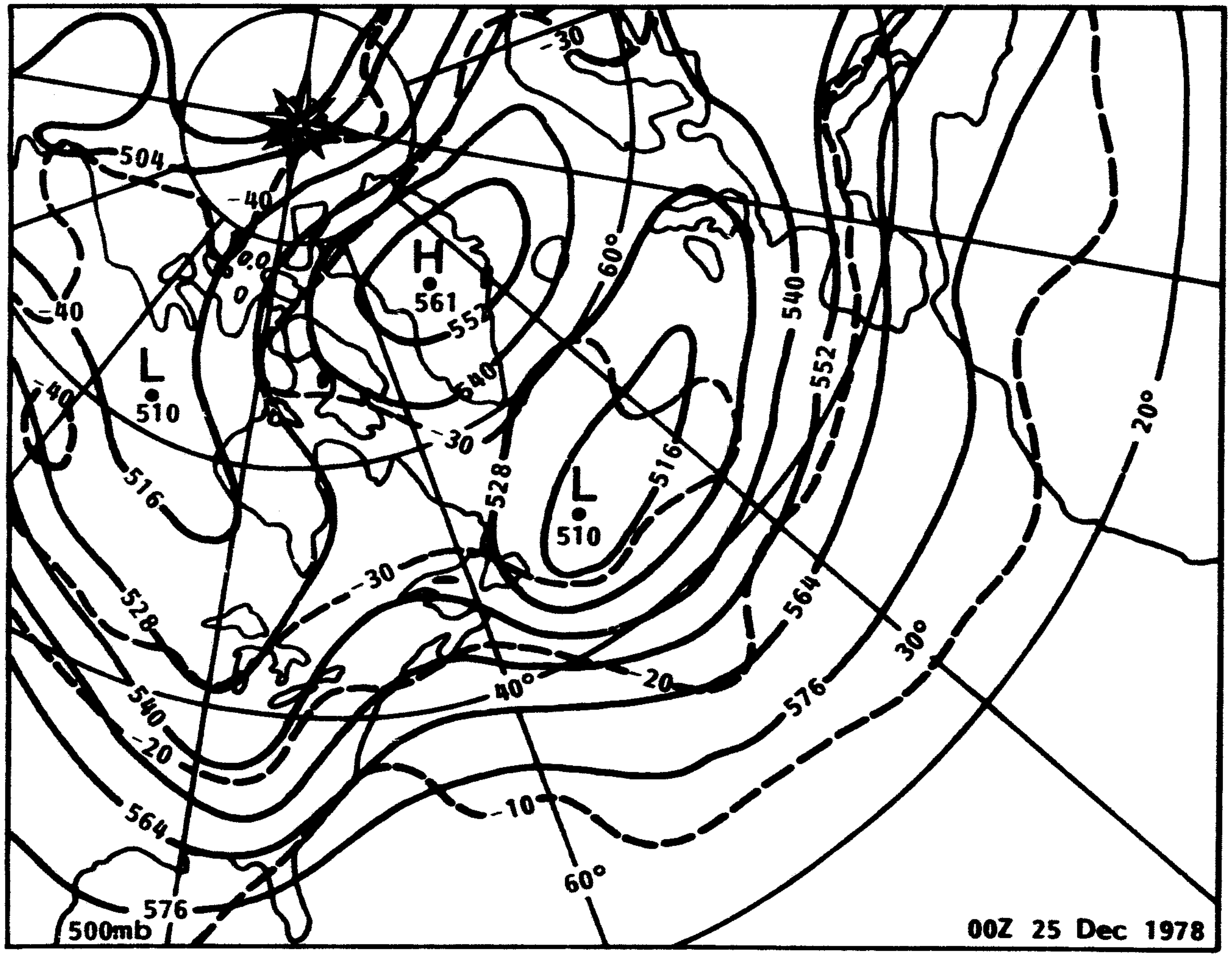
500mb
00Z 25 Dec 1978
H
561
L
510
L
510
504
516
528
540
552
564
576
-40
-30
-20
-10
20°
30°
40°
60°

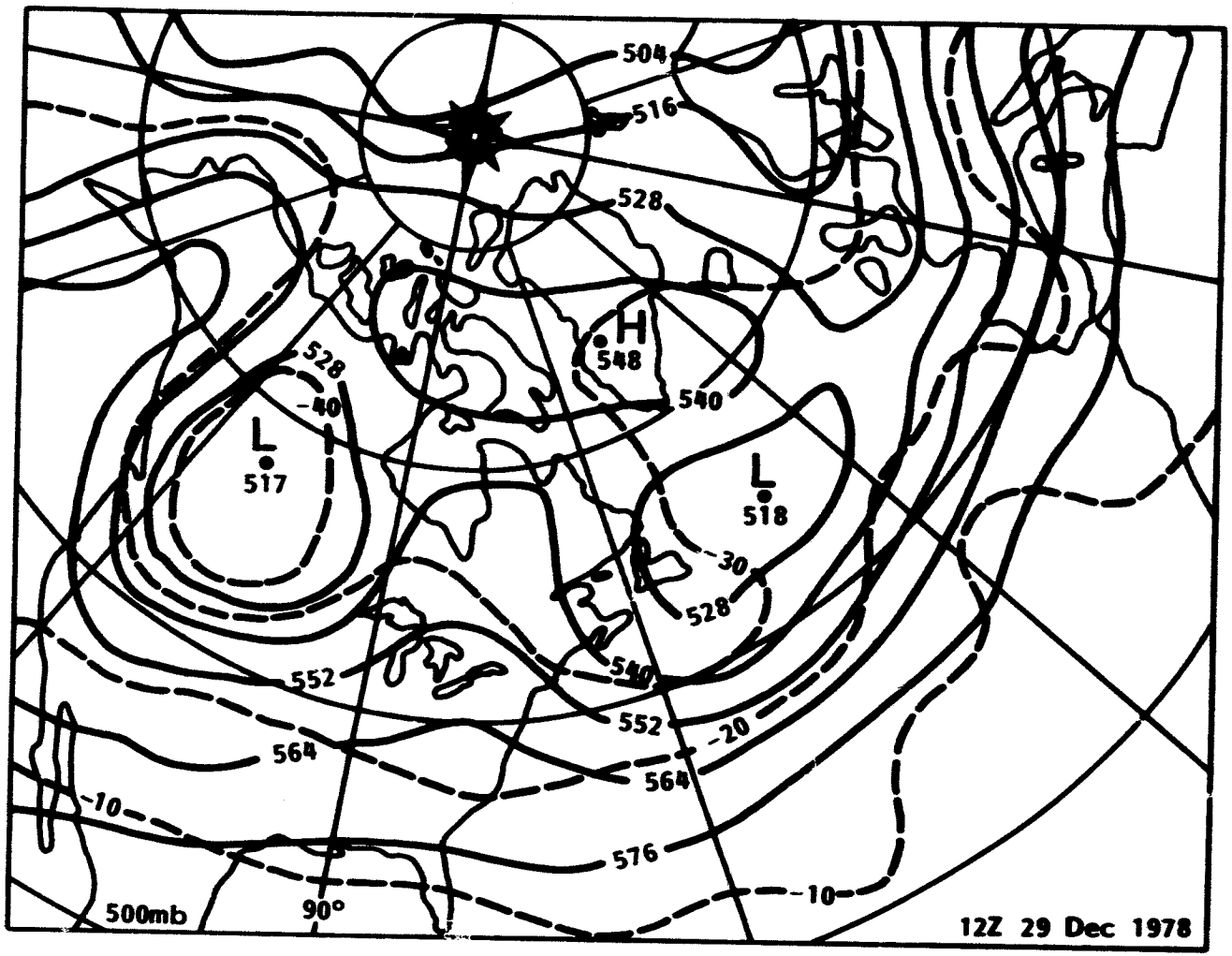
504
516
528
H
548
528
-40
540
L
517
L
518
-30
528
552
540
552
-20
564
564
-10
576
-10
500mb
90°
12Z 29 Dec 1978

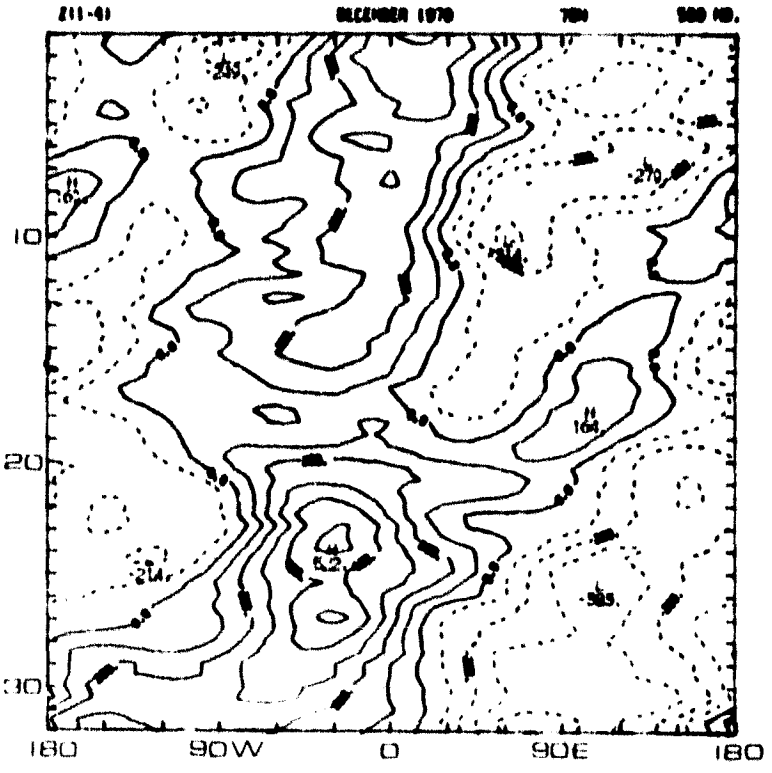
10
20
30
180
90W
0
90E
180

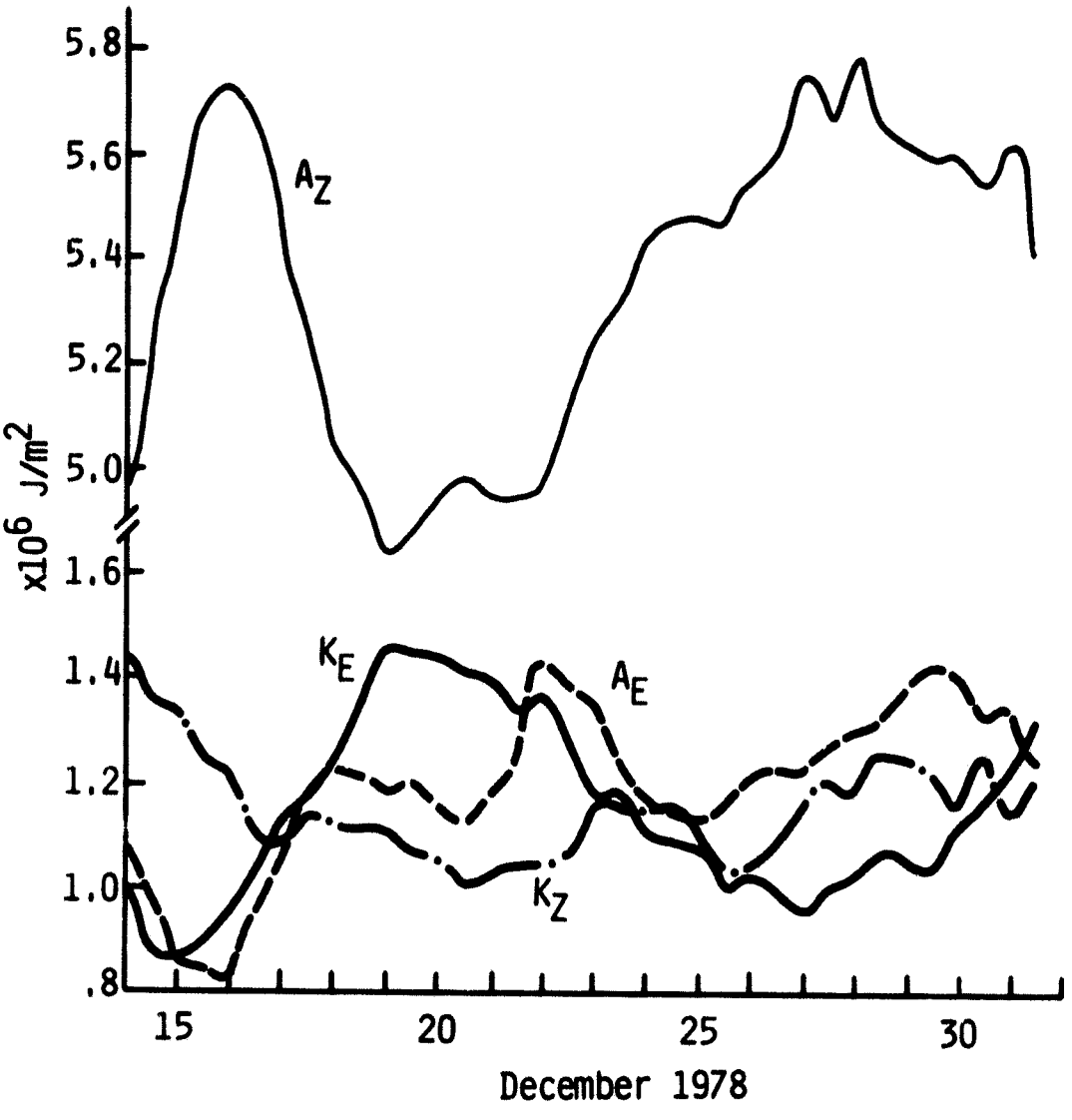
5.8
5.6
5.4
5.2
5.0
1.6
1.4
1.2
1.0
.8
x10^6 J/m^2
A_Z
K_E
A_E
K_Z
15
20
25
30
December 1978

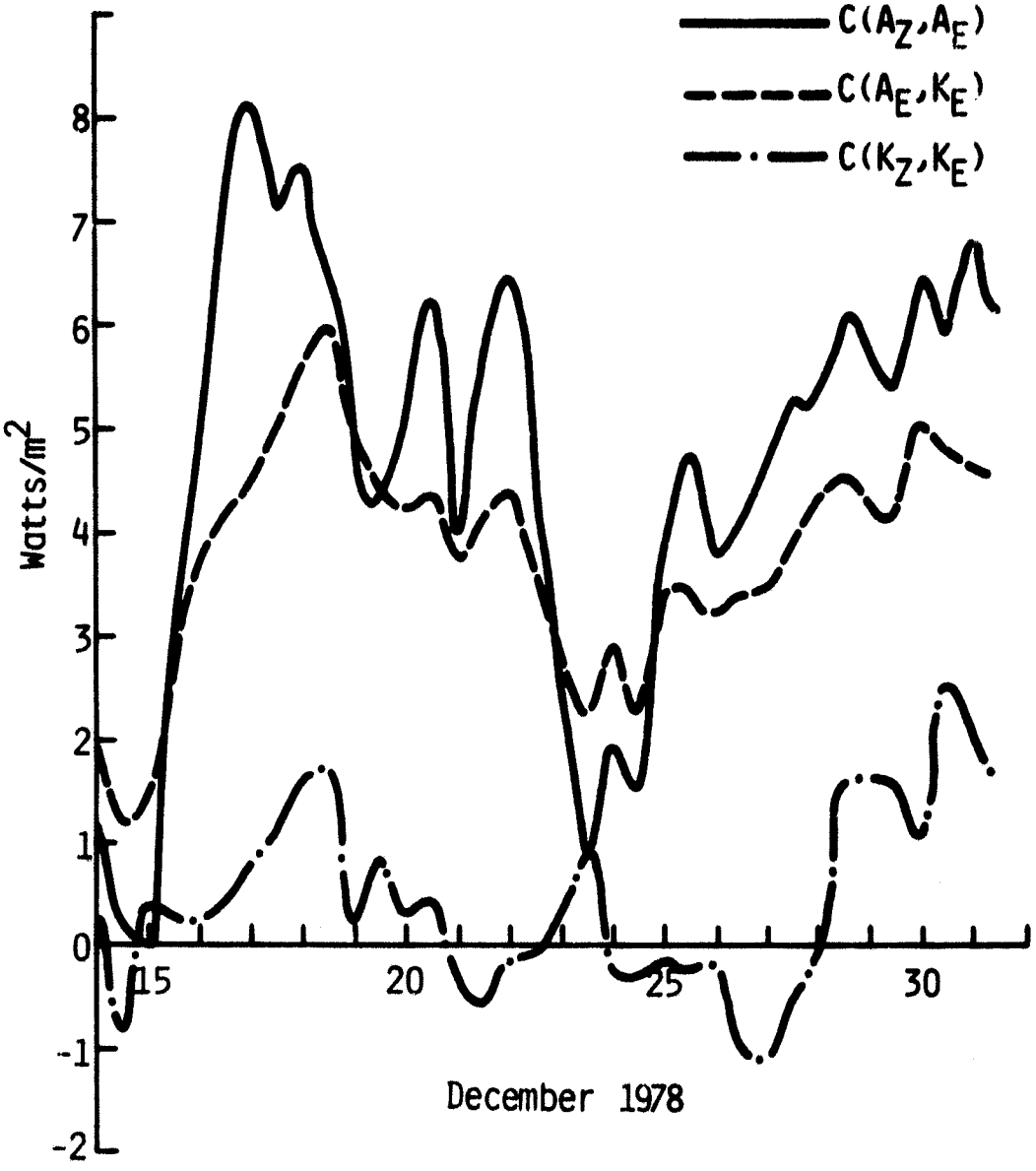
C(A_Z, A_E)
C(A_E, K_E)
C(K_Z, K_E)
Watts/m²
8
7
6
5
4
3
2
1
0
-1
-2
15
20
25
30
December 1978

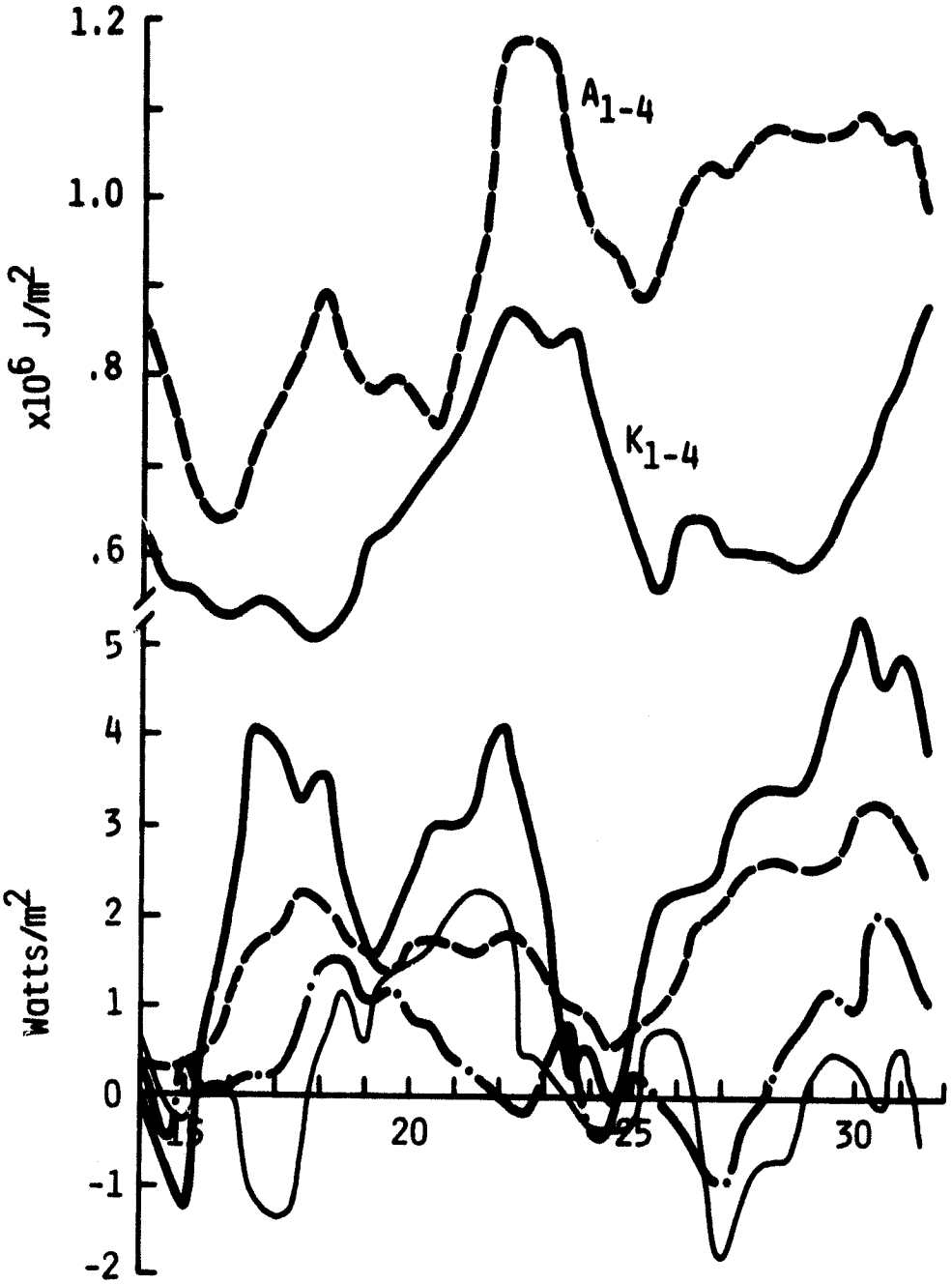
1.2
1.0
.8
.6
x10^6 J/m^2
A1-4
K1-4
5
4
3
2
1
0
-1
-2
Watts/m^2
15
20
25
30
December 1978

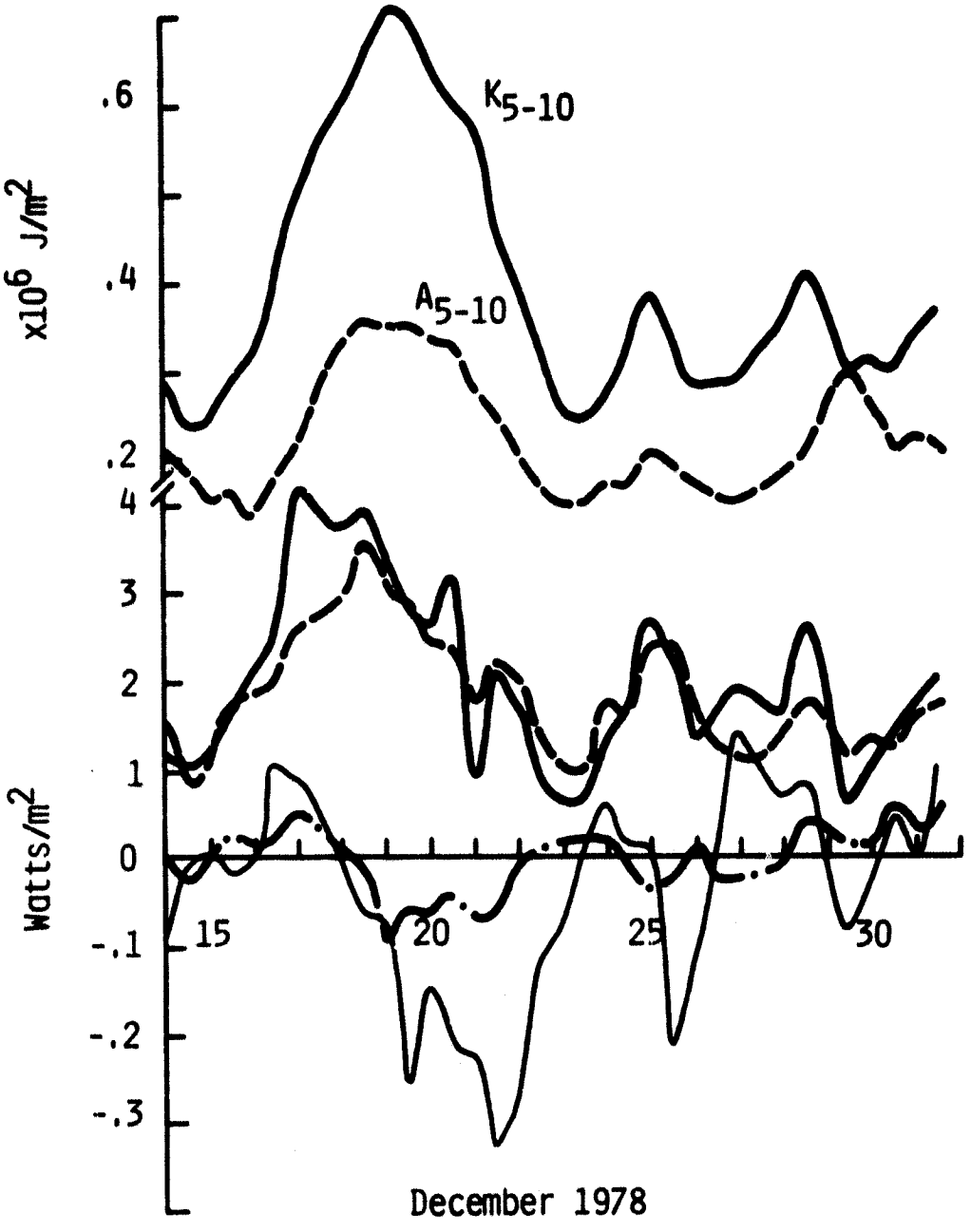
.6
.4
.2
x10^6 J/m^2
K5-10
A5-10
4
3
2
1
0
-.1
-.2
-.3
Watts/m^2
15
20
25
30
December 1978

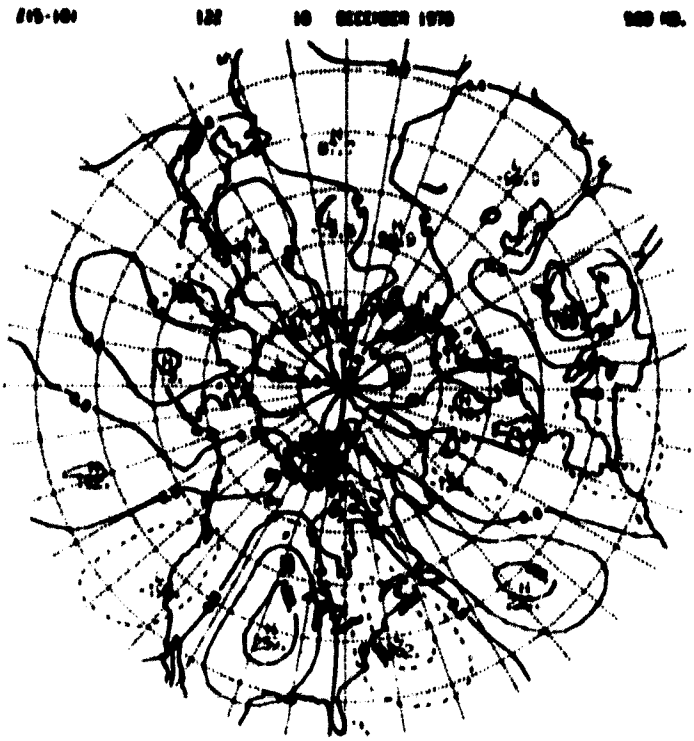

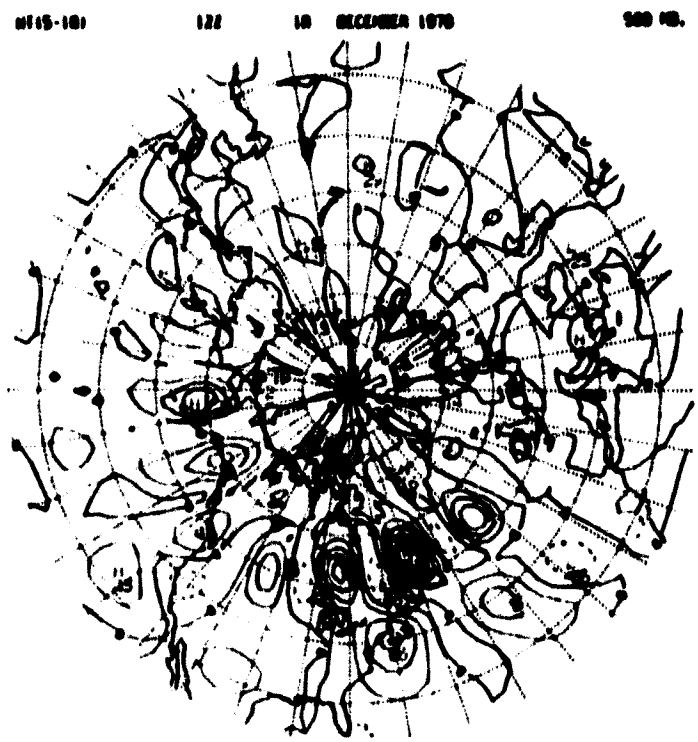

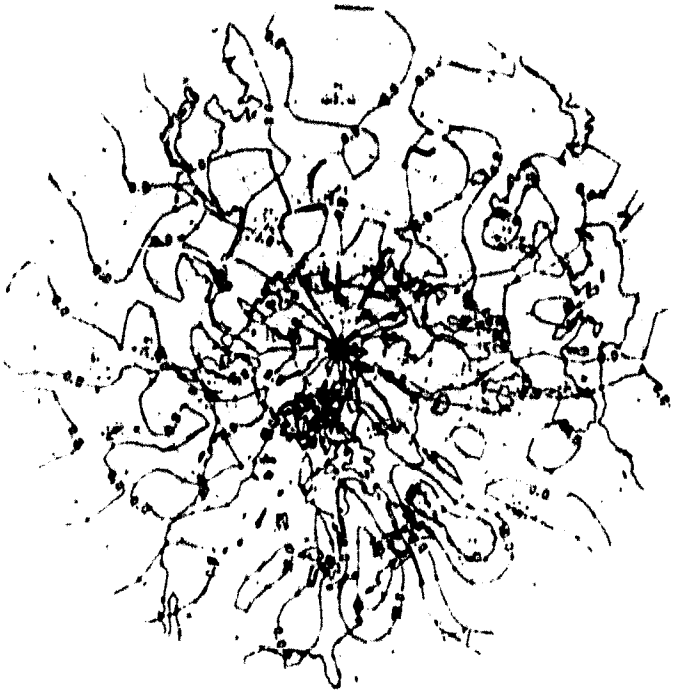

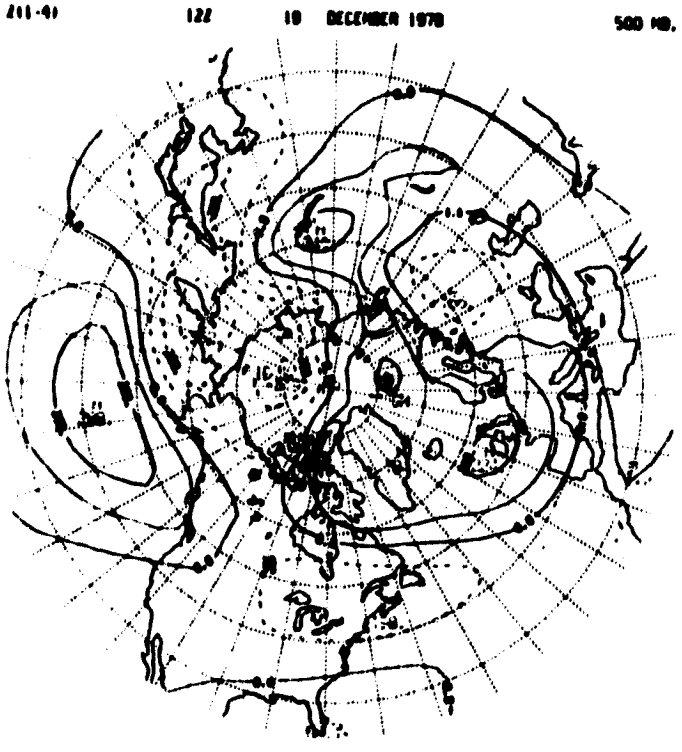


122
19 DECEMBER 1970
500 MB.

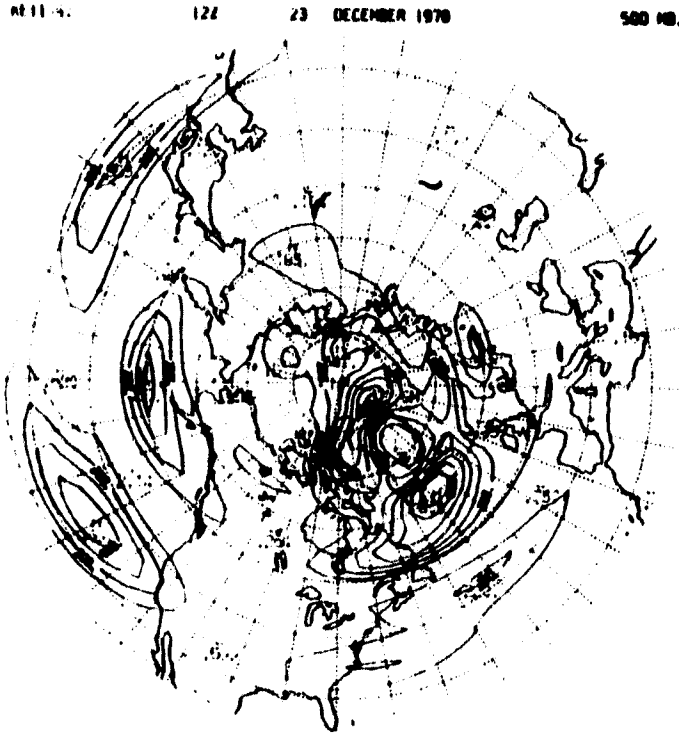
122
23 DECEMBER 1970
500 MB.

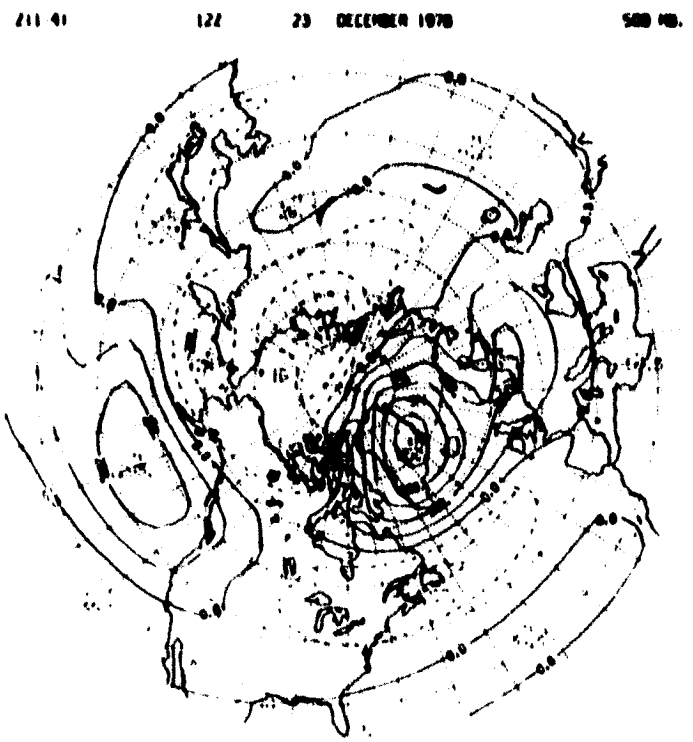
Z11 41 122 23 DECEMBER 1970 500 MB.

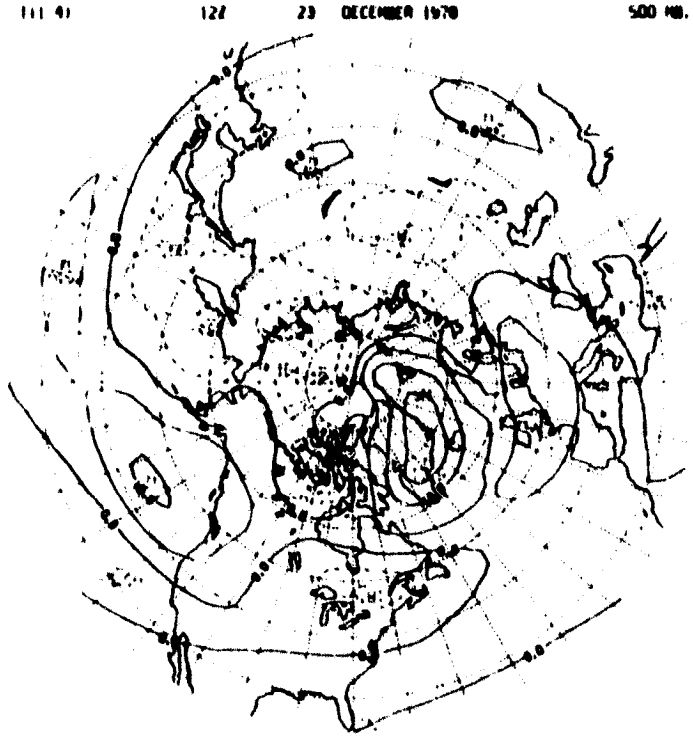
111 41 122 23 DECEMBER 1970 500 MB.


VIII-01
122
21 DECEMBER 1970
500 MB.

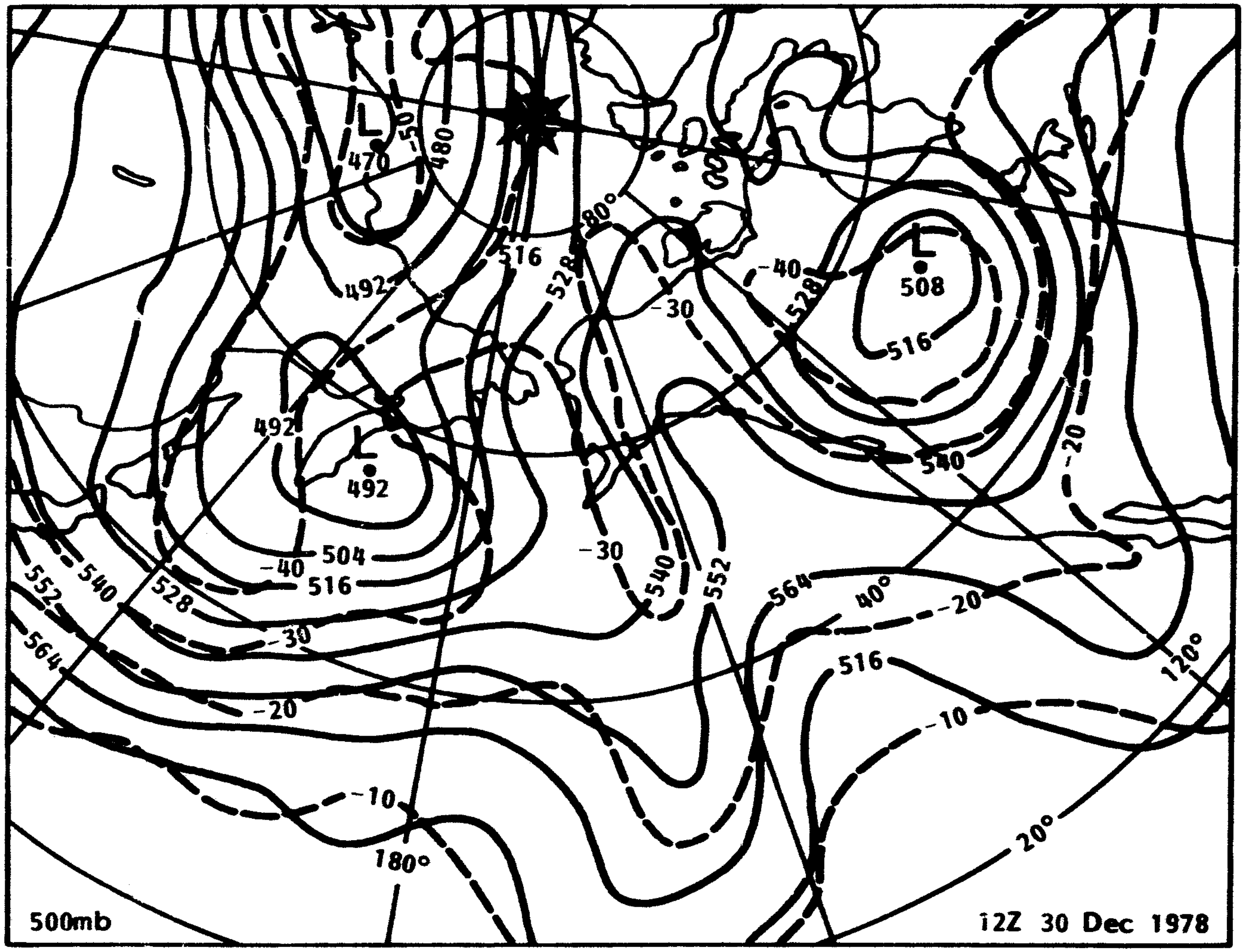
L
470
-50
480
516
528
80°
492
-40
L
508
-30
528
516
492
L
492
540
-20
504
-40
516
-30
540
552
564
40°
-20
516
540
552
564
528
-30
-20
-10
120°
-10
180°
20°
500mb
12Z 30 Dec 1978

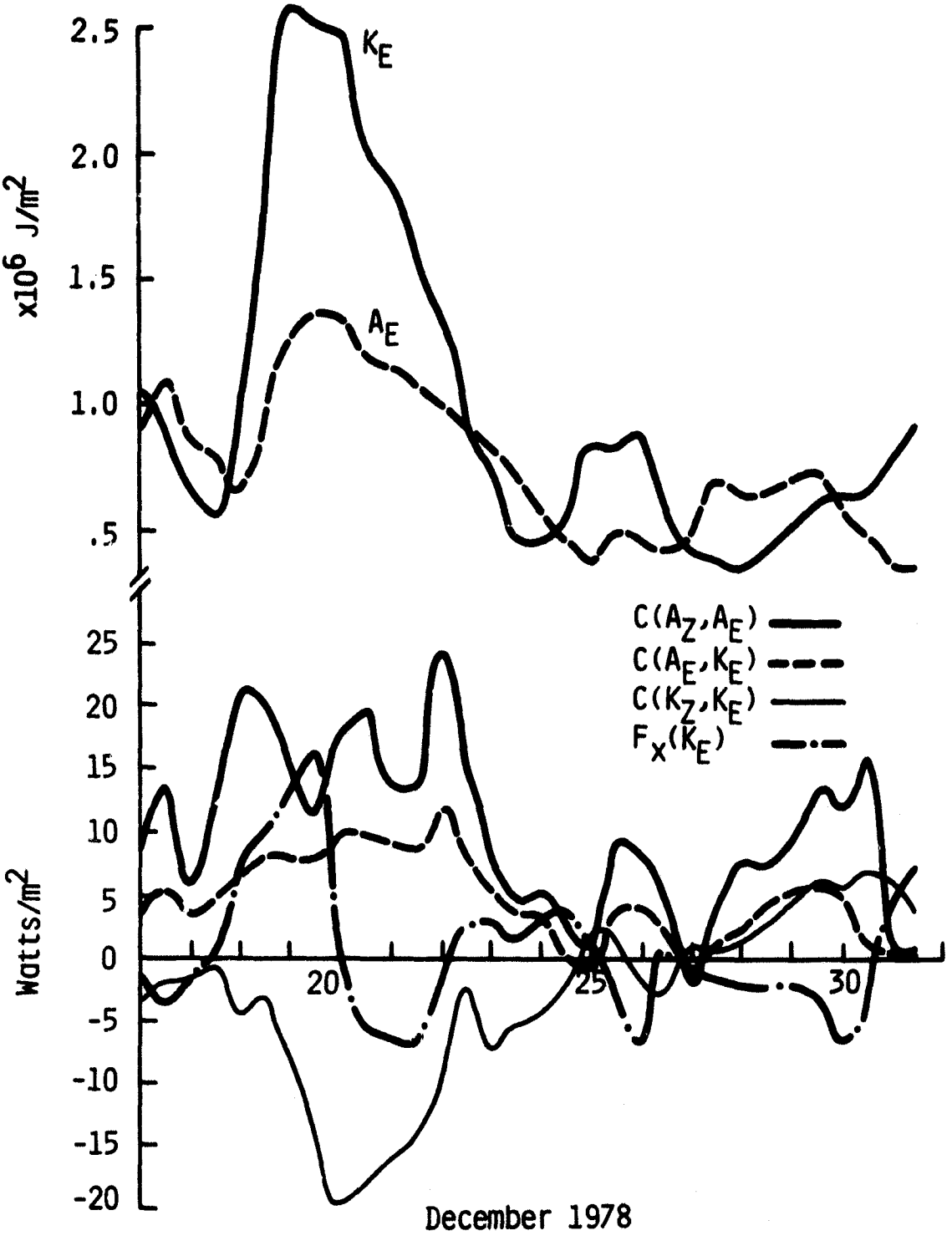
2.5
2.0
1.5
1.0
.5
x10^6 J/m^2
K_E
A_E
25
20
15
10
5
0
-5
-10
-15
-20
Watts/m^2
C(A_Z, A_E)
C(A_E, K_E)
C(K_Z, K_E)
F_X(K_E)
20
25
30
December 1978

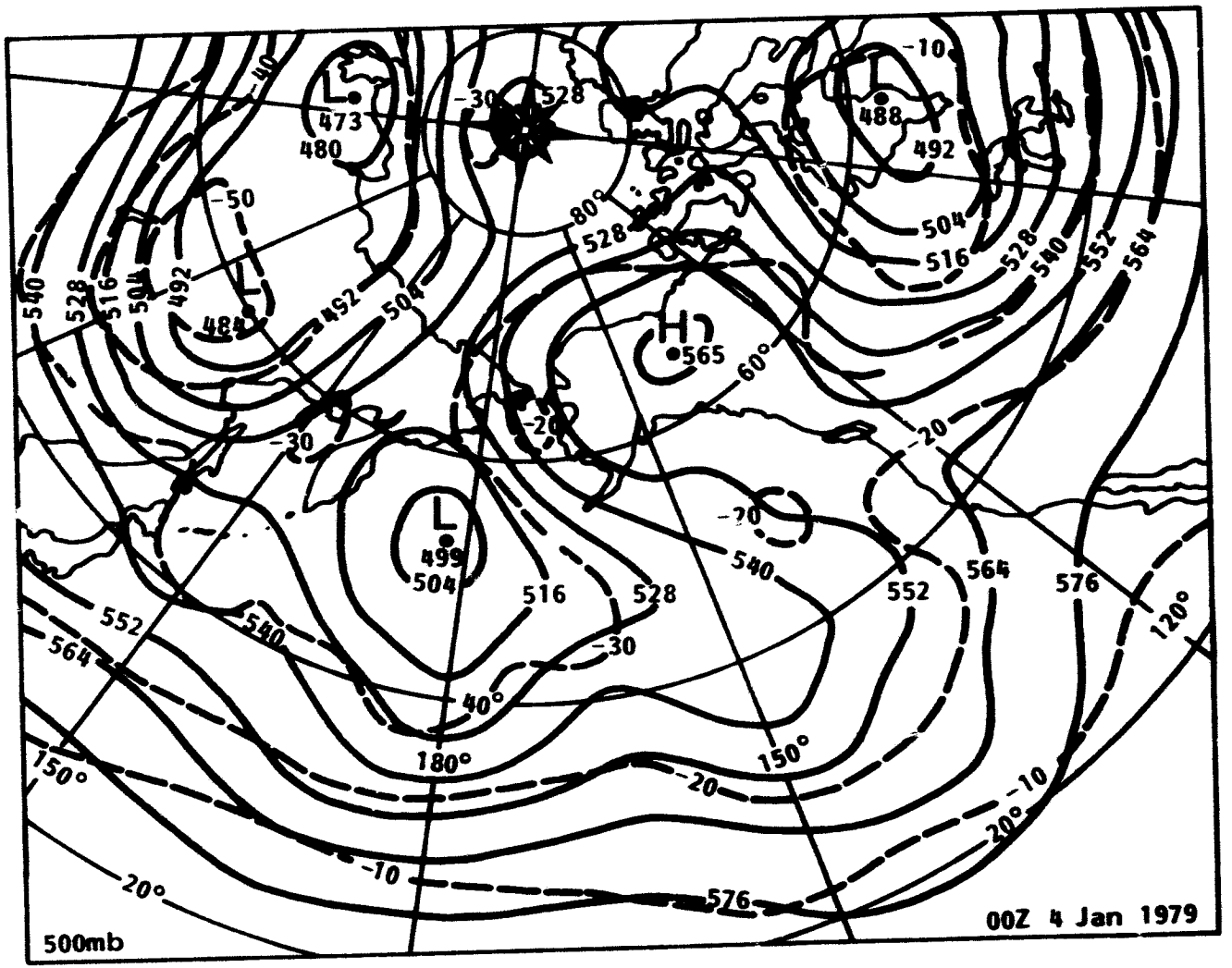
500mb
00Z 4 Jan 1979

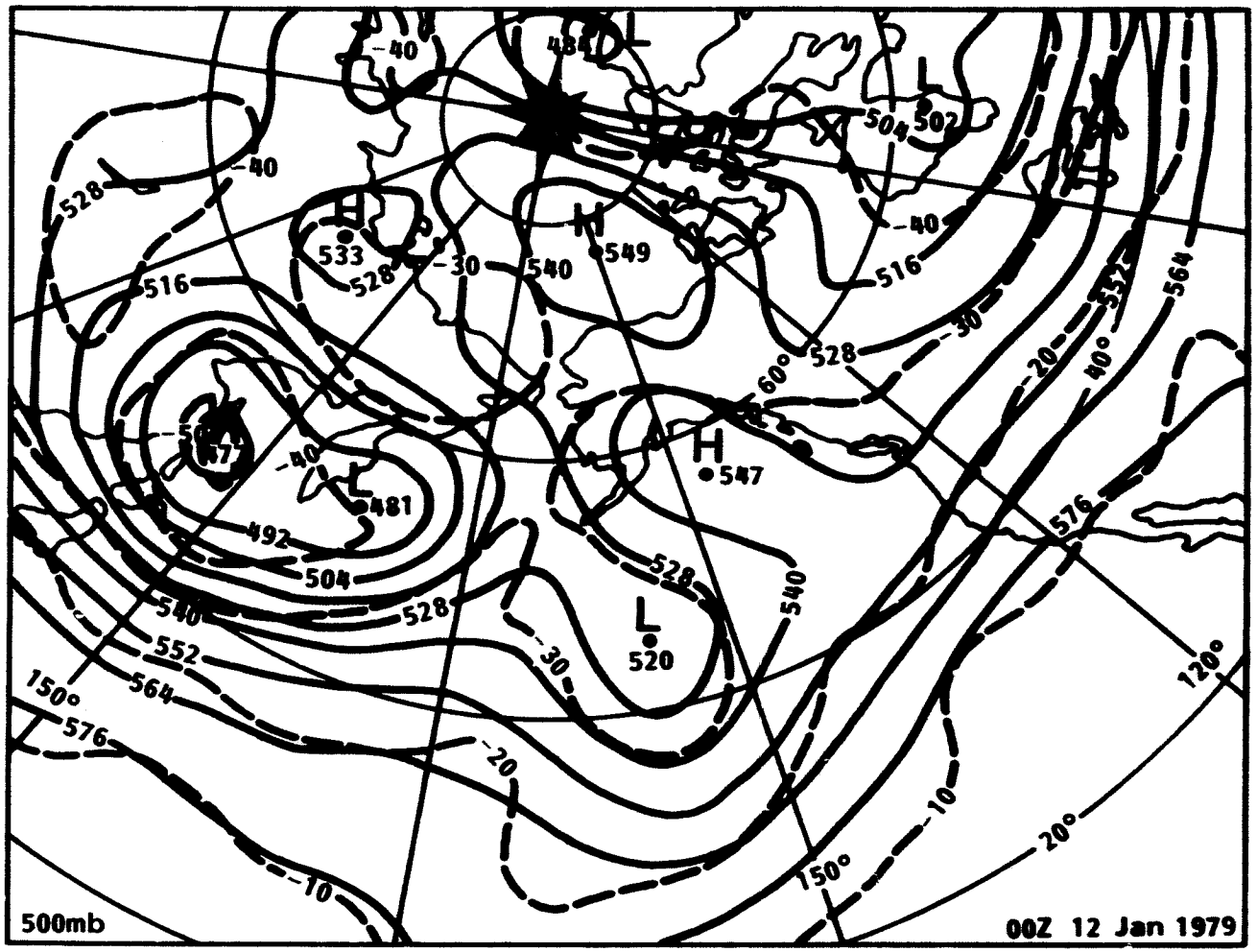
500mb
00Z 12 Jan 1979

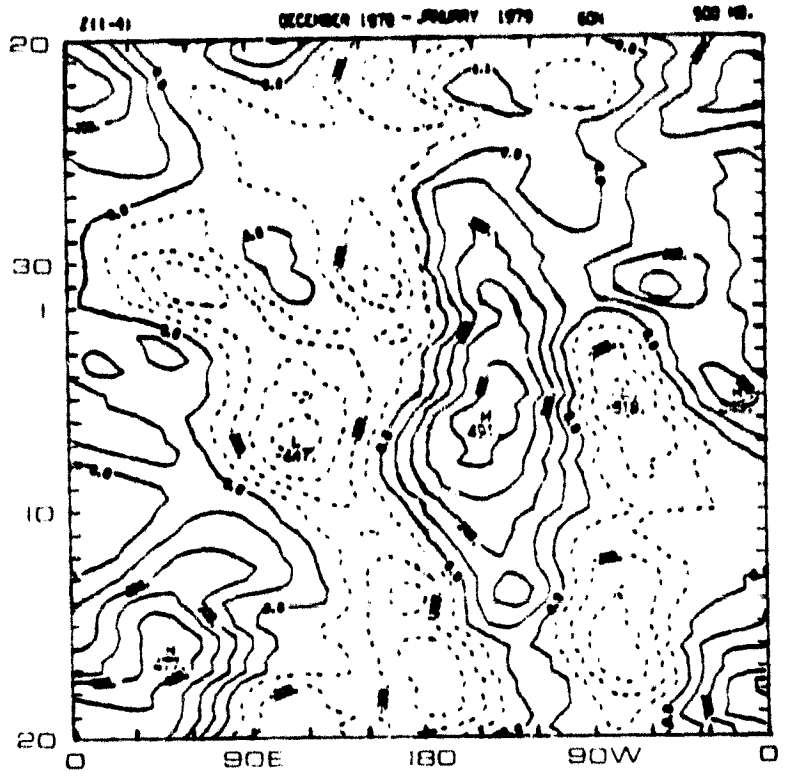
20
30
1
10
20
0
90E
180
90W
0

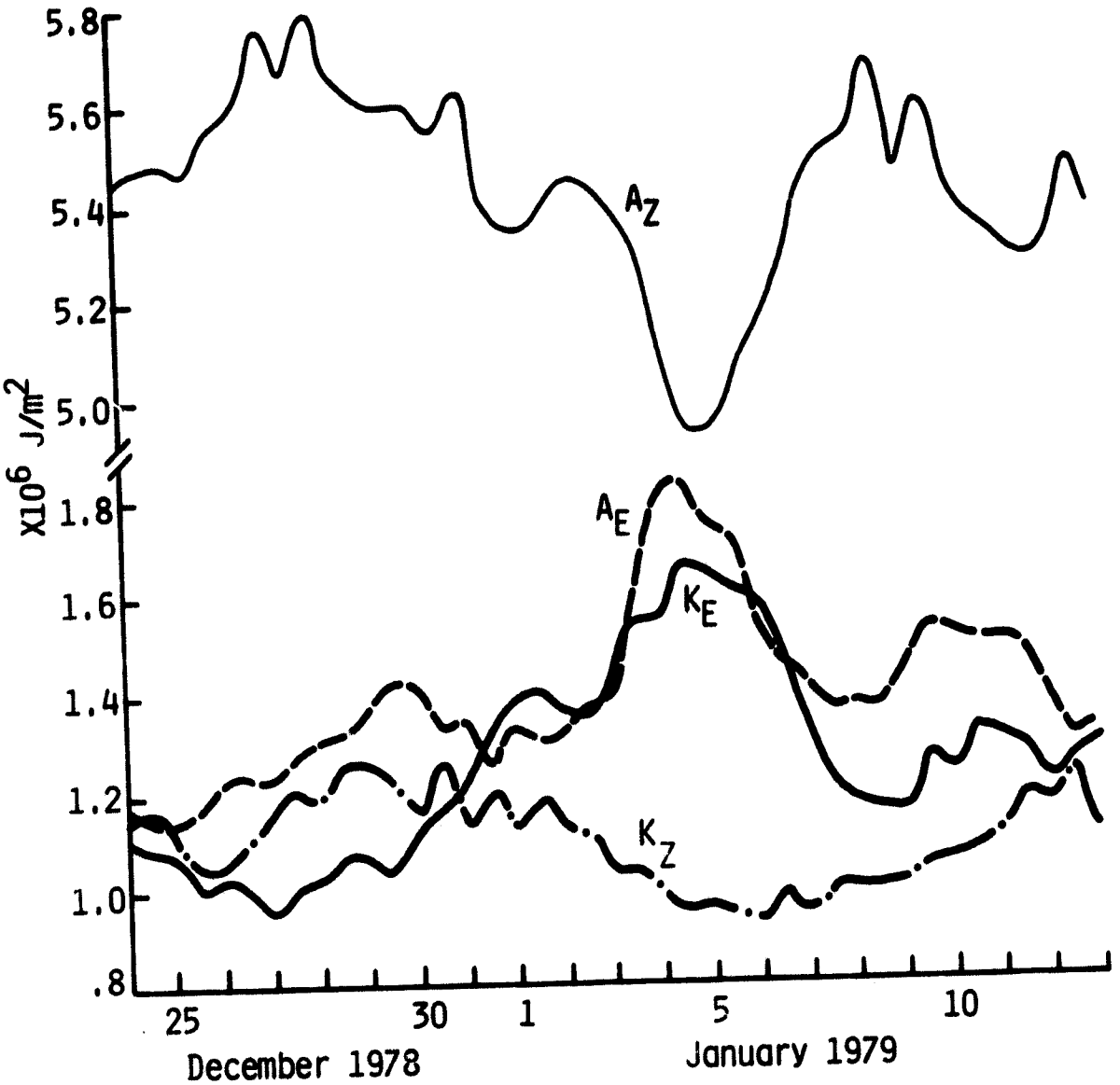
5.8
5.6
5.4
5.2
5.0
A_Z
$X10^6$ J/m^2
1.8
1.6
1.4
1.2
1.0
.8
A_E
K_E
K_Z
25
30
1
5
10
December 1978
January 1979

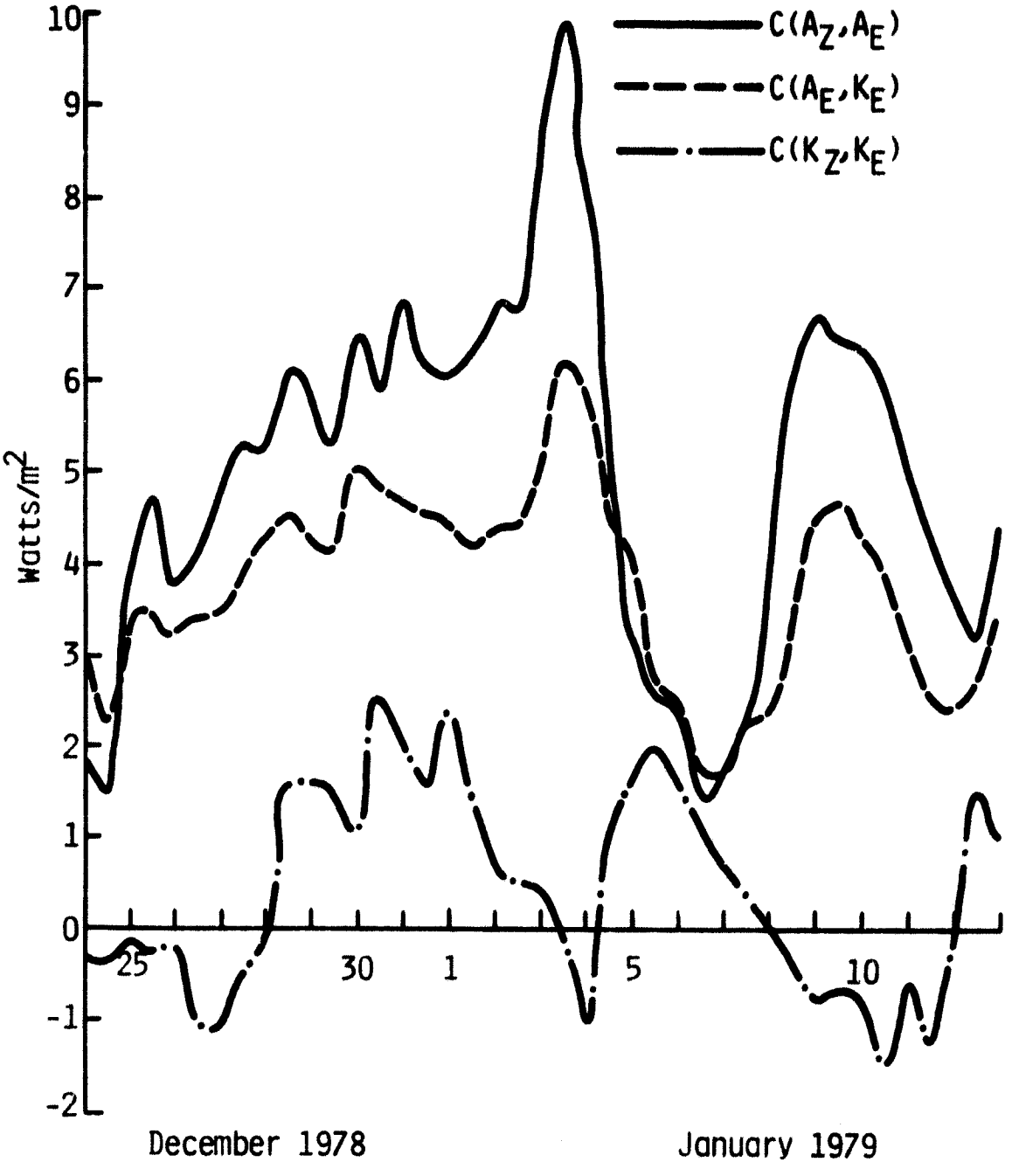
10
9
8
7
6
5
4
3
2
1
0
-1
-2
Watts/m²
C(A_Z, A_E)
C(A_E, K_E)
C(K_Z, K_E)
25
30
1
5
10
December 1978
January 1979

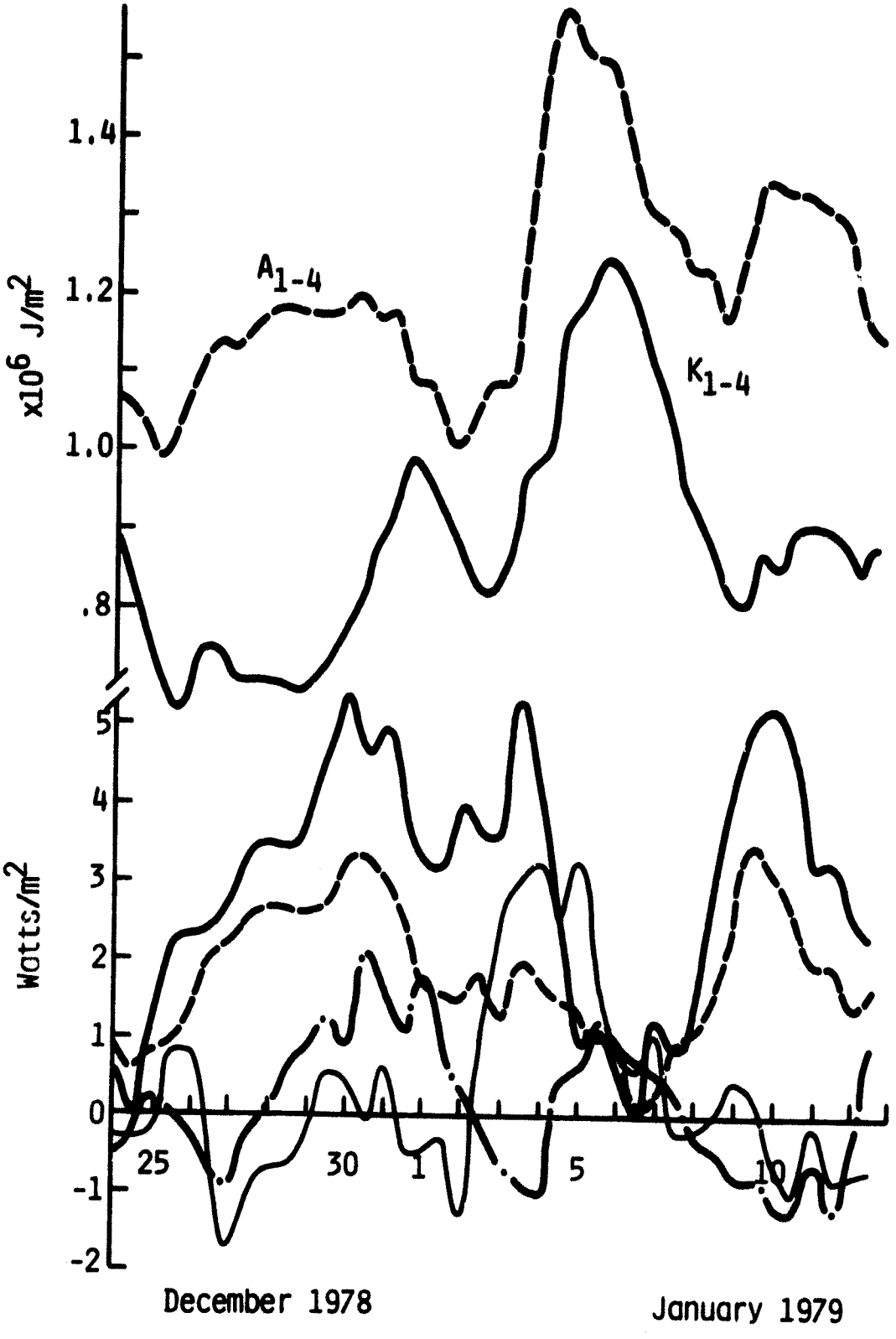
1.4
1.2
1.0
.8
x10^6 J/m^2
A1-4
K1-4
5
4
3
2
1
0
-1
-2
Watts/m^2
25
30
1
5
10
December 1978
January 1979

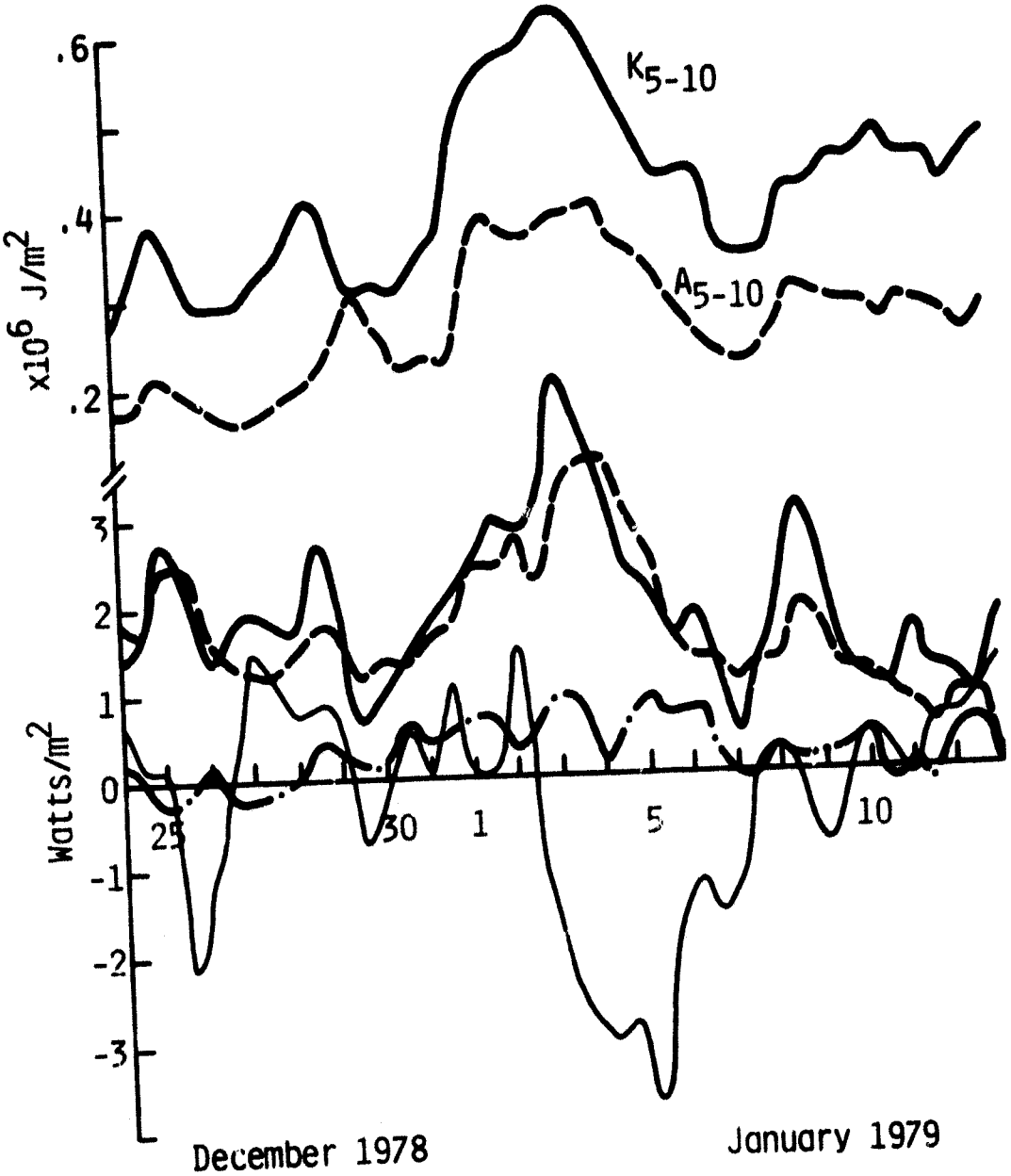
.6
.4
.2
K_{5-10}
A_{5-10}
$x10^6$ J/m^2
3
2
1
0
-1
-2
-3
Watts/m^2
25
30
1
5
10
December 1978
January 1979

VII 41 122 30 DECEMBER 1970 500 MB.

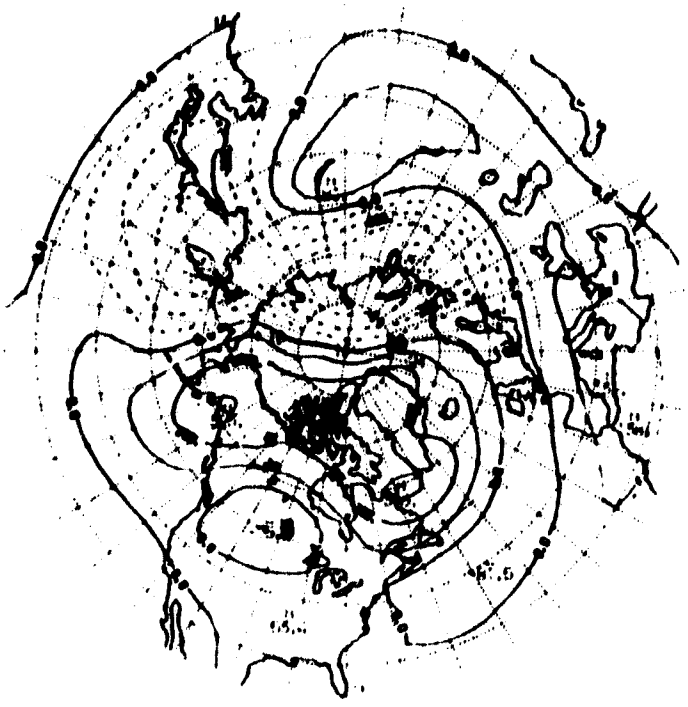

VIII 41 122 30 DECEMBER 1970 500 MB.


122 30 DECEMBER 1978 500 MB.

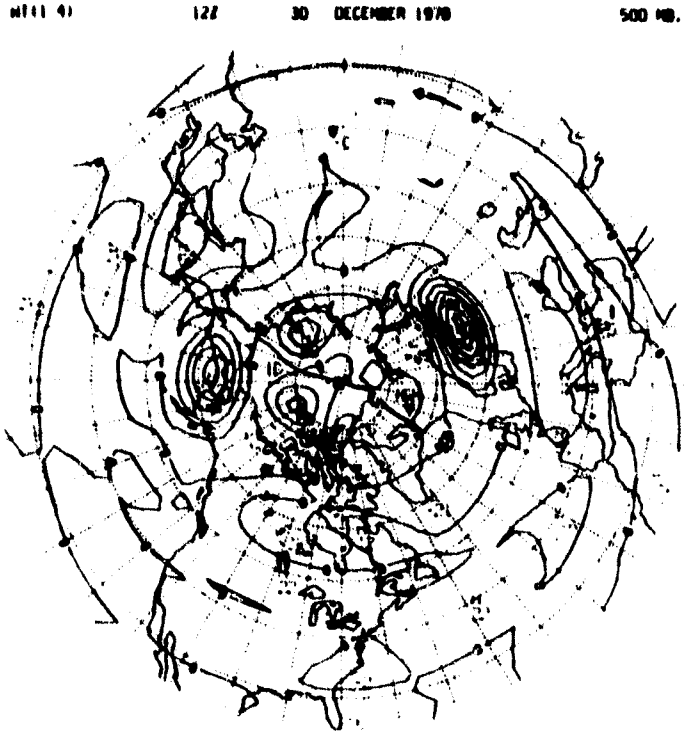
122 30 DECEMBER 1978 500 MB.

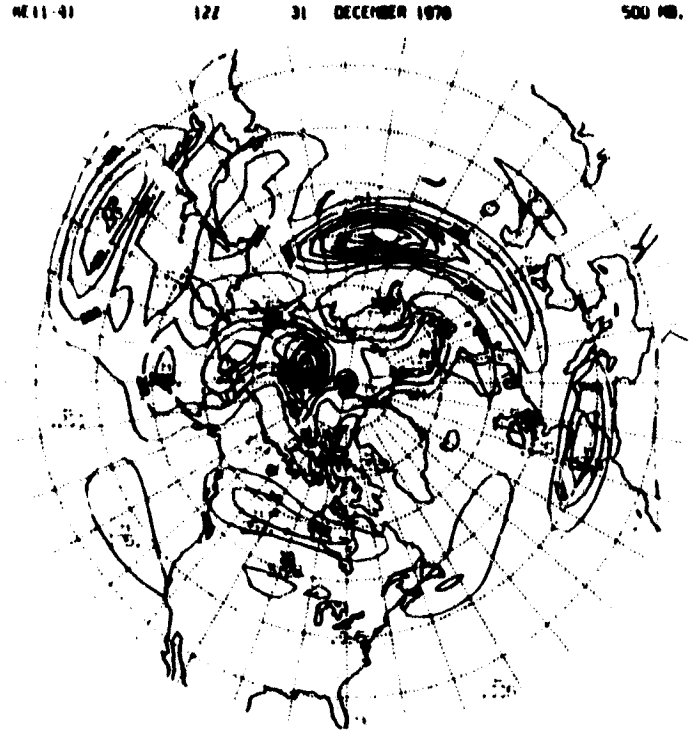

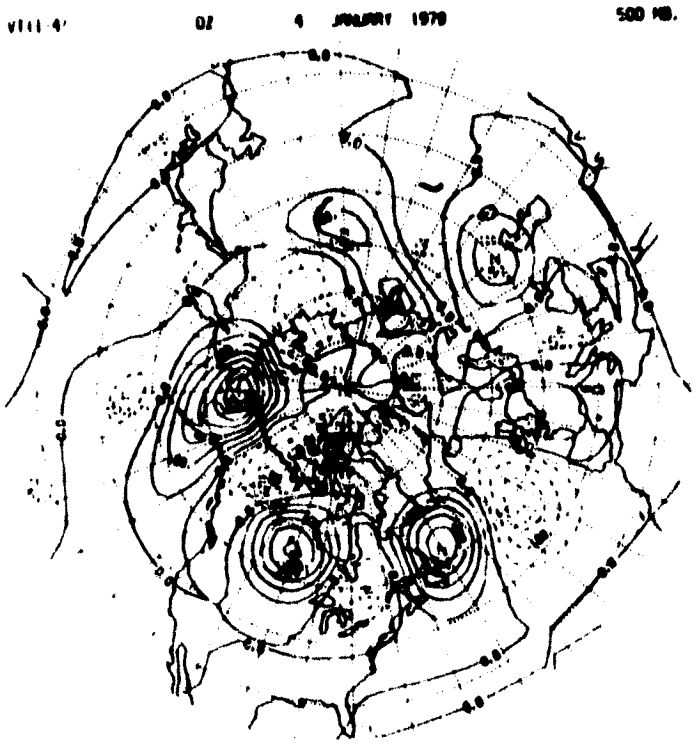
VIII 4'
02
4 JANUARY 1979
500 MB.

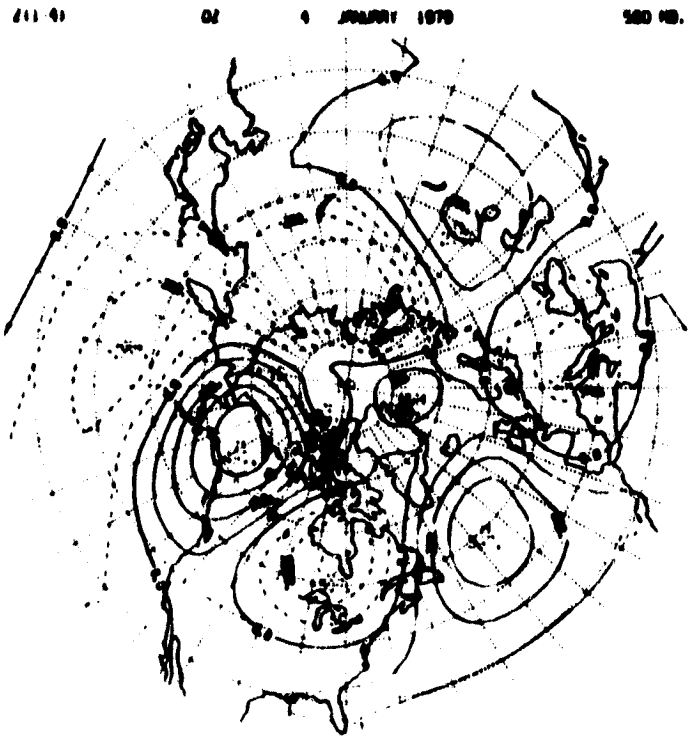

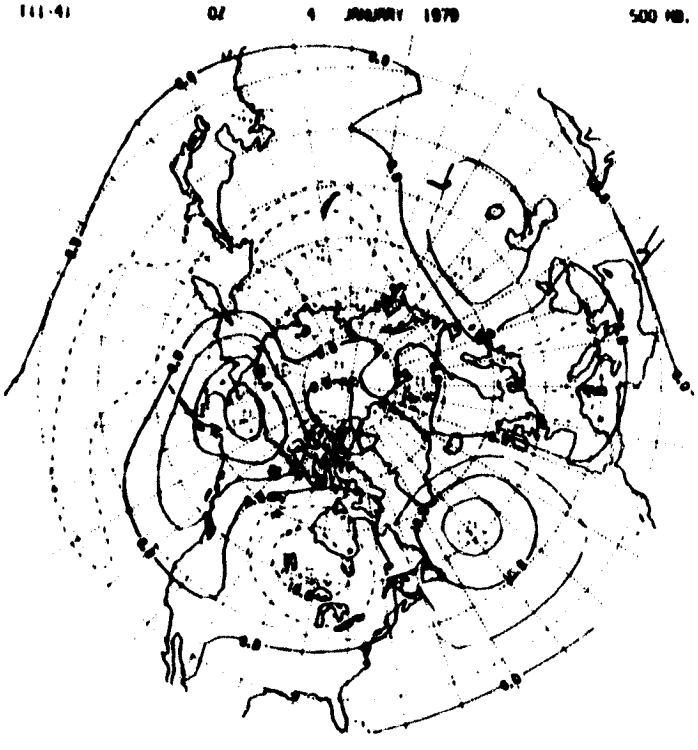

A Note on the Release of Available Potential Energy

by

Tsing-Chang Chen and Anthony R. Hansen

Department of Earth Sciences

Iowa State Unviersity

Ames, Iowa 50011

Joseph J. Tribbia

National Center for Atmospheric Research

Boulder, Colorado 80803

ABSTRACT

The height and temperature fields at the mandatory levels during a two-month period (December 1977-January 1978) are used to evaluate the conversion between available potential energy (A) and kinetic energy (K), C(A,K). The results reveal:

1. The energy conversion due to the mean meridional circulation, $C(A_Z, K_Z) = -0.18\ Wm^{-2}$, and due to the eddy motions, $C(A_E, K_E) = 2.6\ Wm^{-2}$.
2. $C(A_Z, K_Z)$ is attributed to the standing (2-month mean) mode, while $C(A_E, K_E)$ is due to the transient eddies.
3. The contributions to $C(A_E, K_E)$ from various wavenumber regimes, long waves (n=1-4), and cyclone and short waves (n=5-15), are:
   a. Transient cyclone and short waves are dominant in the midlatitudes and the middle layer of atmosphere.
   b. Transient long waves are significant in the middle layer of the atmosphere at mid- and high latitudes.
   c. Standing long waves are not negligible in the midlatitudes and the middle layer of atmosphere.

Introduction

The conversion between available potential energy (A) and kinetic energy (K), C(A, K), is regarded as the baroclinic process that maintains the atmospheric circulation (Wiin-Nielsen, 1968). Tomatsu (1979) recently made an extensive computation of this energy conversion employing multilevel data. However, he has noted that there had been very few analyses of C(A, K) for the hemisphere. This might well be due to the difficulty of evaluating the ω field in the atmosphere.

Recently, we used an alternative mathematical algorithm to solve the ω equation (see Appendix) rather than the conventional relaxation method. Some interesting features of C(A, K) were found in our computations using a two-month (December 1977-January 1978) multilevel data set analyzed at the National Meteorological Center (NMC). The purpose of this note is to report these C(A, K) results in the wavenumber regime and the contributions to C(A, K) from the standing and transient modes of the atmospheric motion.

Computation and Data

The conversion between A and K,

$$C(A, K) = \frac{1}{g} \int_0^{p_0} \int_S -\frac{R}{p} \omega T ds dp,$$

can be expressed in terms of a Fourier expansion representing the contribution from various wave components.

$$C(A,\ K) = \frac{1}{g}\int_0^{p_0}\int_\phi -\frac{R}{p}\omega_0 T_0 \cos\phi d\phi dp + \frac{1}{g}\int_0^{p_0}\int_\phi \sum_{n=1}^{N} -\frac{R}{p}(\omega_n T_n^* + \omega_n^* T_n)\cos\phi d\phi dp$$

$$C(0) \qquad\qquad \sum_{n=1}^{N} C(n) \qquad (1)$$

$$C(A_Z,\ K_Z) \qquad\qquad C(A_E,\ K_E)$$

The notations used are conventional and $(\ )^*$ = complex conjugate of $(\ )$. The two terms on the right-hand side of (1) are the energy conversions due to the mean meridional and eddy motions, respectively.

The expression of C(A, K) can also be resolved further to examine the contributions from the standing and transient modes of the atmospheric circulation,

$$\overline{C(A,\ K)} = \frac{1}{g}\int_0^{p_0}\int_\phi -\frac{R}{p}\bar{\omega}_0\bar{T}_0 \cos\phi d\phi dp + \frac{1}{g}\int_0^{p_0}\int_\phi -\frac{R}{p}\overline{\omega_0' T_0'} \cos\phi d\phi dp$$

$$C(0)_S \qquad\qquad C(0)_T$$

$$C(A_Z,\ K_Z)_S \qquad\qquad C(A_Z,\ K_Z)_T \qquad (2)$$

$$+ \frac{1}{g}\int_0^{p_0}\int_\phi \sum_{n-1}^{N} -\frac{R}{p}(\bar{\omega}_n\bar{T}_n^* + \bar{\omega}_n^*\bar{T}_n)\cos\phi d\phi dp + \frac{1}{g}\int_0^{p_0}\int_\phi \sum_{n=1}^{N} -\frac{R}{p}(\overline{\omega_n' T_n'^*} + \overline{\omega_n'^* T_n'})\cos\phi d\phi dp$$

$$\sum_{n-1}^{N} C(n)_S \qquad\qquad \sum_{n=1}^{N} C(n)_T$$

$$C(A_E,\ K_E)_S \qquad\qquad C(A_E,\ K_E)_T$$

where $\bar{(\ )}$ = time mean and $(\ )' = (\ ) - \bar{(\ )}$, is the transient mode. The subscripts S and T denote the standing and transient modes, respectively. N = 15 and the time mean is a two-month average in this study.

The p vertical motion of the atmosphere is evaluated by using the ω equation of the quasi-geostrophic model. The ω equation has the form of Poisson's

equation and conventionally is solved by the relaxation method (e.g., Krishnamurti, 1968). In this study, an alternative approach employing the tech..que of spherical harmonics to solve the ω equation is used. The ω field can be obtained through a matrix equation which relates the spectral coefficients of ω and the forcing functions in the ω equation. Our experience reveals hat this approach is computationally faster than the conventional relaxation method. The detailed algorithm of this approach is shown in the Appendix. The boundary conditions used in this study are $\omega = 0$ at 1000 and 100 mb for the simplicity of computations.

The computations of this study use the twice daily height and temperature fields on the 2.5° x 2.5° grid of the NMC analysis for December 1977 and January 1978. The data are at the mandatory levels; 1000, 850, 700, 500, 400, 300, 250, 200, 150, and 100 mb. The domain of integration in (7) and (2) is from 20°N to 85°N and from 1000 mb to 100 mb.

Results

An overall view of the conversion between available potential energy and kinetic energy for various modes of the atmospheric motion is provided in Table 1. Note that the eddy conversion is also divided into two groups: $\sum_{n=1}^{4} C(n)$ represents the long-wave regime and $\sum_{n=5}^{15} C(n)$ the cyclone and short-wave regime. The numerical values of $C(A_Z, K_Z) = -0.18\ Wm^{-2}$ and $C(A_E, K_E) = 2.6\ Wm^{-2}$ in the present study. Tomatsu obtains a two-month (December and January) mean values of $C(A_Z, K_Z) = -0.6\ \overline{Wm}^{-2}$ and $C(A_E, K_E) = 3.14\ \overline{Wm}^{-2}$. Our results are somewhat smaller than Tomatsu's, but not unrealistic. In fact, our results are also close to Oerlemans' (1980) recent estimate of $C(A_E, K_E)$ which is $2.1\ \overline{Wm}^{-2}$ in winter. The salient features shown in Table 1 are:

(1) $\sum_{n=1}^{4} C(n)$ and $\sum_{n=5}^{15} C(n)$ are comparable; (2) $C(A_Z, K_Z)$ is attributed to the standing mode and $C(A_E, K_E)$ is mainly contributed by the transient eddies; (3) the major amount of $\sum_{n=1}^{4} C(n)$ is due to the transient eddies, but the contribution from the standing eddies is not insignificant, and; (4) $\sum_{n=5}^{15} C(n)$ is mainly provided by the transient eddies.

The spectral distribution of C(n) is shown in Figure 1. The maximum values C(n) in this study appear at wave numbers 2 and 6. This is in agreement with the spectral energetics results compiled by Saltzman (1970). Tomatsu's computation shows that the maximum C(n) occurs at waves 1 and 3 in winter. The hatched area of Figure 1 represents the spectrum of $C(n)_T$. The maximum value of $C(n)_T$ occurs at wave 6. The contribution of $C(n)_S$ comes from waves 1-3.

In order to have a better view of the climatology of the conversion between A and K, Figure 2 displays the latitudinal height distribution of the energy conversion for various modes of atmospheric motions and various wavenumber regimes. The distribution of $C(A_Z, K_Z)$, Figure 2a, is similar to that shown in Tomatsu's study. The negative values appear between 50°N and 70°N which may be the result of the Ferrel circulation. The positive values occur between 35°N and 50°N, and in the polar area, north of 70°N. Although the areal average of $C(A_Z, K_Z)$ is smaller in this study, the numerical values in the $C(A_Z, K_Z)$ distribution in the current study are larger than Tomatsu's. This indicates that the intensity of the mean meridional circulation in the winter analyzed in this study is stronger.

The distribution of $C(A_E, K_E)$, Figure 2b, shows three areas of maximum value at 500 mb: 45°N (major one), 65°N and 75°N. Tomatsu's result only shows a maximum value at 600 mb and 50°N. It is of interest to examine the contribution of different wave regimes to $C(A_E, K_E)$. The comparison between

$C(A_E, K_E)$, $\sum_{n=1}^{4} C(n)$ (Figure 2c) and $\sum_{n=5}^{15} C(n)$ (Figure 2d) shows very clearly that the major maximum of $C(A_E, K_E)$ at 45°N is mainly attributed to the cyclone and short waves. The two minor maxima of $C(A_E, K_E)$ at 65°N and 75°N are due to the long waves. This may indicate that the wave activities in the high latitudes are dominated by the long waves, while in the mid-latitudes cyclone and short waves are active, in addition to the long waves.

In the right-hand column of Figure 2, we display the latitude-height distributions of either the standing or transient modes of those four quantities discussed above depending upon which provides the dominant contribution to their totals, respectively. The $C(A_Z, K_Z)$ distribution is more or less decided by $C(A_Z, K_Z)_S$, while the $C(A_E, K_E)$ distribution is determined by $C(A_E, K_E)_T$. The further breakdown of $C(A_E, K_E)_T$ into $\sum_{n=1}^{4} C(n)_T$ and $\sum_{n=5}^{15} C(n)_T$ shows that $\sum_{n=5}^{15} C(n)$ distribution is almost identical to $\sum_{n=5}^{15} C(n)_T$. However, $\sum_{n=1}^{4} C(n)$ and $\sum_{n=1}^{4} C(n)_T$ has some significant difference over the location where the maximum value of $C(A_E, K_E)$ occurs, i.e. 500 mb and 45°N. The difference between these two quantities indicates that the major contribution of the standing eddies appears at 500 mb and 45°N.

The idea of computating the energy conversion between A and K is not new. However, very few studies have been made to evaluate this energy conversion using multilevel observational data. Some interesting features shown in our C(A, K) computations may be useful in evaluating model simulations of the atmospheric general circulation.

Acknowledgment

This study is supported in part by the NSF grant ATM-7915800 and the NASA grant NSG-5339.

Table 1. Contributions to conversion between available potential energy (A) and kinetic energy (K) from various modes of atmospheric motions. Unit: Wm^{-2}.

	Total (S+T)	Standing (S)	Transient (T)
$C(A_Z, K_Z)$	-0.18	-0.22	0.04
$C(A_E, K_E)$	2.60	0.40	2.20
$\sum_{n=1}^{4} C(n)$	1.15	0.36	0.79
$\sum_{n=5}^{15} C(n)$	1.45	0.04	1.44

Appendix

The ω equation of the quasi-geostrophic model may be written as

$$\nabla^2\omega + \frac{f^2}{\sigma}\frac{\partial^2\omega}{\partial p^2} = F \,, \tag{A1}$$

where $$F = \frac{f}{\sigma}\frac{\partial}{\partial p} J(\psi, \zeta + f) + \frac{1}{\sigma}\nabla^2 J(\psi, \frac{\partial\phi}{\partial p}) \,.$$

$\sigma = \sigma(p)$ and ϕ is geopotential. The forcing of function in (A1) contains only the vertical differentiation of vorticity advection and the Laplacian of thermal advection. Let us express ω and F in terms of solid spherical harmonics (Platzman, 1960).

$$\omega = \sum_m \sum_n \omega_n^m \, Y_n^m \tag{A2}$$

and

$$F = \sum_m \sum_n F_n^m \, Y_n^m \tag{A3}$$

where $Y_n^m = P_n^m e^{im\lambda}$ and $P_n^m(\mu)$ is the Associated Legendre function of the latitude, ϕ, at which $\mu = \sin\phi$. ω_n^m and F_n^m are the spectral coefficients of ω and the forcing function, respectively. Substitution (A2) and (A3) into (A4), we can obtain the spectral form of (A2),

$$-\frac{n(n+1)}{a^2}\omega_n^m + \frac{f^2}{\sigma}\frac{\partial^2\omega_n^m}{\partial p^2} = F_n^m \tag{A4}$$

where a is the earth's radius. The second-order derivative of ω_n^m in (A4) is evaluated by the finite difference scheme illustrated in Figure A1. The second-order derivative of ω_n^m at the level K is evaluated by dividing the difference between the first-order derivative of ω_n^m in the middle of levels (K + 1 , K) and of levels (K, K-1) by $\frac{1}{2}(\Delta p_K + \Delta p_{K+1})$. Therefore, (A4) can be written as,

$$A_{K+1}\,\omega_n^m(K+1) - B_K\,\omega_n^m(K) + C_{K-1}\,\omega_n^m(K-1) = F_n^m(K) \qquad \text{(A5)}$$

where

$$A_{K+1} = \frac{2f^2}{\sigma\Delta p_{K+1}(\Delta p_{K+1} + \Delta p_K)}$$

$$B_K = \frac{n(n+1)}{a^2} + \frac{2f^2}{\sigma\,\Delta p_K\,\Delta p_{K+1}}$$

$$C_{K-1} = \frac{2f^2}{\sigma\,\Delta p_K\,(\Delta p_{K+1} + \Delta p_K)} \cdot$$

Applying (A5) to every level, we can obtain a linear system which can be expressed in terms of a matrix equation,

$$\bar{M}\,\bar{\omega} = \bar{F}$$

where

$$\bar{M} = \begin{pmatrix} -B_1 & A_2 & 0 & \cdots & 0 \\ C_1 & -B_2 & A_3 & \cdots & 0 \\ \cdot & \cdot & \cdot & \cdots & \cdot \\ \cdot & \cdot & \cdot & \cdots & \cdot \\ \cdot & \cdot & \cdot & \cdots & A_N \\ 0 & 0 & \cdot & \cdots & C_{N-1} \quad -B_N \end{pmatrix}, \quad \bar{\omega} = \begin{pmatrix} \omega_n^m(1) \\ \omega_n^m(2) \\ \cdot \\ \cdot \\ \cdot \\ \omega_n^m(N) \end{pmatrix} \text{ and } \quad \bar{F} = \begin{pmatrix} F_n^m(1) \\ F_n^m(2) \\ \cdot \\ \cdot \\ \cdot \\ F_n^m(N) \end{pmatrix} \qquad \text{(A6)}$$

C-3

N is the maximum number of vertical levels, $\bar{M}$ is a triadiagonal square matrix and ω_n^m at the various levels can be obtained by solving (A6).

The procedures are as follows: (a) calculate the forcing function of the ω equation on the 2.5° x 2.5° grid; (b) use Ellsaesser's (1966) scheme to create the spectral coefficients of the forcing functions; (c) the spectral coefficients of the vertical motion are solved by equation (A6); and (d) the ω field is constructed by equation (A2).

The spectral truncation used in this study is triangular with $0 \leq |m| \leq 25$ and $0 \leq n \leq 25$. Since only hemispherical data is available, we must make some assumption concerning the parity at the physical variables. We assume that ω and F are even.

References

Ellsaesser, H.W., 1966. Expansion of hemispheric meteorological data in antisymmetric surface spherical harmonic (Laplace) series. J. Appl. Meteor. 5:263-276.

Krishnamurti, T.N., 1968. A diagnostic balance model for studies of weather systems of low and high latitudes, Rossby number less than 1. Mon. Wea. Rev. 96:197-207.

Oerlemans, J., 1980. An observational study of the upward sensible heat flux by synoptic-scale transients. Tellus 32:6-14.

Platzman, G.W., 1960: The spectral form of the vorticity equation J. Meteor. 17:635-644.

Saltzman, B., 1970. Large scale atmospheric energetics in the wave number domain. Rev. Geophys. Space Phys. 8:289-302.

Tomatsu, K., 1979. Spectral energetics of the troposphere and lower stratosphere. Advances in Geophysics, Vol. 21, Academic Press, 289-405.

Wiin-Nielsen, A., 1968. On the intensity of the general circulation of the atmosphere. Rev. Geophys. 6:559-879.

Figure Captions

Figure 1. Spectral distributions of C(n) (solid line), $C(n)_T$ (solid line enclosing the hatched area) and $C(n)_S$ (dashed line). Unit: 10^{-1} Wm^{-2}.

Figure 2. Latitudinal-height distribution of (a) $C(A_Z, K_Z)$, (b) $C(A_E, K_E)$, (c) $\sum_{n=1}^{4} C(n)$, (d) $\sum_{n=5}^{15} C(n)$, (e) $C(A_Z, K_Z)_S$, (f) $C(A_E, K_E)_T$, (g) $\sum_{n=1}^{4} C(n)_T$ and (h) $\sum_{n=5}^{15} C(n)_T$. Unit: 10^{-3} Wm^{-2} mb^{-1}.

Figure A-1. Schematic diagram for the computation of the vertical derivative for ω_n^m.

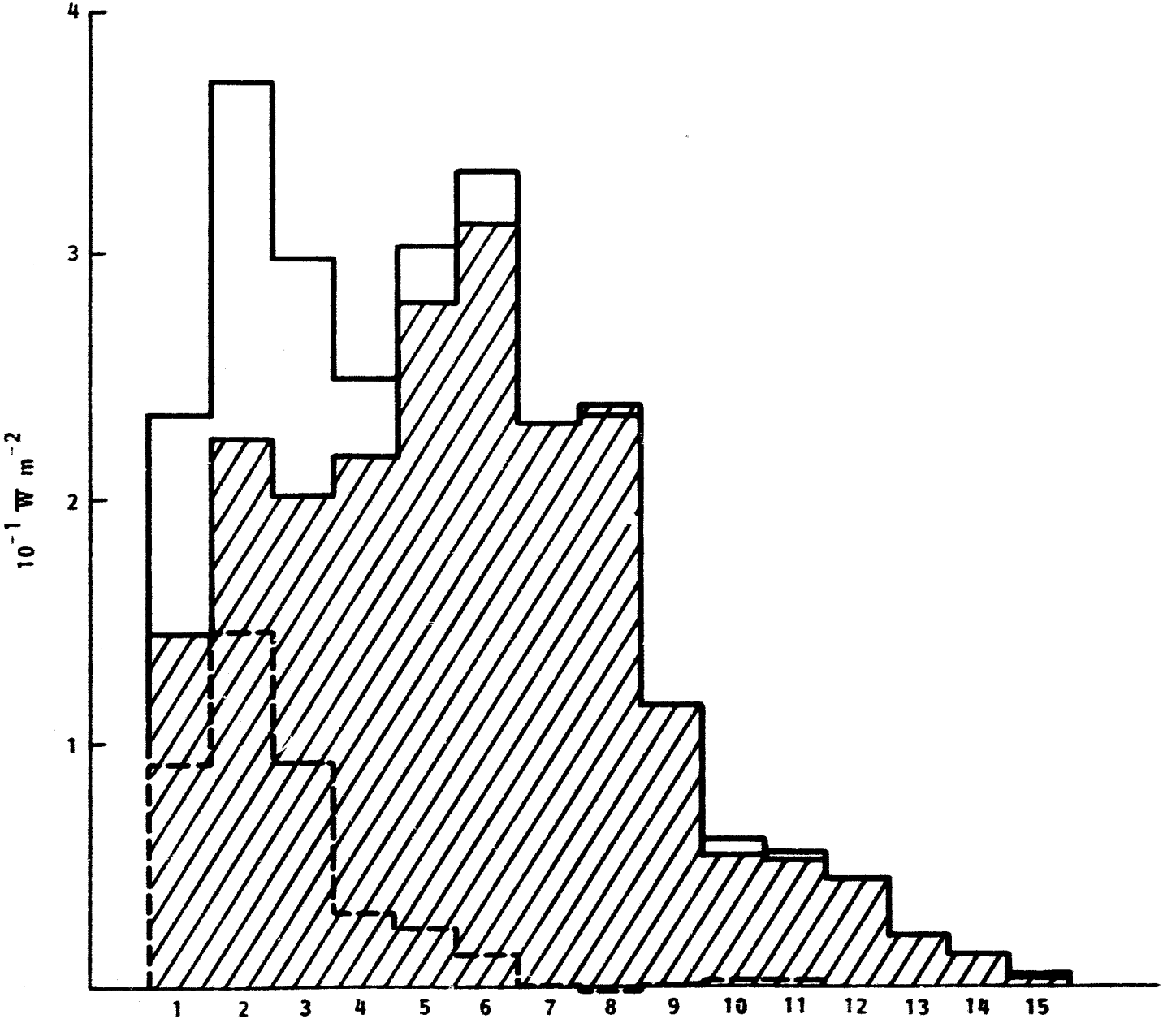

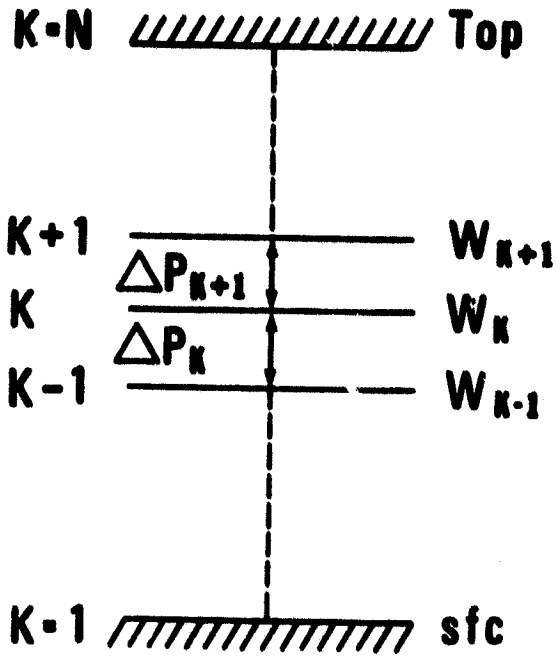
K=N
Top
K+1
W_{K+1}
ΔP_{K+1}
K
W_K
ΔP_K
K-1
W_{K-1}
K=1
sfc

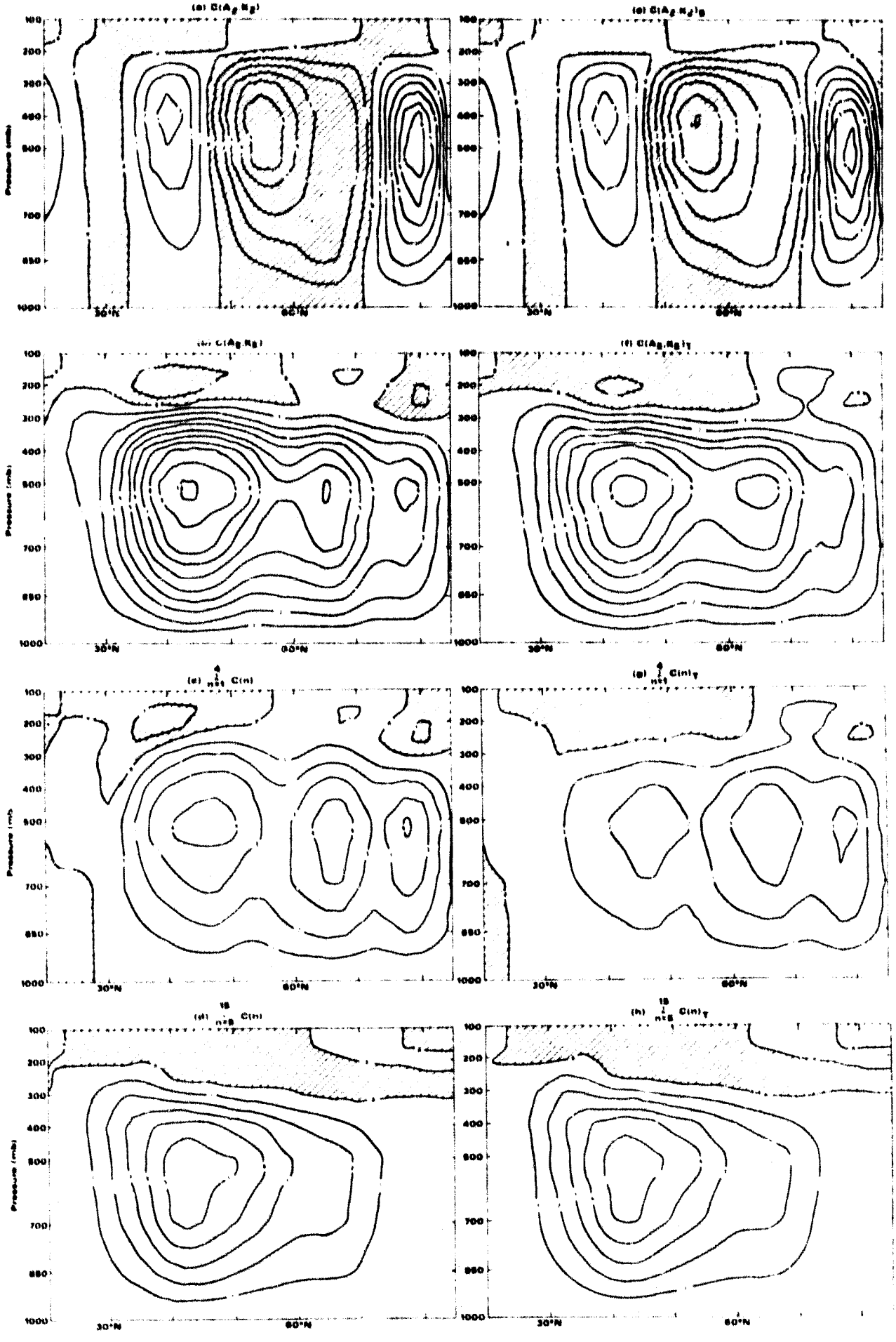
(a) C(A_E, K_E)
(b) C(A_E, K_E)_S
(c) C(A_E, K_E)
(f) C(A_E, K_E)_T
(e) Σ_{n=1}^{7} C(n)
(g) Σ_{n=1}^{7} C(n)_T
(d) Σ_{n=8}^{15} C(n)
(h) Σ_{n=8}^{15} C(n)_T
Pressure (mb)
100
200
300
400
500
700
850
1000
30°N
60°N

On the warming of the polar troposphere during the stratospheric warming of January 1977

Anthony R. Hansen and Tsing-Chang Chen

Department of Earth Sciences
Iowa State University
Ames, IA, 50011

On the warming of the polar troposphere during the stratospheric warming of January 1977

Anthony R. Hansen and Tsing-Chang Chen

Department of Earth Sciences
Iowa State University
Ames, IA, 50011

Abstract

In January 1977, a warming of the polar troposphere occurred following a major stratospheric warming. The temperature increase in the polar troposphere is found to be larger below 400 mb than in the upper troposphere. Analysis of the heat budget of the polar troposphere shows that the eddy heat flux convergence is the major factor responsible for the tropospheric warming.

Introduction

During January 1977, a major sudden warming in the stratosphere was followed by a striking temperature increase in the polar troposphere (Quiroz, 1977). This sequence of events raises the question of causal connection between these two occurrances. It would be interesting to investigate whether there is a direct connection between the stratospheric and tropospheric warmings. Recently, Koermer and Kao (1980) studied the evolution of the kinetic and thermal energy as well as the heat and momentum flux convergence in the stratosphere and troposphere during this warming compared to the minor warming of 1975-76. O'Neill and Taylor (1979) investigated the 20 mb and 300 mb heat and momentum budgets and found that warming in the polar upper troposphere in early January was due to increased subsidence that was forced by southward eddy momentum transport.

We have computed the heat budget in the troposphere where we found that the largest temperature increase over the polar cap in mid-January 1977 occurred below 400 mb. Taylor and Perry (1977) have pointed out that an unusually large number of 1000-500 mb thickness anomolies centered around 80°N latitude occurred during mid-January of this year. The purpose of this note is to show that the lower tropospheric warming was primarily the result of strong eddy heat flux convergence in the lower troposphere. Although a complete explanation of the cause of the enhanced eddy transport of sensible heat into the polar tropcaphere is beyond the scope of the present report, a possible mechanism is proposed.

Analysis Method and Data

The heat budget of the polar trophosphere is investigated by using the zonally averaged form of the thermodynamic equation:

$$\frac{\partial T_z}{\partial t} = -\frac{1}{a\cos}\frac{\partial}{\partial\phi}\left(\left(V_E T_E\right)_z \cos\phi\right) - \frac{1}{a\cos\phi}\frac{\partial}{\partial\phi}\left(V_z T_z \cos\phi\right) -$$

$$-\left(\frac{\partial T_z}{\partial p} - \frac{R}{c_p p} T_z\right)\omega_z - \left[\left(\frac{\partial T_E}{\partial p} - \frac{R}{c_p p} T_E\right)\omega_E\right]_z + \frac{1}{c_p} H_z$$

The z subscript denotes variables that were averaged around a latitude circle and the E subscript denotes eddy quantities that were departures from the zonal average. The term on the left-hand side is the local rate of change of the zonally averaged temperature. The terms on the right-hand side are the temperature change due to 1) eddy heat flux convergence; 2) convergence of the zonal mean heat flux; 3) adiabatic warming (or cooling) due to zonal mean vertical motion; 4) adiabatic warming due to eddy vertical motion; and

5) diabatic heating.

Data from the objective analysis scheme of the National Meteorological Center (NMC) for every 2.5° of longitude at the 10 mandatory levels (1000, 850, 700, 500, 400, 300, 250, 200, 150, and 100 mb) in the troposphere are used to evaluate the various terms in this equation at 70°N and 80°N. NMC employed the Flattery analysis scheme (Flattery, 1970) in 1976-77 which removes the divergent component of the wind from the horizontal motion field. $V_z = 0$ in the Flattery analysis so the residual in the heat budget represents not only the effects of diabatic heating but also changes in T_z due to the actual convergence of the zonal mean heat flux as well as any effects due to errors in the data. The exact quality of the data at polar latitudes is difficult to determine, but for the sake of discussion, changes in or contributions to changes in T_z with magnitudes of 1°K/day or less may be considered to be noise. The vertical motion is computed from the quasi-geostrophic form of the ω-equation assuming $\omega = 0$ at 1000 mb and 100 mb (Chen et al., 1981). The ω-equation includes the effects of both dynamic and thermodynamic forcing on the vertical motion field (Wiin-Nielsen, 1964). These include the vertical differentiation of the absolute vorticity advection and the Laplacian of the thermal advection. The ω values obtained from this method may be underestimated to some extent due to excessive smoothing of the height field by the objective analysis scheme in data sparse regions (Wiin-Nielsen, 1968).

Discussion and Speculation

Figure 1 shows the average cross-section of the zonal mean temperature for 10-18 January 1977. The following discussion will concentrate on the results at 80°N because the largest tropospheric temperature rise occurred at or north of 80°N (Figure 1).

The zonal mean temperature at 80°N as a function of height and time is shown in Figure 2. The largest temperature rise occurs in the lower troposphere, below 700 mb, from 9 to 12 January with a slightly smaller temperature increase in the mid-troposphere. Very little temperature rise is evident in the upper troposphere (300-200 mb). The largest rate of temperature increase occurs at low and mid levels (Figure 3a), but warming extended throughout the troposphere below 300 mb from 1200 GMT 9 January through 0000 GMT 12 January. Significant heating due to eddy heat flux convergence occurs in the layer below 400 mb from 1200 GMT 9 January through 0000 GMT 12 January (Figure 3b) and coincides almost exactly with the observed temperature increase. The maximum warming due to eddy sensible heat transport is 4°K/day between 700 and 1000 mb. Comparison of Figures 3a and b shows that the eddy heat flux accounts for almost the entire observed temperature rise in mid-January. A similar relationship between the rate of change of the zonal mean temperature and positive eddy heat flux convergence in the lower troposphere is also apparent in the heat budget results at 70°N (not shown).

Warming due to zonal mean adiabatic descent at 80°N is present throughout a deep layer on 8-9 January with a maximum value of 3°K/day between 200 mb and 300 mb (Figure 3c). However this effect is not reflected in a rise in T_z. The adiabatic warming in our calculation is compensated by the residual (Figure 3d). The effects of vertical motion are unimportant at 70°N (not shown). The large eddy heat flux convergence in the lower troposphere from 9 to 12 January would force upward vertical motion and diabatic cooling. However, subsidence is indicated in Figure 3c on 9 and 10 January. Apparently, the strong southward eddy momentum flux occurring at this time at polar latitudes

(O'Neill and Taylor, 1979) forced descending motion that dominated the effect of the northward eddy heat flux on the mean vertical velocity. The insignificance of adiabatic warming together with the absence of a large temperature rise in the upper troposphere (Figure 2) indicate, as O'Neill and Taylor (1979) have already shown, that warming due to adiabatic descent did not propagate downward from the stratosphere into the troposphere. Eddy vertical motion did not significantly effect the polar heat budget.

Koermer and Kao (1980) note that once the 1976-77 major warming was in progress, there was a decoupling of the stratospheric and tropospheric circulation and blocking in the troposphere. Under normal conditions, the band of strongest zonal mean westerly winds acts as a waveguide for vertically propagating planetary-scale waves (Dickinson, 1968). During a major stratospheric warming the westerly jet in the stratosphere is replaced by mean easterlies preventing the normal upward propagation of planetary waves (Charney and Drazin, 1961). Although easterly winds appeared almost simultaneously at polar latitudes in both the lower stratosphere and troposphere shortly before 10 January 1977 (Quiroz, 1977; O'Neill and Taylor, 1979), substantial warming in the middle and upper stratosphere occurred from 28 December 1976 to 3 January 1977 (Quiroz, 1977). Reversal of the zonal wind and temperature gradient occurred in the upper stratosphere before extending downward (Koermer and Kao, 1980). This warming pulse in late December and early January may have initiated the disruption of the westerly wave guide in the stratosphere. As a result, amplifying tropospheric planetary waves associated with Atlantic blocking in the first 10 days of January may have been unable to propagate vertically. The tropospheric planetary waves reached their maximum amplitude at about the same time or shortly after easterly winds appeared in the lower stratosphere (Table 1).

The easterly mean flow in the lower stratosphere would completely disrupt the westerly wave-guide. The coincidence of tropospheric wave amplification with the appearance of stratospheric easterlies may have lead to the observed eddy heat flux convergence at polar latitudes. With the waves unable to propagate upward away from their source region, the northward heat transport normally associated with vertically propagating waves may have manifested itself in the large observed sensible heat transport into the polar troposphere. The heat transport accompanying the amplifying waves lead to warming near the pole instead of upward wave propagation.

McGuirk (1977) noted that major perturbations of the zonal mean tropospheric temperatures with high latitude warming and mid-latitude cooling occur after the commencement of stratospheric warmings. Labitzke (1965) has shown that tropospheric blocking patterns occur roughly 10 days after the onset of stratospheric warmings. In blocking, a pronounced warming occurs in the northern part of the blocked zone with cooling in the southern part (Rex, 1950). Consequently, a mechanism similar to one presently proposed may have been responsible for the growth of the blocks studied by Labitzke and for the pattern of T_z changes noted by McGuirk.

In conclusion, the tropospheric polar warming in January 1977 was principally the result of eddy heat flux convergence in the middle and lower troposphere. It appears that the tropospheric warming was not due to adiabatic descent within the troposphere. This warming may have been a manifestation of the trapping of vertically propagating planetary waves beneath stratospheric easterlies. Thus, the stratospheric warming may have had an indirect effect on the tropospheric circulation.

Acknowledgements

This study was supported in part by the National Aeronautics and Space Administration under Grant NSG-5339, and the National Science Foundation under Grant ATM-7924568.

Table 1. Dates of the maximum 500 m amplitude of the sum of zonal harmonic height waves 1 through 4 over the Atlantic in early January 1977

Latitude	Date	Maximum Wave Amplitude	Longitude
50°N	8 Jan	475 m	25 W
60°N	10 Jan	419 m	30 W
70°N	11 Jan	378 m	40 W

FIGURE CAPTIONS

Figure 1. The average meridional cross section of T_Z(°K) for 0000 GMT 10 January 1977 through 1200 GMT 18 January 1977.

Figure 2. The zonally averaged temperature, T_Z(°K), at 80°N as a function of height and time.

Figure 3. Height-time sections of the terms in the heat budget at 80°N: a) the time rate of change of the zonally averaged temperature, $\partial T_z/\partial t$; b) eddy heat flux convergence, $-\frac{1}{a\cos\phi}\frac{\partial}{\partial\phi}\left[\left(V_E T_E\right)_z \cos\phi\right]$ c) adiabatic warming (cooling) due to zonal mean vertical motion, and; d) the residual. The units are °K/day with positive values shaded.

REFERENCES

Chen, T.C., A.R. Hansen, and J.J. Tribbia, A note on the release of available potential energy. Submitted to J. Meteorol. Soc. of Japan, 1981.

Dickinson, R.E., Planetary Rossby waves propagating through weak westerly wind wave guides. J. Atmos. Sci., 25, 269-279, 1968.

Flattery, T., Spectral models for global analysis and forecasting. Proceedings of the Sixth AWS Technical Exchange Conference, U.S. Naval Academy, Air Weather Service Technical Report 242, pp. 42-54, 1970.

Koermer, J.P., and S.K. Kao, Major and minor stratospheric warmings and their interactions on the troposphere. Pageoph, 118, 428-451, 1980.

Labitzke, K., On the mutual relation between stratosphere and troposphere during periods of stratospheric warmings in winter. J. Appl. Meteorol. 4, 91-99, 1965.

McGuirk, J.P., Planetary-scale forcing of the Janaury 1977 weather. Science 199, 293-295, 1978.

O'Neill, A., and B.F. Taylor, A study of the major stratospheric warming of 1976/77. Quart. J. Roy. Meteorol. Soc., 105, 71-92, 1979.

Quiroz, R.S., The tropospheric-stratospheric polar vortex breakdown of January 1977. Geophys. Res. Lett., 4, 151-154, 1977.

Rex, D.F., Blocking action in the middle troposphere and its effect on regional climate. I. An aerological study of blocking action. Tellus, 2, 196-211, 1950.

Taylor, B.F., and J.D. Perry, The major stratospheric warming of 1976-1977. Nature, 267, 417-418, 1977.

Wiin-Nielsen, A., On the intensity of the general circulation of the atmosphere. Rev. Geophys., 6, 559-579, 1968.

Wiin-Nielsen, A., On energy conversion calculations. Mon. Wea. Rev., 92, 161-167. 1964.

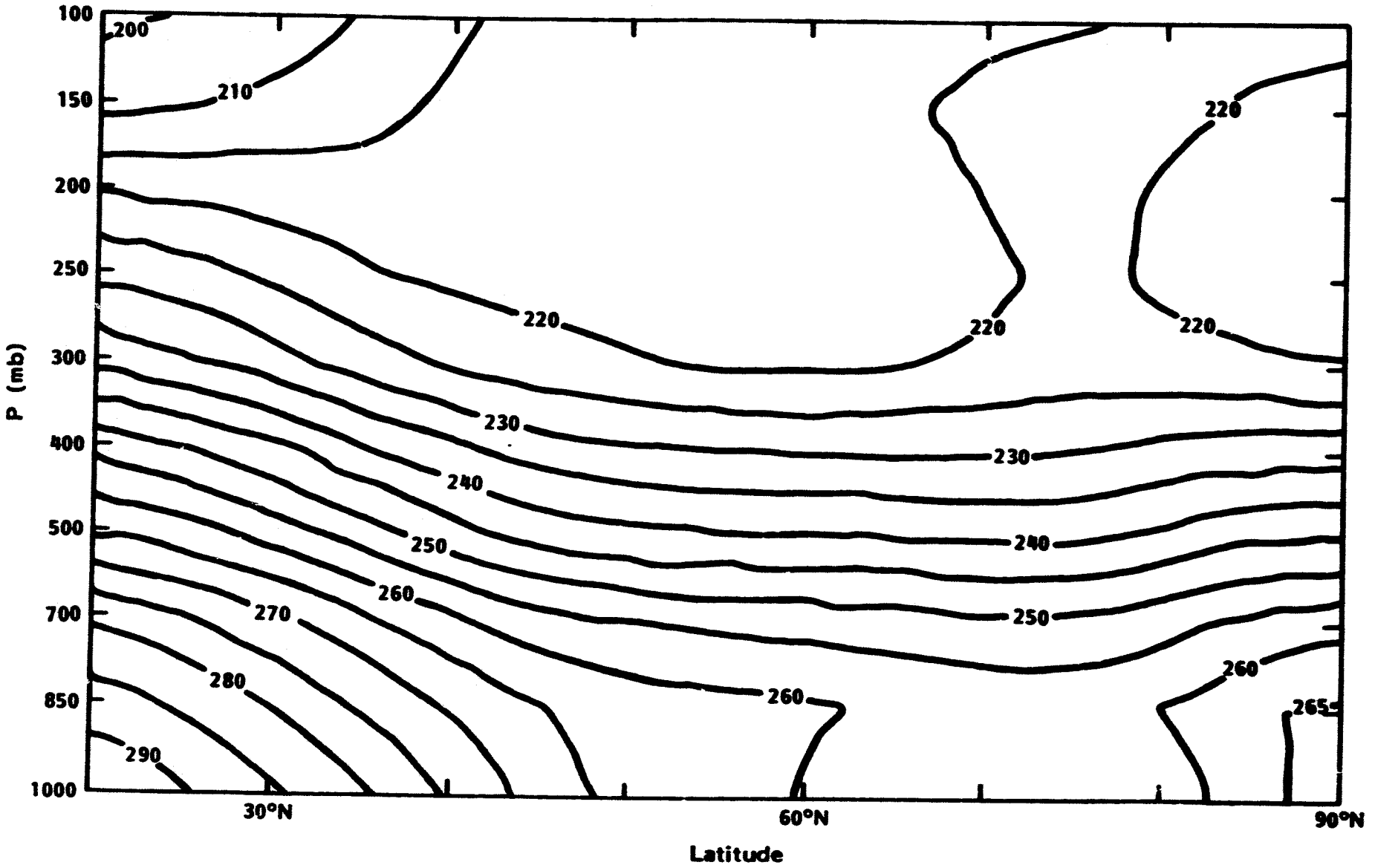
100
150
200
250
300
400
500
700
850
1000
P (mb)
200
210
220
220
220
220
230
230
240
240
250
250
260
260
270
280
290
260
265
30°N
60°N
90°N
Latitude

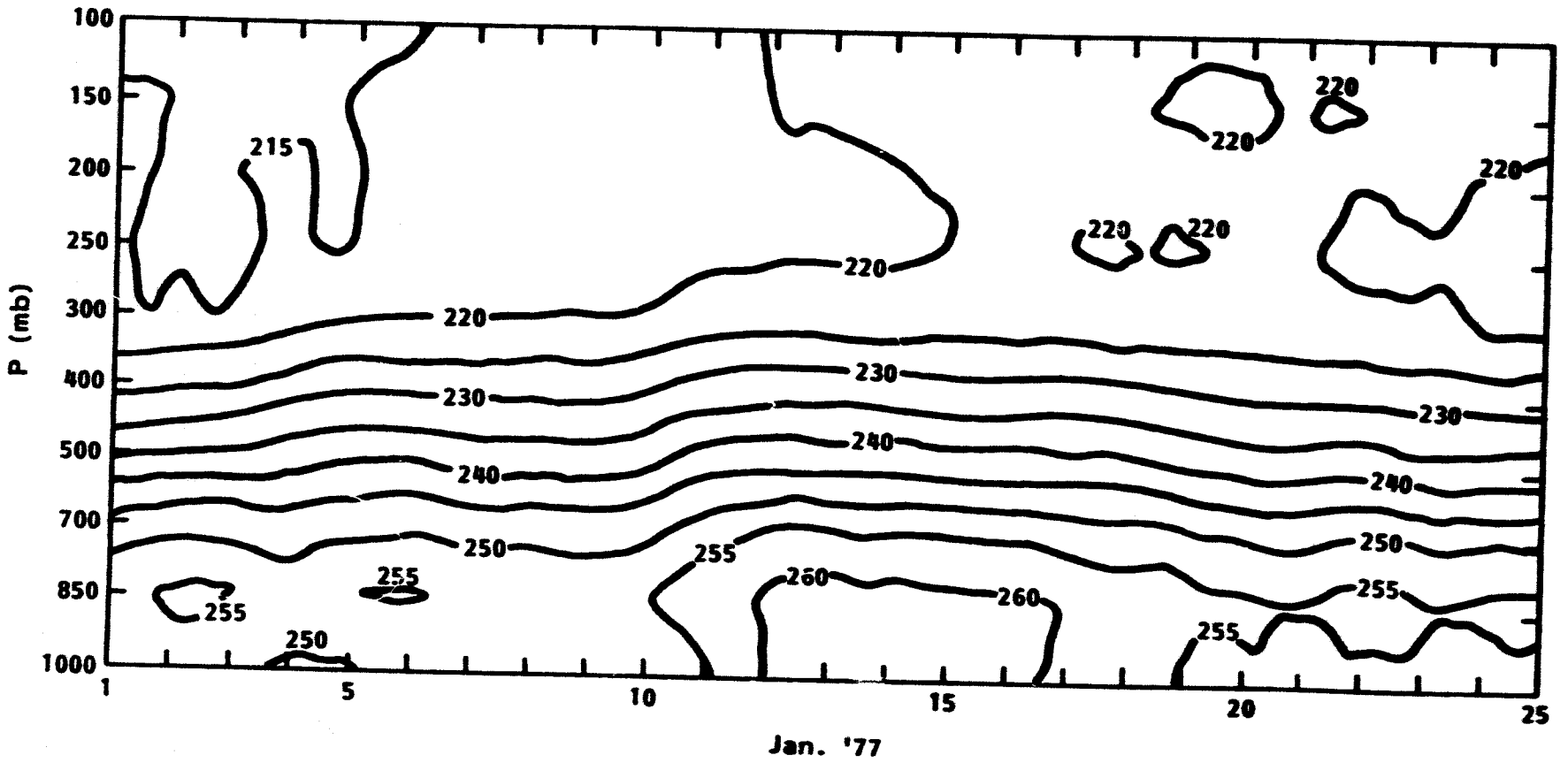
100
150
200
250
300
400
500
700
850
1000
P (mb)
215
220
220
220
220
220
220
230
230
230
240
240
240
250
250
255
255
255
260
260
255
1
5
10
15
20
25
Jan. '77

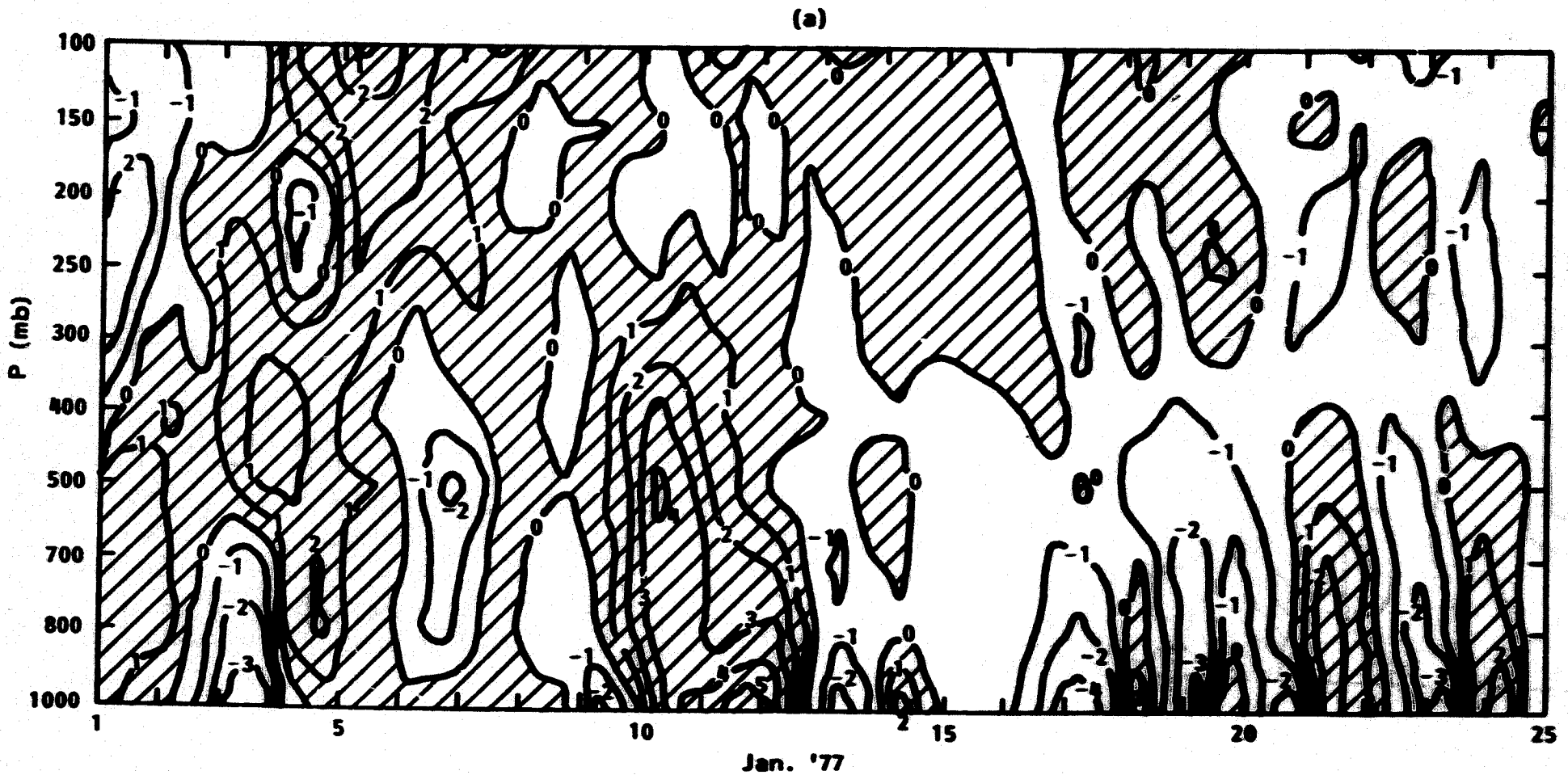
(a)
P (mb)
100
150
200
250
300
400
500
700
800
1000
1
5
10
15
20
25
Jan. '77

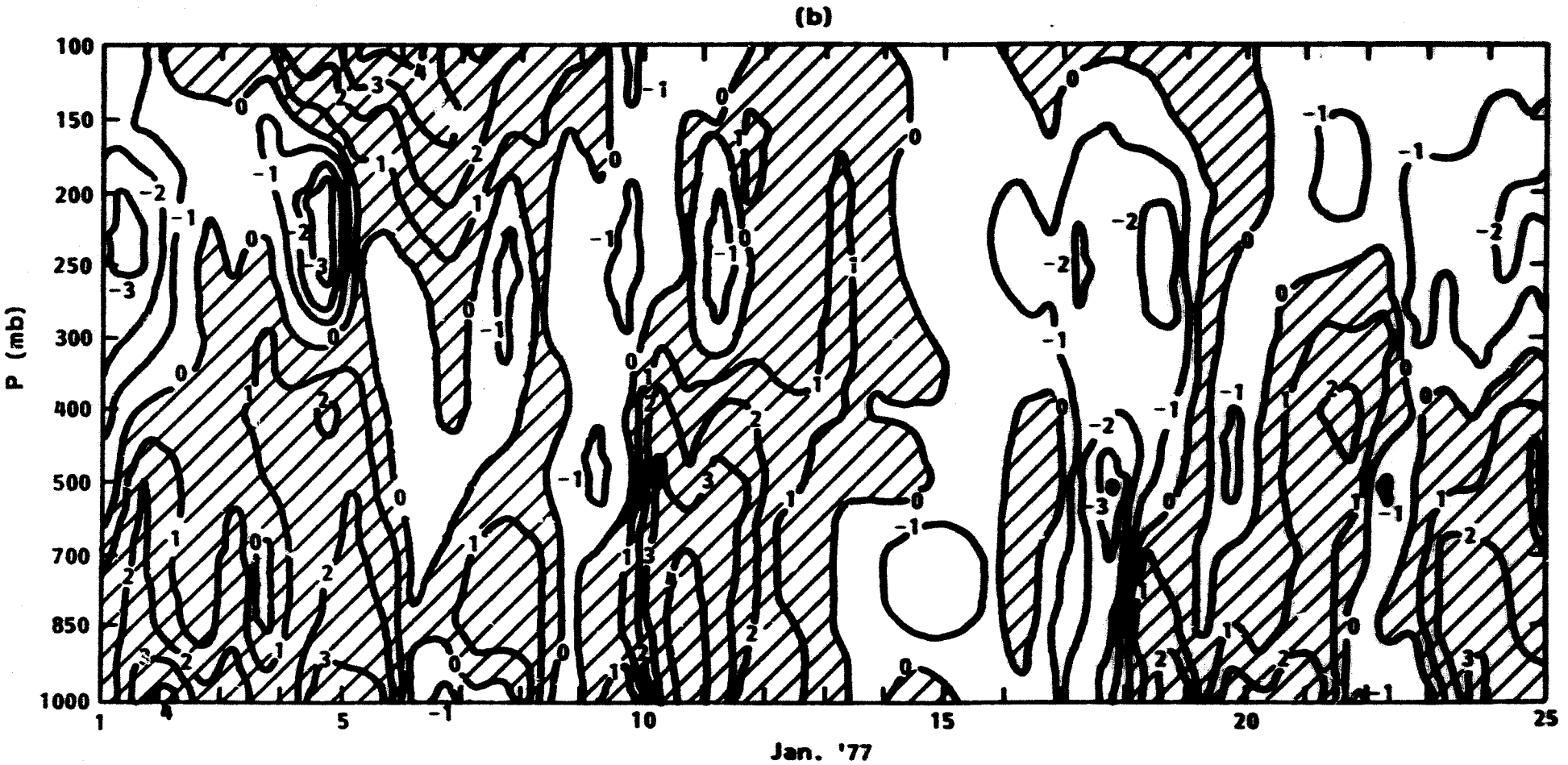
(b)
P (mb)
100
150
200
250
300
400
500
700
850
1000
1
5
10
15
20
25
Jan. '77

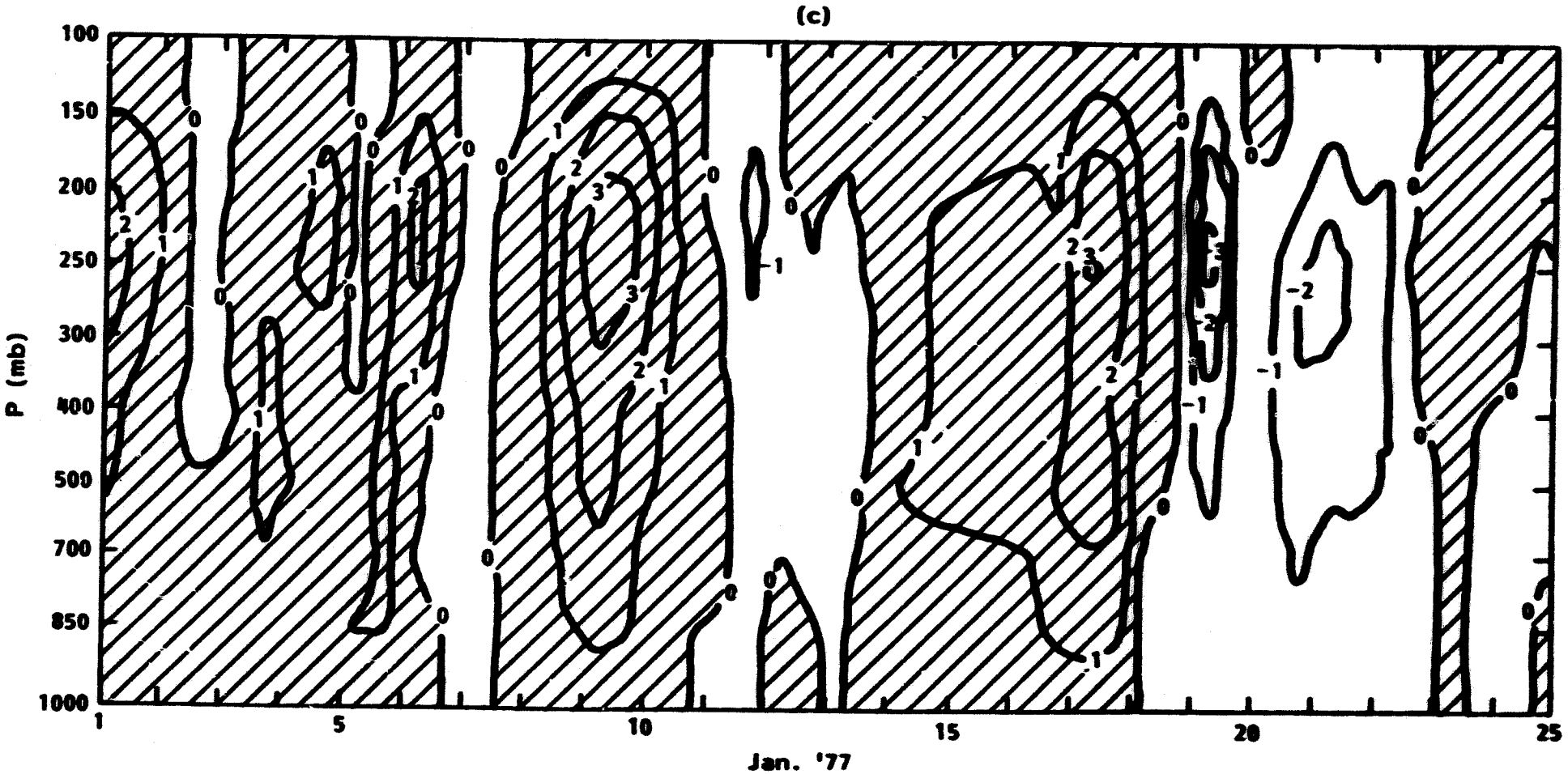
(c)
P (mb)
100
150
200
250
300
400
500
700
850
1000
1
5
10
15
20
25
Jan. '77

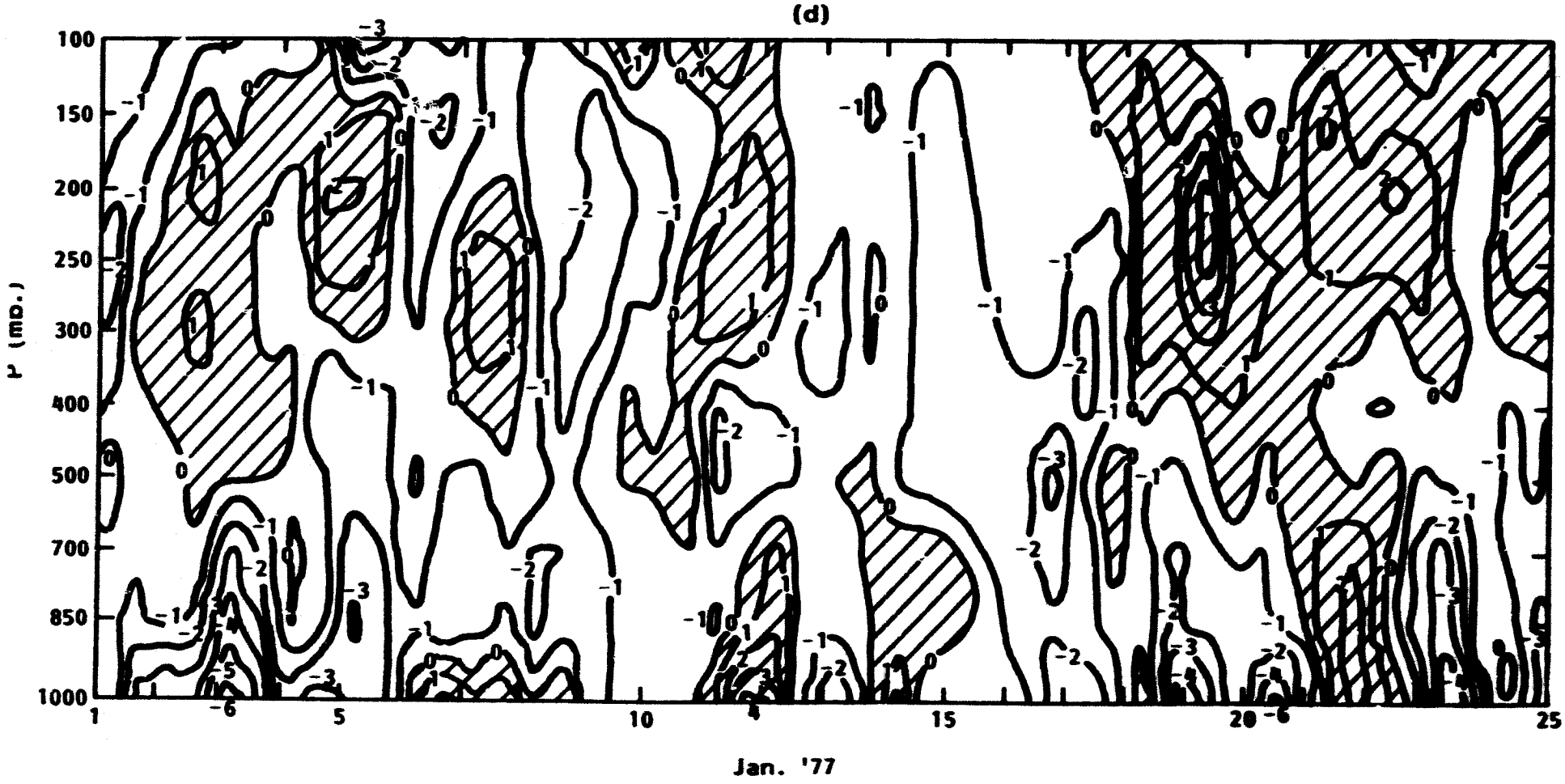
(d)
100
150
200
250
300
400
500
700
850
1000
P (MB.)
1
5
10
15
20
25
Jan. '77